OSCCAR:
FUTURE OCCUPANT SAFETY FOR CRASHES IN CARS

Validated and Computationally Robust Active HBMs

Document Type	Deliverable
Document Number	D3.2
Primary Author(s)	Johan Davidsson | Chalmers
Document Version / Status	1.2 | Final
Distribution Level	PU (public)

Project Acronym	OSCCAR
Project Title	FUTURE OCCUPANT SAFETY FOR CRASHES IN CARS
Project Website	www.osccarproject.eu
Project Coordinator	Werner Leitgeb | VIF | werner.leitgeb@v2c2.at
Grant Agreement Number	768947
Date of latest version of Annex I against which the assessment will be made	2021-02-05
Upload by coordinator:	First submitted: 2021-12-21 Re-submitted: 2022-04-11

OSCCAR has received funding from the European Union's Horizon 2020 research and innovation programme under grant agreement No 768947.

CONTRIBUTORS

Name	Organization	Name	Organization
Muriel Beaugonin	ESI	Christoph Klein	VIF
Stefanos Vlachoutsis	ESI	Peter Wimmer	VIF
Morgan Cameron	ESI	Jason Fice	Chalmers
Nico Erlinger	TU Graz	Johan Davidsson	Chalmers
Desiree Kofler	TU Graz	Anders Jaber	Chalmers
Corina Klug	TU Graz	Emma Larsson	Chalmers
Lennart Nölle	USTUTT	Atul Mishra	MBRDI
Oleksandr Martynenko	USTUTT	María González-García	Volkswagen AG
Syn Schmitt	USTUTT	Jens Weber	Volkswagen AG
Tanmoy Banik	USTUTT	Richard Lancashire	Siemens
Eduardo Herrera Alfaro	USTUTT		

FORMAL REVIEWERS

Name	Organization	Date
Jonas Östh	Volvo Cars	2021-12-06
Swen Schaub	ZF	2021-12-19

DOCUMENT HISTORY

Revision	Date	Author / Organization	Description
0.1	2021-11-13	Johan Davidsson / Chalmers	First draft for review
0.2	2021-12-10	Johan Davidsson / Chalmers	Second draft for second review
1.1	2021-12-20	Johan Davidsson / Chalmers	Final version
1.2	2022-04-07	Manuela Klocker / VIF	Update after EU Review

TABLE OF CONTENTS

1 EXECUTIVE SUMMARY 10

2 OBJECTIVES 11

3 DESCRIPTION OF WORK 12

3.1 Volunteer data for the development of active and reactive HBMs 12

3.1.1 Review of data for the development of active and reactive HBMs 12
3.1.2 OM4IS2 volunteer data 13
3.1.3 PRECOONI volunteer data 14
3.1.4 TNO volunteer data 14
3.1.5 AHBM2 data – Autonomous braking volunteer data 15
3.1.6 AHBM3 – Autonomous lane-change volunteer data 17
3.1.7 Female response in AHBM3 volunteer tests 18
3.1.8 Data analysis of volunteer tests in the driver and passenger seat 19
3.1.9 Response corridors for the development of active HBMs of all occupants 25

3.2 Models for the use of volunteer data 26

3.2.1 Models of the loading environments used in the OM4IS2 and PRECOONI tests 26
3.2.2 Models of the loading environments used in the TNO tests 27
3.2.3 Models of the loading environments used in the AHBM2 and AHBM3 tests 27
3.2.4 Boundary conditions - setting priorities for volunteer tests 28

3.3 Muscle models for active and reactive HBMs 32

3.3.1 Hill muscle model with serial damping and eccentric force-velocity relation 32
3.3.2 Implementation of extended Hill-type material in LS-DYNA models 33
3.3.3 Implementation of extended Hill-type material model in VPS 35
3.3.4 Implementation of extended Hill-type material model in active THUMS TUC 42

3.4 Control systems for active HBMs 44

3.4.1 General muscle control systems 44
3.4.2 Shoulder muscle feedback controller for HBMs 49
3.4.3 Improved kinematic controllers for the Madymo AHBM 50
3.4.4 Torque controller for active HBMs 53
3.4.5 VPS-Simulation X coupling 59

3.5 Validated and computationally robust active and reactive HBMs 60

3.5.1 Validation of the THUMS TUC-VW AHBM 60
3.5.2 Literature review on age related active muscle properties 68
3.5.3 Modelling of changes to active muscle properties related to these changes. 69
3.5.4 Modelling an elderly population with active HBMs 72
3.5.5 Development of eastern anthropometry small female active HBM 75
3.5.6 Special focus on occupants with reduced mobility 79
3.5.7 Simulations of both the pre-crash phase and the in-crash phase 80
3.5.8 Lower Limb Control in the Madymo AHM 83

4 DISSEMINATION, EXPLOITATION AND STANDARDISATION 86

5 CONCLUSIONS 87

6 REFERENCES 90

A. APPENDIX - REVIEW OF DATA FOR THE DEVELOPMENT OF ACTIVE HBMS 96

Summary **96**
Methods of literature review of volunteers in pre-crash events **96**
Description of each study **97**

Autoliv Germany (1999) In vehicle passengers in emergency braking 97
Summary 97
U. Munich (2005) Lane change and sinusoidal manoeuvres 98
Hongik U. (2005) Bracing volunteers on sled 99
MIRA Ltd. (2005) Volunteer postures in vehicle pre-crash 100
Exponent (2005) Initiation of roll over in vehicle 101
U. Munich (2005) On sled lateral acceleration & initiation of roll-over 103
Delphi (2006) Lateral acceleration on sled. 104
JARI (2007) Pre-crash braking on sled. 105
JARI (2008) Pre-crash braking on sled 107
UMRT24 (2010) Driver simulator and in vehicle pre-crash braking 109
Autoliv. Sweden (2013) Children in vehicle braking and cornering 110
Chalmers (2011) On road manual and autonomous braking 111
Graz U. (2011) On sled lateral and braking acceleration 113
JARI (2012) Lateral accelerations on sled 114
VIF, Graz. (2013) In vehicle lane change manoeuvres 116
TNO (2013) On sled lateral and lateral/yaw accelerations 117
Chalmers (2012) In vehicle autonomous braking with pre-tensioned belts 119
JARI (2013) On sled braking acceleration with belt pre-tensioner 120
VIF, Graz (2014) Braking, lane change, and combined manoeuvres in vehicle 122
Chalmers (2016) On sled multidirectional horizontal plane accelerations. 124
IfF (2017) Different automation levels in pre-crash braking. 125
Chalmers (2018) Autonomous lane change manoeuvres in vehicle 126
UMTRI (2018) Age and BMI influence, in vehicle braking, lane change, and cornering 128
VIF (2018) PRECOONI Sled Tests 130
VIF (2018) Daimler Steering Tests 131

B. APPENDIX – DATA FOR THE DEVELOPMENT OF ACTIVE HBMS 132

OM4IS2 data **132**

Ethics 132
Disclaimer 132
Methods 133
Data Description 143
References 158

PRECOONI data **159**

Ethics 159

Disclaimer 159
Methods 159
Data Description 167

TNO data 174

Introduction 174
Methods 174

AHBM 2 data 176

Ethics 176
Disclaimer 177
Methods 177
Data Description 184
References 186

AHBM 3 data 187

Ethics 187
Disclaimer 187
Data Description 188

C. APPENDIX - MODELS OF THE LOADING ENVIRONMENTS USED IN THE VOLUNTEER TESTS 192

Models for the use of OM4IS2 and PRECOONI data 192

Development of the OM4IS2 and PRECOONI seat model 192
Calibration of the OM4IS2 and PRECOONI seat model 193

Models for the use of AHBM 2 and AHBM 3 data 197

Development of the generic AHBM 2 and 3 seat model 197
Tuning of the AHBM 2 and 3 seat model 198
Validation of the AHBM 2 and 3 seat model 199

D. APPENDIX – IMPLEMENTATION OF EHTM MODEL IN VPS 204

VPS EHTM model input 204
Evaluation of the VPS EHTM under isometric concentric load cases 204

E. APPENDIX - A SUMMARY OF VALIDATION DATA IN STUDIES OF SHOULDER JOINT STABILITY 208

F. ABBREVIATIONS AND DEFINITIONS 210

G. DISCLAIMER 211

LIST OF FIGURES

Figure 1: The coordinate system in the test vehicle. 21

Figure 2: Photos of the car interior used in the AHBM3 volunteer tests. 21

Figure 3: Photo of a volunteer with head, T1 skin, sternum skin and acromion skin markers attached. 21

Figure 4: Steering wheel angular change in LBPT load cases with the volunteer in the driver seat (time scale adjustments pending – initiation of manoeuvre starts at -1 s). Females to the left and males to the right. 22

Figure 5: Belt pay-out and belt loads in LBSB load cases with the volunteers in the driver seat (time scale adjustments pending – initiation of manoeuvre starts at approximately -1 s). Females to the left and males to the right. 23

Figure 6: Mean and mean ± SD male passenger head rotations around x-axis (roll, upper row) and translations in y-direction (lateral excursion, lower row) for LSB (left) and USB40 (right). 24

Figure 7: Mean and mean ± SD male passenger T1 rotations around x-axis (roll) for LSB (left) and USB40 (right). 24

Figure 8: PRECOONI and OM4IS seat model 27

Figure 9: Model schematic 27

Figure 10: Comparison of passive 1D-elements (blue) and 1D-elements (red) belonging to the muscle model for THUMS Version 4.02 (left), Version 5.03 (middle) and Version 6.02 (right) 28

Figure 11: Volunteer tests P03T02 and P03T03 compared to various THUMS models (passive and reactive) at time 0.8 s 30

Figure 12: Forward head excursion over time of positioned HBM models compared to volunteer results (P03T02: hand sliding comparable to simulations, P03T03: hands not sliding) 31

Figure 13: Schematic structures of Hill-type muscle models: a) Structure of LS-DYNA *MAT_MUSCLE; b) Structure of EHTM 32

Figure 14: A-THUMS-D Arm Model with FE Muscles (red) 33

Figure 15: Overlay of A-THUMS-D Arm model kinematics with test data from Kistemaker *et al.* [13] 34

Figure 16: Stimulation signal recorded in primary arm flexors 35

Figure 17: Concentric, Isometric and quick contraction experiments [6] [1] 37

Figure 18: Piglet VPS EHTM characterization (Units: mm, kg, ms) 37

Figure 19: Isometric contraction load case – stimulation curve for piglet and cat 38

Figure 20: Piglet – isometric contraction – VPS EHTM – muscle total force 39

Figure 21: Piglet – isometric contraction – VPS EHTM - muscle active state versus time 39

Figure 22: Piglet – concentric contraction – VPS EHTM - muscle velocity 40

Figure 23: Piglet – concentric contraction – VPS EHTM Hatze vs VPS HTM vs Guenther experiment 40

Figure 24: Piglet – Quick Release – VPS EHTM - Muscle total force vs velocity 41

Figure 25: Initial boundary conditions defined with the THUMS TUC-AHBM in a supine position 42

Figure 26: Vertical displacement of the centre of gravity of the THUMS TUC-VW AHBM head modelled with Hill-type and EHTM muscle models 43

Figure 27: Vertical displacement trajectories for simulations with the reflex muscle controller active 46

Figure 28: CORA quantitative rating for different load cases 46

Figure 29: A-THUMS-D F05 CNIS Arm model with muscles 48

Figure 30: Kinematics of A-THUMS-D Arm model with VHC and Baseline Hy-C 48

Figure 31: Vertical hand displacement (blue = left, red = right) in arm drop test. Top graph: before modification, bottom graph: after modifications 51

Figure 32: Change in impactor force between original AHM (green) and updated shoulder model (yellow) 52

Figure 33: Relative orientation of coordinate systems using Bryant angles 53

Figure 34: Concept for torque controller 54

Figure 35: Controller architecture 54

Figure 36: Longitudinal and lateral acceleration for combined (braking, steering) manoeuvre in OM4IS 55

Figure 37: ISO view of the surrogate model 55

Figure 38: Side view of the surrogate model (without seat) 55

Figure 39: Controller architecture for stabilization without pulse 57

Figure 40: Controller architecture for stabilization with pulse 57

Figure 41: Controller architecture for determination of time delay and controller parameters with direct and inverse surrogate model 58

Figure 42: Head angle of torque controlled THUMS v3 with OM4IS corridors for combined manoeuvre 58

Figure 43: VPS-SimulationX workflow 59

Figure 44: Visual systems-CosimVPS model-coupling components for muscle management 60

Figure 45: THUMS TUC-VW AHBM including 602 muscles 60

Figure 46: Updates of THUMS TUC-VW AHBM: a) curved muscle path with via-points and b) distributed load at the muscle insertion area of the bone [72] 61

Figure 47: Flowchart of the VPS-SimulationX coupling established for muscle feedback control in THUMS TUC-VW AHBM. q_0 is the muscle tone and ND – the neural delay 62

Figure 48: Reduction of the CPU time by increasing the sampling time between the software VPS and SimulationX using 64 CPUs 63

Figure 49: THUMS TUC-VW AHBM responses and volunteer corridors. Forward (top) and vertical (bottom) displacements under the OM4IS braking condition starting with a 50 km/h initial velocity. HT: highly tensed, MT: moderately tensed, LT: low tensed and R: relaxed 65

Figure 50: THUMS TUC-VW AHBM and volunteer corridor lateral excursion under the OM4IS lane change to the left (left) and right (right) condition 66

Figure 51: THUMS TUC-VW AHBM and volunteer corridor of the forward (left) and lateral excursions under (right) the OM4IS combined condition 67

Figure 52: THUMS TUC-VW AHBM and volunteer corridor of the forward excursion (left) under the Chalmers autobraking condition and lateral excursion (right) under the Chalmers lane change condition 67

Figure 53: Model and volunteer head rotational and linear kinematics from a 73 km/h lane change to the right [30]. 70

Figure 54: Model and volunteer head kinematics from a 73 km/h lane change to the right [30]. Comparing the baseline model (baseline) with a model with active muscle PCSA reduced by 19% (PCSA19) and a model with the peak isometric stress reduces by 30% (PIS30). 71

Figure 55: Time history curves of a) steering wheel force and b) brake pedal force for scenarios I to IV 74

Figure 56: A-THUMS-D F05 CNIS 75

Figure 57: Kinematics of A-THUMS-D in OM4IS phase 2 braking simulations 77

Figure 58: Kinematics of A-THUMS-D F05 CNIS in autobraking event as per Ólafsdóttir et al. [20] 78

Figure 59: Resultant displacement over time for a) COG of upper leg and b) COG of lower leg.... 80

Figure 60: On the left-hand side, the THUMS TUC-VW AHBM positioned in the vehicle interior on the passenger seat with the hands on the thighs. On the right-hand side, the pulse applied to the vehicle is shown. 81

Figure 61: Comparison of the centre of gravity of the head trajectories between the THUMS TUC-VW AHBM using two control strategies during the in-crash phase and a the THUMS TUC passive HBM..... 82

Figure 62: Lower limb kinematics in lane change manoeuvre 83

Figure 63: Development of lower limb dysfunction under 1 sec. constant lateral acceleration..... 83

Figure 64: The positions of the medially-rotating muscles in the AHM..... 84

Figure 65: Lower limb kinematics of the modified AHM in lane change manoeuvre 85

LIST OF TABLES

Table 1: A summary of datasets chosen by the WP3.2.1. subtask group for the validation of active HBMs to predict pre-crash responses. 13

Table 2: Manoeuvres carried out in the AHBM3 tests with the volunteer in the passenger seat. ... 20

Table 3: Manoeuvres carried out in the AHBM3 tests with the volunteer in the driver seat. 20

Table 4: Muscle Non-Specific Parameters for EHTM used in A-THUMS-D Arm [14]. 33

Table 5: Calculation time comparison between MAT_MUSCLE and EHTM used with Hy-C in LS-DYNA..... 35

Table 6: Computational cost using the two muscle material types, Hill-type and EHTM 44

Table 7: Maximal vertical displacements and CORA rating for different strain threshold values 46

Table 8: Calculation time Comparison Between VHC and Baseline Hy-C in LS-DYNA™ 48

Table 9: Simulation matrix used for the validation of the THUMS TUC-VW AHBM. X: performed simulation, -: data available, but simulation was not performed, n/a: data not available 64

Table 10: Elderly vs. young person active muscle architectural changes. Generally, in these studies, elderly persons were defined as individuals approximately 70-90 years of age, while young persons were defined as individuals approximately 20-40 years of age. 68

Table 11: Maximum Forces and corresponding time steps 75

1 EXECUTIVE SUMMARY

The OSCCAR project addresses occupant protection in vehicle crashes by the development of advanced virtual test tools and their use to design safe restraints when both the pre- and in-crash phases are included in the simulation. The pre-crash phase frequently includes some sort of avoidance manoeuvre, such as harsh vehicle braking or swift steering, which will alter the occupants´ postures and their risk of injury in the crash. Unprepared occupants have been shown to change posture more than those that are prepared. The number of avoidance manoeuvres are expected to increase as well as the proportion of unaware occupants in a car, and also the driver may be unprepared when these avoidance manoeuvres are carried out by a vehicle installed safety system.

Since avoidance manoeuvres include low level vehicle accelerations, in relation to in-crash accelerations, and can last for up to a few seconds muscle activity may significantly influence the occupant response in the pre-crash phase. While state-of-the-art crash test dummies, and the virtual models of these, are designed for studies of the in-crash phase, Human Body Models (HBMs) can, partly because they are models of humans, be fitted with active muscles to enable the prediction of humanlike responses in simulations of avoidance manoeuvres and other pre-crash events. These models, referred to as active HBMs, were at the start of the project capable of reproducing the human response in braking events but additional research and developments are required before these models can predict the responses in all types of avoidance manoeuvres or all pre-crash events.

To further develop the active HBMs several tasks were carried out within the OSCCAR project and reported here. Firstly, original volunteer test data, that is required for the development and validation of these active HBMs, were reviewed and extensively analysed. Secondly, models of the original test setups and knowledge that guides the use the original data were generated. Thirdly, muscle models, kinematic control systems, and muscle control systems for these active HBMs were enhanced. These models and controllers were made code independent in the work towards harmonized use of active HBMs. Finally, HBMs fitted with these new muscle models and/or muscle or joint torque controllers, were optimized and validated. The updated models were made available for their use in OSCCAR WP4 and WP5 and to some extent in WP2.

Keywords: volunteer test data, validation data, muscle models, muscle controllers, joint torque controllers, Active Human Body Models (HBMs), pre-crash modelling

2 OBJECTIVES

The main objectives of the work reported in this deliverable were three:

To provide biomechanical data that facilitated the development of active HBMs with responses similar to real life occupants in existing and future occupant positions in pre-crash situations. This objective was reached via an extensive review and analysis of past volunteer test data. In addition, a study was carried out, exploring the influence of boundary conditions on occupant kinematics to guide future volunteers test series and use of volunteer data in pre-crash situations. Finally, data that can be used in the development of mathematical models of the loading environments used in the past volunteer tests was analysed and made available.

To develop muscle models, kinematic control systems, and muscle control systems for active HBMs. These controllers should preferably be capable of modelling occupant reflex response from vehicle kinematics, voluntary occupant response (such as actively braking and steering), purposeful movement generation, and reflex response from awareness of a possible crash. In addition, these models and controllers should preferably be code independent. To develop muscle models and control systems for active HBMs intended for pre-crash situations that are representative of the entire population at risk.

To develop and validate omnidirectional HBMs for prediction of active and reactive human responses in pre-crash scenarios. To reach this objective, muscle models or controllers were implemented in several HBMs, the controllers were optimized, and the HBMs were validated.

3 DESCRIPTION OF WORK

3.1 Volunteer data for the development of active and reactive HBMs

3.1.1 Review of data for the development of active and reactive HBMs

Pre-crash responses due to bracing, steering, braking etc. may alter occupant position relative to safety systems and change injury risk if there is a crash. An important tool to assess these risks is HBMs with some form of muscle control system which often are referred to as active HBMs (AHBM). For the development and advance of these models, validation and tuning data are necessary. The purpose of this review was to collect information and data from experiments that have measured volunteer kinematic and muscle activity responses to simulated or actual pre-crash events and assess their applicability as validation data for HBMs with muscle control systems.

3.1.1.1 Methods of literature review

The focus of the review was to assess the suitability of the datasets to being used for validation/tuning of HBMs. Mostly datasets that have been published were included in this review, and partner organizations have suggested reports with additional unpublished data.

Publications were added to this review if they met two criteria: 1) experiments on human volunteers and 2) the volunteer's response to pre-crash scenarios was elicited by exposure to appropriate accelerations (<1.5 g). For this review only pre-crash events that included occupant bracing, vehicle or sled braking, vehicle or sled lane change, vehicle or sled cornering or any combination of these were included. The publications were found by searching "pre-crash volunteer" and "pre-impact volunteer" in google scholar. In addition, the references of publications found were checked for further publications that should be included.

The datasets found were reviewed by the WP3.2.1 subtask group in a series of meetings. The WP3.2.1. subtask group targeted three loading conditions: lane-change, braking, and a combination of these. A target was set to have at least one dataset for each case in a laboratory environment, to have more precise boundary conditions, and in-vehicle environment, to mimic real-world conditions more closely. Specifically, the datasets were reviewed for their applicability in validation/tuning of HBMs. The loading conditions were considered reproducible if time histories of all the relevant sled or vehicle dynamics were available. Boundary conditions were considered reproducible if enough information about the geometry of the seat, the type of restraints, and occupant initial position etc. had been made available. Electromyographic (EMG) recordings of muscle activity data that were normalized by maximum voluntary isometric contracts (MVIC) were considered suitable for validation or tuning. This is because in the Hill muscle model activation scales the maximum muscle force, and EMG data normalized by MVIC is interpretable in this context.

3.1.1.2 Results

A total of 25 datasets were identified that involved applying accelerations that mimic pre-crash events to human volunteers. Most of these were from published sources and three additional ones came from unpublished data. The subtask group choose five datasets to be shared with the OSCCAR partners (Table 1). See Appendix A for a summary of all 25 datasets reviewed. Biomechanical data for the development of active and reactive HBMs

Vehicle/sled manoeuvre	Laboratory Environment	In-vehicle Environment
Braking	Precooni	AHBM 2 and OM4IS2
Lane-change	TNO - Robot lane-change	AHBM3 and OM4IS2
Braking and lane-change	n/a	AHBM3 and OM4IS2

Table 1: A summary of datasets chosen by the WP3.2.1. subtask group for the validation of active HBMs to predict pre-crash responses.

3.1.2 OM4IS2 volunteer data

A rough overview of the OM4IS2 test series and the available data is given in this chapter. The complete report can be found in this document in the Appendix B. Additional details can be found in the original publications by Huber et al. (2013) [1], Huber et al. (2014) [2], Huber et al. (2015) [3] and Kirschbichler et al (2014) [4].

3.1.2.1 Vehicle and manoeuvres

- Series production car
- Following manoeuvres were performed
  - Emergency braking manoeuvres at 12 km/h and 50 km/h,
  - Single lane change manoeuvres to the left and right side at 50 km/h and
  - Combined braking and steering manoeuvres also at 50 km/h were performed.
- For the braking as well as the combined manoeuvres acceleration level was set to the peak value which could be reached (~ 1g).

3.1.2.2 Volunteers

The focus of the movement studies was on the kinematics of 50th percentile subjects. 27 male and 6 female subjects were measured.

Three awareness states were investigated.

In total 33 subjects - six female (mass: 63.0 ± 10.4 kg, height: 169.0 ± 4.1 cm, age: 31.5 ± 9.3 y) and twenty-seven male (mass: 77.8 ± 8.4 kg, height: 179.1 ± 4.7 cm, age: 25.4 ± 9.6 y) subjects were tested in this series in various tests.

3.1.2.3 Measurements

- Kinematic detection with a Vicon V612 motion capturing system with eight near infra-red cameras (Head and Thorax)
- Vehicle states: (Acceleration in x- and y-direction, steering wheel angle, angular velocity, and brake status)
- Belt forces (Shoulder, Buckle)
- Muscle activity with EMG for 5 subjects

3.1.2.4 Data

Test data for the OM4IS load cases are published under https://doi.org/10.5281/zenodo.5747370

3.1.3 PRECOONI volunteer data

An overview of the PRECOONI test series and the available data is given in this chapter. The complete report can be found in this document in the Appendix B.

3.1.3.1 Sled and manoeuvres

A modified serial seat, the OM4IS2 seat with new foam material, was positioned in the driving direction on a sled. The sled was accelerated from static to a predefined velocity and decelerated at 0.5 g maximum.

3.1.3.2 Volunteers

Six subjects, close to the 50th percentile male anthropometry, were tested: with average age, stature and weight of 30.5 years,174.5 cm, and 75.2 kg, respectively.

Detailed seated anthropometrics were measured.

The volunteers were belted and exposed to distractions.

As the behaviour of the volunteers was very different, it was decided to use the individual test results instead of corridors, which could be misleading. The three test cases include one volunteer with activated neck muscles already at the beginning of the tests and two with no activation at t0, one with the highest head displacement and one with medium head displacement compared to the other non pretensed volunteers and trials.

3.1.3.3 Measurements

- 3D kinematic were reconstructed for head, shoulder, elbow, wrist, knee and ankle
- Belt forces (shoulder and buckle)
- Force between seat and platform
- Force on footrest
- Pressure on seat surface
- Muscle activity with MVC normalised EMG

3.1.3.4 Data

Test data for the three selected load cases are published under https://doi.org/10.5281/zenodo.5747369

3.1.4 TNO volunteer data

An overview of the TNO volunteer tests and the available data is given in this chapter. The objective of the TNO tests was to quantify kinematic behaviour and muscle activation in simulated steering tests in several realistic conditions. A complete report can be found in this document in the Appendix B.

3.1.4.1 Car and manoeuvres

Volunteers sat in a custom designed remote-controlled test sled/vehicle with hands on a non-functional steering wheel and feet on a footplate. A rigid rally sport type seat was used.

A four-point harness with inertial reel on the shoulder straps was mounted as well.

The volunteers underwent purely lateral manoeuvres at 5 m/s^2 deceleration or simulated lane change manoeuvres at 5 m/s^2 peak acceleration and peak yaw velocity of 25°/s. Both left and right direction test were undertaken.

3.1.4.2 Volunteers

Ten males participated with average (SD) height of 1.77 (0.04) m, weight of 73.3 (4.5) kg, and age of 41 (9) years.

3.1.4.3 Measurements

Subjects were instrumented with photo markers that were tracked with 3D high-speed stereo cameras:

Left glenohumeral joint

Left elbow joint

Left and right wrist joint

Left knee joint.

Skin overlaying the spinous process of vertebra T1

Head

Bilateral surface EMG recorded activity of the sternocleidomastoid and longus capitis muscles for all subjects. Other muscle measured on some subjects included bilateral longissimus, obliquus externus abdominis, biceps femoris, and triceps brachii muscles.

EMG was normalized based on the largest activity recorded across trials for each muscle and subject.

3.1.4.4 Publications

Original publication for this work was were done by van Rooij et al. [5].

Test data for the selected load cases are published under: https://doi.org/10.5281/zenodo.5786677

3.1.5 AHBM2 data – Autonomous braking volunteer data

An overview of the tests and the available data from volunteer tests where the car was braked autonomously is given in this chapter. A more complete description of methods used, and data generated can be found in two publications and the Appendix B:

- Östh et al. [65].
- Ólafsdóttir [20].

3.1.5.1 Volunteers

In brief, this series of tests exposed 20 volunteers to full braking. There were 11 males, with average age of 32.7 years, height of 178.2 cm and weight 77.5 kg, and 9 females, with average age of 28.8 years, height of 166.6 cm and weight 59.4 kg.

3.1.5.2 Car and manoeuvres

The car was a standard 2012 Volvo V60 T4 with leather upholstery seats.

The vehicle's three-point seat belt retractor was replaced with an Autoliv supplied reversible pre-tension retractor. In reversible pre-tension trials, 170 N was applied to the belt 200 ms before autonomous braking. In standard seat belt trials, no pre-tension was applied, and the retractor locked at 0.45 g vehicle acceleration, or 1.5 g belt pull-out acceleration.

Occupants in the passenger seat were exposed to autonomous braking with either a reversible pre-tensioner or regular seat belt. Occupants in the driver seat were exposed to the same braking events with same seat belt systems but with the additional load case of manual braking with a standard belt. In these experiments a reversible pre-tensioner seat belt is one that tensions the seatbelt before an aggressive braking manoeuvre.

The braking peaked at 1.1 g and was started from an initial car speed of 70 km/h; the speed change was 50 km/h. These autonomous braking events were triggered by a researcher in the back seat without any warning to the occupant.

Volunteers adjusted the car seat for a comfortable fit (fore-aft, seat back angle, steering wheel position and angle). The seat cushion was at its lowest angle and adjustments of height and angle were not permitted.

3.1.5.3 Measurements

During these experiments the occupant's kinematics were measured with markers tracked by cameras, kinetics was measured with pedal, belt, and steering wheel loadcells, and muscle activity was recorded in 8 bilateral muscles in the neck, torso, and upper extremities. Muscle activity was normalized to maximum voluntary isometric contractions.

3.1.5.4 Data

Electronic data from the original Autobrake test series with volunteers were shared with OSCCAR partners. For this reason, the dataset was repackaged, a mathematical model of the seat and restraints were developed, and reports were developed to aid in the use of this data and model for validating HBMs. The data and the full report may not be shared outside of OSCCAR. However, some of the diagrams of the original publications have been digitized and the data have been made available for the public. Also, the mathematical model of the seat and restraints have been made available for the public.

Please see Appendix B for further details about how this dataset was collected and how it can be used to validate active HBMs during pre-crash events.

Some of the published data has been digitized and is available: https://doi.org/10.5281/zenodo.5774088

3.1.6 AHBM3 – Autonomous lane-change volunteer data

This dataset is from a 2016 series of human volunteer tests in which volunteers were exposed to autonomous manoeuvres when driving in 73 km/h at an airfield. An overview of the tests and the available data from volunteer tests where the car autonomously caried out a lane-change and lane-change with braking is given in this chapter. A more complete description of methods used, and data generated can be found in the following two publications:

- Ghaffari et al. [30].
- Ghaffari et al. [63].

3.1.6.1 Car and manoeuvres

The car was a standard 2016 Volvo V60 with leather upholstery seats.

The lane-change and lane-change with braking manoeuvres were carried out by a steering and braking robot. All manoeuvres reported here were initiated when the car speed was 73 km/h. A lane change produced a maximum lateral acceleration of 5.8 m/s^2, while a lane change with braking manoeuvre produced a maximum lateral acceleration of 5 m/s^2 and a longitudinal acceleration of -5.6 m/s^2

All tests were repeated three times for each condition and with a reversible pre-tensioner or a standard seatbelt. The latter applied a 170 N belt force; the belt was activated approximately 200 ms before autonomous manoeuvre started.

3.1.6.2 Volunteers

Nine males were passengers in the test vehicle during these manoeuvres and analysed.

3.1.6.3 Measurements

Vehicle kinematics were measured with a roof mounted Inertial Measurement Unit (IMU) and Global Positioning System (GPS); data analysis provided the acceleration of the vehicle at the approximate the H-point location of the volunteers in the midline of the vehicle.

Participant head, torso, and shoulder kinematics were measured with videos cameras that tracked white spheres affixed to anatomical landmarks.

Shoulder belt, lap belt, and footwell forces were measured along with shoulder belt pay-out. Muscle activity was measured with surface EMG on 38 muscles in the neck, upper extremities, the torso, and lower extremities. Muscle activity was scaled to maximum voluntary contractions.

3.1.6.4 Data

Electronic data from the lane change and lane change with braking test series with volunteers were shared with OSCCAR partners. For this reason, the dataset was repackaged, a mathematical model of the seat and restraints were developed, and reports were developed to aid in the use of this data and model for validating HBMs. The data and the full report may not be shared outside of the OSCCAR project. However, some of the diagrams of the original publications have been digitized and the data have been made available for the public along with the mathematical model of the seat and restraints have been made available for the public.

Please see Appendix B for further details about how this dataset was collected and how it can be used to validate active HBMs during pre-crash events.

Some of the published data has been digitized and is available: https://doi.org/10.5281/zenodo.5784240

3.1.7 Female response in AHBM3 volunteer tests

3.1.7.1 Introduction

The tests with volunteers carried out within the AHBM3 project in 2016 included also female volunteers. In this study lane change to the right and lane change to the right with braking have been analysed. These tests were carried out either with a standard belt or a reversible pre-tension belt. An overview of the study is presented below while a more complete description of methods used, the results obtained, and conclusions drawn are to be found in:

Ghaffari and Davidsson [64]

3.1.7.1.1 Objective

The primary aim of this works was to study female occupant kinematics and muscle activations in vehicle manoeuvres potentially occurring in pre-crash situations and with different seat belt configurations. Another aim was to provide validation data for active HBMs of female occupants in these manoeuvres.

3.1.7.1.2 Methods

Nine front-seat female passengers wearing a standard or reversible pre-tensioning three-point seat belt were subjected to multiple autonomously-carried-out lane change and lane change with braking manoeuvres while traveling at 73 km/h. Head centre of gravity and T1 vertebra body linear and rotational displacements were quantified. This study also includes surface electromyography (EMG) data collected from 38 muscles in the neck, torso, upper and lower extremities. All EMG data was normalized by maximum voluntary contraction (MVC). The raw EMG data were filtered, rectified and smoothed.

For statistical analysis of the analysed data, separate Wilcoxon signed ranks tests were performed on EMG onset and amplitude as well as peak displacements of Head and T1 considering two paired samples with the belt configuration as an independent variable.

3.1.7.1.3 Results

Significantly ($p<0.05$) smaller lateral and forward displacements for Head and T1 were found with the reversible pre-tensioning belt versus the standard belt. Averaged muscle activity in the neck and lumbar extensor and abdominal muscles increased up to 16% MVC immediately after the vehicle accelerated in lateral direction. Muscles in the right and left side of the body displayed differences in activation time and amplitude relative to the vehicle's lateral motion.

For specific muscles, lane changes with the pre-pretensioner belt resulted in earlier muscle activation onsets and significantly ($p<0.05$) smaller activation amplitudes compared to the standard belt.

3.1.7.1.4 Conclusions

The presented results from female passengers complement the previously published results from male passengers subjected to the same loading scenarios. The data provided in this paper can be used for validation of AHBMs of female occupants in both sagittal and lateral loading scenarios potentially occurring prior to a crash. Additionally, our results show that pre-pretensioner belt decreases muscle activation onset and amplitude as well as forward and lateral displacements of Head and T1 compared to standard belt confirming previously published results.

3.1.8 Data analysis of volunteer tests in the driver and passenger seat

3.1.8.1 Introduction

The volunteer test series carried out within the AHBM3 project in 2016 included other combinations of seating positions and vehicle kinematics than those published and reported in 3.1.6. For front row passengers these were U-turns and braking with regular belt fit and with predefined belt slack. In the U-turns, the volunteers were either aware or not aware of the upcoming turn. For drivers these were lane change to the left, lane change to the left with braking, braking and manual lane change to the left. Most of these tests were carried out with either a standard belt or a reversible pre-tension belt. These tests were analysed within the OSCCAR project with the ambition to make data for tuning/validation of active HBMs readily available. Some of these test conditions were far more time consuming than originally planned and publications are pending. However, an overview of the tests and the available data from these volunteer tests is provided in this chapter. A more complete description of methods used, the data generated and any conclusions on the data analysis will be found in near future publications.

3.1.8.1.1 Methods

The methods used in these volunteer tests were similar to these presented in 3.1.6 and were carried out following the protocol approved by the Ethical Review Board at the University of Göteborg, application 602-15. All volunteers gave their informed consent.

In brief, front-seat female and male passengers and drivers wearing a 3-point seat belt, with either standard or pre-pre-tensioning functionality, were subjected to multiple autonomously-carried-out manoeuvres. Passengers were exposed to lane changes to the right and lane changes to the right with braking (previously published in [30], [63] and [64]) braking to full stop without any belt slack or with a predefined belt slack. The braking was carried out at a vehicle speed of 73 km/h to full stop with a deceleration of 9.4 m/s^2. Passengers were also exposed to U-turns at 40 and 30 km/h with a vehicle lateral acceleration of 8.2 m/s^2 and 5.6 m/s^2, respectively. In the 40 km/h U-turns, the volunteers were either aware or not aware of the upcoming turn. Drivers were exposed to lane change to the left, lane change to the left with braking, braking and manual lane change to the left. All tests with the volunteer in the driver seat was carried out at or with an initial vehicle speed of 73 km/h. Please see Table 2 and Table 3 for details.

The analysis quantified vehicle and body kinematics, Head centre of gravity and T1 vertebra body linear and projected rotational displacements, and kinetics. In these analysis, surface electromyography (EMG) data and seat cushion data were not analysed. Data analysis was done in MATLAB v. R2020b. For each loading condition response corridors were established using mean and mean ± one SD for all available test data.

Manoeuvre	Belt condition	Initial veh speed (km/h)	Acronym
Lane change right	Std belt	73	LSB
Lane change right	Reversible pre-tension belt	73	LPT
Lane change right and braking	Std belt	73	LBSB
Lane change right and braking	Reversible pre-tension belt	73	LBPT
Braking	Reversible pre-tension belt	73	BPT
Braking	Std belt	73	BSB

Manoeuvre	Belt condition	Initial veh speed (km/h)	Acronym
Braking	Std belt- SLACK	73	BSBS
U turn	Std belt	40	USB40
U turn	Std belt	30	USB30
U turn	Pre-pre-tensioned belt	40	UPT40
U turn – aware of turn	Std belt	40	MUSB40

Table 2: Manoeuvres carried out in the AHBM3 tests with the volunteer in the passenger seat.

Manoeuvre	Belt condition	Initial veh speed (km/h)	Acronym
Lane change left	Std belt	73	LSB
Lane change left	Reversible pre-tension belt	73	LPT
Lane change left and braking	Std belt	73	LBSB
Lane change left and braking	Reversible pre-tension belt	73	LBPT
Braking	Reversible pre-tension belt	73	BPT
Braking	Std belt	73	BSB
Manual lane change left	Std belt	73	MLSB

Table 3: Manoeuvres carried out in the AHBM3 tests with the volunteer in the driver seat.

Volunteers were selected based on the following criteria:

- Inclusion criterion was that the volunteers did not have any history of neck pain, poor general health or other medical conditions that could cause an increased injury risk.
- Exclusion criteria were volunteers not in neutral posture (sitting still and looking forward) before the beginning of the manoeuvre. More specifically these criteria were head angle deviations >20 deg, head angular change >5 deg during the 0.5 s just before initiation of vehicle manoeuvre. Data was also excluded if none of the following were available; three complete video recordings per test, reference target video recording, vehicle kinematics and belt load and position data.

325 tests with 13 males and 318 tests with 9 females were included in the analysis of passenger data. 160 tests with 11 males and 111 tests with 8 females were included in the analysis of driver data.

Instrumentations - Film analysis of the video data from the front, side (Figure 2) and rear cameras was performed using TEMA Automotive version 3.5-17 (Image Systems, Linköping, Sweden). Note that in Figure 2 the pressure sensor mattress (Conformat Sensor 5330, version 7.60-30I, Tekscan, Inc., Boston, USA) were temporary on top of the dashboard, when testing this unit was mounted to the seat cushion. Note also that only one camera capturing videos from the side was mounted at the time; volunteers did not ride with a camera mounted to the nearside window. Linear and projected angular displacement of Head and upper torso (T1) were estimated from markers attached to the skin of the volunteer (Figure 3) using same methods as explained in Equation 3 and Equation 4 in Ghaffari et al. [30], respectively; except for upper torso (T1) linear displacements and rotation around y-axis which were estimated using the average coordinate of the markers attached to the skin nearby the T1 processes and upper region of the sternum. Upper torso (T1) rotation around the x- and z-axis were estimated from the markers attached to the skin nearby the T1 and the acromion closest

to the window of the car. All rotation angles were estimated using projection of angles on each plane made up of two axes. Figure 1 presents the coordinate system used in the AHBM3 volunteer study.

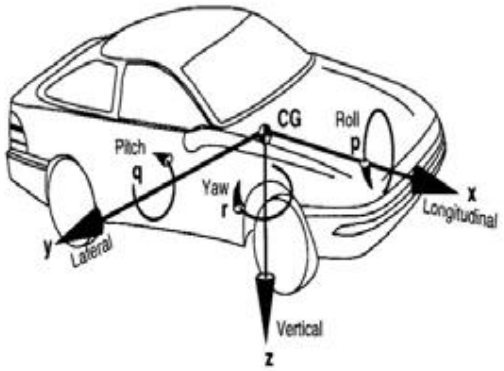

Figure 1: The coordinate system in the test vehicle.

Figure 2: Photos of the car interior used in the AHBM3 volunteer tests.

Figure 3: Photo of a volunteer with head, T1 skin, sternum skin and acromion skin markers attached.

3.1.8.1.2 Results and discussion

For LSB, LPT, LBSB and LBPT when the volunteer was the driver of the car the steering wheel data clearly shows that a few volunteers resisted steering wheel turning, which was carried out by a robot (Figure 4). To facilitate the construction of response corridors for proper lane-changes, an additional exclusion criterion was developed that required proper steering wheel turning (the wheel should reach a minimum of -45 degrees within 0.45 s from initiation of manoeuvre).

For each loading scenario, vehicle dynamics, shoulder- and lap-belt interaction forces, shoulder pay-in and pay-out and volunteer kinematics corridors were established using mean and mean ± one standard deviation (S.D.) with available volunteer data sets. These data will be published in scientific papers soon; below is a few of the results presented.

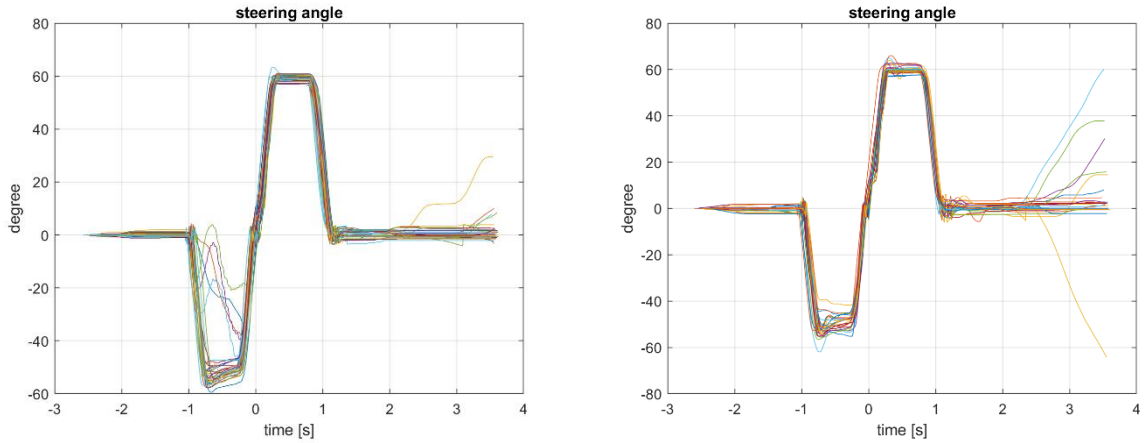

Figure 4: Steering wheel angular change in LBPT load cases with the volunteer in the driver seat (time scale adjustments pending – initiation of manoeuvre starts at -1 s). Females to the left and males to the right.

The belt pay-out and belt loads in tests with standard belt settings (Figure 5) were not very different between drivers and front seat passengers (see [63]and [30] for passenger data). The data suggest that drivers did not restrain themselves using the steering wheel. This is in contradiction to the results presented in [65] and [20] and leads to the speculation that volunteers in the AHBM3 volunteer study avoided restraining their forward and sideways motions using the steering wheel when the steering wheel was turned by the robot.

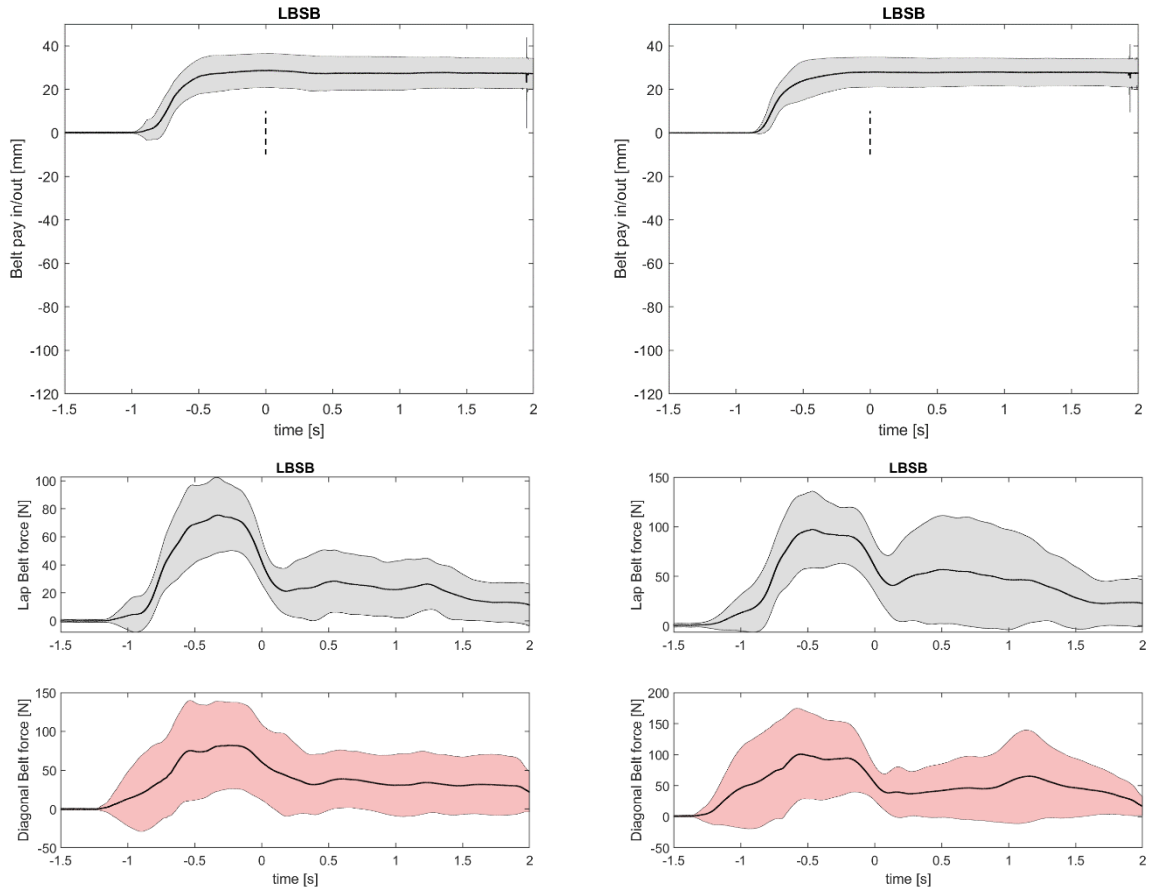

Figure 5: Belt pay-out and belt loads in LBSB load cases with the volunteers in the driver seat (time scale adjustments pending – initiation of manoeuvre starts at approximately -1 s). Females to the left and males to the right.

Smaller head excursions towards the left of the car and counter-clockwise head roll (negative values) were observed for male passengers when exposed to U-turns to the right with a vehicle speed of 40 km/h relative lane changes to the right at 73 km/h with the standard belt (Figure 6). These differences may not origin in differences in peak lateral vehicle accelerations; the lateral acceleration was somewhat higher in U-turns compared to lane-changes. However, it took longer time for the steering robot to reach the larger maximum steering wheel angles used in the U-turns than those used in the lane changes. This additional time may have allowed the volunteer to respond to the manoeuvre earlier in relation to peak sideways acceleration and by that limit the head excursions and head rolls. Also, the T1 excursions were smaller in the U-turns compared to the lane changes.

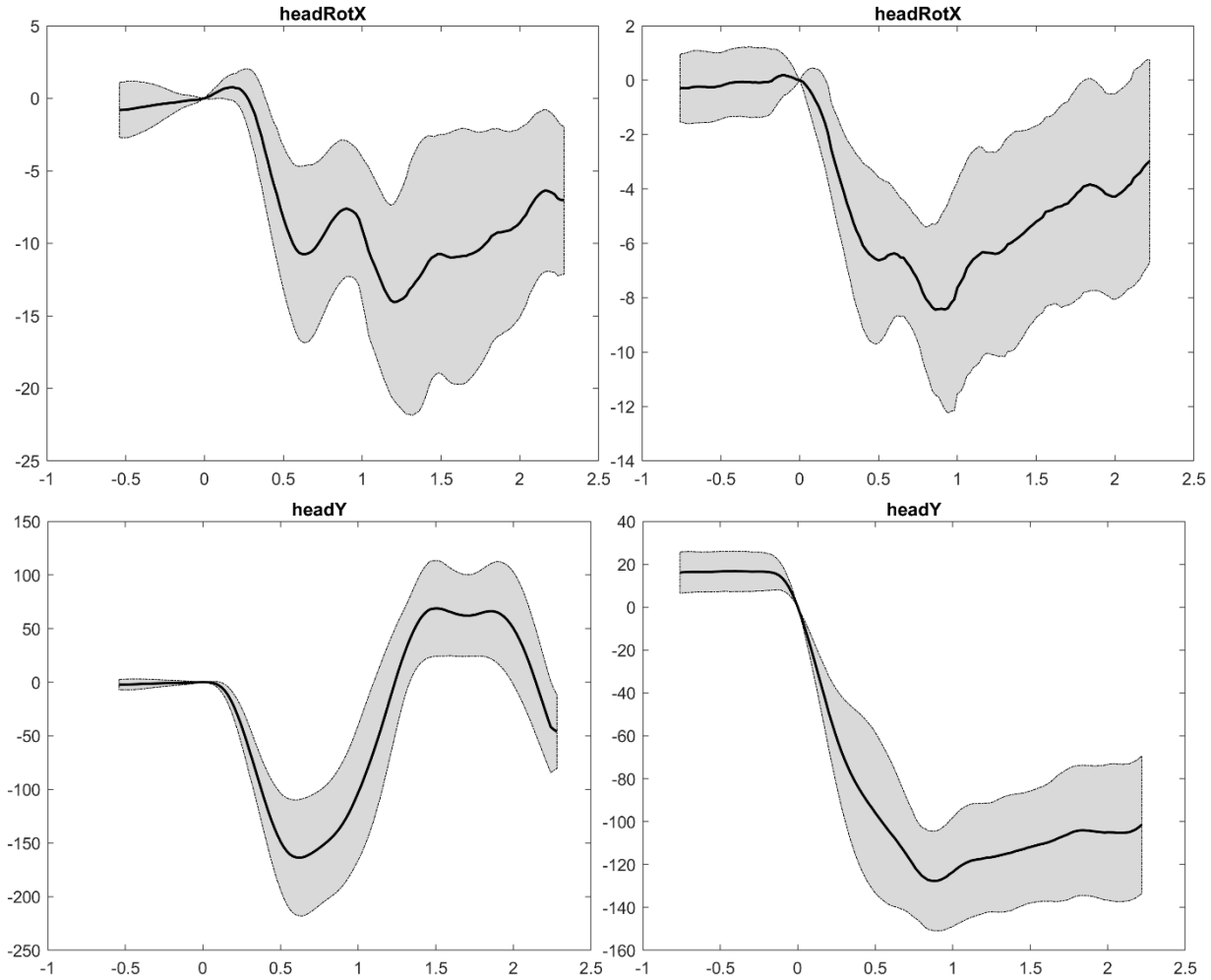

Figure 6: Mean and mean ± SD male passenger head rotations around x-axis (roll, upper row) and translations in y-direction (lateral excursion, lower row) for LSB (left) and USB40 (right).

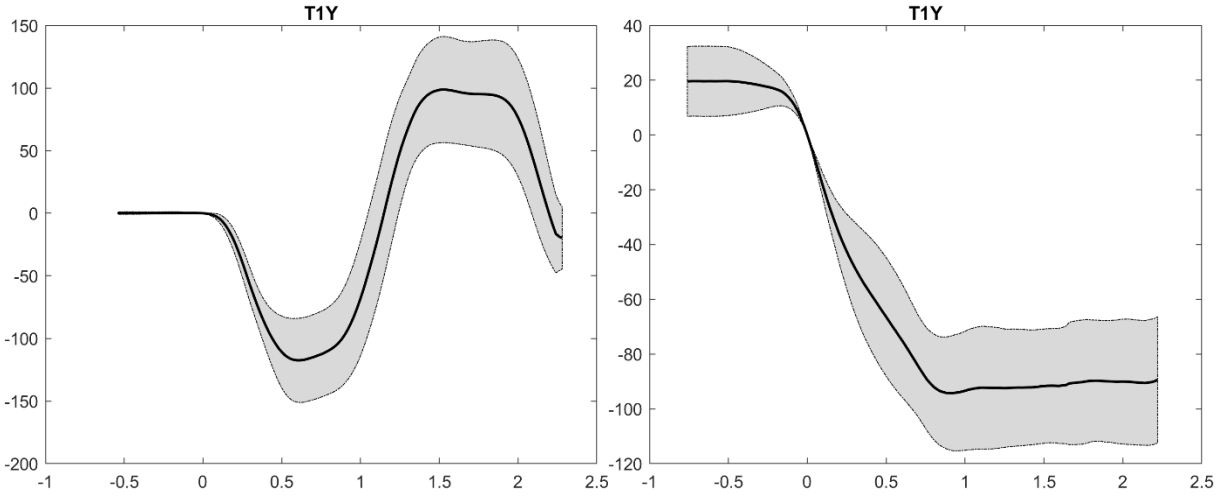

Figure 7: Mean and mean ± SD male passenger T1 rotations around x-axis (roll) for LSB (left) and USB40 (right).

3.1.8.1.3 Conclusions

The analysis of AHBM3 data provided data for female and male passengers and drivers subjected to a large range of loading scenarios will complement the previously published results from male and female passengers subjected to the lane change and lane change with braking. The data provided in the analysis can be used for validation of active HBMs of male and female occupants in both sagittal and lateral loading scenarios potentially occurring prior to a crash. While some of the data may seem to be redundant, some dataset can be used for tuning while others can be used for validation of these HBMs. Additionally, the new data show that pre-pretensioner belt decreases forward and sideways head excursions also in U-turns and braking load cases (as compared to lane change and lane change with braking).

The AHBM3 data analysed within the OSCCAR project took longer time then planed and publications are still being prepared for submission.

3.1.9 Response corridors for the development of active HBMs of all occupants

3.1.9.1 Introduction

Previous research indicates large variabilities among volunteer responses to evasive manoeuvres representative of pre-crash situations. Within the OSCCAR project a study was carried out to explore the influence of occupant characteristics (age, stature, and sex) on their body kinematics in evasive manoeuvres. The study also targeted the development of a statistical model that can be used to predict body kinematics of volunteers with any age, stature, and sex.

3.1.9.1.1 Methods

The dataset explored includes head and upper torso kinematics of 9 male and 9 female passengers exposed to multiple autonomous lane change manoeuvres. The data has previously been presented in [30] and [64]. The included volunteers' body mass indices were from 18 to 23 and were, hence, mostly within the normal range. Volunteer age and stature varied greatly from 23 to 71 years of age.

A Principal component analysis (PCA) was done on the selected time series of head and upper torso forward and lateral displacements. Based on the scores of the first three principal components (PCs) for the selected displacements and their maximums were then used in the development of a linear mixed model (LMM). This model was used to examine the effects of age, stature, and sex on body kinematics.

The variability between volunteers, was set as a random effect while age, stature and sex were fixed effect (treated as predictors). Two-way interactions of these predictors and the residuals, the variability within volunteers, were included in the models. A conditional and marginal R-square value recommended to be used with the LMM were estimated to indicate the proportion of the variance explained by the entire model including both fixed and random effects and the proportion of the variance explained by only the fixed effects.

3.1.9.1.2 Results

The first three PCs together explained around 94 - 98% of the variance in the studied volunteer responses. An analysis using the developed LMM provided that sex, stature and their interaction effects were statistically significant ($p < 0.05$) for the first PCs of the head and upper torso forward and lateral displacements as well as for the maximum lateral displacements. Age was not a significant effect.

Using the developed LMM enabled the researchers to developed corridors of head and upper torso displacements for specified sex and stature. These corridors will be provided for an average female, a 5th percentile female, an average male and a 95th percentile male in a paper (ready for submission).

3.1.9.1.3 Conclusions

Using PCA and LMM enabled the researchers to analyse the variances in kinematic responses of volunteers seated in the passenger seat of a regular car and exposed to lane change manoeuvres that can potentially occur in scenarios proceeding a car crash.

Several kinematic response corridors were modelled and will be provided in a paper. These can be used in evaluation of HBMs of different age, stature, and sex for the development of improved safety systems.

Working title and authors of the paper ready for submission: *The effect of age, stature, and sex on passenger kinematics in lane change manoeuvres.* By Ghazaleh Ghaffari, Johan Iraeus, and Johan Davidsson

3.2 Models for the use of volunteer data

3.2.1 Models of the loading environments used in the OM4IS2 and PRECOONI tests

The seat model represents the simplified serial seat, which has been used in the PRECOONI and OM4IS tests. Wooden plates were screwed on a serial seat and covered with foam and leather in the tests. The seat geometry was captured with a 3D Laserscan after the PRECOONI test series. The model was meshed by MBRDI. The foam was calibrated according to available test data of samples from the used foam.

To mimic the stiffness of the seat structure, generic springs were included. These were calibrated within the OSCCAR project by TU Graz based on test data, which was available from the APPROVE project. The seat model is shown in Figure 8. As a slightly different foam was used in PRECOONI compared to OM4IS, the model is modular, and a parameter is included to switch from one foam material to the other.

Details on the seat calibration and validation are shown in Appendix C. The seat model is publicly available on the openVT platform: https://openvt.eu/osccar/precrash_seat_models/precooni-om4is

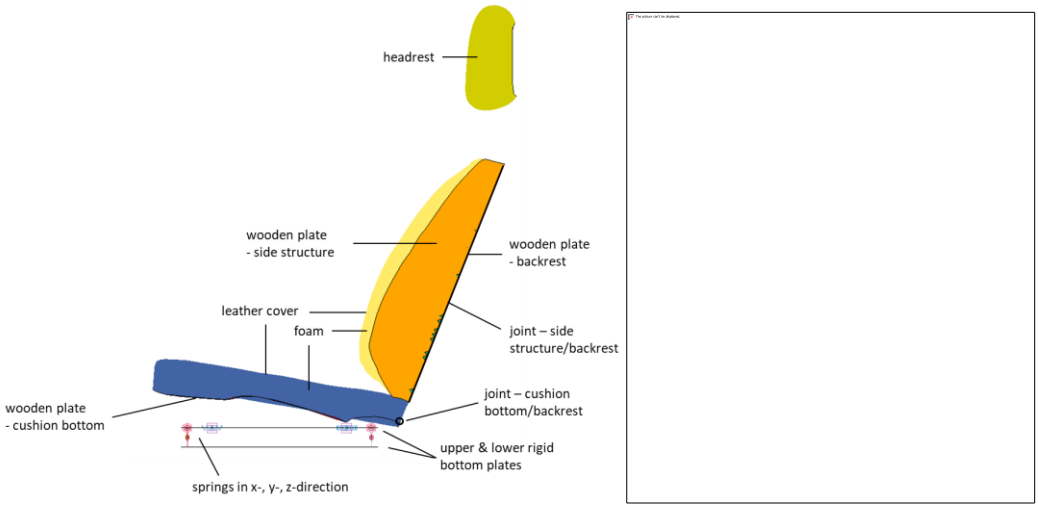

Figure 8: PRECOONI and OM4IS seat model

3.2.2 Models of the loading environments used in the TNO tests

A Simcenter Madymo model of the test set-up used in the TNO tests with volunteers were established and shared with OSCCAR partners for their use. The model is available on request from Siemens Industry Software Netherlands BV.

The model provides the dimensions of the test apparatus, a geometrical (rigid FE) mesh of the monocoque seat, (see Figure 9), and the seat belt characteristics.

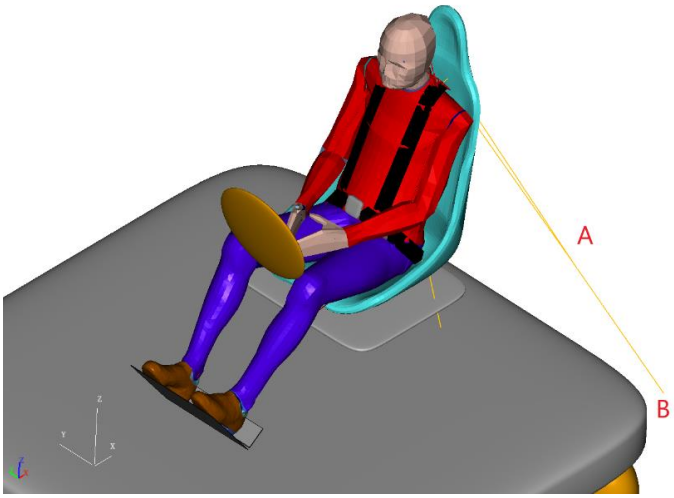

Figure 9: Model schematic

3.2.3 Models of the loading environments used in the AHBM2 and AHBM3 tests

As part of the goal of OSCCAR, to provide pre-crash validation data, it was decided that a seat model was an essential part of using the Chalmers validation data for active HBM development. A simplified seat model was developed that didn't utilize IP belonging to Volvo cars for this task. This simplified seat model was shared with the OSCCAR partners and made available for the public on the Virtual open VT platform at: https://openvt.eu/osccar/precrash_seat_models/safer-ahbm_2-3

The test vehicle used in the 2012 autobrake experiments was a 2012 Volvo V60 T4. In the 2016 lane change experiments, a 2016 Volvo V60 was utilized. Note that the simplified seat model is suitable for use with both experiments. Chalmers internal results have shown that the geometry and mechanical stiffness of these two experimental seats are very similar.

The geometry and construction of this simplified seat model were based on a generic seat model developed by Johan Iraeus (J. Iraeus, PhD Thesis, 2015) and this generic seat was morphed to match the surface geometry of a Volvo supplied V60 driver's seat model. The foam properties of the seat back and seat pan of the simplified model were tuned to match indentation testing performed on the physical Volvo V60 seat used in the Chalmers 2012 Autobrake test series. Further, the kinematics of the SAFER HBM v9 were compared for the simplified seat and the Volvo supplied seat model for a lane-change with braking load case from the 2016 Chalmers lane-change dataset. It was found that the HBM's kinematic responses were very similar for the two seat models, and thus it is believed the simplified seat model was well suited for HBM validation with the Chalmers test series that were included as part of the OSCCAR project (sections 4 & 5 below).

3.2.4 Boundary conditions - setting priorities for volunteer tests

3.2.4.1 Introduction

Although volunteer tests in production cars have the advantage that they are performed in a most realistic environment, they have some limitations when it comes to measuring possibilities. In some of the tests, information is lacking which are needed to reproduce them virtually, when calibrating or validating active HBMs. See Figure 10 for a comparison of 1D elements of a passive and two active HBMs. Furthermore, the detailed anthropometry of the individuals (e.g., arm length) usually differs from the HBM, but morphing an active HBM is not straightforward. Within this study, simplified laboratory tests have been used, where detailed information was available, and sensitivities have been analysed to identify the key influencing parameters affecting the HBM kinematics. The study should serve as a guideline how to best reproduce volunteer tests virtually with an active HBM and which kind of information is essential to be captured in future volunteer tests.

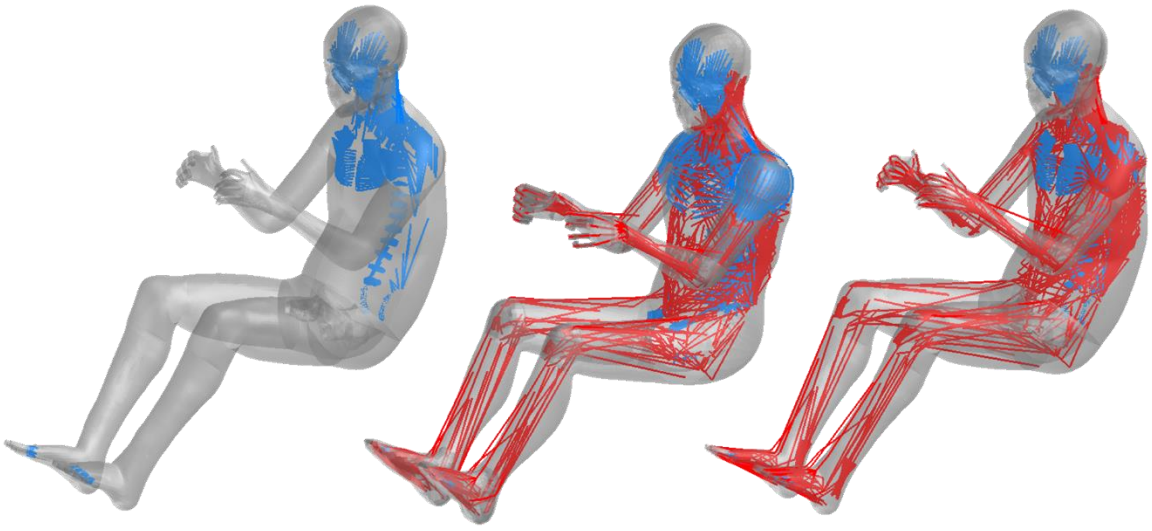

Figure 10: Comparison of passive 1D-elements (blue) and 1D-elements (red) belonging to the muscle model for THUMS Version 4.02 (left), Version 5.03 (middle) and Version 6.02 (right)

3.2.4.1.1 Methods

Volunteer sled tests with an acceleration of about 0.5 g in combination with a backward mounted automotive seat were carried out in the PRECOONI project. The arms of the volunteers were resting on their thighs, representing a co-driver or automated driving. In total, 19 tests with five male volunteers with an anthropometry close to 50th percentile were performed (mean weight 75 kg (SD 2.5 kg), mean height 174.5 cm (SD 2.8 cm)). Muscle activity, kinematics and interaction forces were measured during the tests. One exemplary test was selected as a baseline, because the volunteer was initially relaxed and showed a medium head excursion (compared to other tests and volunteers). The initial posture measured from the volunteer served as target posture for the subsequent HBM simulations. To get a comprehensive overview of the influence of the initial HBM posture, the HBM model was positioned to four additional postures (arms, legs separate and combined, spine). In a further step, different versions of the THUMS model (THUMS Version 4.02, THUMS Version 5.03, THUMS Version 6.02) were chosen in order to reconfirm observed trends with different model versions and also to compare the effect of using different models compared to the positioning effect. Figure 11 shows the response of two selected volunteer tests and the utilized THUMS models. The kinematics of Version 5.03 and 6.02 were analysed for both, passive and reactive (=originally relaxed) muscle state. The reactive THUMS models use a posture controller, which is calculating the muscle response depending to the posture change compared to the initial posture (Kato et al. [10]). Additionally, seat material (deformable/rigid), seat geometry, settling method, friction between HBM and seat and friction of the arms on the thighs was varied Evaluation focused on the head excursions (used for all simulations), additional hip and wrist displacement was compared among a subset of simulations (variation of seat and skin friction). Stress distribution on the seat after settling was plotted and compared to volunteer results.

P03T02

P03T03

THUMS V4 PASSIVE THUMS V5 PASSIVE THUMS V5 REACTIVE

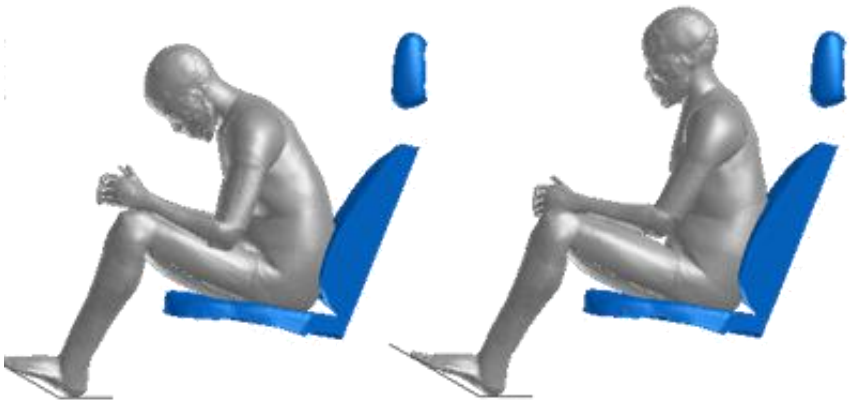

THUMS V6 PASSIVE THUMS V6 REACTIVE

Figure 11: Volunteer tests P03T02 and P03T03 compared to various THUMS models (passive and reactive) at time 0.8 s

3.2.4.1.2 Results

The results of the posture parameter study showed the importance of the loading path via the arms to support the torso. Especially for the relaxed HBM models, this circumstance had a major influence on the peak head excursion (relaxed HBM approx. -60%, passive HBM approx. -30% compared to original driver posture). It was also possible to reconfirm this trend within the volunteer test results (sliding of arms in things increased the head excursion). Different leg postures showed a smaller influence and no differences between active and passive models were observed. Also, here, the effect was confirmed within the volunteer tests, where the angle of the footrest was varied for one volunteer. The adjustment of the spine (4 degrees more upright sitting posture) showed only little effect on the head excursion with one exception, where the changed spine posture caused sliding of the hands on the thigs. This caused less torso support and therefore increased the head excursion significantly. Passive HBM models showed about double the head excursion than the model with initially relaxed muscle state. Asymmetries found in the seat geometry caused lateral movements of passive and relaxed HBM models. This effect was not present in the volunteer study. In general, observed head excursions of active HBM models were in the range of test data, as shown in Figure 12.

Furthermore, the results suggested that the modelling of a deformable seat with both, realistic geometry and realistic material properties is important as the mean peak head excursion increased drastically by switching to a rigid and flat seat.

Variation of the skin friction coefficient showed notable influence on the relative movement of the arms on the things and thus also on the peak head excursion of the head. For the full positioned THUMS Version 5 (relaxed) a reduction of 73% wrist excursion led to a 34% lower head excursion.

The results of the settling parameter study suggest gravity-based settling (0.2 s ramp) as the most suitable method for the investigated setup. Prescribed motion settling caused additional settling movement especially for the active HBM.

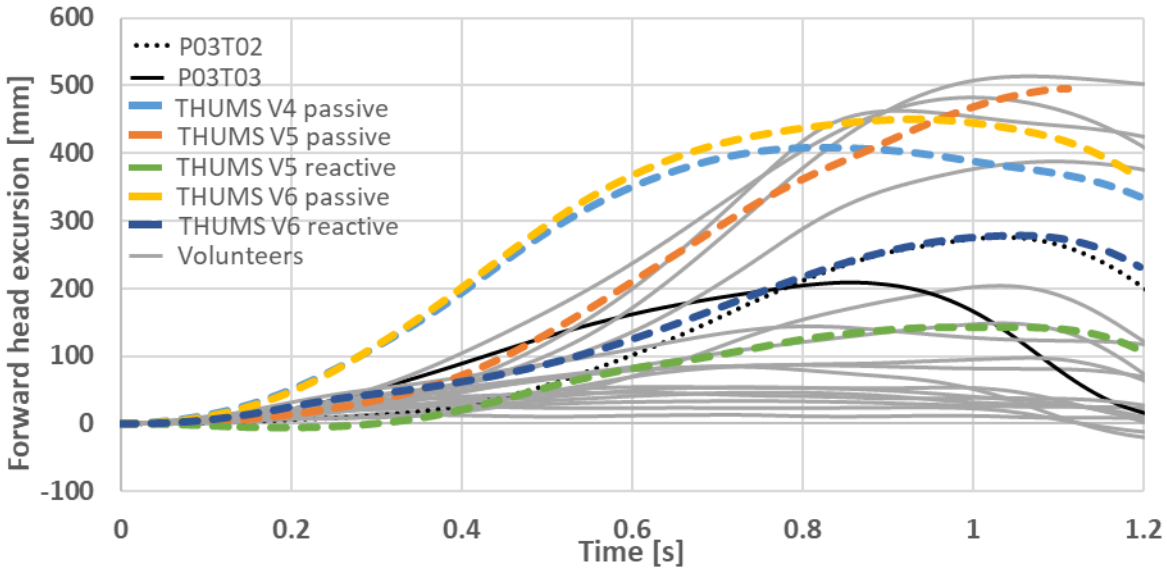

Figure 12: Forward head excursion over time of positioned HBM models compared to volunteer results (P03T02: hand sliding comparable to simulations, P03T03: hands not sliding)

3.2.4.1.3 Conclusion

In general, the results of the conducted HBM simulations showed a good correlation with the selected volunteer test. Activation of relaxed muscles reduced the peak head excursion by about half compared to a passive HBM, which resulted in excursions close to the selected volunteer. The results highlighted the importance of the arms-thigs loading path for torso support of active HBM models and presumably also for volunteers in respect to the peak head excursion. Whereas positioning of the legs seems to have less of an impact on head excursion and no notable differences between active and passive models were observed. Both, active and passive HBM models showed an excessive reaction to asymmetries of the seat leading to lateral tilting, which was not present in the volunteer study and therefore indicates, that the muscle modelling might need further improvement. Data from seat pressure mats fixed on the test seat was compared to stress distribution in the foam of simulation results. The contact area of the backrest showed differences between the applied THUMS models and when compared to the volunteer. The overall contact area in the simulations is smaller, which is probably caused by stiffer soft tissue model (increases the model stability) in the HBM models compared to a real person.

The results of this study showed, that for future volunteer tests the arm support of the torso should be more in focus, as it has been in the past. The relative posture of the wrists on the arms should be consistent between simulations and tests. If the wrists are sliding on the thigs in the simulations, but not in the tests, no meaningful comparison of the head excursion can be done. If the difference in anthropometry is causing this difference, the arm length and/or thigh length should be morphed. As some effects observed in the volunteer study, as well as in the simulations are not completely understood, future experimental data including different arm postures will be beneficial.

The importance of proper measurement of the initial posture was shown. Recommendations on volunteer tests derived from this study will be summarised in Deliverable 5.2.

3.3 Muscle models for active and reactive HBMs

3.3.1 Hill muscle model with serial damping and eccentric force-velocity relation

The extended Hill-type material (EHTM) is an improved version of the Hill-type muscle models which are typically used in biomechanical simulations. It was developed by Günther et al. [7] and Häufle et al. [41] and is characterised by a more realistic serial dampening behaviour and eccentric force-velocity relation than previous models. The EHTM is made up of four elements with the contractile element (CE) and the parallel elastic element (PEE) representing the muscle, a serial elastic element (SEE) and a serial dampening element (SDE) acting as the tendon of the muscle-tendon-unit (MTU). The EHTM therefore differs from the regular three element structure of Hill-type models such as the LS-DYNA-internal *MAT_MUSCLE where muscle and tendon form a single lumped unit (Figure 13). The EHTM was first implemented as a user-defined material into LS-DYNA by Kleinbach et al. [6] and was updated during the OSCCAR project to work for single and double precision versions of both symmetric multiprocessing and massively parallel processing executables of LS-DYNA. Its current state is documented in the work of Wochner et al. [12]. In addition to its more biophysiological behaviour, the LS-DYNA variant of EHTM also offers four biologically motivated internal low-level muscle control functions. These control functions consist of the open-loop alpha controller, the length-based closed-loop lambda controller, a hybrid controller which combines the alpha and lambda control approaches and a length-based reflex controller [12] and [17]. The use of these internal control functions can result in a significant speed up of AHBM simulations [42] while offering a more biofidelic kinematic behaviour compared to regular Hill-type muscles.

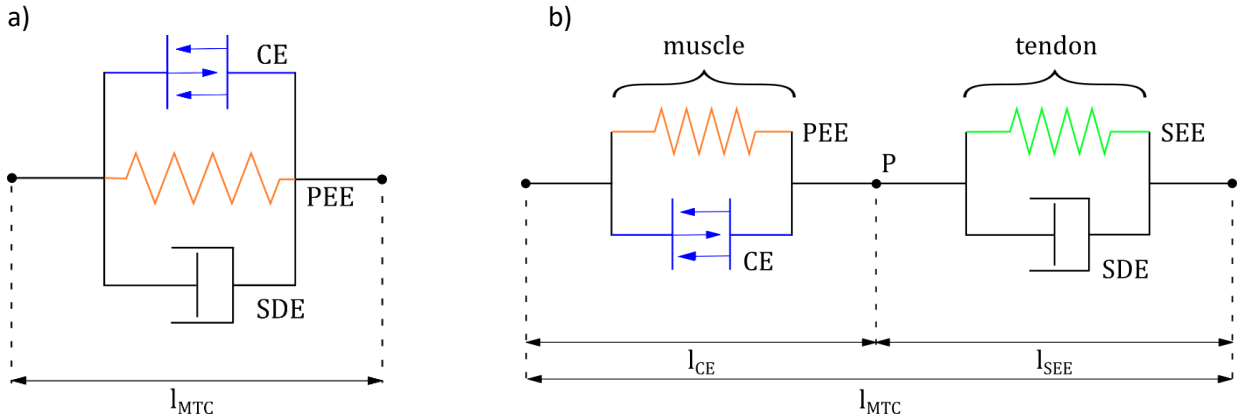

Figure 13: Schematic structures of Hill-type muscle models: a) Structure of LS-DYNA *MAT_MUSCLE; b) Structure of EHTM

The implementation of the EHTM to models in LS-DYNA and VPS is described in the following chapters.

3.3.2 Implementation of extended Hill-type material in LS-DYNA models

3.3.2.1 Methods

Extended Hill Type Muscle (EHTM) material [6] and [12] was added as *USER_DEFINED_MATERIAL_MODELS (MT = -41) in LS-Dyna and assigned to muscles in A-THUMS-D. A-THUMS-D is a 50th %ile male Active Human Body Model developed for pre-crash and related applications by Mercedes-Benz AG. The right arm from the A-THUMS-D model (Figure 14) was separated and constrained appropriately to replicate the same load case as Kistemaker *et al.* [13] in simulation environment. Eight muscle elements representing the muscles which actuate the elbow joint were implemented with EHTM and used in the simulations

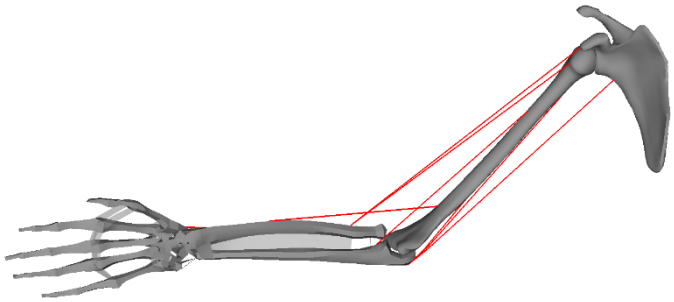

Figure 14: A-THUMS-D Arm Model with FE Muscles (red)

Numerous parameters are needed for EHTM for appropriate modelling of muscles in LS-DYNA^{TM} and these were derived by conducting a literature survey. Some parameters were considered common for all muscles and were referred to as muscle non-specific parameters and are listed in Table 4.

Hy-C	k_p	k_d	□	Neural Delay □□□□[ms]
	$1/l_{lopt}$	$10/l_{opt}$	Preset Value	25
Activation Dynamics [46]	q_{min}	c [mol/L]	□□[L/mol]	k
	0.005	1.37 e^{-4}	5.27 e^{4}	2.9

Table 4: Muscle Non-Specific Parameters for EHTM used in A-THUMS-D Arm [14].

Muscle specific parameters including peak force (F_{Max}) and tendon length (L_{SEE}) were derived for individual muscles from Peterson et al. [15] and Östh et al. [16].

The EMG data for volunteers given in Kistemaker *et al.* [13] was used as a basis to determine the target length (lambda, λ) input to the model for calculation of muscle stimulation by the Hybrid Equilibrium-Point Controller (Hy-C) [17] built into EHTM.

Elbow joint flexion from 45 deg to 145 deg as per volunteer test data [13], was replicated in the simulation environment. Muscle behaviour was monitored by tracking arm motion and muscle stimulation and resulting muscle activity.

The traditional muscle material in A-THUMS-D is LS-DYNA^{TM} MAT_MUSCLE. Hy-C was coded externally using LS-DYNA *DEFINE_FUNCTION keyword and was coupled with MAT_MUSCLE as reported by [17]. Since EHTM was introduced newly to A-THUMS-D muscles, a benchmarking study with traditional LS-DYNA^{TM} muscle modelling approach using MAT_MUSCLE was required. A-

THUMS-D arm featuring muscles modelled using LS-DYNA™ MAT_MUSCLE, coupled with Hy-C defined using *DEFINE_FUNCTION keyword for calculation of muscle stimulation (u) and activity (a), as described in [17], was used for this study. Benchmarking of new modelling approach (using EHTM) with previous modelling (done using MAT_MUSCLE+ External Hy-C) was done by comparing model kinematics and calculation time required, as one of the primary benefits of EHTM is fast calculation of muscle behaviour.

3.3.2.2 Results and discussion

A-THUMS-D arm kinematics, shown in Figure 15 were close to volunteer responses reported in Kistemaker et al. [13]. The peak angle achieved was smaller than the volunteer's due to the simplified elbow modelling which leads to early stacking up of bones at the completely flexed position. Stimulation (u) vales recorded in arm flexors during course of the simulation are reported in Figure 16. High stimulation (u) in the holding phase allows holding of the arm in completely flexed position.

Comparison between A-THUMS-D arm model with muscles modelled using EHTM and MAT_MUSCLE shows comparable kinematics in the motion phase as shown in Figure 15. The difference in the arm angle in the holding phase (after ~250 ms) is driven by difference in the nature of stacking up of bones at the completely flexed position in the A-THUMS-D arm. Since, the muscle driven motion is of primary importance in this study, the aforementioned modelling-induced effect, resulting in difference in the final arm angle, was neglected. A significant gain in calculation speed, however, was achieved with EHTM which shows 91.8% reduction in calculation time as compared to Hy-C coupled externally with MAT_MUSCLE as tabulated in Table 5 .

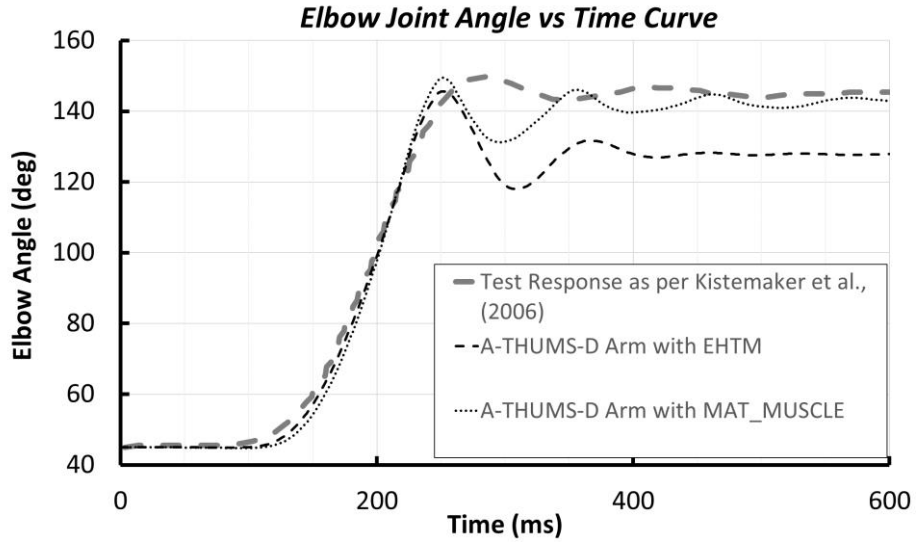

Figure 15: Overlay of A-THUMS-D Arm model kinematics with test data from Kistemaker *et al.* [13]

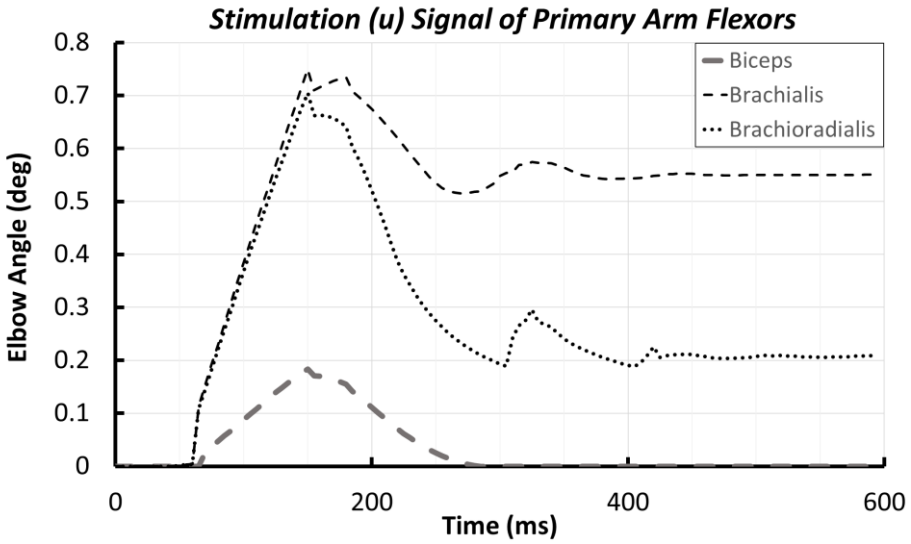

Figure 16: Stimulation signal recorded in primary arm flexors

Muscle Type	Calculation Time (s)
MAT_MUSCLE Coupled with Hy-C	7176
EHTM with Hy-C	585

Table 5: Calculation time comparison between MAT_MUSCLE and EHTM used with Hy-C in LS-DYNA

The results demonstrated a successful implementation of EHTM to A-THUMS-D arm muscles in LS-DYNA™ and form a basis for further implementation to entire musculature of A-THUMS-D comprising of 552 FE muscle strands representing major skeletal muscles in humans.

3.3.3 Implementation of extended Hill-type material model in VPS

Based on the implementation of Extended Hill-type muscle (EHTM) material model in LS-Dyna done by USTUTT reported in [6] and on corresponding code sources, an equivalent EHTM model has been developed in VPS, called 'VPS EHTM'-model.

In VPS, a standard Hill-type muscle material representing the muscle belly only, is available and called 'MATER type 240' hereafter. To ensure consistency with already available standard VPS MATER type 240, the same implementation architecture has been proposed.

VPS EHTM model implementation

VPS EHTM model consists of three sections: Part definition, EHTM material definition and Fascicle activation definition (see Figure A - 61 in appendix D).

Firstly, Part section specifies the type of the material as 'MUSCLE' and defines the geometrical parameters. As for MATER type 240, muscle, the main muscle geometrical parameters (physiological cross-sectional area, total mass, resting length) must be entered. The quantity $\mathrm{L0fib} = l_{PEE,0}$ is the muscle resting length of the fibre in VPS and LS-DYNA respectively.

$$l_{PEE,0} = \mathrm{L0fib} \tag{1}$$

where:

$l_{PEE,0}$ is the muscle fibre's resting length r in LS-Dyna

$\mathrm{L0fib}$ is the muscle fibre's resting length in VPS

The other muscle geometrical parameters (Alf, pennation angle of muscle fibre), which are not proposed in LS-DYNA EHTM material, are not available for VPS EHTM model.

Then, EHTM material section manages the muscle physical parameters and behaviours. For VPS EHTM model, a new muscle material has been developed called 'MATER type 241' hereafter. This material contains specific parameters as defined in LS-Dyna EHTM material implemented by USTUTT, except of $\mathcal{L}_{PEE,0}$ which is calculated from already defined parameter ALopt, as in MATER type 240, managing equivalence between LS-Dyna and VPS.

$$l_{PEE,0} = \mathcal{L}_{PEE,0} \cdot l_{CE,opt} \tag{2}$$

$$l_{CE,opt} = \mathrm{ALopt} \cdot \mathrm{L0fib} \tag{3}$$

$$\mathrm{ALopt} = \frac{1}{\mathcal{L}_{PEE,0}} \tag{4}$$

where:

$l_{PEE,0}$ is the muscle fibre's resting length in LS-DYNA

$l_{CE,opt}$ is the optimal muscle fibre length at which the isometric force reaches the maximum value

$\mathcal{L}_{PEE,0}$ is the muscle fibre's resting length normalized by $l_{CE,opt}$

$\mathrm{L0fib}$ is the muscle fibre's resting length in VPS

ALopt is the ratio of muscle fibre's resting length in VPS to determine muscle optimal length

A choice of four following damping models as implemented in LS-Dyna is proposed:

$$\mathrm{Damp} = \begin{cases} 0 : \text{No damping} \\ 1 : \text{Parallel damping} \\ 2 : \text{Serial damping} \\ 3 : \text{Serial force} - \text{dependent damping} \end{cases}$$

A filter based on a defined interval in number of cycles can be applied to smooth the muscle's lengthening/shortening elongation rate.

Finally, fascicle activation section contains the muscle activation parameters. For VPS ETHM model, three activation models are available. The first option is to manage muscle activation by a time-dependent activation level curve. The second option is to control muscle activation with a time-dependent stimulation curve, as proposed in Zajac dynamic activation model depending on the neural activation level. The third option is to define muscle activation depending on the neural activation level and on length-dependent sensitivity of Ca^{2+} level change, based on Hatze dynamic activation model.

3.3.3.1 VPS EHTM model validation

The validation of implemented VPS EHTM model has been performed with the same experimental load cases used for USTUTT EHTM implementation in LS-DYNA (see [6] and [7]). 3 load cases are proposed as illustrated in Figure 17: isometric contraction, concentric contraction, and quick release.

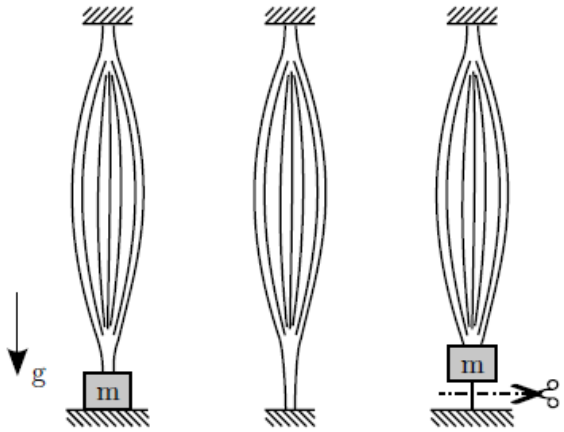

Figure 17: Concentric, Isometric and quick contraction experiments [6] [1]

- 3 animal muscles
  - Piglet
  - Cat
  - Rat

Tests results are available for muscles of piglet, cat and rat. In these past experiments, while rat and cat muscles have been tested in Isometric Contraction load case only, piglet muscles experiments results have been reported for the three load cases [7]. Hereafter the evaluation of VPS ETHM model for Piglet muscle under these three loadings is presented. For the Cat and Rat muscle, VPS EHTM model definition as well as their evaluation are provided in appendix D. In the comparison of the VPS ETHM with Piglet muscle data, the following VPS EHTM material type 241 definition, presented in Figure 18, were used.

```
$#          IDMAT    MATYP              RHO    ISINT     ISHG  ISTRAT    IFROZ
MATER /        11      241             1E-6        0        0
$# BLANK                                                    QVM             IDMPD
                                                             1.                 0
$      kN
NAME Muscle type 241 - piglet calf (Gunther)
$#  FMax            ALopt
0.03                 1.11
$                                                 in ms-1
$#          dWdes  nCEdes   dWasc  nCEasc    Arel0   Brel0     Secc     Fecc
             0.14      3.    0.57      4.      0.1   0.001       2.      1.8
$                                       mm                      kN
$#                    nPEE     FPEE   lSEE0 dUSEEnl  dUSEEl  dFSEE0
                       2.5       1.     45.  0.1825   0.073    0.06
$#          IDAMP SCALFSE DAMPFSE           NCYCLE
                3     0.3    0.01                1
```

```
$#        IDFASCI
FASCI /     10101
NAME Piglet Muscle Fascicle - Hatze model
$#    ACT     NACT NACTfac
        3     1101       0.
$# BLANK      ALF     PCSA     WMAS QUALIFY    L0fib
               0.       0.    0.08CONSTANT     13.5
$#             q0        c      ETA        k        m
          0.0050.000137  52700.      2.9     11.3
        PART       101
        END
```

```
$#        IDFASCI
FASCI /     10101
NAME Piglet Muscle Fascicle - Zajac model
$#    ACT     NACT NACTfac
        2     1101       0.
$# BLANK      ALF     PCSA     WMAS QUALIFY    L0fib
               0.       0.    0.08CONSTANT     13.5
$#             q0   PARAM1   PARAM2
          0.0001    0.025      0.5
        PART       101
        END
```

Figure 18: Piglet VPS EHTM characterization (Units: mm, kg, ms)

- Isometric Contraction load case:

Both muscle extremities were fixed. Simulation have been made for different initial muscle lengths expressed as ratio of muscle length (h), with a variation from 0.85 to 1.10. Figure 19 presents the stimulation curve used.

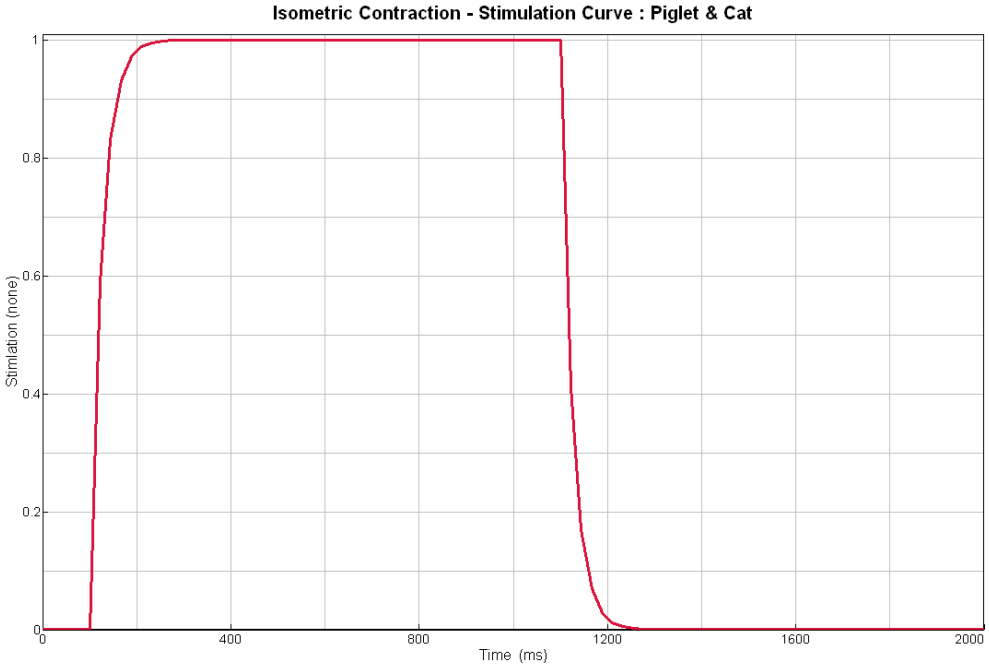

Figure 19: Isometric contraction load case – stimulation curve for piglet and cat

For each initial muscle length variant, the VPS EHTM model results, for Zajac and Hatze activation models, are compared to experimental results (see Figure 20).

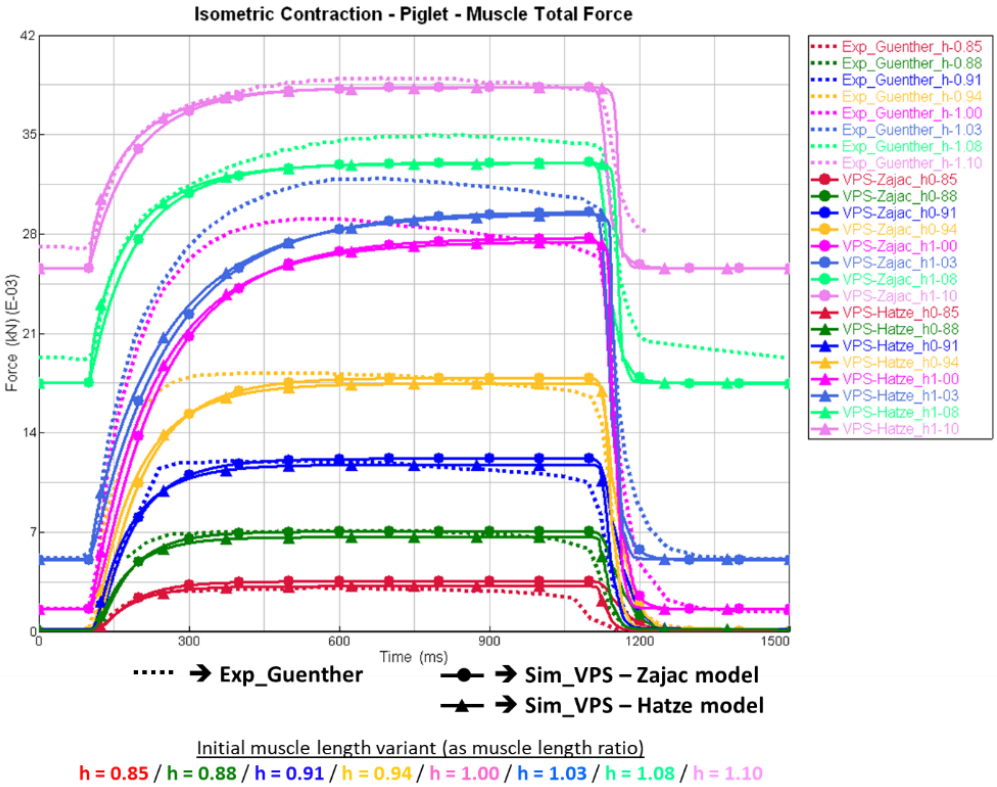

Figure 20: Piglet – isometric contraction – VPS EHTM – muscle total force

Both Activation models of VPS EHTM model present similar behaviour depending on muscle length variants. Equivalent qualitative results are observed for LS-DYNA EHTM model results and for VPS EHTM model in comparison to experiment measurements.

Concerning VPS EHTM model, the effect of the dynamic activation model choice, Zajac or Hatze, is shown on muscle active state versus time curve, as presented in Figure 21.

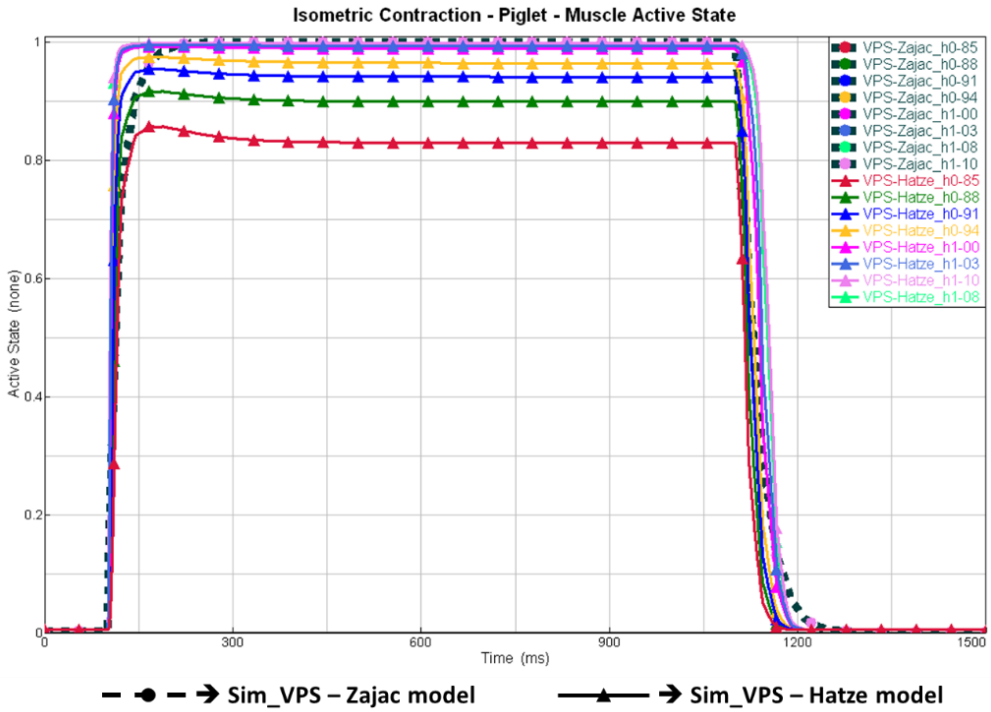

Figure 21: Piglet – isometric contraction – VPS EHTM - muscle active state versus time

As expected, while with Hatze activation model muscle active state evolves based on muscle length variants, Zajac activation model provides similar active state whatever muscle length is.

For both other load cases, VPS EHTM models using the Hatze and Zajac dynamic activation models are evaluated.

- Concentric Contraction load case:

The muscle initial length is defined at muscle length of 59.7 mm.

Muscle top end is fixed, while its bottom end is loaded with a mass which varies from 0.1 kg to 1.8 kg.

A full stimulation constant is used.

The behaviour of VPS EHTM muscle velocity is compared to experiment measurement (see Figure 22).

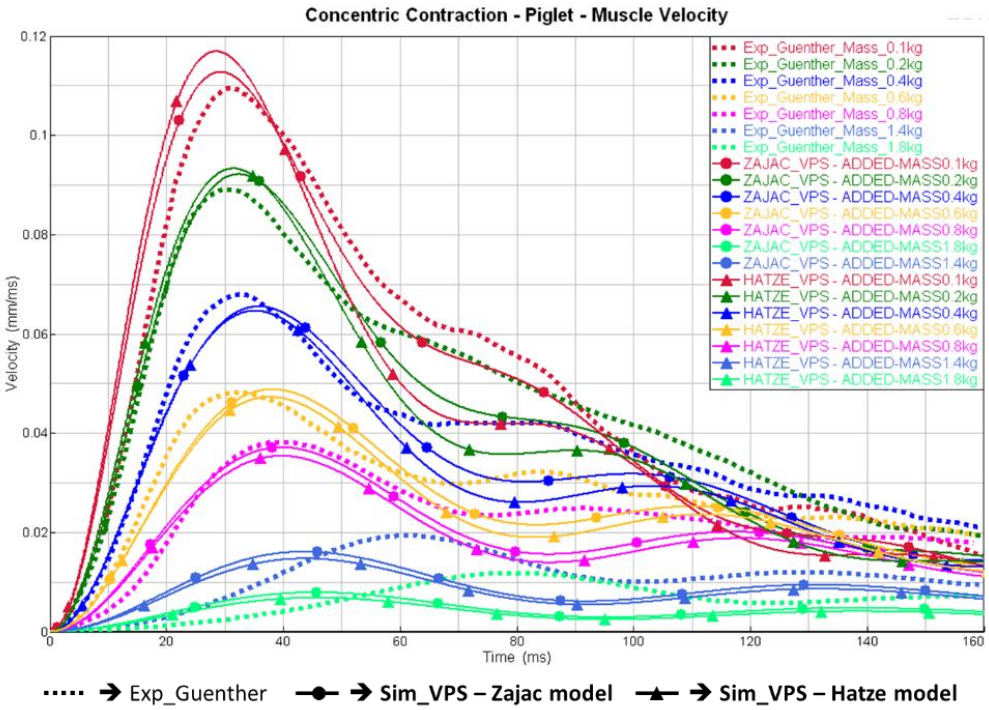

Figure 22: Piglet – concentric contraction – VPS EHTM - muscle velocity

For both dynamic activation models, Zajac and Hatze respectively, VPS EHTM model results were in agreement with experiments measurements. The effect of mass increase was similar between experiments and VPS simulation results.

This Concentric Contraction load case has been done with VPS HTM (MATER type 240) to illustrate the improvement of simulated behaviour with VPS EHTM (MATER type 241) with Hatze activation model, as presented in Figure 23.

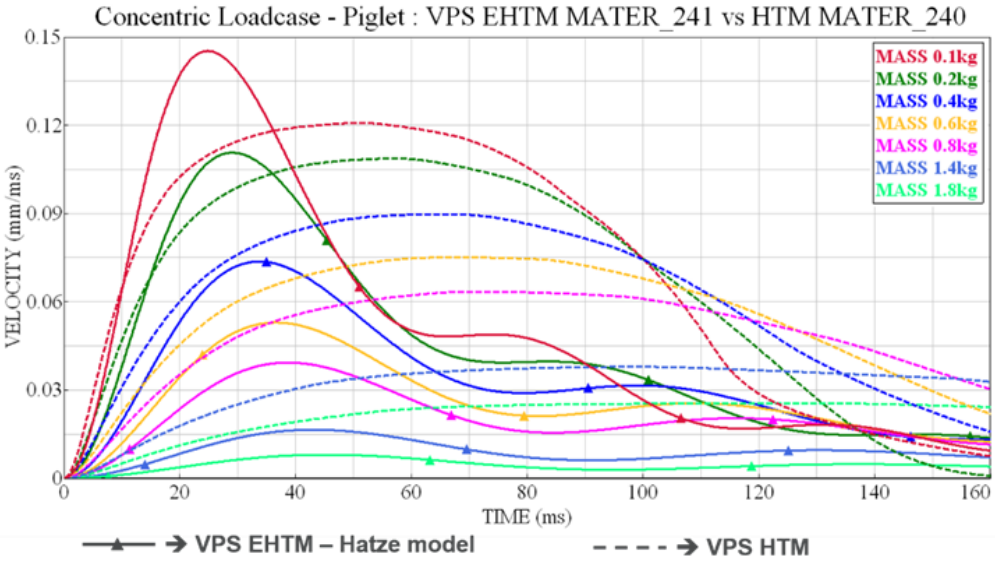

Figure 23: Piglet – concentric contraction – VPS EHTM Hatze vs VPS HTM vs Guenther experiment

A comparable initial contraction velocity is simulated with VPS MATER type 240 and type 241, in particular for higher masses. Nevertheless, the VPS MATER type 240 model cannot be able to

represent muscle velocity decrease, as it is the case of VPS EHTM model in agreement with experiment results. It has been noted a non-negligible effect of damping parameter in VPS MATER type 240. A tuning of this parameter could improve the obtained maximum velocity.

- Quick Release load case:

The muscle initial length is defined at muscle length of 60.3 mm.

Muscle top end is fixed, while its bottom end is loaded with a mass which varies from 0.1 kg to 1.5 kg.

From 0 ms to 1300 ms a full stimulation constant is used. Then the Piglet muscle is considered fully relaxed, so stimulation falls to 0 at 1600ms and until 3000 ms.

Like LS-Dyna EHTM model, VPS EHTM model defined with each dynamic activation model, Zajac and Hatze, presents comparable results to experimental results, in terms of relationship between muscle total force and its velocity, as shown in Figure 24.

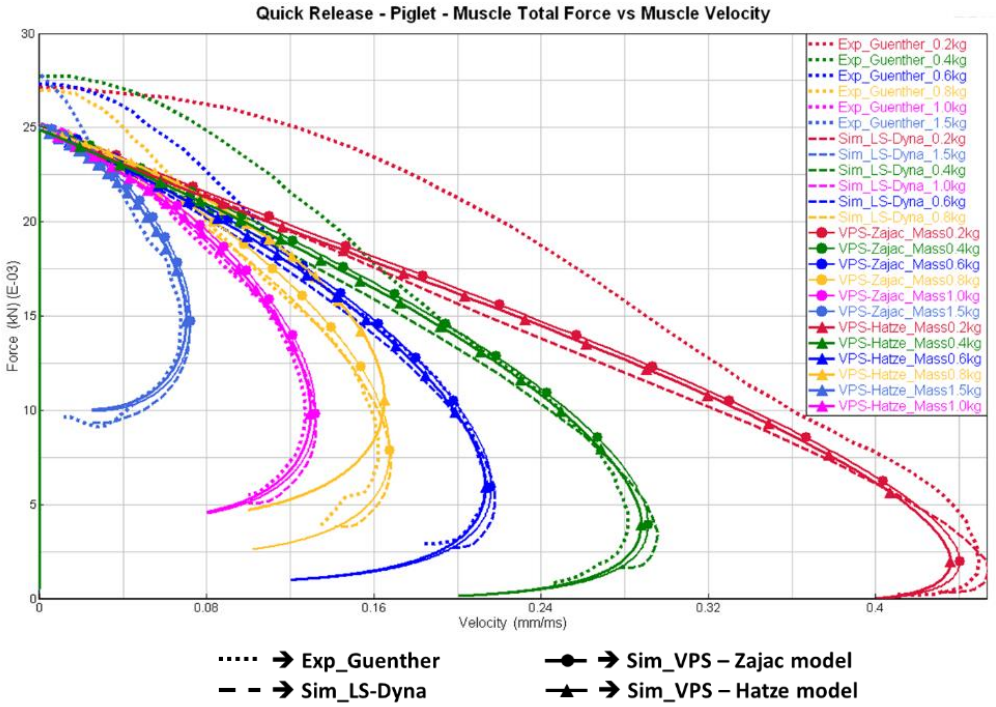

Figure 24: Piglet – Quick Release – VPS EHTM - Muscle total force vs velocity

Based on the available validation data, the implemented VPS EHTM model has been evaluated. Its capabilities to reproduce muscle behaviour measured in experiments is comparable to LS-Dyna EHTM model. For concentric contraction load case, VPS EHTM model proposes a better representation in comparison to VPS MATER type 240.

3.3.4 Implementation of extended Hill-type material model in active THUMS TUC

3.3.4.1 Methods

The THUMS TUC-VW AHBM is the active model used and developed by Volkswagen AG. This model is based on the THUMS TUC 2019 version realised in the VPS code [67][68]. And originally based on THUMS version 3.0 developed by Toyota Central R&D Labs., Inc. [69]. This model represents a 50th percentile male.

Originally, the THUMS TUC-VW AHBM was developed using the Hill-type material 240 in the VPS code. In the current study the newly developed EHTM material 241 accounting for both the muscle and the tendon, has been implemented in the THUMS TUC-VW AHBM neck region. To this aim, the length of the original 1D muscle elements needed to be divided into the muscle (l_{0fib}) and tendon length (l_{see0}), respectively. The proportion of muscle/tendon for the neck muscles was provided by the USTUTT based on publicly available data [70]. Afterwards, this data was scaled to the length of the muscles in the AHBM. However, the relation between tendon and muscle length was not available for all the muscles included in the neck of the THUMS TUC-VW AHBM. For the muscles, for which no values were available in the literature, a tendon length of 1 mm was defined.

The material 241 enables three types of muscle control: 1) time dependent activation defined by an input curve, 2) Zajac dynamic activation and 3) Hatze dynamic activation. The THUMS TUC-VW AHBM controls its muscle activation by a muscle length closed-loop algorithm. The muscle activation is therefore defined by a time dependent activation curve. Thus, flag 1 has been selected in the corresponding muscle fascicle (FASCI) card. Please refer to the subchapter 3.4.5 for a more detailed description of the THUMS TUC-VW AHBM muscle control.

3.3.4.2 Evaluation

An extension of the head-neck complex under gravity was selected as the evaluation load case for the comparison of Hill-type and EHTM material type behaviour and performance in the THUMS TUC-VW AHBM. The boundary conditions were defined to represent the volunteer relaxed experiments reported by Wochner et al. [12]. The THUMS TUC-VW AHBM was placed in a supine position on a flat, horizontal, and rigid surface, as it is shown in Figure 25. The upper and lower limbs were removed, and the sacrum was fixed in X- and Z-direction. The whole active HBM was subjected to gravity, thus, the head, which was not supported, was free to move until the muscle activation was able to stop the extension and move the head upwards.

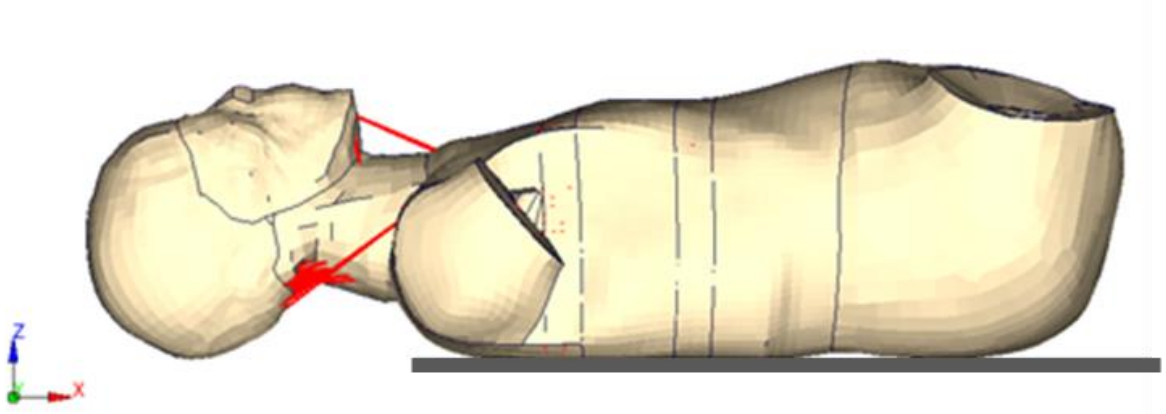

Figure 25: Initial boundary conditions defined with the THUMS TUC-AHBM in a supine position

3.3.4.3 Results

The vertical displacement of the centre of gravity of the head was analysed for two simulations:

- Hill-type material 240 with the THUMS TUC-VW AHBM muscle control
- Extended Hill-type material 241 with the THUMS TUC-VW AHBM muscle control

In these simulations, a neural delay of 25 ms was considered for the neck muscles [74].

As it can be seen in Figure 26, the THUMS TUC-VW AHBM with the EHTM implementation shows higher extension of the neck than the one modelled with the Hill-type material model. Moreover, higher number of muscles are activated if the Hill-type muscle material modelling is used.

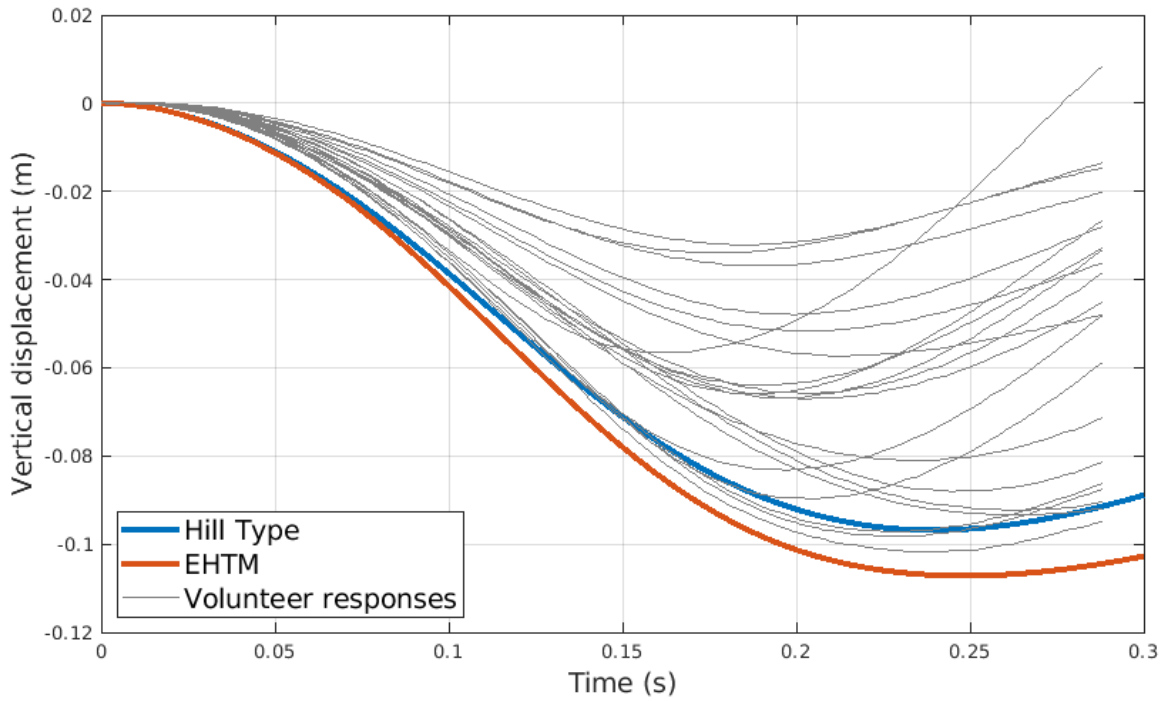

Figure 26: Vertical displacement of the centre of gravity of the THUMS TUC-VW AHBM head modelled with Hill-type and EHTM muscle models

In this study, the same control parameters were used for both muscle models. Furthermore, the target length defined for the THUMS TUC-VW AHBM was the total muscle length and the total muscle tendon unit (MTU) length at t_0 for the Hill-type and the EHTM, respectively. The proportion of the tendon is stiffer than the muscle, therefore less MTU elongation is expected. Since the feedback control is muscle length-based, the activation is lower for the MTU. Furthermore, the muscle control implemented in the THUMS TUC-VW AHBM does not account for the muscle length, when using the EHTM material model, but rather for the MTU length. Since the stimulation is proportional to the inverse of the length, the stimulation would be higher if only the muscle length would be considered.

Regarding the computational time, in case of muscle control by SimulationX coupling, both material models, Hill-type and EHTM consume the same computational cost independent of the material type (Table 6). However, further investigations have shown that if the HBM is used without the muscular control, the CPU cost with EHTM is reduced by approximately 10%. The CPU times reported in Table 6 were obtained running the two simulations using 64 CPUs for a run time of 700 ms.

	CPU Time (s)	CPU Time/CPU Baseline
Hill-type – Muscle control THUMS TUC-VW AHBM	5483	Baseline
EHTM – Muscle control THUMS TUC-VW AHBM	5511	1.005

Table 6: Computational cost using the two muscle material types, Hill-type and EHTM

3.3.4.4 Conclusions

The EHTM material has demonstrated to better depict the muscle behaviour than available models. However, the muscle parameters used in the THUMS TUC-VW HBM muscle control need to be further optimised for this material type. It has been shown in Figure 26 that, if the same parameters are used the model response is weaker and needs more time to react.

3.4 Control systems for active HBMs

3.4.1 General muscle control systems

3.4.1.1 Reflex controller

The EHTM provides the user with two different options for closed-loop control strategies based on the muscle length feedback: (1) the reflex controller; and (2) the Lambda controller [6] and [43]. The main difference between these approaches is how the controlled variable is set before and monitored during the simulation. Moreover, it has a different workflow depending on the software code used. The implementation of the material in VPS was discussed in the chapter 3.3.3 above. Here, the muscle controller functioning in LS-DYNA will be reviewed.

The reflex controller functionality was included in the user-defined muscle material in the previous studies[43] [44] and [45] to determine the muscle stimulation u_i based on the current strain. It is a stretch-based muscle length controller that activates muscle at maximum stimulation level $u_i = 1$ as soon as a particular pre-set strain threshold ω is exceeded. Although the muscle stimulation signal with is generated using “bang-bang” approach, it undergoes Hatze activation dynamics [46] to be transformed into a muscle activation signal leading to the muscle contraction. As shown in (Bayer, Schmitt, Günther, & Haeufle, 2017) on the Figure 7 (a), the applied activation dynamics has the properties of a low-pass filter, which results in a smooth and continuous activation signal.

Four parameters can be defined in the material card prior to the simulation:

- t_{contr} – the reflex controller activation time,
- τ – the neural delay time,
- $l_{CE,ref}$ – the reference length of the contractile element,
- ω – the strain threshold.

The controller signal starts to be generated once the current simulation time t exceeds the sum of t_{contr} and τ. Such a modelling approach allows for the repositioning of the model without a controller being activated till the t_{contr} and to for the representation of the biophysiological neural delay τ present in the human nervous system. Once activated, the contractile element strain ε_{CE} is calculated using Equation (1):

$$\varepsilon_{CE} = \frac{l_{CE,delay} - l_{CE,ref}}{l_{CE,ref}} \quad (1)$$

where

$$l_{CE,delay} = l_{CE}(t - \tau). \quad (2)$$

Constant stimulation signal $u_i = [0,1]$ is generated based on the relation between ε_{CE} and ω as following:

- $\varepsilon_{CE} > \omega \xrightarrow{yields} u_i = 1,$
- $\varepsilon_{CE} \leq \omega \xrightarrow{yields} u_r = 0.$

Based on the previous studies neural delay time $\tau = 0.025$ s as well as strain thresholds $\omega = 0.05$ were selected for the simulations with different AHBMS [12]. THUMS v5, A-THUMS-D and THUMS TUC-VW AHBM models were positioned to replicate the experimental setup described in the same publication. An example position is shown in Figure 25. Volunteers were lying down on a horizontal table in an unrestrained the supine position with the arms placed on the abdomen and the T1 vertebra placed over the table's edge. They were asked to completely relax their muscles, which was monitored by surface EMG measurements. Each experiment started with a sudden release of a specifically designed trapdoor that supported the head, which lead to a sudden application of the gravitational load to the head-neck complex. Consequently, it moved downwards until the person contracted respective muscles, trying to compensate for the head fall movement. All the simulations were run with the EHTM reflex controller active and the muscle activation thresholds values provided above.

Simulation results for all three AHBMs with the boundary and initial conditions remaining consistent through all the simulations are displayed in Figure 27. As anticipated, the displacement trajectories with a lower reflex threshold lies above the trajectories with a higher one for all models. The lower results boundary is set by the THUMS TUC-VW AHBM EHTM with the threshold ω=0.05 and the upper results boundary by A-THUMS-D EHTM with ω=0.02, having the range [-0.078 – -0.116]. Maximal vertical displacements and CORA quantitative rating ranging [0.349 – 0. 656] for different strain threshold values are provided in Table 7 supplemented by the graphical representation for CORA values in Figure 28.

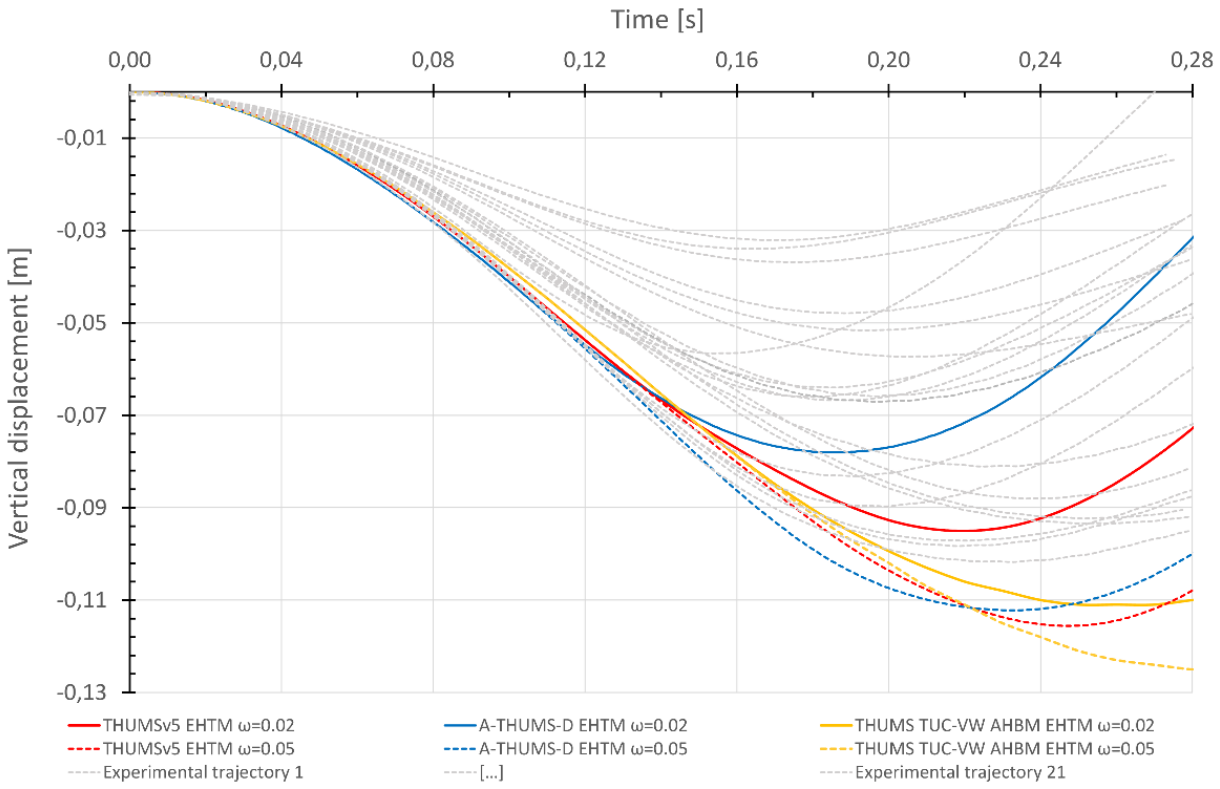

Figure 27: Vertical displacement trajectories for simulations with the reflex muscle controller active

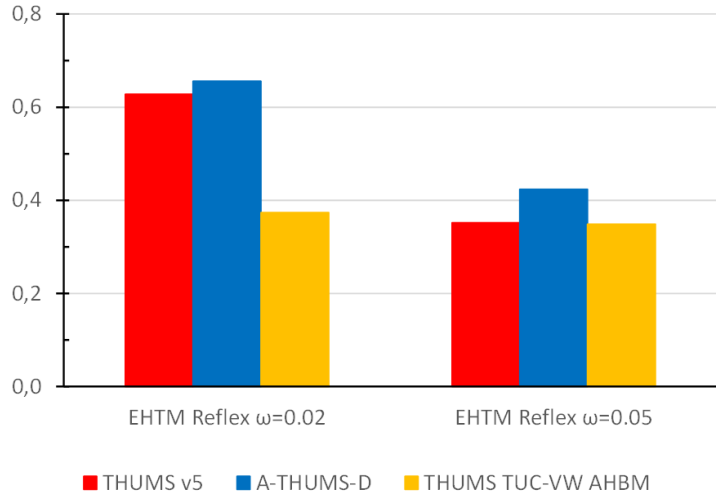

Figure 28: CORA quantitative rating for different load cases

Model	ω = 0.02		ω = 0.05	
	Displacement [m]	Cora rating	Displacement [m]	Cora rating
THUMS v5	-0.095	0.628	-0.116	0.352
A-THUMS-D	-0.078	0.656	-0.112	0.424
THUMS TUC-VW AHBM	-0.111	0.374	-0.125	0.349

Table 7: Maximal vertical displacements and CORA rating for different strain threshold values

The simulations provide results slightly different comparing to the experimental volunteer's behaviour. Besides, the maximal displacement was reached at different times for the three AHBMs. Such a behaviour could be explained by the discrepancy in soft tissues material properties between the models and the difference in the EHTM Reflex controller implementation between LS-DYNA and VPS. For both THUMS v5 and A-THUMS-D, the strain calculation is based solely on the muscle fibre length l_{CE} and does not include the tendon length. In contrast, the THUMS TUC-VW AHBM controller in VPS does not distinguish between muscle and tendon length and operates on the whole MTU-length l_{MTU}. Hence, the calculated muscle strain for the whole MTU will increase slower than the one in the CE alone, leading to a slightly delayed AHBM response and lower activation levels. This explains why THUMS TUC-VW AHBM reaches its maximal excursion later than the other two models while using the same controller parameters and reflex strategy. More details on this topic can be found in [60].

3.4.1.2 Vectorized hierarchical controller

The calculation of controller signals and activation dynamics [46] for each muscle in an AHBM can be very time consuming, especially if done by external functions, i.e., control and activity functions written in LS-DYNA keywords. Bypassing these calculations and using experimentally derived stimulation signals in the form of EMG is also not viable in most cases, as EMG signals are seldomly available for all muscles but are mostly measured for singular main muscle strands only. Although there are alternative solutions to calculate controller signals that are much more efficient then presented in [46], an attractive alternative is to adopt a new muscle control approach called the Vectorized Hierarchical Controller (VHC). Its purpose is to derive the stimulation signals of many so-called child-muscles from the few stim signals of singular parent-muscles. This calculation is based on the percentage contribution of muscles to movements across specific joints as detailed in the work of Iwamoto and Nakahira [47]. As described there, joints in the human body allow for a maximum of six types of movements: Flexion, extension, inversion, eversion, internal rotation and external rotation. Depending on which movements can be performed around a given joint, a suitable number of parent muscles has to be defined to provide input from one parent muscle per movement type. To ensure a correct calculation of child-muscle stimulations, the percentage contributions of the child-muscles should be normalized to percentage contributions of the parent-muscles. The STIM of a child-muscle $STIM_C$ can therefore be calculated according to Equation 1:

$$STIM_C = \sum_{1}^{n} x_{pc,n}\, STIM_{P,n} \tag{1}$$

where:

n is the number of parent-muscles between 1 and 6

$x_{pc,n}$ is the normalized relatedness factor between parent and child muscle for parent-muscle n

$STIM_{P,n}$ is the stimulation signal input of parent-muscle n

It should be noted that biarticulate parent-muscles can provide stimulation signals for child-muscles of two joints if desired.

Application of Vectorized Hierarchical Controller (VHC)

The VHC was implemented to an A-THUMS-D F05 CNIS arm to the muscles actuating the elbow joint and an arm flexion from 45^0 to most flexed arm position was conducted. The Brachialis was considered as the parent muscle for all flexor muscles implemented in the arm model (Figure 29)

and was controlled by Hybrid Equilibrium Point Controller (Hy-C) described in [17] with the child muscles stimulated with signals generated as per Equation 1.

A Baseline simulation was conducted with all arm flexors stimulated independently with Hy-C.

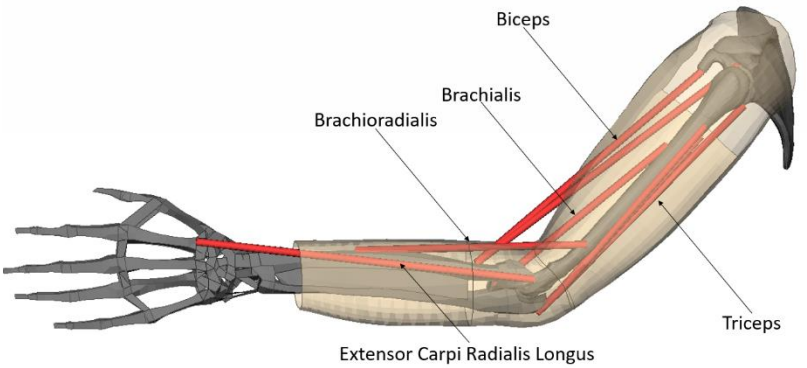

Figure 29: A-THUMS-D F05 CNIS Arm model with muscles

Arm kinematics and calculation times were compared between VHC and Baseline simulations and are presented in Figure 30. below. VHC shows kinematics comparable to baseline case where all muscles are controlled independently. However, there was a significant improvement in calculation time (32%) with VHC resulting in faster calculation speeds as listed in Table 8. VHC also simplifies controller inputs as only few parent muscles need to be assigned target lengths for Hy-C and stimulation signals for multiple child muscles are derived subsequently. Improved calculation time and simplified controller inputs are important steps towards the industrial usability of Active HBMs.

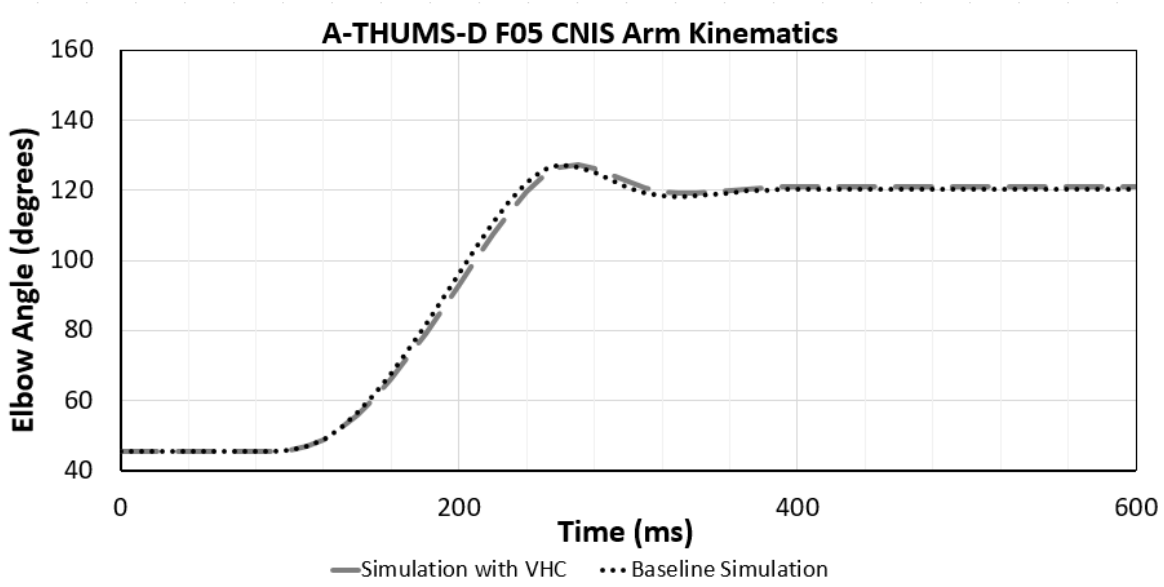

Figure 30: Kinematics of A-THUMS-D Arm model with VHC and Baseline Hy-C

Table 8: Calculation time Comparison Between VHC and Baseline Hy-C in LS-DYNA™

Simulation Case	Time (sec)
Baseline	14896
VHC	10133
Difference	4783

Simulation Case	Time (sec)
% Difference	32 %

VHC, however poses limitations in terms of applicability to entire HBM over all muscles as other joints in the body, for example the head-neck joint doesn't have muscles with absolute contribution in all 3 DOFs. Thus, identifying parent muscles and subsequent distribution of stimulation signal to child muscles becomes complex. Further work on the refinement of the ideas and the approach derived in the development of VHC for industrialization of Active HBMs needs to be done in the future.

3.4.2 Shoulder muscle feedback controller for HBMs

HBMs have been fitted with active musculature and control systems to regulate muscle activation to model occupant pre-crash behaviours. Several active HBMs have been developed in the past and used in the design of restraints. Most state-of-the-art models can predict the passenger kinematics in braking and steering events while a few also predicts driver kinematics in these events. The ability of drivers' to actively engage their arms during a manoeuvre may introduce differences between a driver and a passenger as well as differences in awareness of the expected vehicle kinematics. An active HBM representative of a driver would probably require an active controller of the muscles spanning the elbow and shoulder joints.

In version 9 of the SAFER HBM lower torso, neck, and arm muscles are controlled by angle changes between body parts. Simulated muscles in six body regions are controlled by the same number of PID controllers. Muscle length feedback can also be used to control the neck and lumbar body regions. The intermuscular load sharing used in the SAFER-HBM are based on data from experiments on volunteers. This approach is supported by other studies that have indicated that the human intermuscular load sharing cannot be determined solely from the muscles' geometrical location: human's contract nearby located muscles to maintain joint stability and to fine tune movements. The shoulder joint is the most freely moving joint in the body and predicting humanlike load sharing of muscles that bridge the shoulder joint is likely essential for the prediction of humanlike shoulder joint kinematics.

The aim of this study was to develop a shoulder muscle controller for FE-HBMs, based on human physiological data, that predicts human-like elbow displacements when exposed to dynamic loading to the elbow. When fully integrated in the SAFER-HBM the model should enable the prediction of humanlike driver kinematics in pre-crash manoeuvres.

The study was mainly carried out in the in the project Active HBMs for virtual occupant response, step 4 (AHBM4). The funding of this study was shared between OSCCAR and the FFI (Strategic Vehicle Research and Innovation), by VINNOVA, the Swedish Transport Administration, the Swedish Energy Agency, and several industrial partners.

3.4.2.1 Methods

In total 179 beam elements were updated or added to the right shoulder of the SAFER HBM v10. The controller strategy from Larsson et al. [33] was adapted to the shoulder. The muscles spanning the glenohumeral joint were controlled with angular position feedback. Intermuscular load sharing based on directionally dependent muscle activation data from volunteer experiments were also introduced. All modelled muscles that were spanning the scapulothoracic joint were controlled using muscle length feedback.

The model was evaluated by simulating volunteer experiments in which dynamic loads were applied to the elbow in eight directions. Peak elbow displacement, time to peak elbow displacement, and

detailed elbow kinematics of the model were compared to the results obtained in the volunteer experiments. In addition, a sensitivity study was undertaken to show the effect of varying the gains of the angular position feedback controller on the elbow responses.

3.4.2.2 Results

The study found that the active controller reduced peak elbow displacement for all eight directions evaluated. The study also showed that for two of the gain combinations, the model was capable of producing peak displacements within one standard deviation of the volunteers, in all eight loading directions. The obtained time to peaks were within one standard deviation in four of the eight directions. The successful prediction of peak elbow displacement showed that the controller is ready to be implemented and evaluated in full-body driver simulations.

3.4.2.3 Presentation of the full study

The study was included in the Licentiate Thesis by Emma Larsson [18] and a scientific paper will be submitted to a scientific journal before the end of 2021.

Authors and title of the paper: Emma Larsson, Jason Fice, Johan Iraeus, Jonas Östh, Bengt Pipkorn and Johan Davidsson *"Development of a shoulder muscle feedback controller for HBMs".*

3.4.3 Improved kinematic controllers for the Madymo AHBM

The behaviour of the upper limbs and shoulders was investigated in support of OSCCAR WP2. The upper limbs provide an important load path during braking and lateral manoeuvring, assisting the occupant in supporting the upper body upright [5]. The shoulder's active response to horizontal arm loading was validated against experimental data [84]; however, responses with vertical loadings were reported to be asymmetrical and unrealistically soft. In addition, partners reported numerical instability in the shoulder that led to simulations aborting.

Investigations into the shoulder design in the AHM revealed that a co-ordinate system had been incorrectly defined, leading to the asymmetry, and that the shoulder joint was insufficiently constrained. In the model a few muscles were not accounted for.

3.4.3.1 Shoulder strength study: methods

A standing model prototype of the AHM with updated coordinate definitions and additional shoulder joint muscles. The model was set up to duplicate tests with volunteers [87] to evaluate the arm responses. The publication reporting on the original volunteer tests are difficult to obtain; hence a summary of the original tests is provided in Appendix E. In these volunteer tests arms were extended forward and supported by strings. When the strings were released the volunteers activated their muscles to recover the initial arm position.

The torso and spine of the AHM were locked, as the flexibility of the trunk in standing loading has not been validated.

3.4.3.2 Results and discussions

The bottom graph in Figure 31 shows the results following changes realised by the updates, with the model behaving fully symmetrically and the displacement reduced as compared to before upper top graph in Figure 31.

The updated model took 1.36 s to return the arms to horizontal; slightly longer than the volunteer response (averaged 1.22 s). Experiment and simulation differed in that the trunk of the body was locked rigid in the numerical model, with all response focussed on the shoulder joint actuator, whereas the volunteers were free standing and supported their core and shoulders with actively posture muscles. The full response of the upper body was therefore not included in the simulation.

While the times used in the control system were taken from the average response of all volunteers include in the study these can be varied to account for age and sex variations.

It was noted that all volunteers overcompensated when recovering their initial posture. The arms passed the original position before settling back to the original posture. This was not seen in the model and is an indication that human active response is less systematically damped than the current AHM control systems model.

Further work can be done on developing displacement corridors for such volunteer testing, allowing the displacement to be either tuned or validated and giving an indication of the recovery overshoot. This would allow the dynamic damping in the shoulder actuator to be empirically tuned or validated.

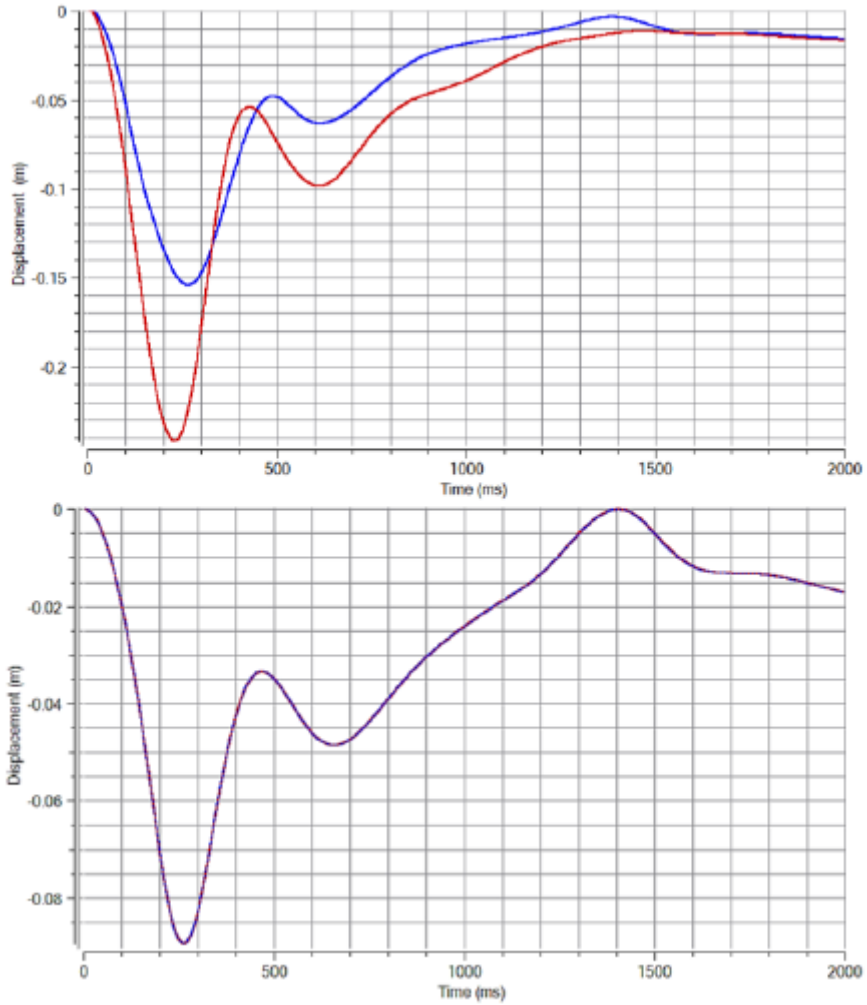

Figure 31: Vertical hand displacement (blue = left, red = right) in arm drop test. Top graph: before modification, bottom graph: after modifications

3.4.3.3 Implementation

Following the modification of the prototype, the new restraint system was implemented into the AHM and the effects on the existing biofidelity validation database, as described in [88], were checked. Further optimisation of the characteristics was identified and carried out until the effects of the implementation on the established biofidelity of the model were minor. As an example, Figure 32 shows the change in the response brought about by the shoulder restraint updates to the impactor response in a simulation of the test described in [90]. In this test a flat, circular impactor of mass 23.4 kg strikes the shoulder of an unsupported PMHS laterally at the head of the humerus, at 5.5 m/s.

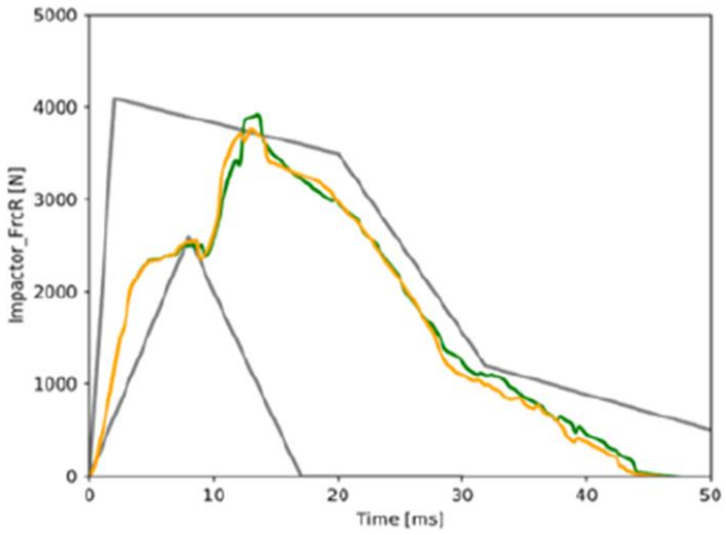

Figure 32: Change in impactor force between original AHM (green) and updated shoulder model (yellow)

The passive response to loading is therefore almost unaffected, while the improvements described show a clear improvement in shoulder stability and response.

Instability

The model was reported to be unstable in an application run by IKA. The simulation aborted due to numerical instability in the shoulder, in the form of a gimbal lock.

Many of the restraints in and around the shoulder joint in the AHM are cardan restraints between two bodies; these apply opposing torques on the connected bodies which depend on the relative angles between them [91]. The relative orientation is described in Madymo by prescribing a set of three successive rotations, known as Bryant angles, which define the orientation of the child system *j* relative to the parent system *i* (see Figure 33)

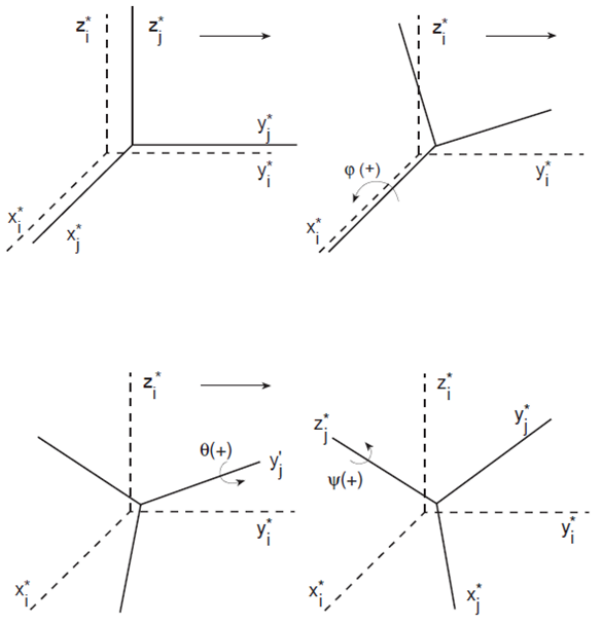

Figure 33: Relative orientation of coordinate systems using Bryant angles

When θ = π/2, the first and third rotation axes are parallel and cannot be numerically discriminated. This leads to the loss of one degree of freedom, which constrains the system rotations into a degenerate 2-D space; this is known as a gimbal lock. For this reason, the Madymo solver requires that - π/2 < θ < π/2 for the second rotation.

The latissimus dorsi restraints connect spine bodies to the humerus. The range of motion of the arm relative to the spine is large, and in OSCCAR simulations or rear-facing occupants in “living room” style AV interiors, the cardan restraint reached a gimbal lock configuration due to the nature of the applied loading. The novelty of the loading regime placed the shoulder joint into an angle that other validation and testing had not managed to cause.

It was necessary to ensure that the second degree of freedom for the cardan restraint corresponded to the least mobile rotation: that of internal/external rotation. That alone was not sufficient to ensure numerical stability, however; following the implementation/validation phase mentioned above it was found that the existing constraint values for the AHM in this degree of freedom were not sufficient to prevent this motion.

The constraints on internal/external rotation of the shoulder beyond voluntary motion from the latissimus dorsi is taken as 125 Nm/rad, and in the range of voluntary control is 0. The model initially had the voluntary range as -1.3 to 3 radians, however, which was far too high; study of the literature suggested a range of -1 to 1 radians [92]. Once this restraint range was corrected, the model was found to be stable in all applications that were showing signs of instability. This had no effect on the existing validation results, as the model was not loaded in ways that caused this range to be exceeded.

3.4.4 Torque controller for active HBMs

This controller concept is not based on the simulation of muscular activity via beams and muscle material models. The developed approach simulates the body kinematics in the pre-crash phase, by applying torque to the skeleton. As the main kinematics in pre-crash manoeuvres takes place in the upper body and head/neck, torque is applied at every vertebra in two direction (x,y). Based on the positions of the vertebras, the necessary torque is calculated by an external Code (Python PyBullet).

The Python code contains a surrogate model of the HBM and the determined torques are applied with a LS-Dyna User Material function. Positions of every vertebra are sent to Python for every FE calculation timestep.

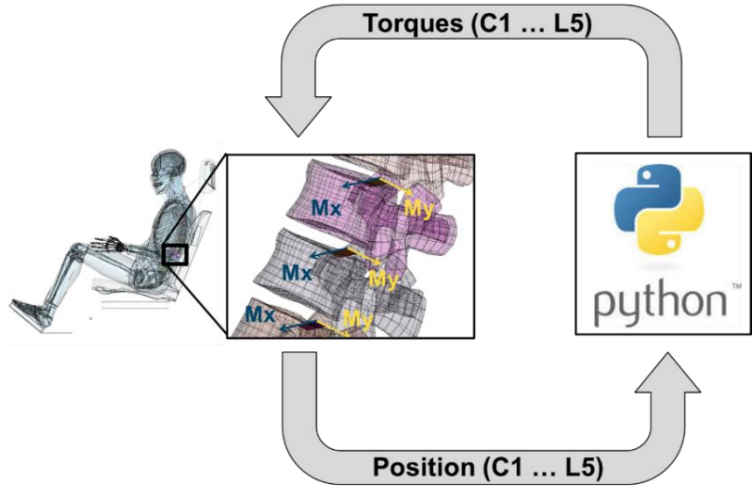

Figure 34: Concept for torque controller

3.4.4.1 Controller architecture and strategy

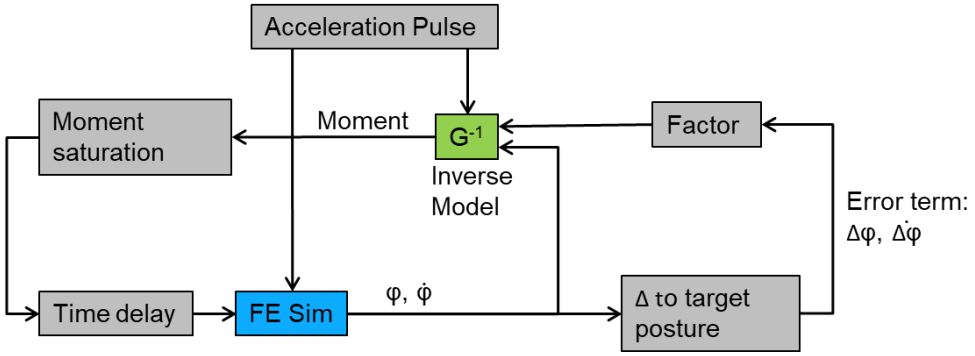

Figure 35: Controller architecture

The main principle of the controller is, to apply the necessary torque, which keeps the HBM in its initial position, even if an acceleration pulse is applied. The torque is calculated for both axis (x,y) based on the current angular position and angular velocity by an inverse surrogate model (description below). To consider the differences to the initial position and velocity, an error term is defined and multiplied by a factor. The calculated moments are limited to avoid overshooting. The limits are defined separately for each spine section (lumbar, thorax, cervical) and direction (x,y).

By applying a time delay, the calculated moments can be shifted in time and leads to a forward motion of the occupant model. Using no time delay leads to an occupant model, which remains in its initial position as mentioned before.

3.4.4.2 Selected dataset for controller development

For the development of the controller, a combined (braking, steering) of the OM4IS dataset (see 3.1.2) was used. Following diagram show the longitudinal and lateral accelerations.

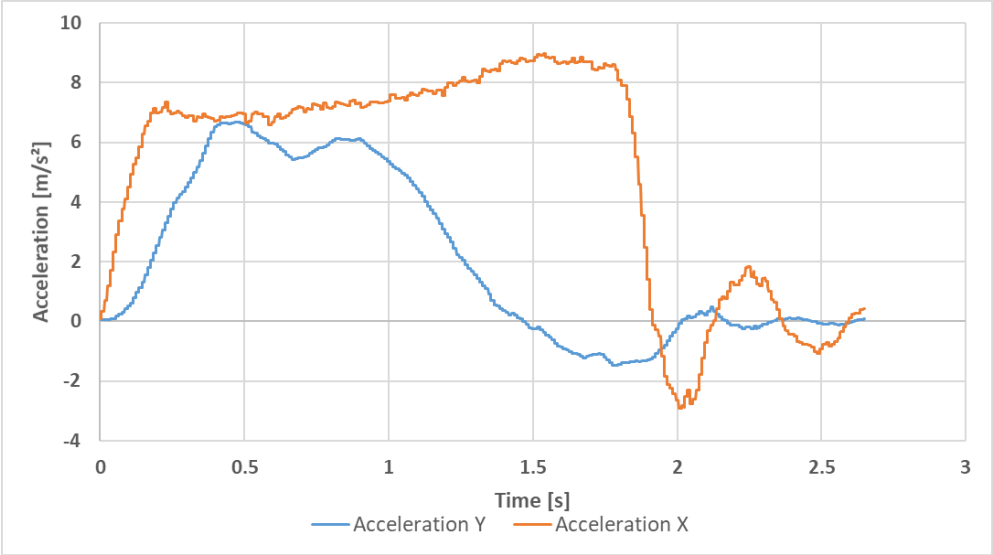

Figure 36: Longitudinal and lateral acceleration for combined (braking, steering) manoeuvre in OM4IS

3.4.4.3 Surrogate model development

The surrogate model is a multibody model which is created with the Python package PyBullet. Basically a “multi-pendulum” approach was chosen, which depicts the upper body and the head (Figure 37 and Figure 38). For every intervertebral disc, two joints were positioned, according to the FE model. They allow the rotation about the X- and Y axis.

Additional to the HBM surrogate, a seat and a seat belt were modelled.

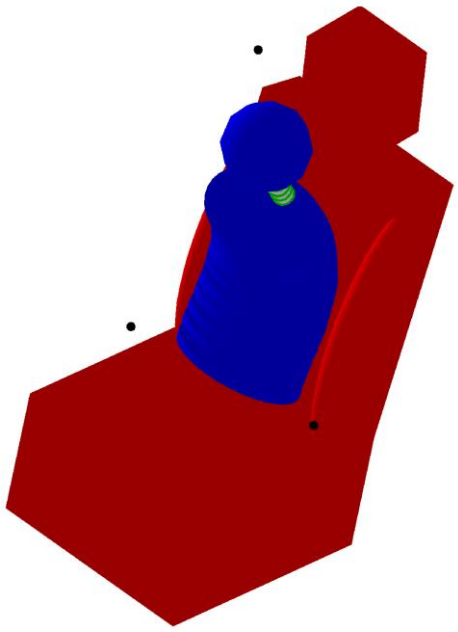

Figure 37: ISO view of the surrogate model

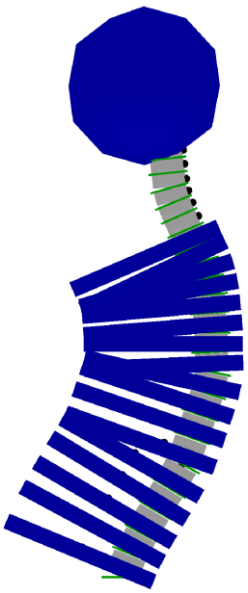

Figure 38: Side view of the surrogate model (without seat)

In order to align the kinematics of the surrogate model and the FE models, two characteristics need to be considered.

- Inertia
- The inertia of the upper body needs to be projected to the vertebras of the surrogate model.

To do so, the masses of each section (Lumbar spine, Thoracic spine, Cervical spine) were evenly distributed to each of the respective vertebrae. The centres of gravity (CoG) were set to positions such that the summarized CoG position of each section matches the CoG position in the THUMS model as closely as possible. The mass moments of inertia are also identical for all vertebrae in each section. The respective values were chosen such that the overall mass moments of inertia per section are a as close as possible to the values measured in the THUMS model.

- Joint stiffness

The stiffness of the upper body also needs to be considered in the surrogate model. That is done by introducing rotational spring and damper parameters to the joints. The parameters are determined by optimization. The target kinematics is the FE HBM kinematics for the acceleration pulse the combined manoeuvre in the OM4IS dataset (Figure 36).

In total, 48 joints are used, which would lead to 96 parameters for the optimization. To reduce that, the spine was divided into three sections (lumbar, thorax, cervical) and it was assumed that the spring and damping parameters are constant within each spine section.

The PyBullet surrogate model can depict the “direct kinematics”, means the excursion caused by a moment, and also the “inverse” kinematics. That allows, to determine the necessary moment to reach a certain position.

3.4.4.4 Controller development

The controller development was done in four steps, which are explained in more detail below.

- Stabilization of the FE model in initial position without a pulse
- Stabilization of the FE model in initial position with a pre-crash pulse

These first to steps are done to evaluate if the surrogate model predicts the FE HBMs kinematic with sufficient precision. The next two steps adapt the controller to match with the volunteer test data.

- Adaption of time delay and controller parameters for the surrogate model to match with OM4IS corridors
- Adaption of time delay and controller parameters for the FE model to match with OM4IS corridors
- Stabilization of the FE model in initial position without a pulse

In the first step, the controller is used to simply stabilize the HBM in its initial position. No external accelerations are applied to the model. Hence the only effect which needs to be compensated by the controller is the gravity. The time delay is also not used in this first step, as shown in Figure 39.

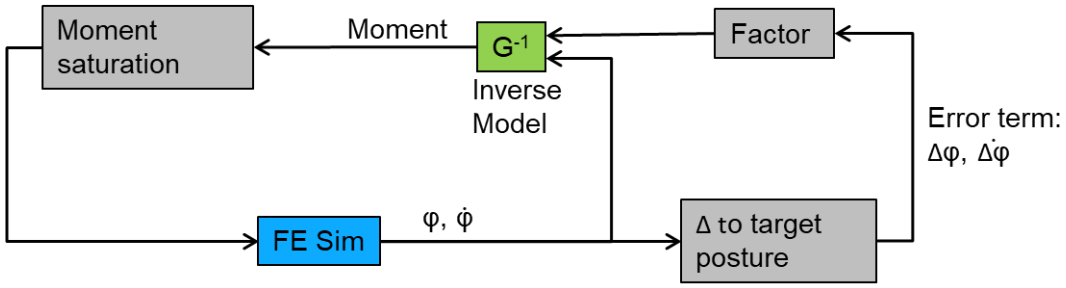

Figure 39: Controller architecture for stabilization without pulse

- Stabilization of the FE model in initial position with a pre-crash pulse

The joint torques are applied on the model without a time delay (Figure 40). That stabilizes the model in its initial position during the pre-crash pulse. The current controller version calculates the torques in y-direction (forward – rearward bending).

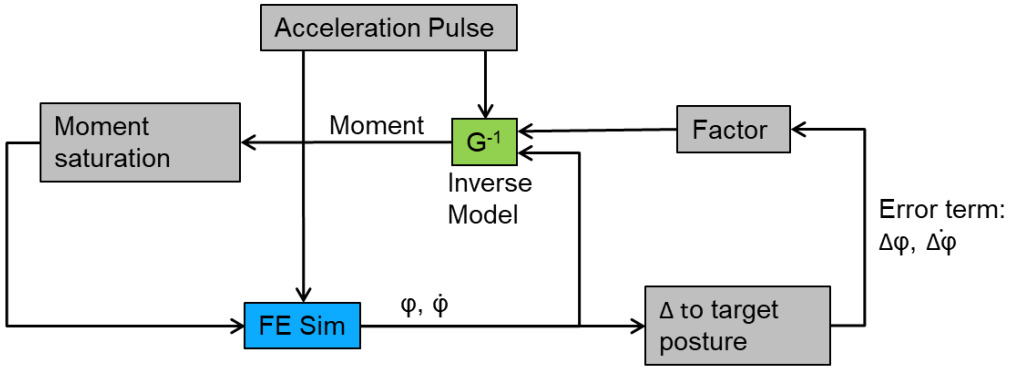

Figure 40: Controller architecture for stabilization with pulse

- Adaption of time delay and controller parameters for the surrogate model to match with OM4IS corridors

The time delay, which is necessary to generate excursion is pre-adjusted by using the direct kinematics of the surrogate model instead of the FE model (Figure 41). That is done due to lower computational cost of the surrogate model compared to the FE model.

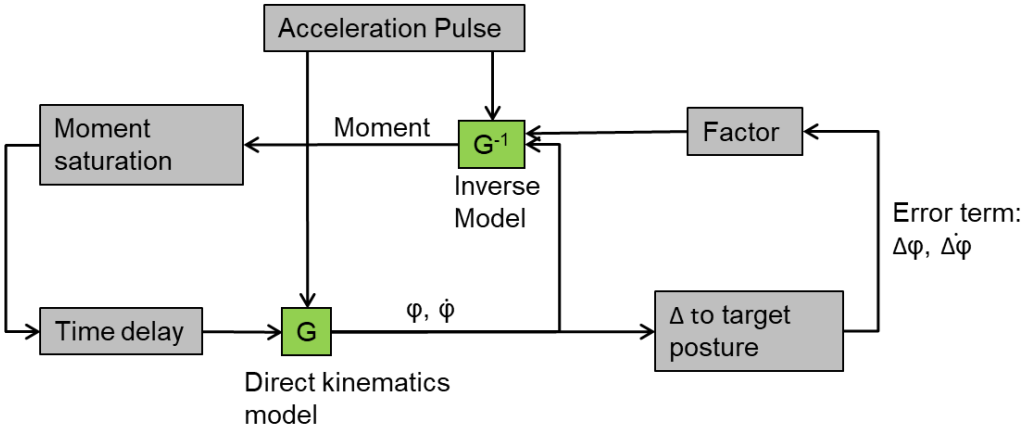

Figure 41: Controller architecture for determination of time delay and controller parameters with direct and inverse surrogate model

The focus of this adaption process is on the head angle since the thorax angle is mostly defined by the belt forces.

- Adaption of time delay and controller parameters for the FE model to match with OM4IS corridors

Last step is to adapt the time delay and parameters of the controller by using the FE model, as it is shown in Figure 35. The parameters determined with the help of the surrogate model serve as the basis to find the parameters with the FE model. Figure 42 shows the head angle (y-axis) for the controlled FE model. A further improvement of the controller is possible, but as the current settings leads to a head angle, which follows the volunteer mean characteristic and stays within the corridor for more than 90% of the simulation time, the current settings are further used for OSCCAR active simulations. As the angle of the Thorax is mainly controlled by the belt, the influence of the controller to the torques in lumbar and thoracic spine is kept low.

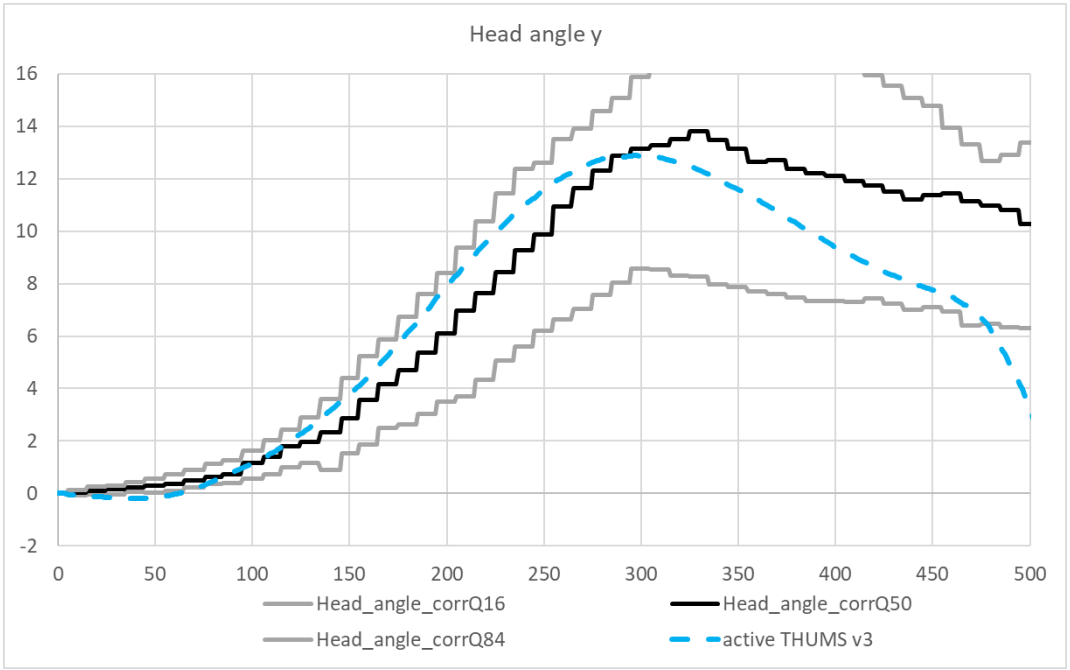

Figure 42: Head angle of torque controlled THUMS v3 with OM4IS corridors for combined manoeuvre

3.4.4.5 Conclusion and Outlook

A kinematic controller was developed, which works with prescription of controlled torques instead of muscle elements. The principle is adaptable to other HBMs as long as a surrogate model (which is invertible) is available.

Controlling the kinematics about the x-axis shows, that some further updates are necessary. Therefore, the developed controller is capable of motion about the y-axis.

3.4.5 VPS-Simulation X coupling

In order to facilitate HBM muscle control during pre-crash or in- crash phase, the coupling solution between VPS and SimulationX has been enhanced by adding support for HBM-specific variables, involving in active muscle modelling.

Developments have been made at two levels as indicated in Figure 43:

The VPS-SimulationX workflow allows the dynamic control of the muscle activation or stimulation level based on muscle parameters exported during the coupled simulation.

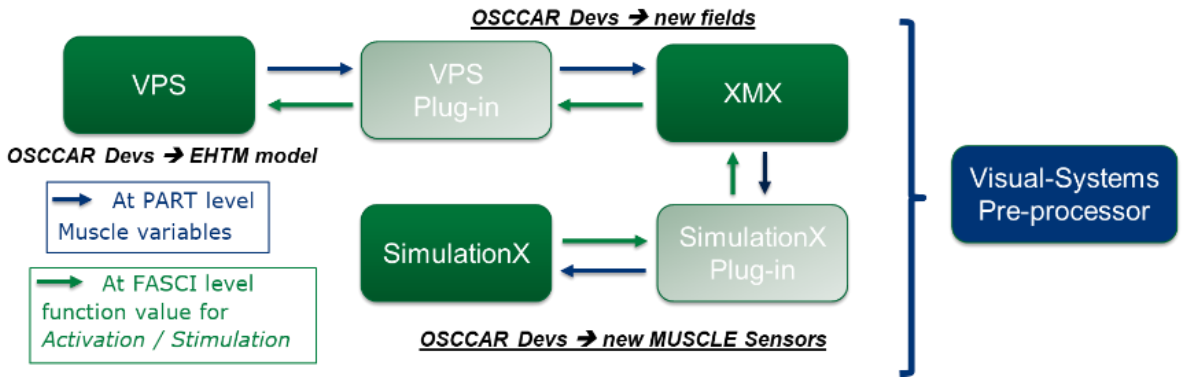

Figure 43: VPS-SimulationX workflow

3.4.5.1 Solver developments

Involved ESI solvers have been adapted to ensure muscle control during load case simulation.

For ESI *VPS* solver, an export of parameters for PART of MUSCLE type has been developed. In particular, muscle length, strain, strain rate and total force magnitude are now available. In parallel, ESI *SimulationX* plug-in has been updated to support the above new fields. Concerning the coupling management made by ESI *XMX* solver, for these new variables associated fields have been added. In addition, coupling management has been improved with an update of the exchange file format (.emf, ESI model file) and the solvers units compatibility at plug-in level

3.4.5.2 Visual-systems developments

For muscle controller definition, Visual-Systems have been adapted (see Figure 44). In *CosimVPS*, a new muscle sensor has been added to the coupling library. Developments have been realized to support the update of the XMX exchange file format and the new PART specification which is used for muscle variables management.

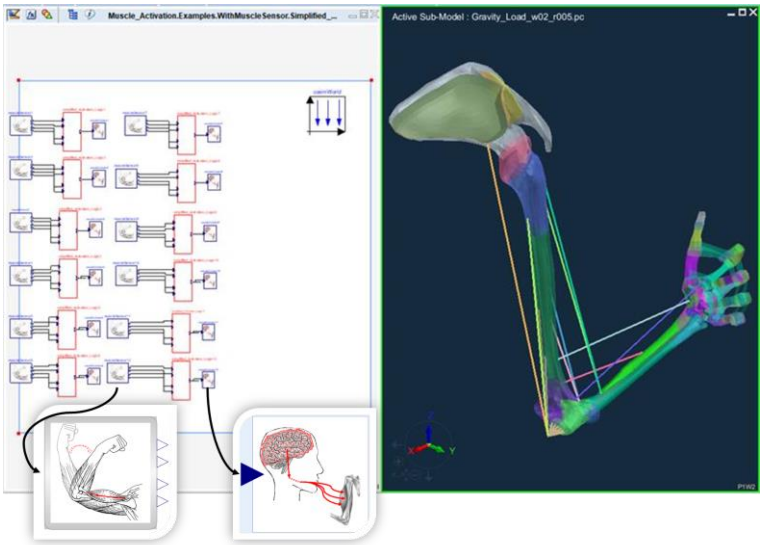

Figure 44: Visual systems-CosimVPS model-coupling components for muscle management

3.5 Validated and computationally robust active and reactive HBMs

3.5.1 Validation of the THUMS TUC-VW AHBM

3.5.1.1 Background

The AHBM used by Volkswagen is the THUMS TUC-VW AHBM (Figure 45). Currently, this model is based on the THUMS TUC 2020 model realised in the VPS code - a passive HBM representing a 50th percentile male, which itself is derived from the original THUMS version 3.0 developed by Toyota Central R&D Labs., Inc. . In the following subchapter 3.5.1, the now extended validation of the THUMS TUC-VW AHBM under frontal and lateral load cases is presented.

The THUMS TUC-VW AHBM includes 602 muscles modelled with 1412 1D-elements being controlled by 66 controllers and represents the latest upgrade compared to the version first published in [71] - including 334 muscles and 20 controllers. Further upgrades, in addition to the implementation of muscles over the whole body, are related to the soft tissue material properties, muscle path and muscle fixation.

Figure 45: THUMS TUC-VW AHBM including 602 muscles

The muscle paths were updated and, if necessary, via-points between muscle origin and insertion were introduced, allowing a more biofidelic curved muscle path rather than one single bar element, and hence straight point to point action line. Figure 46 shows an example of the curved path approach for the gluteus medius muscle. The curved path was defined according to anatomical literature and educational anatomy models, for example [27]. The correctness of the muscle path is crucial if large rotations occur at the joint, since the action line might pass its rotation centre, which will change the functionality of the muscle, for example from extensor to flexor or vice versa.

The second major improvement regarding the muscle modelling is related to the fixation of the muscles on the bones. The muscle origin and insertion points were originally modelled by shared nodes between the 1D-element of the muscle and a single node on a shell element of the bone. The improved modelling method of the current AHBM distributes the insertion on an area of the bone, mostly using about six nodes, which connect the muscle bar node by the OTMCO linkage available in VPS. This modelling method represents a more biofidelic modelling of the muscle insertion, since the load applied to the bone is distributed to a larger area, therefore avoiding concentrated loads on a single node. This is a valuable improvement, in case the AHBM is used for an injury risk evaluation based on bone strains, rather than just for kinematic analyses.

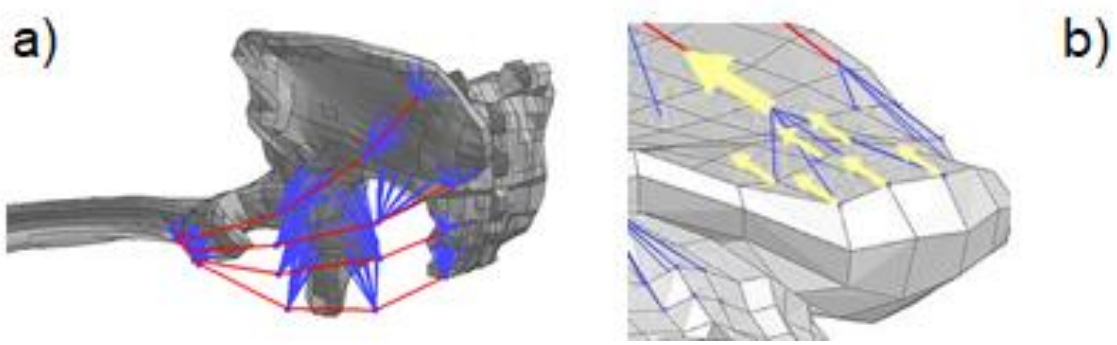

Figure 46: Updates of THUMS TUC-VW AHBM: a) curved muscle path with via-points and b) distributed load at the muscle insertion area of the bone [72]

Finally, the soft tissue materials applied to the neck ligaments and passive muscle tissue were further improved with respect to both their biofidelity, according to experimental data from the literature [21][26], and numerical stability in relation to large deformations occurring in an in-crash phase.

The newly developed soft tissue materials in OSCCAR Task 3.1 and reported in D3.1 were not included in the THUMS TUC-VW AHBM used in this study, since their evaluation was conducted in parallel to the AHBM validation and requires further analyses before its implementation to the AHBM can be done.

Currently, AHBMs are mainly used for pre-crash phase analyses. These simulations are computationally expensive in comparison to in-crash phase simulations. While the pre-crash phase may last for several seconds, the in-crash phase only lasts about 150 milliseconds depending on the crash scenario. To consider the muscle activation, while keeping the computational time low, the muscles of the THUMS TUC-VW AHBM have been clustered into groups depending on their functionality, e.g., flexors and extensors, resulting in 66 muscle controllers.

In the analysis presented here, the muscle material used is the Hill-type, referred as material 240 in VPS. Please refer to subchapter 3.3.4 for further details about the implementation of the newly Extended Hill-type material model in the THUMS TUC-VW AHBM.

Finally, the THUMS TUC-VW AHBM muscular control has been further enhanced since its first version [71], aiming to improve its muscle response, biofidelity and computational cost. Initially, the muscle control was integrated in the finite element HBM by implementing the control algorithm in Python, using the PYFUNC keyword available in VPS. The algorithm updated an activation time-dependent curve, namely called NACT, which enabled the calculation of the active muscle forces. The here mentioned Python functions were given access to variables such as the length and the strain rate of the contractile element. However, this approach is time consuming since the muscle activation was calculated at each time step of the simulation. Additionally, the mathematical functions available for PYFUNC in VPS were limited and thus, restricted the further development of the muscle control.

The new approach enabling the further enhancement of the muscle control of the THUMS TUC-VW HBM is the coupling between the software VPS and SimulationX [73]. This solver coupling is explained in detail in the following subchapter 3.4.5. In Figure 47, a flowchart with the closed-loop feedback control implemented with the THUMS TUC-VW AHBM is shown.

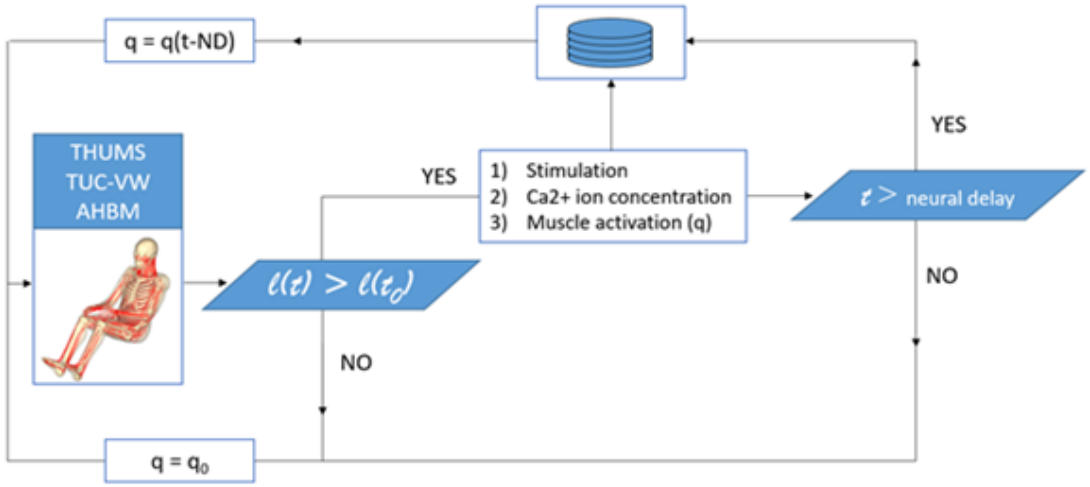

Figure 47: Flowchart of the VPS-SimulationX coupling established for muscle feedback control in THUMS TUC-VW AHBM. q_0 is the muscle tone and ND – the neural delay

The coupling of these two software enables the definition of a sampling rate. This means, that the coupling and exchange of parameters does not have to occur at each time step, but at each sampling step, which can be defined by the user. In Figure 48, the advantage of reducing the sampling rate on the reduction of the CPU time is shown. This has been evaluated with the THUMS TUC-VW AHBM under the falling head boundary conditions (Figure 45). The simulation run time chosen was 700 ms using 64 CPUs. The sampling time of 0.001 ms would represent an exchange at almost each time step. If a sampling time of 0.05 ms is chosen instead, a reduction of 20% in the CPU time has been attained. However, it is important to ensure that the kinematics and activation of the muscles is not altered by the sampling rate. For this study, it was proven, that the used sampling rates applied did not alter the outcome.

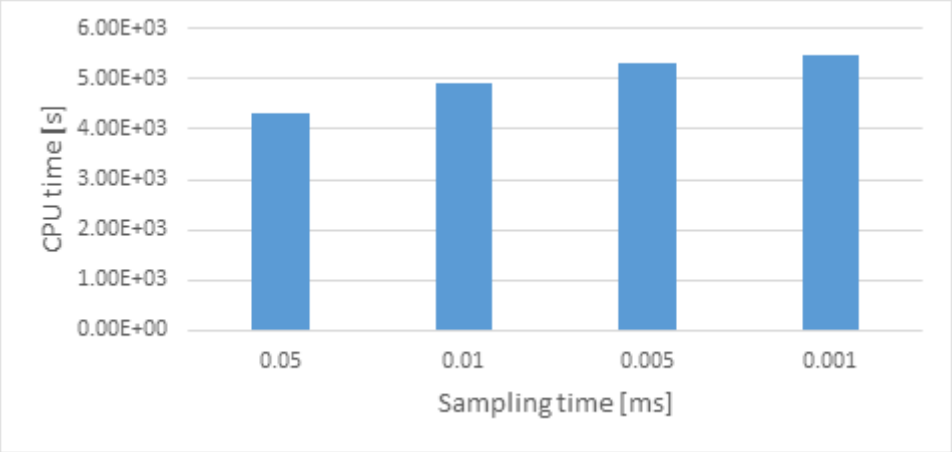

Figure 48: Reduction of the CPU time by increasing the sampling time between the software VPS and SimulationX using 64 CPUs

The principal target of the model control is to react by activating the muscles to return to the position prior to an external perturbation. For this purpose, the target length is defined as the initial length of the muscles. If the muscles are extended, i.e., if the length of the muscles is greater than the original muscle length, the outburst of the activation starts. If the muscle length is shorter than the initial one, the muscle does not contract and it remains with its muscle tone activation, called q_0 in the Figure 47. This algorithm represents the neuromuscular action of the muscle spindles, which are stretch receptors detecting changes in the length of the muscle.

If the muscle is extended, the muscle contracts to return to its initial length. To this end, the stimulation of the reference muscles is calculated based on their current length and strain rate [7]. Furthermore, three parameters need to be defined: activation gain, co-contraction, and strain weight; depending on the values chosen for these parameters different activation levels can be reached. Afterwards, the Hatze's activation dynamics function [46] is used to calculate the free-calcium-ion concentration and finally the activation value. The activation can reach values from q_0, muscle tone, to 1, full activation of the muscles. The contractile element exerts an active force after an onset defined by the neural delay. The neural delays used in this model are 30, 70 and 100 ms for neck, upper body, and lower body, respectively 94.

3.5.1.2 Methods

The updated version of the THUMS TUC-VW AHBM described in the subchapter 3.4.5 has been further validated within the OSCCAR project, using the volunteer experimental data reported in the subchapters 3.1.2 and 3.1.5. These validation data include representative load cases of braking [3] and [20], lane change [3] and [30] and combined manoeuvres [3]. The validation test matrix performed with the THUMS TUC-VW AHBM is presented in the Table 9. Data of the driver behaviour has been documented in [20], however in this study merely the passenger position has been considered, expecting that in an autonomous driving scenario all the vehicle occupants will be passengers.

	Braking	Lane Change		Combined	
		Right	Left	Right	Left
OM4IS	x	x	x	x	-

	Braking	Lane Change		Combined	
Chalmers	x	x	n/a	-	n/a

Table 9: Simulation matrix used for the validation of the THUMS TUC-VW AHBM. X: performed simulation, -: data available, but simulation was not performed, n/a: data not available

The activation level of the THUMS TUC-VW AHBM can be defined by the selection of a parameter set for the muscle control. In this study the levels *highly, moderately,* and *low tensed* are shown for the OM4IS braking validation load case. Moreover, a simulation without muscle control, in which a constant activation value of 5 percent was defined for all the muscles, intended to resemble a relaxed state, has also been carried out under the OM4IS and Chalmers braking conditions. In total 10 validation simulations were performed. For the other load cases the moderately tensed parameter set has been demonstrated in this study.

Additionally, before the validation simulations, two positioning simulations were carried out for the two environments. The hands of the THUMS TUC-VW AHBM were moved from its original position (driver position) to achieve a position as similar as possible to the volunteers (resting on the thighs). The deformation of the soft tissues and the seat foam was imprinted in the validation simulations by using the Picking functionality available in VPS, which considers, among others, stresses and strains from a previous simulation run.

3.5.1.3 Results - OM4IS braking

In the Figure 49, the cyan coloured curve shows the head centre of gravity (COG) forward and vertical excursion of the AHBM representing relaxed behaviour. As expected, the curve lie outside the volunteer's corridor presented in Huber at el. [2] and [3], since the model does not react to the external perturbation, namely the braking pulse. The curves representing the relaxed state conditions are included here exemplarily to demonstrate, that the model without muscle control does not show the behaviour in the range of the volunteers, but above in terms of the maximum excursions.

Furthermore, three parameter sets were selected to represent three different activation levels*: highly, moderately,* and *low tensed*. The aim of selecting different parameter sets is to not only resemble the average behaviour, but to cover the whole range of volunteer reactions, as shown in Figure 49 by the AHBM.

It can be observed that the highly and low tensed models are stabilised after 2500 ms, whereas the moderately tensed model is less stable and showed larger oscillations. Moreover, the low tensed model matches the lower boundary of the Head COG corridor well with respect to forward excursion (Figure 49, top). The highly tensed model represents a stiffer behaviour than the average volunteer. On the other hand, the moderately tensed model’s forward excursion was close to the lower boundary of the corridor behaviour. This parameter will have to be further optimised to better represent a moderately tensed behaviour.

On Figure 49 bottom, the vertical displacement of the head COG is shown. During the first 100 ms the model settles down, thus an offset in the Z-excursion was calculated with the respective vertical displacements obtained at this time point by each of the models. This is issue is under investigation and the model stability in the vertical direction at the start of the simulation needs to be further enhanced.

In the Z-excursion the highly and low tensed parameter sets match well the outer boundaries of the volunteer's corridor. On the other hand, the moderately tensed behaviour needs further improvement to reduce the oscillations.

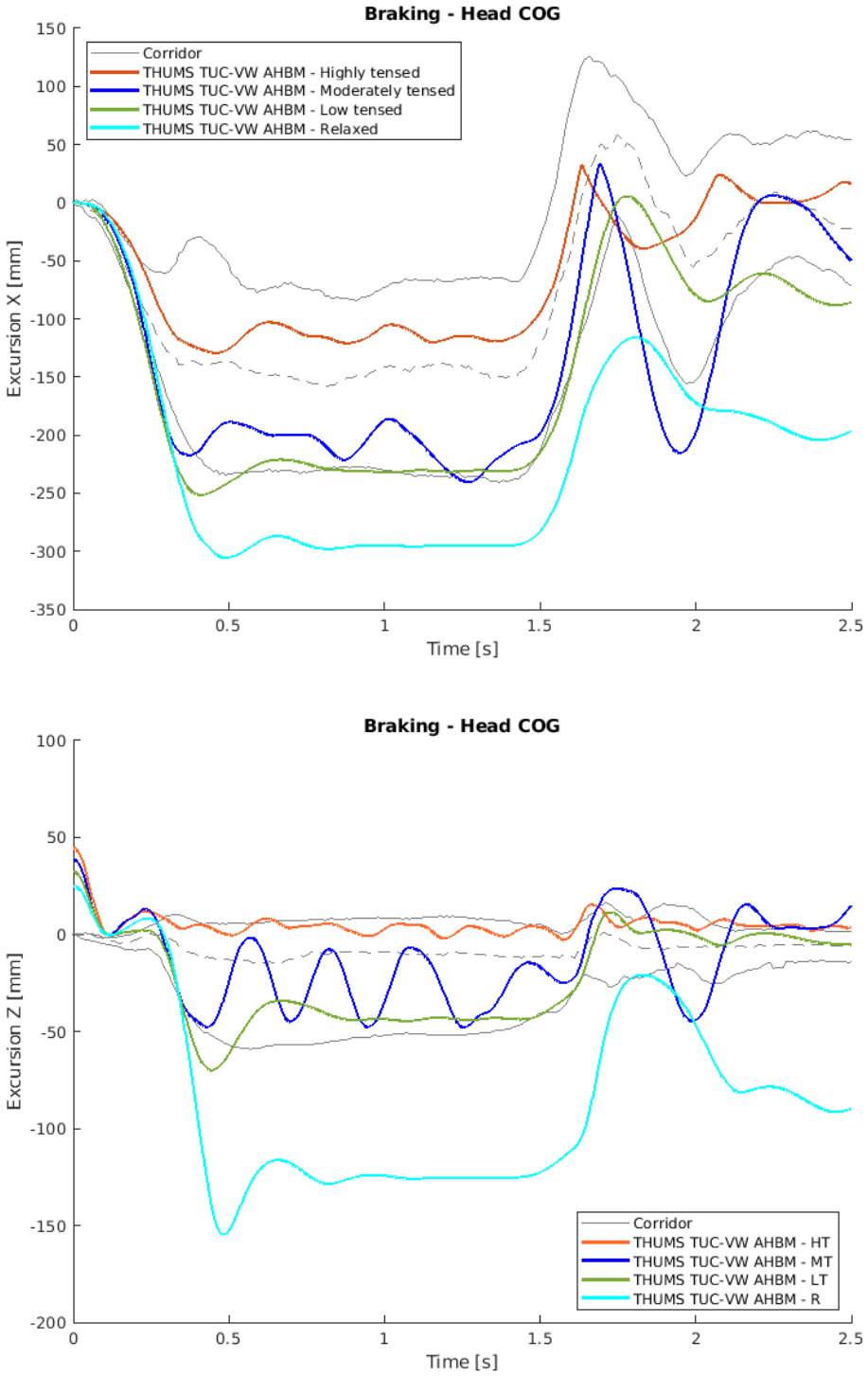

Figure 49: THUMS TUC-VW AHBM responses and volunteer corridors. Forward (top) and vertical (bottom) displacements under the OM4IS braking condition starting with a 50 km/h initial velocity. HT: highly tensed, MT: moderately tensed, LT: low tensed and R: relaxed

3.5.1.4 Results - OM4IS lane change

The lateral excursion of the AHBM's head COG under the lane change pulse, first to the to the left, exceeds the lateral excursion of the volunteer's corridor [3] to both sides. It has been stated in previous research studies that the environment surrounding the occupant plays an important role in its reaction [76], e.g., trying to avoid a contact with the vehicle's interior structure, e.g., the B-pillar. This effect can also be seen in the volunteer corridor: the first movement peak for the lane change, first to the left, is around 50 mm shorter than the peak in the lane change when moving first to the right. This avoidance is considered as an active movement, that is not yet implemented in the current THUMS TUC-VW AHBM version.

Moreover, it has been observed, that the seatbelt slips off the shoulder of the AHBM when moving to the left, whereas this was not seen in the volunteer experiments. This might be the reason why larger excursions are also observed to the left in the second peak of the lane change, first to the left.

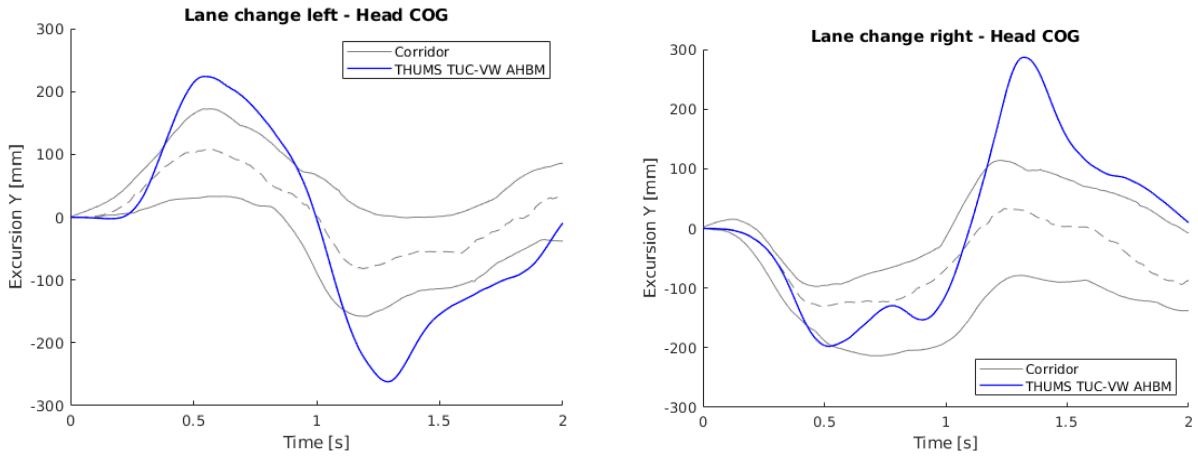

Figure 50: THUMS TUC-VW AHBM and volunteer corridor lateral excursion under the OM4IS lane change to the left (left) and right (right) condition

In the lane change, first to the right, the AHBM movement remains within the corridor in the first peak to the left, whereas it leaves the upper bound of the corridor in the second peak to the right (Figure 50). This is the same case as the first peak in the lane change to the left, the THUMS TUC-VW AHBM does not have the ability to actively rotate the head trying to avoid the contact with the side structure.

3.5.1.5 Results - OM4IS combined

The AHBM head kinematics match well the volunteer's corridor from Huber at el. [2] and [3], under the combined load case with respect to the shape of the kinematics (Figure 51). However, the moderately tensed behaviour, in the same way as for the braking load case (Figure 44), represents the lower boundary of the corridor instead of a stiffer behaviour.

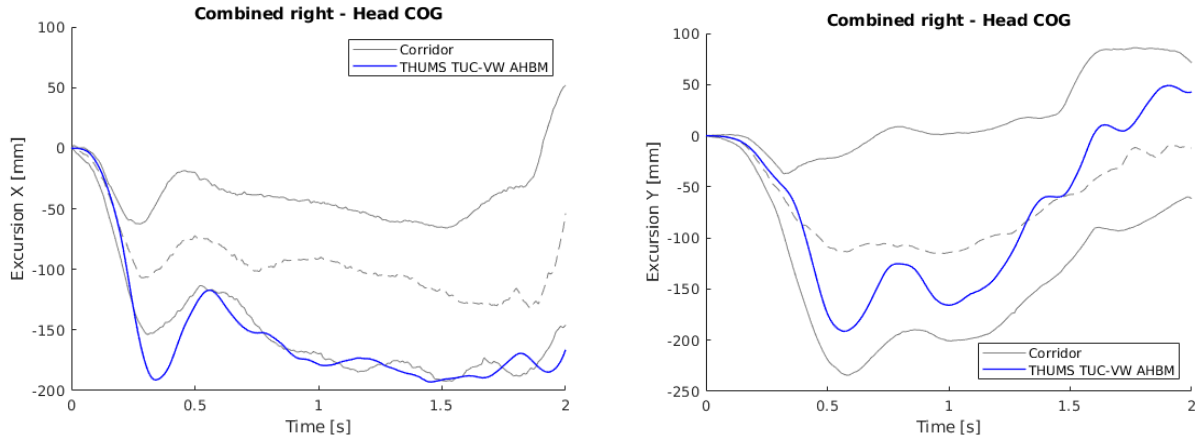

Figure 51: THUMS TUC-VW AHBM and volunteer corridor of the forward (left) and lateral excursions under (right) the OM4IS combined condition

3.5.1.6 Results - Chalmers autobraking and lane change [20] and [30]

The trend in the head forward and lateral excursion of the moderately tensed THUMS TUC-VW AHBM is comparable to the volunteer corridor under braking and lane change, for both, shape, and value (Figure 52).

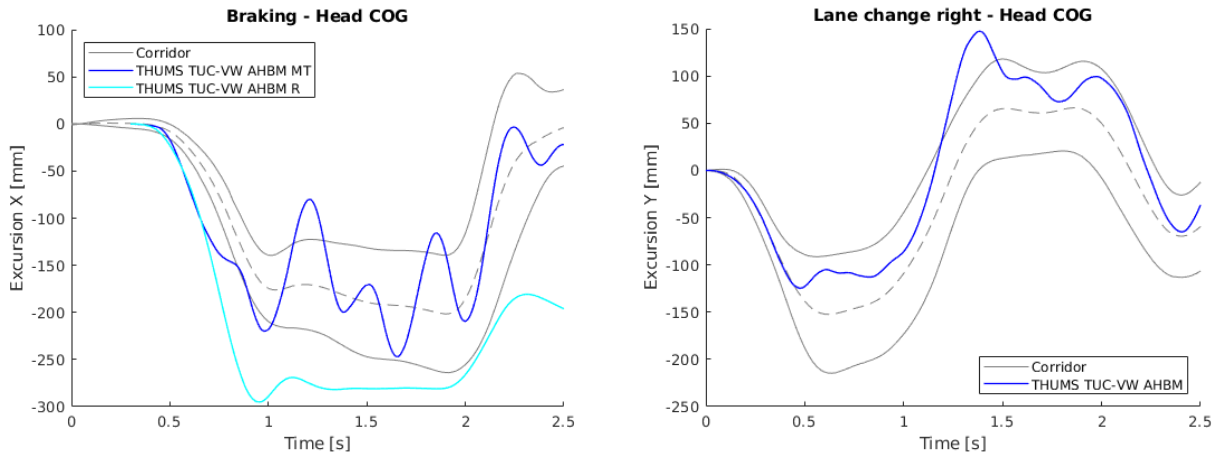

Figure 52: THUMS TUC-VW AHBM and volunteer corridor of the forward excursion (left) under the Chalmers autobraking condition and lateral excursion (right) under the Chalmers lane change condition

However, as already seen in the OM4IS braking load case, the moderately tensed condition in braking leads to relatively large oscillations.

Furthermore, the light blue curve in Figure 52 (left) represents the relaxed active state. Similarly, as in Figure 49, the model does not react to the external perturbation and thus, the curve lies outside the volunteer's corridor, as expected.

3.5.1.7 Conclusions

The THUMS TUC-VW AHBM matches well the head COG gravity kinematics under the presented load cases. However, further improvements are yet to be done. This AHBM can reproduce different levels of activation, nonetheless, the moderately tensed behaviour needs to be further enhanced in

terms of stability. Furthermore, the kinematics of the model under lateral pulses in a vehicle environment are larger than those of the volunteers. Further enhancement of the muscular control in the model is planned for the next steps, taking into account active movement control.

3.5.2 Literature review on age related active muscle properties

The goal of this work was to assess the impact of age-related changes in active muscle properties on pre-crash occupant kinematics.

Sarcopenia is an age-related loss of muscle mass that is very common in elderly populations. While the changes in muscle architecture that come with aging are well studied, the influence of these changes on occupants during pre-crash manoeuvres are less clear. The goal of this work was two-fold, to review the muscle architectural changes expected with age, and to model these changes during a pre-crash manoeuvre.

Physiological cross-sectional area (PCSA) is proportional to the force producing capabilities of a muscle as it considers both the anatomical CSA and the pennation angle (i.e., the angular deviation of muscle fibres relative to the origin-insertion line). PCSA can be calculated as the volume of a muscle divided by its fibre length. It has been found that muscle volume decreases as we age, with declines becoming significant by the fifth decade, and larger changes in the lower limbs compared to the upper body [31]. Similarly, muscle fibre length has also been found to decrease with age and muscles become less pennate [61]. While the decrease in muscle fibre length would cause an increase in PCSA, the decrease in muscle volume is a relatively larger change and several authors report a decrease in PCSA of 14-19% for elderly compared to young volunteers (Table 10).

In addition to the reduction in PCSA of elderly persons, authors have also noted that the specific force (i.e., force generating capacity of an individual muscle fibre) also decreases with age. It is thought that this decline in specific force is due to a breaking down in the excitation-contraction coupling that generates force due to an electrical signal [28]. This reduction in specific force in elderly compared to young has been found to range from 11-30% (Table 10).

Finally, the maximum velocity of muscle shortening may change with age. Maximum shortening velocity increases with decreasing pennation angle and decreases with a smaller ratio of fibre length over muscle length. While most studies report that muscle length tends to decrease in proportion to decreases in fibre length with age, maintaining a constant ratio [37]. Pennation angle is also known to decrease with age [37] and [61]. Taken together, it would be expected that maximum shortening velocity should remain constant or increase slightly with age. This is in contrast with the only available data this author could find which estimated maximum shortening velocity to decrease by 38% ([34]; Table 10) in elderly compared to young people by fitting voluntary contraction data to a hill muscle model. More data is required to understand this discrepancy.

	Range	References
PCSA	Decrease: 14-19%	[32], [61], [34], [38]
Specific force	Decrease: 11-30%	[32], [37]
Max shortening velocity	Decrease: 38%	[34]

Table 10: Elderly vs. young person active muscle architectural changes. Generally, in these studies, elderly persons were defined as individuals approximately 70-90 years of age, while young persons were defined as individuals approximately 20-40 years of age.

3.5.3 Modelling of changes to active muscle properties related to these changes

3.5.3.1 Methods

To investigate the influence of architectural active muscle property changes we implemented these changes in the SAFER HBM v9 [33]. The loading case was based on reproducing a 70 km/h lane-change with standard seat belts from Ghaffari et al. [30]. Details of the model, boundary conditions, and loading conditions can be seen in Larsson et al. [33].

To isolate the architectural active muscle properties changes from the influence of the active muscle controller, we recorded the muscle activation as a function of time from all hill-type active muscle elements in the model from the model during the load case used in this study while using APF-Y feedback control [33]. This muscle activity was then fed to the model in open-loop control. In this way the muscle activation timing and intensity was constant for all the architectural active muscle changes modelled.

The architectural active muscle property changes modelled were applied consistently on all Hill-type active beam elements in the model. Physiological cross-sectional area (PCSA) changes were implemented by reducing the cross-sectional area of the hill-type active muscle beam sections. Muscle specific force was changed in the model by adjusting the peak isometric stress (PIS) in the Hill-type muscle model.

A total of three simulations were included. 1) baseline open-loop control without any architectural changes made. This was simulated to allow comparison to the previous feed-back control model from Larsson et al. [33]. 2) baseline with PCSA reduced by 19%. 3) baseline with PIS reduced by 30%. These changes in active muscle architecture represent the largest mean differences reported between young and elderly volunteers in the data reviewed (Table 10).

3.5.3.2 Results

As expected, the head kinematics of the baseline model with open-loop active muscle control matched the response of the baseline model with feed-back controlled active muscles (Figure 53). This result was expected because the open-loop muscle activation scheme was based on the feed-back controlled model [33].

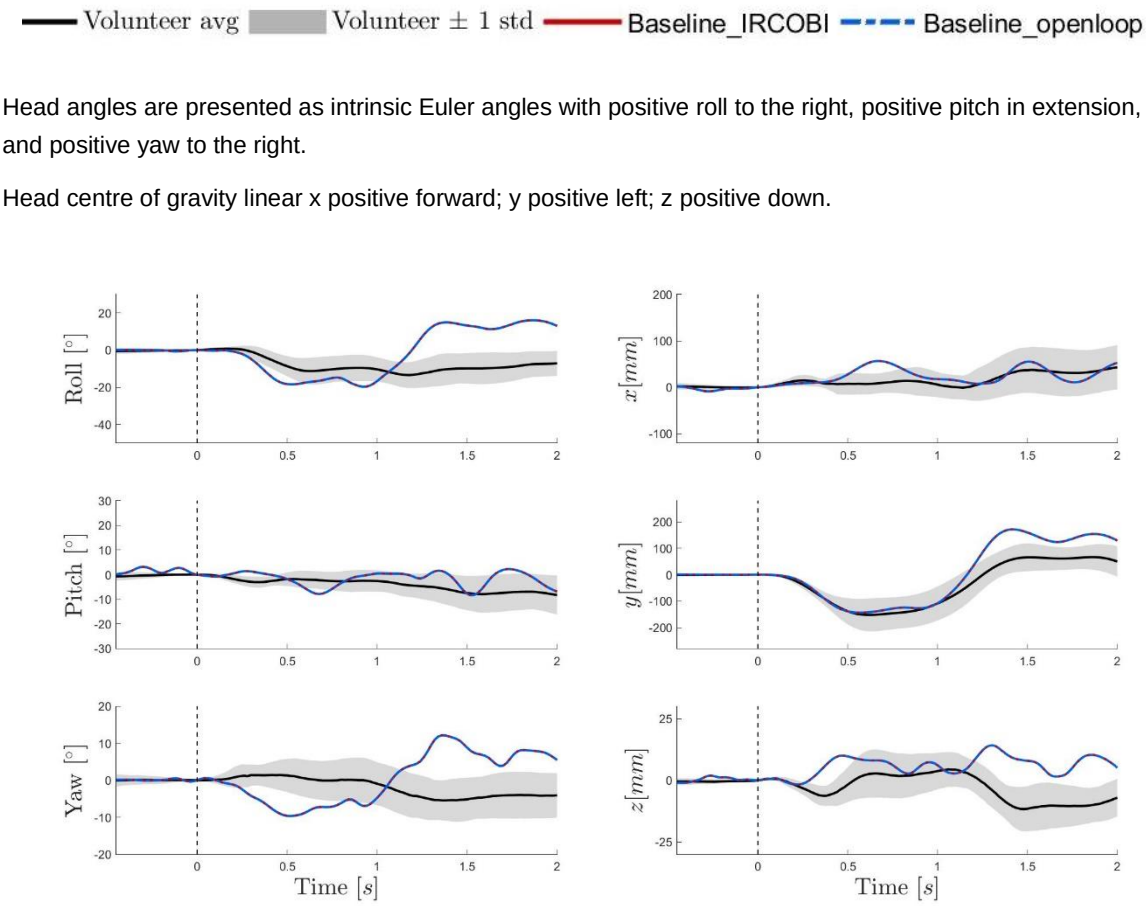

Head angles are presented as intrinsic Euler angles with positive roll to the right, positive pitch in extension, and positive yaw to the right.

Head centre of gravity linear x positive forward; y positive left; z positive down.

Figure 53: Model and volunteer head rotational and linear kinematics from a 73 km/h lane change to the right [30].

The head kinematics of the model were also generally consistent when comparing the baseline model, representing a young male, to the model with active muscle architectural changes to represent an elderly population (Figure 54). All models use the same open-loop active muscle activation scheme based on a feed-back control strategy presented in Larsson et al. [33]. The largest changes in head kinematics were seen in head roll, with peak increases of 2.9 and 4.2° (18 and 23% differences) over the baseline model for the PCSA and PIS reduced models respectively. The lateral linear displacement of the head increased by 9.1 and 12.7mm (7 and 10% difference) between the baseline model and the model with PCSA and PIS changes respectively. The timing of these four peak differences ranged from 0.70 to 0.79s after initiation of the lane-change manoeuvre.

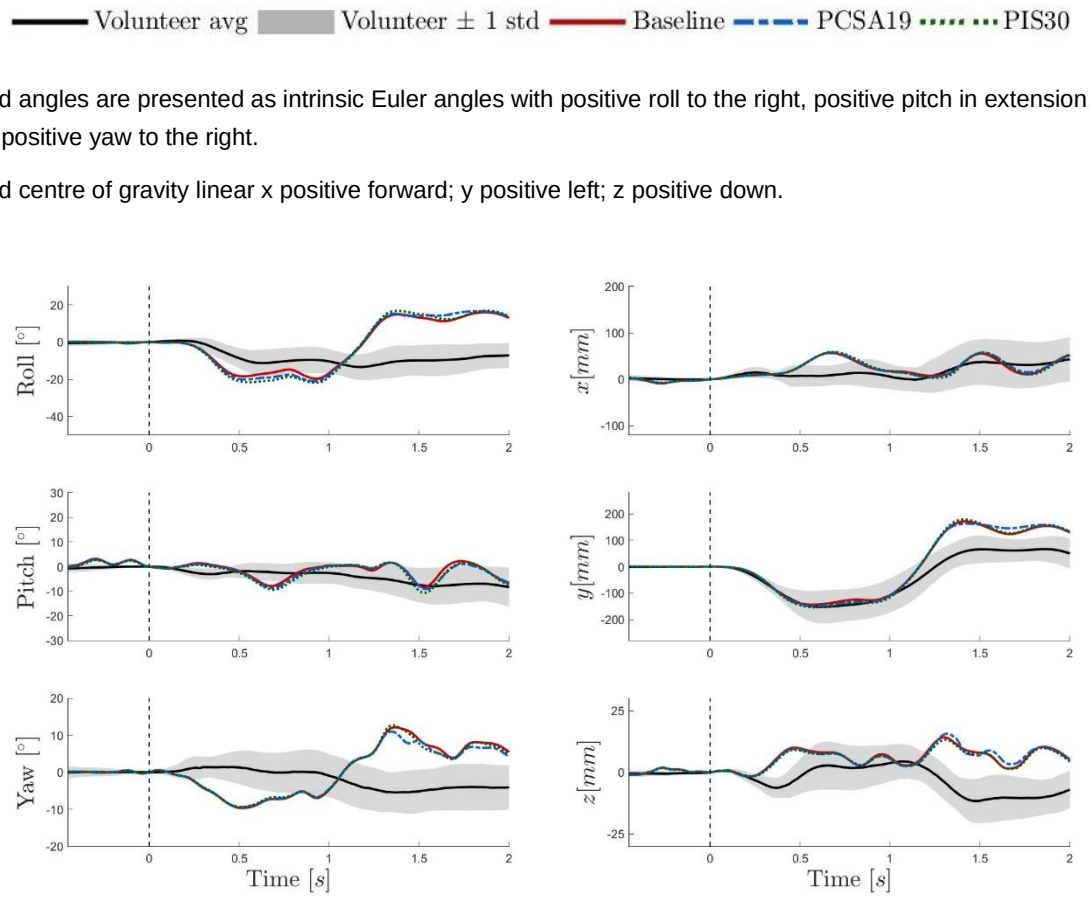

Head angles are presented as intrinsic Euler angles with positive roll to the right, positive pitch in extension, and positive yaw to the right.

Head centre of gravity linear x positive forward; y positive left; z positive down.

Figure 54: Model and volunteer head kinematics from a 73 km/h lane change to the right [30]. Comparing the baseline model (baseline) with a model with active muscle PCSA reduced by 19% (PCSA19) and a model with the peak isometric stress reduces by 30% (PIS30).

3.5.3.3 Discussion

The goal of this work was to explore the influence of architectural muscular changes associated with old age on occupant kinematics during a pre-crash manoeuvre. The SAFER HBM v9 was exposed to a 70 km/h lane change event with either baseline muscle properties representing a young male, or decreased PCSA or decreased PIS representative of an elderly male. We found modest changes as a result of these architectural muscular changes. Specifically, a maximum change of 4.2deg or 23% reduction in head roll with reduced PIS in elderly compared to young. Thus, architectural muscular changes associated with aging on their own may not be critical to model elderly occupants for a lane-change pre-crash event. However, the change in kinematics due to these muscular changes may combine with other variables associated with aging and produce important changes in occupant response during pre-crash events.

For example, both body mass index and stature are both know to vary with age [29]. These factors could be important to consider along with muscle architectural differences for pre-crash kinematic responses. Further, other neuromuscular changes may alter muscle activity with aging. Reaction time and potentially neurological delays may alter elderly driver's responses [62]. While some authors have shown altered neuromuscular control in elderly compared to young volunteers, through an increase in antagonist co-contraction [32], [35] and [36], although this finding is not universal [39].

Further, it has also been shown that changes in neuromuscular control are secondary to muscle architectural changes [37].

It should be noted that the modest changes in head kinematics of the model because of architectural muscular changes representing elderly populations were the largest mean changes in a spread of experimental findings (Table 10). It is expected that the changes in head kinematics seen in the model would be smaller if fewer extreme findings were used to set the values for architectural changes. The goal of these study was to study the influence of architectural muscular changes, and thus we wanted to see what the largest changes could be. Further, we maintained a consistent muscle activity scheme to isolate the changes in muscle architecture, but it is expected that a feed-back controller would reduce the changes we saw in head kinematics by increasing muscle activity.

One limitation of this work is that the architectural changes were applied uniformly across different body regions. This contrasts with findings that larger changes in muscle volume were seen in the lower limbs compared to the upper body [31]. Currently there is not enough data to specify body region specific muscle architecture changes.

3.5.3.4 Conclusion

While the PCSA and PIS changes associated with elderly persons investigated in this WP may not alone contribute a large amount to changes in pre-impact kinematic responses, their contribution should be further investigated with all the other variables that may change with age.

3.5.3.5 Further work

Combine the architectural active muscle changes studied here with other factors like changes in BMI and stature that are also associated with ageing.

3.5.4 Modelling an elderly population with active HBMs

The ability to react to road traffic emergency scenarios quickly and efficiently through actions such as steering, braking and lane changing is a fundamental skill in driving. However, studies have shown that the motor performance slows down with increasing age [48] and [49], potentially diminishing the ability of elderly drivers to react to dangerous traffic scenarios. The reaction time (RT), defined as the time interval between stimulus activation and response initiation, is a commonly used measurement to quantify this slowdown. Several biological factors, such as a slower rate of motor unit recruitment and transmission along with a delayed spread of the action potential across the muscle fibres were found to be key reasons behind RT elongation in the elderly [50]. Similarly, the motor capabilities of elderly people are also characterised through a reduction of the muscles' maximum isometric force F_{max}. As the amount of force produced by a muscle depends on the aggregate of individual motor units, a reduction of available motor units with age could limit F_{max}. while also resulting in longer RTs [51]. Moreover, a decrease in volume of fast twitch fibres combined with an increase in non-contractile material in the muscles such as fat and connective tissues play a significant role in the decrease of force production with age [52]. Having identified two main factors influencing the motor skills of elderly people, namely an elongation of RT and a change in F_{max} and contraction dynamics, appropriate scaling factors were derived from literature and simulations were performed to illustrate the effects of these factors on the force development characteristics while steering and the braking.

For the elderly population group, ages between 60 to 65 years were considered. Experimental data for the trends of force production in the different age groups were obtained from [53], where an overall decrease of the average force of 45% was found in elderly people. Furthermore, a 25% lesser

maximal force and a 40% lesser maximal shortening velocity in the elderly in comparison to younger people is described in [54]. Experimental data from [52], where an overall increase in RT of 15 ms in the elderly population was observed, were referenced to incorporate the reaction time delay.

3.5.4.1 Methods

All sample simulations were performed with the Total Human Model for Safety (THUMS) Adult Male 50th percentile Occupant model of version 5.02.1 acquired under academic license which, in its original state, is representative of a 30- to 40-year-old average American male. It was subjected to the bracing scenario supplied in the model validation catalogue alongside with the model. Here, the occupant pushes his right foot on a brake pedal and grips the steering wheel with his hands with a pre-defined muscle stimulation intensity. Changes were made to the settings of the LS-DYNA internal muscle material *MAT_156 [55] to account for the effects of ageing. The Peak Isometric Stress (PIS) value was reduced by 45% for all the muscles to incorporate the reduction of F_{max} described in [53]. Modifications were also done to the contraction dynamics of the muscles by scaling down the Stress vs Strain Rate (SVR curve) according to the directions given in [54], which corresponds to the muscle's force-velocity relationship. Lastly, the muscle activation curves were modified to incorporate the RT delay of 15 ms observed in [52].

Four distinct scenarios were considered as a comparative study of the steering and pedal forces resulting from the applied bracing scenario and the changes to RT, F_{max} and the contraction dynamics. (I) Young subject age 30 to 40 years with standard THUMS properties, (II) Elderly subject with reaction time delay, (III) Elderly subject with reduced F_{max} and adjusted contraction dynamics and (IV) Elderly subject with RT delay, reduced F_{max}, and adjusted contraction dynamics. The time history curves of steering wheel and brake pedal forces for each of these scenarios can be seen in Figure 55. The achieved maximum forces and the time it took to reach them are listed in Table 11.

a)

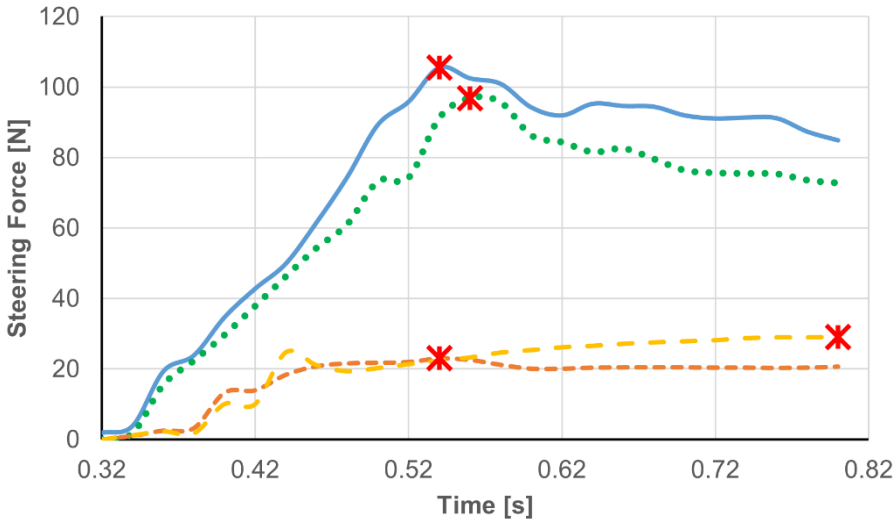

b)

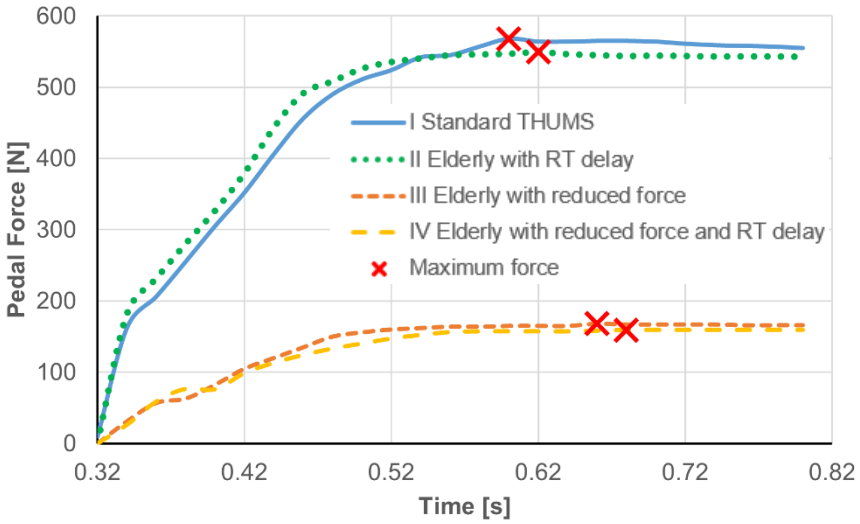

Figure 55: Time history curves of a) steering wheel force and b) brake pedal force for scenarios I to IV

3.5.4.2 Results

The baseline simulation in scenario I yielded a maximum steering force of 105.5 N and a pedal force of 568 N at 540 ms and 600 ms respectively [56]. The induced reaction time delay of scenario (II) resulted in a change in curve characteristics which went beyond a simple temporal curve shift (Figure 55b). This could be attributed to the fact that the difference in muscle activation timing could have influenced synergetic muscle effects caused through otherwise synchronous activation, leading to a quicker rise in brake pedal force than in the baseline simulation. An even greater change in force can be seen in scenarios III and IV, where the downscaling of F_{max} and the adjusted contraction dynamics lead to a maximum force reduction of roughly 70%. The additional elongation of RT in scenario IV further delays the point of maximum force for both pedal and steering forces. Scenario IV, which is representative of an elderly driver with reduced force production capabilities and an elongated reaction time, therefore not only yielded lower maximum steering and pedal forces than the middle-aged occupant modelled in scenario I but also took the longest out of all scenarios to produce maximal forces. When viewed as a whole, the sample simulations indicate that incorporating the properties associated with an elderly subject influence both the reaction time and the maximal forces which the driver can produce. This effect should be considered when developing active safety systems. However, to assess the driving capabilities of the elderly and to gain a more comprehensive perspective on the functioning of the combined effects of reaction time delay and reduced force-velocity relationship, further detailed research must be conducted in the future.

Scenario No.	Steering Wheel Force		Brake Pedal Force	
	Force [N]	Time [ms]	Force [N]	Time [ms]
Scenario I	105.5	540	568	600
Scenario II	96.8	560	549.5	620
Scenario III	23	540	168	660

Scenario No.	Steering Wheel Force		Brake Pedal Force	
Scenario IV	29.1	800	159	680

Table 11: Maximum Forces and corresponding time steps

3.5.5 Development of eastern anthropometry small female active HBM

3.5.5.1 Methods and model

Active HBMs are developed to capture human responses in low g loading scenarios, which are characteristic of the pre-crash phase. Significant progress has been made in the past decade over development of mid-size male Active HBMs. The priority at present is to create methods that allow the creation of Active HBMs of different anthropometries to address the topic of integrated safety for all vehicle occupants.

As a step in this direction, a method to transfer muscle Physiological Cross-Sectional Area (PCSA) values from A-THUMS-D M50 50th %ile male Active HBM (Active Human Body Model developed by Mercedes-Benz AG) to A-THUMS-D F05 CNIS 5th %ile female Active HBM was developed based on data available in literature and easily measurable physical quantities. The dependency of this method on easily measurable physical quantities makes this method applicable to other anthropometries as well, for example, child models. A detailed description of the method is reported in Mishra *et al.* [18].

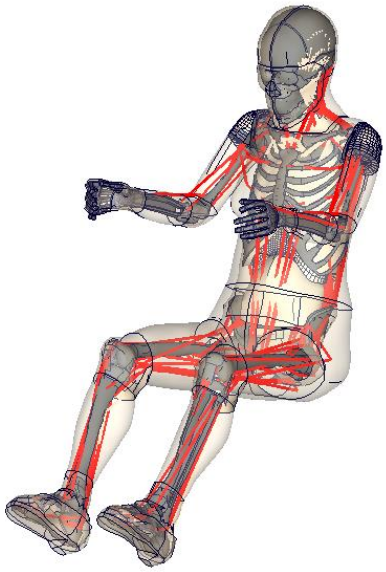

Figure 56: A-THUMS-D F05 CNIS

A-THUMS-D F05 CNIS (Figure 56) represents a 5th percentile Chinese anthropometry female with a height of 1,484 mm and weight of 55 kg developed based on the China National Institute of Standardization (CNIS) database. The model features 172 muscle groups (86 on each body side) represented with 878 LS-DYNA™ ELFORM 3 beams. Muscle elements are assigned with LS-DYNA™ MAT_MUSCLE (MAT_156) governed by Hybrid Equilibrium Point Controller (Hy-C) [17]. Relaxation of the model was done as per recommendations from Shelat *et al.* [11]. Muscles in the model are routed around the joints to capture curved muscle paths.

A part of *performance evaluation* of A-THUMS-D F05 CNIS was conducted in the course of OSCCAR project and will be extended into OSCCAR China project. Following load cases were studied in the current work:

a) OM4IS Phase 2 1*g* braking

Braking manoeuvre tests involving volunteers seated in co-driver position were conducted by Huber *et al.* [3] and data for vehicle acceleration, head excursions (at ear level), torso excursions (T5 level) have been reported. A representative sled model from the test vehicle (Mercedes-Benz S-Class) with A-THUMS-D F05 CNIS seated in simplified test seat (Kirschbichler *et al*. [4]) in co-driver position was prepared for LS-DYNA™ simulations. Motion pulse from (Huber *et al.* [3]) was prescribed to the simplified vehicle model and 2500ms simulations were conducted in two configurations, namely ‘Active’ and ‘Relaxed’.

- *Active Configuration* – Configuration of A-THUMS-D F05 CNIS implemented with active muscles.

- *Relaxed Configuration* – Configuration A-THUMS-D F05 CNIS where FE muscles are present but have no activity is referred to as ‘Relaxed’ configuration.

A-THUMS-D F05 CNIS simulations in Relaxed configuration were conducted to clearly understand the influence of muscles on the kinematics based on the difference between kinematics of Active and Relaxed configuration.

b) Autobraking Event as per Ólafsdóttir *et al.* [20]

Volunteer tests involving autobraking event were reported by Ólafsdóttir *et al.* [20] with male and female volunteers both in presence and absence of an active belt pre-pretensioner. The The FE environment representative of the tests has been described in described in detail in Section 3.2.3. In the current work, autobraking event with standard belt (active pre-pretensioner absent) was simulated with A-THUMS-D F05 CNIS in active and relaxed configuration.

It should be noted that volunteer test data for active occupant behaviour is not readily available. Therefore, the A-THUMS-D F05 CNIS model performance is evaluated with the above volunteer data representing average male and female anthropometry. A discussion of the consequences is found in the following section.

3.5.5.2 Results and discussion

a) OM4IS Phase 2 1*g* braking

The kinematics of Relaxed A-THUMS-D F05 CNIS revealed torso excursions within the maximum excursions reported in Huber *et al.* [3]. This was attributed to restraint offered by the shoulder belt, which operated in locked regime in majority of the severe braking event simulated in the load case. The effect of lumbar and back muscles recruited in the case is also to restrict motion of torso, hence, the excursions of A-THUMS-D F05 CNIS in Active configuration are lower as compared to relaxed configuration. The target length inputs required for Hy-C governing the muscles were iteratively modified to achieve a good fit with the corridors reported in literature.

Figure 57 illustrates the kinematic comparison between Relaxed and Active HBM and difference between kinematics of the two models can be clearly seen.

It must, however, be highlighted that the corridors reported in Huber *et al.* [3] were developed for mid-sized male anthropometry and may not be directly applicable to A-THUMS-D F05 CNIS model which represents an Eastern anthropometry small female. For this reason, the term ‘performance evaluation’ has been used in the study instead of ‘validation’. Methods for scaling existing AHBM validation corridors, to make them applicable for validating AHBMs of other anthropometries are needed as the focus shifts towards development of a population of such models, see Section 3.1.3.

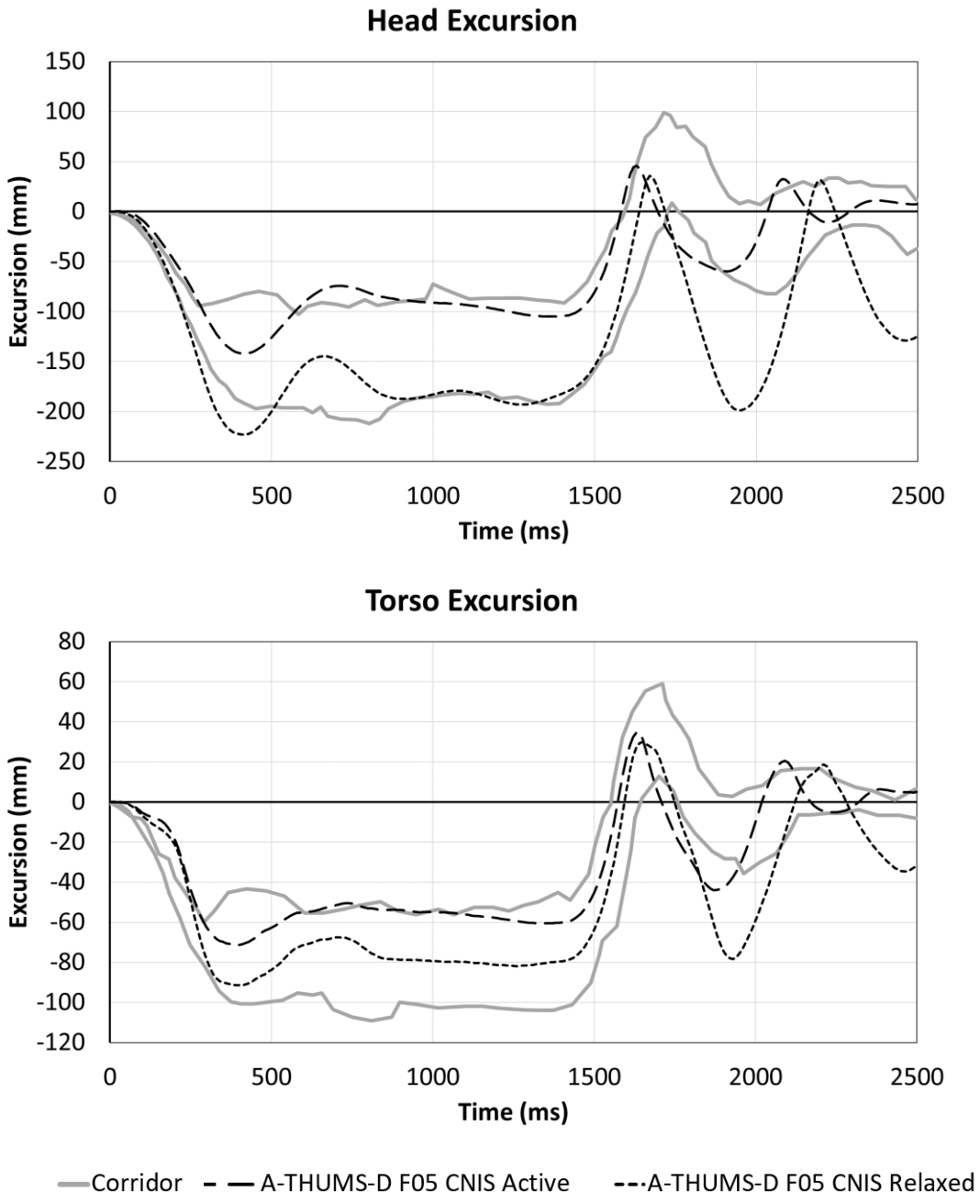

Figure 57: Kinematics of A-THUMS-D in OM4IS phase 2 braking simulations

b) Autobraking event as per Ólafsdóttir *et al.* [20]

The kinematics of A-THUMS-D F05 CNIS overlayed with volunteer corridors are shown in Figure 58. The simulated kinematics of head and T1 in the current case show a trend similar to the head and T5 excursions in OM4IS Phase 2 emergency braking, both for relaxed and active configuration. For the relaxed configuration, the head COG movement exceeds the corridor initially and then stays around the maximum excursion reported in tests. T1 excursions stay inside the corridors for majority of the simulated event. In active configuration, excursions are reduced relative to relaxed configuration and correlate well with the volunteer corridors.

Kinematic corridors for females reported in Ólafsdóttir *et al.* [20] were used for the performance evaluation but may not be directly applicable for A-THUMS-D F05 CNIS since these corridors were developed from the tests involving female volunteers with a different anthropometry (average height

= 166.6 cm) as compared to A-THUMS-D F05 CNIS (height = 148.4 cm). This is similar to the limitation highlighted in the previous section describing OM4IS Phase 2 braking simulation results. As such e.g., head excursion can be expected to be smaller for the model in comparison to the volunteer data. As the trajectories of the active model are found at the lower boundary of the volunteer corridor, the results could be interpreted in a way that supports this assumption. Nevertheless, other factors also contribute to reduced excursion and more validation is advised.

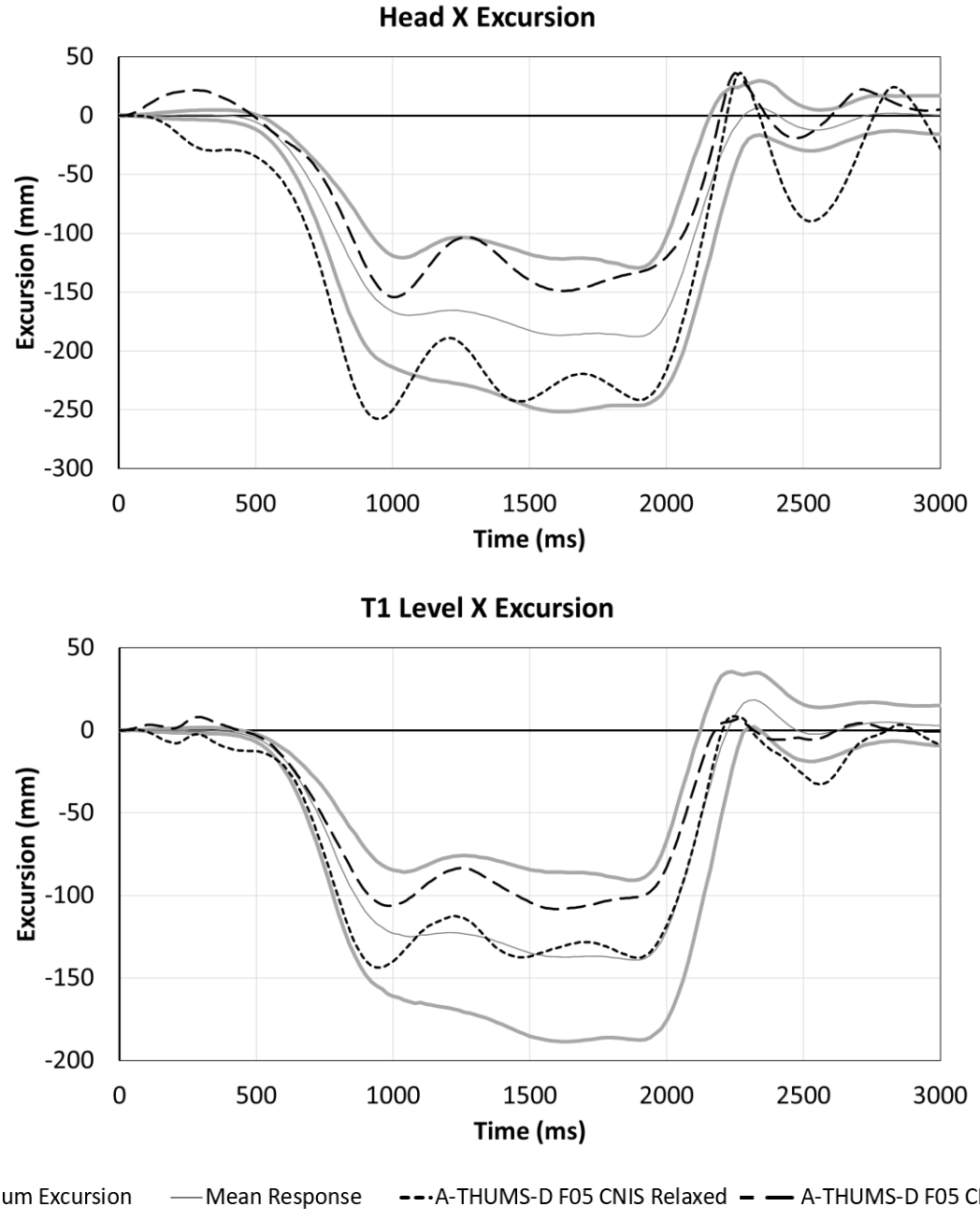

Figure 58: Kinematics of A-THUMS-D F05 CNIS in autobraking event as per Ólafsdóttir et al. [20]

In both braking cases simulated, by OM4IS (a) and Ólafsdóttir *et al.*(b), a *wobbling behaviour* can be seen during the initial phase of motion with the model moving forward and then rebounding before stabilizing. This causes a local minimum in the trajectories. This effect is not so pronounced in motion recorded from volunteers [3] and [20]. The motion is damped in volunteers. One of the contributing factors is probably co-contraction of different muscles acting on head-neck and thoracic joints. This

effect is not captured by the Hy-C present in A-THUMS-D F05 CNIS in this study which primarily activated only the extensors in these regions to restrict forward motion.

Further work on performance evaluation of A-THUMS-D F05 CNIS including body region level validation of arm and HBM level validation using cases also involving lateral accelerations will be done in the OSCCAR China Project.

3.5.6 Special focus on occupants with reduced mobility

An often-overlooked group of drivers in the assessment of vehicle safety is the one of the wheelchair-bound occupants. This is especially troubling seeing that 87% of American wheelchair users surveyed by Brinkey et al. [57] not only had access to a privately owned vehicle, 55% of them solely used this mode of transportation [57]. Despite this clearly visible need for the use of automotive vehicles, methods to secure wheelchairs in the vehicle itself are still far from optimal. A study of car crashes involving occupants seated in wheelchairs performed by Schneider et al. [58] showed that nearly 25% of them died due to injuries related to the crash or related medical complications even though the crash events were of minor or moderate severity [58]. As it is most likely that these crashes would not have resulted in life-threatening injuries if the standard vehicle's seat and seatbelt systems had been used, the overview study of Schneider et al. [59] came to the conclusion that wheelchair-bound occupants should utilize the vehicle seat instead of a wheelchair secured in the car's interior.

Considering that highly automated vehicles could be an attractive mobility option for wheelchair-bound occupants because of their extensive assist features while driving, two AHBM simulations were performed to illustrate the kinematic differences resulting from a loss of lower limb control. All simulations were done with the Total Human Model for Safety (THUMS) Adult Male 50th percentile Occupant model of version 5.02.1 acquired under academic license. Because it has been established that most secure method of seating for both healthy and mobility impaired occupants is the standard car seat provided by the vehicle's manufacturer, the car interior, seatbelt, and seat were taken from the bracing scenario supplied alongside in the model validation catalogue. All muscles of the healthy occupant were activated using the stimulation curves provided with the bracing scenario while the stimulation of the leg muscles was disabled for the wheelchair user. Model movement was introduced by recreating the seat rotation movement from protection principle 1 described in OSCCAR deliverable 2.4 [85] where the occupant's seat was rotated 30° in a time frame of 350 ms. The leg kinematics of the healthy and wheelchair bound occupants were quantified by comparing the trajectories of the centres of gravity (COG) of the upper and lower left leg (Figure 59).

While the resultant displacement curves for both occupant types follow the same basic trajectory, the leg bracing movement of the healthy passenger leads to a larger displacement of both the upper and lower leg's COG because it shifts the occupant's seating position to the left during the rotation.

The results presented here are by no means an extensive study of the effects of lower limb paralysis on occupant behaviour during pre-crash repositioning manoeuvres. However, they do illustrate a clear difference in leg kinematics between healthy and occupants who use wheelchairs, which should be accounted for during the development of active safety systems. This is especially relevant as low acceleration volunteer studies conducted by [89] showed that the pre-impact contraction of the musculature caused a shift in the load distribution so that larger loads were redirected through the legs towards the vehicle's floor. Such a pre-contraction of the leg muscles would be impossible for occupants with paralysed lower limbs, which places higher loads on the restraint systems. Hence, further detailed research and simulation work should be conducted to evaluate the additional risks for occupants with reduced mobility in car crash scenarios.

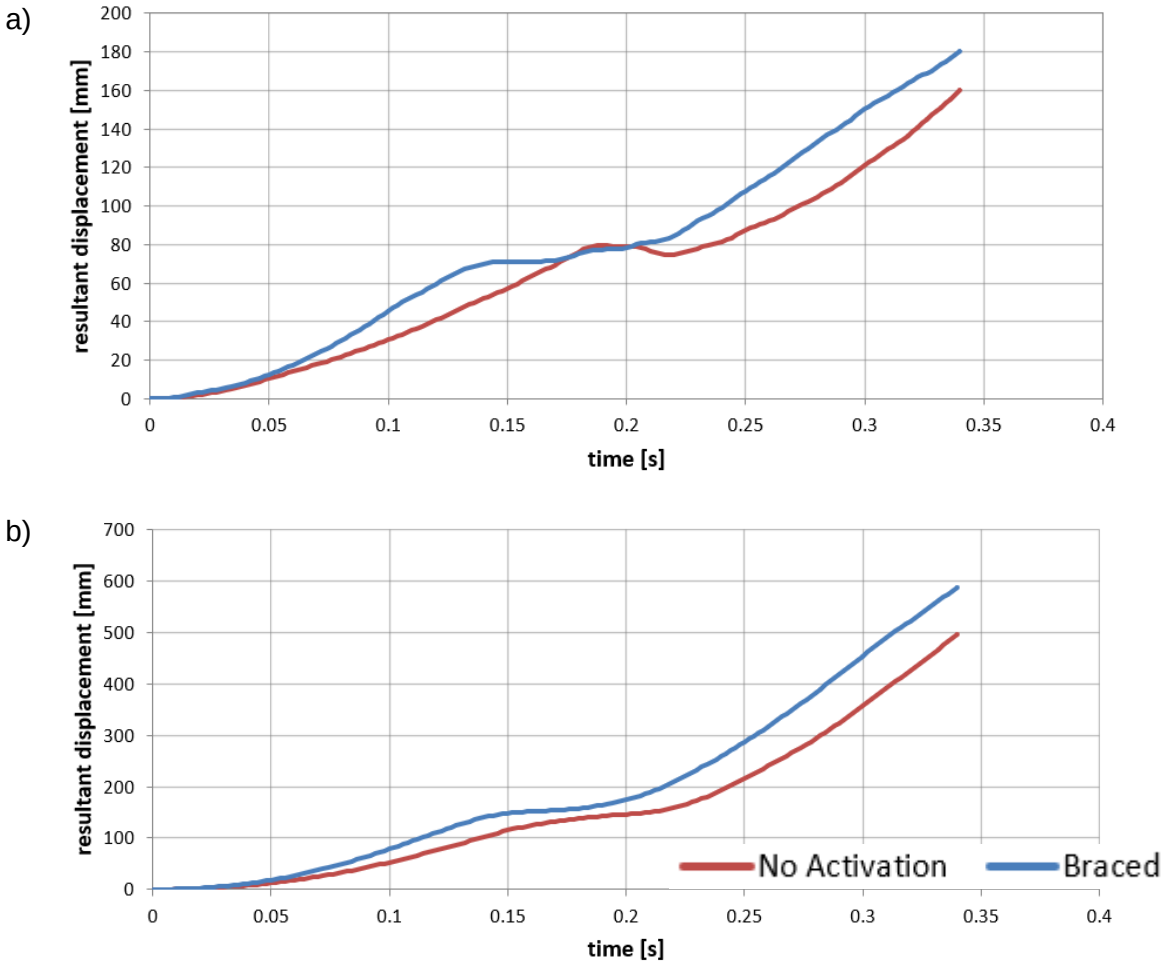

Figure 59: Resultant displacement over time for a) COG of upper leg and b) COG of lower leg

3.5.7 Simulations of both the pre-crash phase and the in-crash phase

Nowadays, active HBMs are merely used during the pre-crash phase under low g-load cases. Many researchers ([1], [2], [3], [30], [65][66]) have stated and proven that occupants have enough time to react by bracing their muscle or performing an avoidance manoeuvre during the pre-crash. These actions may change their position prior to the crash, influencing the kinematics and the injury outcome. Due to the short duration and the high level of the loading of the in-crash phase, no active muscle response of the occupants is expected, thus, researchers have decided to use AHBM in the pre-crash phase and passive ones in the in-crash phase. However, as previously mentioned, it is important to take into account the position of the HBM after the pre-crash phase. The most common approach to do so is to transfer the posture and velocity from the AHBM after the pre-crash phase to the initial state of the passive HBM in the in-crash phase [77].

Another approach is to perform seamless simulation of the pre- to in-crash phase using one single model, namely an active HBM [78] and [80]. If this approach is followed, then the first question that arises is whether the effect of the active HBM influences the outcome of the study [78], [81]. The second question that needs to be answered is how to handle the activation of the HBM in the in-crash phase [78], [81]. Few experiments have been performed with volunteers under high accelerations (>10 g) [82], [83] and to the authors' knowledge in none of them the muscle activation

was measured. Thus, currently no data regarding neuromuscular control under such conditions has been analysed.

3.5.7.1 Methods

To evaluate the potential effect of the pre-activation of the muscles during the pre-crash phase a numerical study has been performed using the THUMS TUC-VW AHBM (Figure 60). Additionally, the THUMS TUC 2019 passive HBM was used as baseline for comparison.

The AHBM was positioned on the vehicle seat model used in Work package 2 in the protection principle 1 [85]. The model was subject to a braking pulse during 500 ms, reaching about 1g at 400 ms. Afterwards, a frontal crash pulse was applied for 100 ms, reaching a maximum of 54 g's at 550 ms.

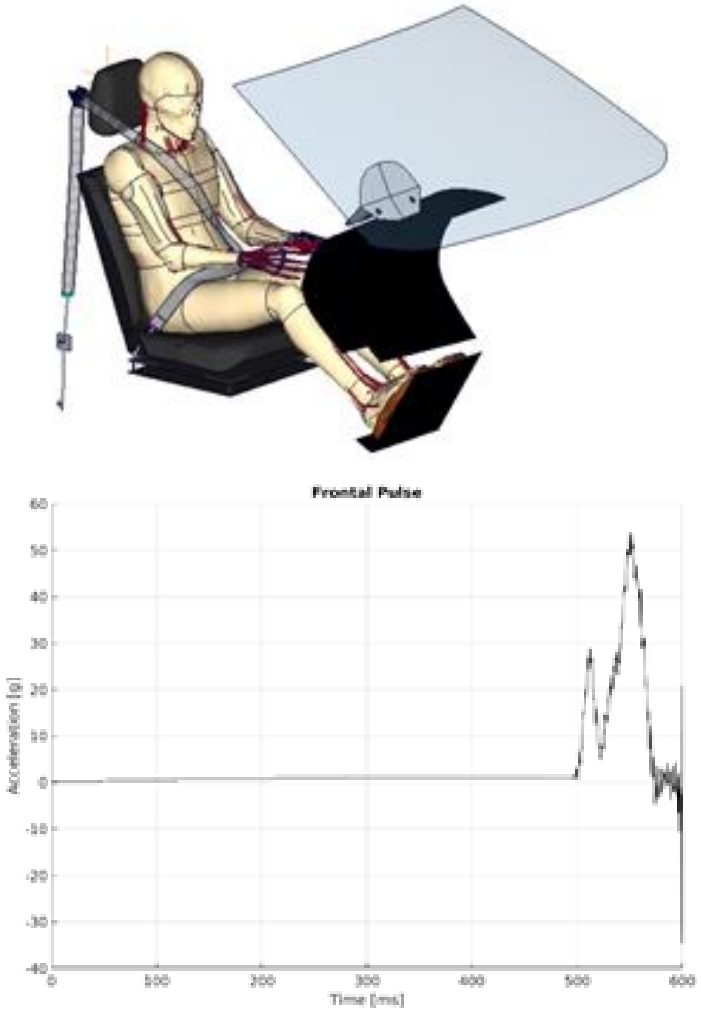

Figure 60: On the left-hand side, the THUMS TUC-VW AHBM positioned in the vehicle interior on the passenger seat with the hands on the thighs. On the right-hand side, the pulse applied to the vehicle is shown.

In this report, two strategies of muscle activation during the in-crash phase with the THUMS TUC-VW AHBM are reported: 1) muscular control and 2) no muscle activation. The former to account for the influence of the muscle activation during the in-crash phase. The later to compare with the

passive THUMS TUC HBM in the in-crash. Additional muscular activation approaches using the same model setup have been previously reported here [78], [81].

3.5.7.2 Results

The trajectories of the centre of gravity of the THUMS TUC-VW AHBM and the passive THUMS TUC model are presented in Figure 61. Both AHBM behave similar until they come into contact with the airbag. Thereafter, the AHBM with the muscular control strategy prevents the head extension. In contrast, the absence of activation (orange curve) subjects the head-neck complex to higher rotations. Thus, for instance the brain injury risk is expected to be higher if the AHBM is used with no muscle activation during the in-crash phase [78], but also neck injury indicators could be affected as well.

Furthermore, the passive HBM has been updated to the posture of the AHBM after the pre-crash phase and subjected to the same in-crash pulse. However, as it is shown in Figure 61 the head of the HBM flexes prior to the interaction with the airbag, therefore the contact point with the airbag is lower than for the AHBM. Additionally, it moves faster than the AHBMs in the rebound phase.

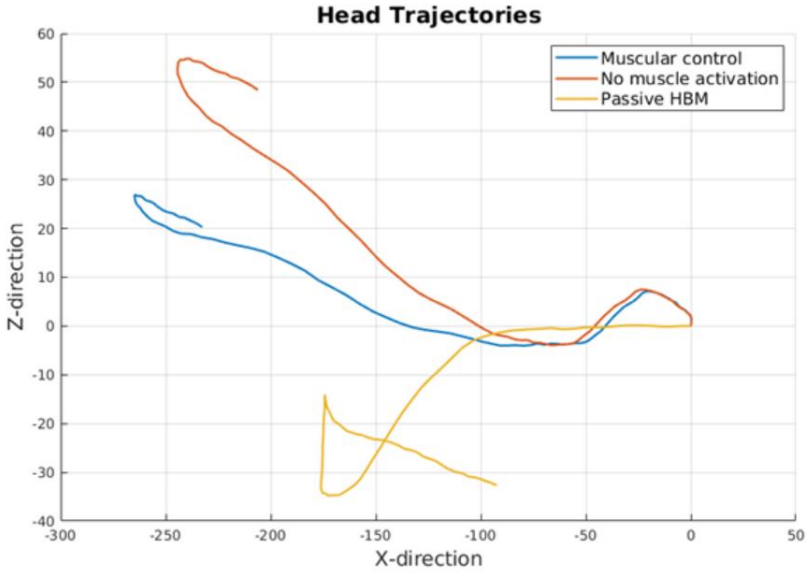

Figure 61: Comparison of the centre of gravity of the head trajectories between the THUMS TUC-VW AHBM using two control strategies during the in-crash phase and a the THUMS TUC passive HBM.

3.5.7.3 Conclusions

The THUMS TUC-VW AHBM is capable of being used in seamless simulations including both, the pre- and in-crash phase. However, there are some open-points on how to handle the muscle activation during the in-crash phase, since to the author's knowledge very limited information is available on the neuromuscular control of humans under high accelerations.

The material properties of the soft tissues were adapted in the THUMS TUC-VW AHBM (Subchapter 3.4.5). However, the passive model has not been re-validated under high g load cases using PMHS experimental data after these changes were performed. This task is planned for the next steps.

3.5.8 Lower Limb Control in the Madymo AHM

In the work described in OSCCAR deliverable 2.4 an issue was encountered with the kinematics of the lower limb. Under certain conditions when modelling precrash situations, the hip rotated strongly medially and the knee flexed (see Figure 62); as this was not prompted by any direct loading of the leg, it was concluded that the source of the motion lay in the active muscle control system of the model.

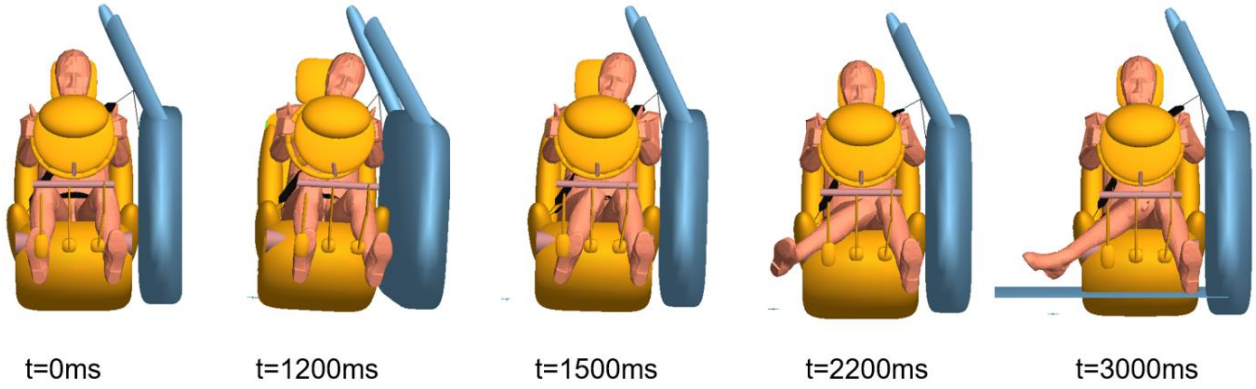

Figure 62: Lower limb kinematics in lane change manoeuvre

To investigate whether the source of the issue lay in the control system, the skin and shoes were removed from the lower half of the AHM, which was then subjected to a series of acceleration loads. It was found that a lateral acceleration of 0.5g triggered the reaction clearly within 1 second of simulation time (see Figure 63)

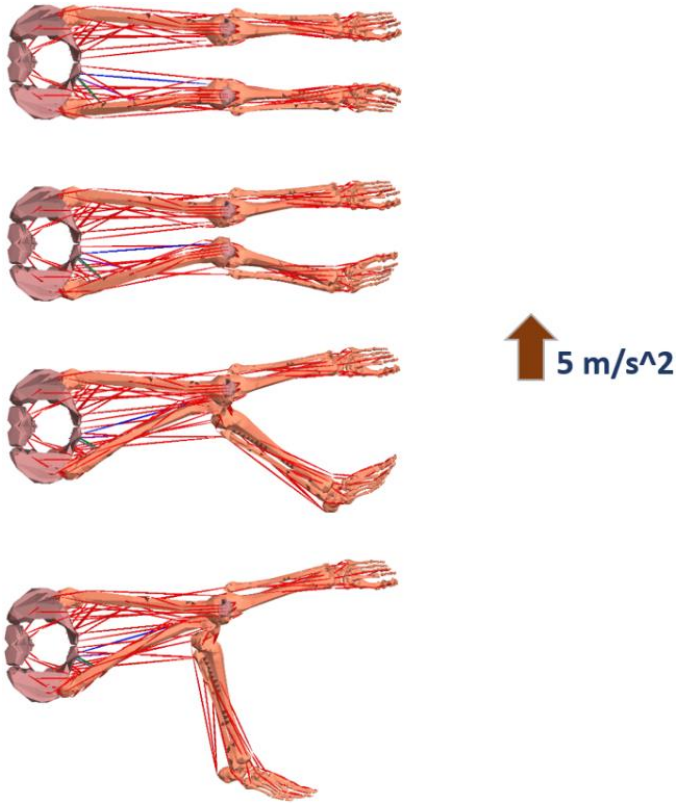

Figure 63: Development of lower limb dysfunction under 1 sec. constant lateral acceleration

The application of the acceleration load as shown above first caused the right leg to adduct.

- This caused the HipR_abduction_only signal to increase to counteract the motion, but in doing so a slight medial rotation was introduced
- As this movement increased, the HipR_lateralrot_only signal attempted to correct this combination of adduction and medial rotation and return the hip to its original position. In doing so, the *biceps femoris longus* muscle was activated, initiating knee flexion
- Finally, the KneeR_extension_only operator was activated to attempt to straighten the leg, but succeeded only in locking the knee as the *biceps femoris longus* was still attempting to counteract the medial rotation

With this ascertained, the muscles recruited under lateral rotation in the sitting AHM could be isolated and examined closely. It was found that the *gluteus medius posterior*, which supports lateral rotation in the standing posture, causes an undesirable rapid medial rotation when the hip is flexed 90 degrees toward the trunk. This renders its action in the sitting AHM undesirable to counteract lateral rotation and was a chief cause of the instability. In addition, the *adductor magnus inferior* is recruited to provide lateral rotation while it in fact provides medial rotation, the moment arm changing with high knee flexion [86]. Figure 64 shows the location of these two muscles in the AHM.

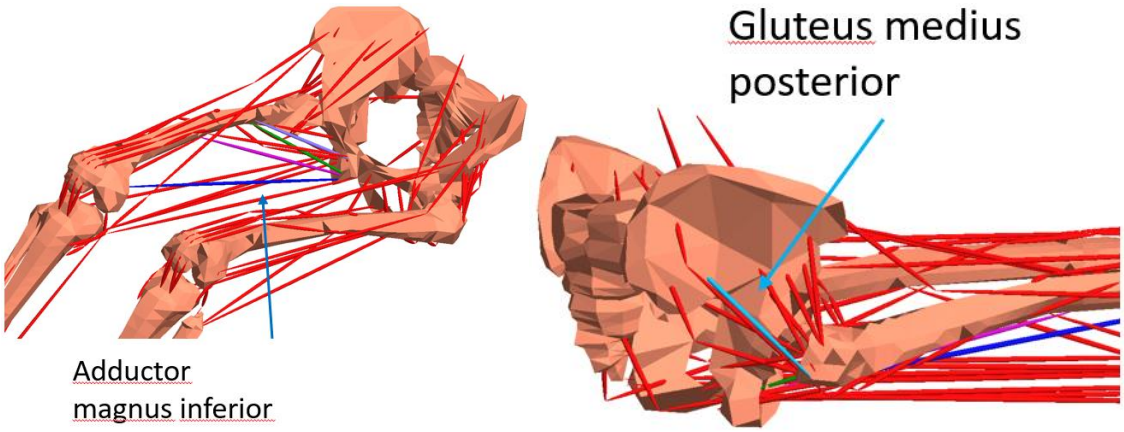

Figure 64: The positions of the medially-rotating muscles in the AHM

The *gluteus medius posterior* in the sitting AHM was removed from the lateral rotation control group, and the *adductor magnus inferior* transferred from lateral rotator to the medial rotator control group.

The modified AHM was then run with a lateral acceleration and the leg motion was found to be stable. Figure 65 shows the kinematics of the modified AHM in the lane change loadcase shown in Figure 62; the excessive medial rotation post-1500 ms is solved. In addition, the complete validation tree of the AHM [87] was run and the response of the model was found to be improved or unchanged.

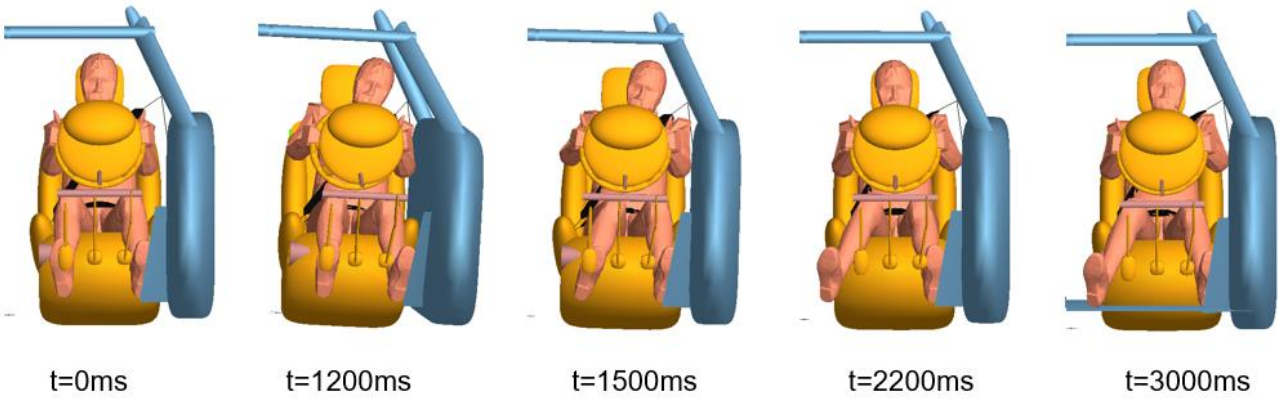

Figure 65: Lower limb kinematics of the modified AHM in lane change manoeuvre

4 DISSEMINATION, EXPLOITATION AND STANDARDISATION

Within this section, it should be described how the performed work can be used for dissemination, exploitation, and standardisation activities. If such activities have already been performed, it should be clearly highlighted and referenced.

Most of the research presented in this report will be available after the OSCCAR project is finished and may be used for the development of active and reactive HBMs. These models are to some extent, and will soon be even more, used in the development of superior restraints. While some works have been shared with third parties via repositories other works will or have already been published in scientific journals or conference proceedings.

5 CONCLUSIONS

Out of the 25 volunteer test datasets that were identified and that involved applying accelerations that mimic pre-crash events to human volunteers the subtask group choose five datasets and shared these with the OSCCAR partners. In addition, models of the original set ups that were used in the original volunteer tests were developed, validated, and made available for evaluations of active HBMs.

Female volunteer test data, from a subset of tests carried out in a project in 2016, were analysed and made available in a publication. The tests included were those where the volunteers were in the passenger seat and exposed to lane change to the right and lane change to the right with braking with a standard belt or with a reversible pre-tension belt. Maximum head and torso excursions, muscle activity and muscle onset times were compared in the publication. The published results complement the previously published results from male passengers subjected to the same loading scenarios. The data provided can be used for validation of AHBMs of female occupants

Male and female volunteer test data, also these from a subset of tests carried out in 2016, were processed. The tests included were those where the volunteers were in the driver seat and in the passenger seat and were exposed to lane changes, with or without braking, braking only and U-turns. In most tests a standard belt was used while in a few test conditions a reversible pre-tension belt was used.

Previous research indicates large variabilities among volunteer responses to evasive manoeuvres representative of pre-crash situations. Within the OSCCAR project a study was carried out to explore the influence of occupant characteristics (age, stature, and sex) on their body kinematics in evasive manoeuvres. The study also targeted the development of a statistical model that can be used to predict body kinematics of volunteers with any age, stature, and sex.

To advance the design of future volunteer tests, a typical volunteer test setup was reproduce using a state-of-the-art active HBM to study the sensitivity of parameters suggested to affect the kinematics. The study will serve as a guideline on what to measure in future volunteer tests and how to best reproduce volunteer tests virtually.

The extended Hill-type material (EHTM), a user-defined material model with more realistic dampening behaviour and eccentric force-velocity relation than previous models, was updated to work in LS-DYNA and VPS. The updated model offers four separate control functions; an open-loop alpha controller, the length-based closed-loop lambda controller, a hybrid controller which combines the alpha and lambda control approaches and a length-based reflex controller. Both the LS-Dyna and the VPS version of the ETHM models were, when implemented in a model of a human arm, found to provide humanlike responses. The EHTM was also implemented in the neck region of the THUMS TUC-VW AHBM developed for VPS. In an evaluation of the model in head drop tests the EHTM better depicted the muscle behaviour of volunteers than did the traditional Hill-type model.

While several active HBMs predicts the passenger kinematics in braking and steering events, few predicts driver kinematics in these events. As part of the development of an active HBM representative of a driver, a controller of the muscles spanning the elbow and shoulder joints were developed. The intermuscular load sharing was based on data from experiments on volunteers as this have been suggested to be essential for the prediction of humanlike shoulder joint kinematics. Then the model was evaluated by simulating volunteer experiments in which dynamic loads were applied to the elbow in eight directions. The study found that the active controller reduced peak elbow displacement and peak displacements were within one standard deviation of the volunteers in all eight loading directions.

In a parallel development, with the aim to develop another active HBM to be representative of a driver, the active response of a shoulder to vertical loadings were evaluated. In this study a standing model was enhanced, including adding shoulder joint muscles. The study found reduced hand displacements as compared to before modifications while the response was somewhat slower than those of the volunteers.

Several HBMs have been fitted active muscles and muscle controllers to enable a proper reproduction of human responses in pre-crash manoeuvres. However, HBMs can also be fitted with active joints that apply torques to the skeletal parts. For this purpose, a controller was developed which can be adopted in several of the existing HBMs. While the evaluation of the new controller provided promising results, some further updates are necessary before model release.

To control muscle models, e.g., when these have been modelled in an HBM, the state of muscles or joint angles or angles between body regions must be provided the controller. To enhance this provision in the VPS solver, the routine that transfer data between VPS and SimulationX has been enhanced by adding support for HBM-specific variables

The THUMS TUC-VW AHBM was validated using volunteer data made available in the OSCCAR project. These validation data include braking, lane change and combinations of these when the volunteers were passengers in the test vehicles. The validation study concluded that the AHBM matches well selected kinematic parameters, but further improvements are yet to be done, e.g., improved stability of the model and modifying the controller of the AHBM to even more accurately reproduce head excursions during lane change manoeuvres.

To learn more about age related effects and how these influence occupant postures in avoidance manoeuvres, age-related changes in muscle properties were reviewed and implemented in an active HBM. When this model was exercised in lane change manoeuvres, the results revealed that the effect of reduced muscle cross section and possibility to generate stress capacity were to a high degree compensated for by the muscle controller. The model of the elderly only exhibited moderately greater peak head displacements compared to baseline model. However, other properties, e.g., muscle distribution and BMI, also change when we grow older and should be investigated.

The ability of car drivers to react to emergency scenarios quickly and efficiently is a fundamental skill in driving. However, studies have shown that the motor performance slows down with increasing age and potentially lessening the ability of elderly drivers to react to dangerous traffic scenarios. To study this, simulations were performed with the Total Human Model for Safety subjected to bracing scenarios. The muscle material model used was modified to account for the aging effects (muscle peak isometric stress was reduced, contraction response slower and activations delayed). The result revealed that the properties associated with an elderly subject influence both the reaction time and the maximal forces which the driver can produce.

There are several active HBMs representative of mid-size males, but few of other anthropometries that can be used in the development of integrated safety. To address this a method to transfer muscle Physiological Cross-Sectional Area (PCSA) from a mid-size active HBM to small size female was developed based on data available in literature and easily measurable physical quantities. The method was used to transfer an active HBM into a small size female and the resulting model was evaluated in several load cases. As the method rely on only easily measurable physical quantities, this method is applicable to other anthropometries as well.

Most active HBMs are merely used during the pre-crash phase. While it is known that occupant position prior to the crash influence the injury outcome, the information obtained in with the active HBMs should also be used in the simulations with HBMs in the in-crash phase. The most common approach to do so is to transfer the posture and velocity from the AHBM after the pre-crash phase to the initial state of a HBM designed for simulations of the in-crash phase. Another approach is to

perform seamless simulation of the pre- to in-crash phase using one single model. Here, the potential effect of the pre-activation of the muscles during the pre-crash phase was studied using the updated THUMS TUC-VW AHBM. The study found that muscle activation during the in-crash phase influenced the kinematics and potentially the injury risk. The study also showed that the THUMS TUC-VW AHBM is capable of being used in seamless simulations including both, the pre- and in-crash phase.

6 REFERENCES

[1] Huber P., Christova M., DÀdetta G.A., Gallasch E., Kirschbichler S., Mayer C., Prüggler A., Rieser A., Sinz W., and Wallner D.: Muscle Activation Onset Latencies and Amplitudes during Lane Change in a Full Vehicle Test; Proceedings of IRCOBI; 2013; pp: 628-640.

[2] Huber P., Kirschbichler S., Prüggler A., and Steidl T.: Three Dimensional Occupant Kinematics during Frontal, Lateral and Combined Emergency Maneuvers; Proceedings of IRCOBI ; 12-10-2014.

[3] Huber P., Kirschbichler S., Prüggler A., Steidl T.: Passenger kinematics in braking, lane change and oblique driving maneuvers; In IRC-15-89.; 2015. p. 783-802.

[4] Kirschbichler S., Huber P., Prüggler A., Steidl T., Sinz W., Mayer C. et al.: Factors Influencing Occupant Kinematics during Braking and Lane Change Maneuvers in a Passenger Vehicle; In Proceedings of IRCOBI Conference 2014; IRC-14-70.; 2014; p. 614-625.

[5] Van Rooij, L., Elrofai, H., Philippens, M. M. G. M., & Daanen, H. A. M. (2013). Volunteer kinematics and reaction in lateral emergency maneuver tests. Stapp car crash journal, 57, 313.

[6] Kleinbach C., Martynenko O., Promies J., Haeufle D., Fehr J. and Schmitt S.: Implementation and validation of the extended Hill-type muscle model with robust routing capabilities in LS-DYNA for active human body models, BioMedical Engineering OnLine (2017) 16:109, DOI 10.1186/s12938-017-0399-7

[7] Günther M., Schmitt S., Wank V.: High-frequency oscillations as a consequence of neglected serial damping in Hill-type muscle models, Biological Cybernetics (2007) 97:63–79, DOI 10.1007/s00422-007-0160-6.

[8] Mörl F, Siebert T, Schmitt S, Blickhan R, Günther M. Electro-mechanical delay in Hill-type muscle models. J Mech Med, Biol. 2012;12(05):1250085–1125008518. doi:10.1142/S0219519412500856.

[9] Siebert T, Till O, Blickhan R. Work partitioning of transversally loaded muscle: experimentation and simulation. Comput Methods Biomech Biomed Eng. 2014;17(3):217–29. doi:10.1080/10255842.2012.675056

[10] Kato, D., Nakahira, A., Atsumi, N., & Iwamoto, M. (2018). Development of Human-Body Model THUMS Version 6 containing Muscle Controllers and Application to Injury Analysis in Frontal Collision after Brake Deceleration. IRCOBI conference 2018.

[11] Shelat, C., Ghosh, P., Chitteti, R. and Mayer, C. (2016). “Relaxed” HBM – an enabler to Pre-Crash safety system evaluation. *Proceedings of IRCOBI conference*.

[12] Wochner I., Noelle L.V., Martynenko O.V., Schmitt S. (2021). Falling Heads: investigating reflexive responses to head-neck perturbations. [submitted].

[13] Kistemaker, DA., Van Soest AJ. and Bobbert MF. (2006). Is Equilibrium Point Control Feasible for Fast Goal-Directed Single-Joint Movements? *J. Neurophysiology*, 95(5), 2898–2912.

[14] Bayer, A., Schmitt, S., Günther, M., and Haeufle, D.F.B. (2017). The influence of biophysical muscle properties on simulating fast human arm movements. *Computer Methods in Biomechanics and Biomedical Engineering*, 20(8), 803–821.

[15] Peterson, S.L., Rayan G.M., (2011). Shoulder and Upper Arm Muscle Architecture. The Journal of hand surgery. 36. 881-9.

[16] Östh, J., Brolin, K. and Happee, R. (2012). Active muscle response using feedback control of a finite element human arm model. *Computer Methods in Biomechanics and Biomedical Engineering*, 15(4), 347–361.

[17] Martynenko, O., Neininger, F. and Schmitt, S. (2019). Development of a Hybrid Muscle Controller for an Active Finite Element Human Body Model in LS-Dyna Capable of Occupant Kinematics Prediction in Frontal and Lateral Maneuvers. *Proceedings: 26th International Technical Conference on the Enhanced Safety of Vehicles, Eindhoven, Netherlands*.

[18] Larsson, E. (2021) Towards a human body model for prediction of vehicle occupant kinematics in omni-directional pre-crash events. Thesis for the degree of Licentiate of Engineering no 2021:06, Department of Mechanics and Maritime Sciences, Chalmers University of Technology, Gothenburg, Sweden.

[19] Mishra, A., Ghosh P., Chitteti R. and Mayer C. (2020). Development of a Chinese 5th Percentile Female Active Human Body Model. *Proceedings of IRCOBI Asia conference*.

[20] Ólafsdóttir, J., Osth, J., Davidsson, J. and Brolin, K. (2013) Passenger kinematics and muscle responses in autonomous braking events with standard and reversible pre-tensioned restraints. *Proceedings of IRCOBI conference*.

[21] Nie X, Cheng J, Chen W, Weerasooriya T. (2010) Dynamic tensile response of porcine muscle. Journal of Applied Mechanics, 78(2). DOI: https://doi.org/10.1115/1.4002580.

[22] Song B, Chen W, Ge Y, Weerasooriya T. (2007) Dynamic and quasi-static compressive response of porcine muscle. Journal of Biomechanics, 40(13): pp.2999–3005. DOI: https://doi.org/10.1016/j.jbiomech.2007.02.001.

[23] Van Loocke M, Lyons CG, Simms CK. (2008) Viscoelastic properties of passive skeletal muscle in compression: Stress-relaxation behavior and constitutive modelling. Journal of Biomechanics, 41(7): pp.1555–1566, DOI: https://doi.org/10.1016/j.jbiomech.2008.02.007.

[24] Mattucci S. (2011) Strain Rate Dependent Properties of Younger Human Cervical Spine Ligaments. Journal of Kyoto Prefectural University of Medicine, 10: pp.216-226.

[25] Mattucci S, Moulton J, Chandrasekhar N, Cronin D. (2012) Strain Rate Dependent Properties of Younger Human Cervical Spine Ligaments. Journal of the Mechanical Behavior of Biomedical Materials, 10, pp. 216–226. DOI: https://doi.org/10.1016/j.jmbbm.2012.02.004.

[26] Kulavi P, Segura RD. (2016) Towards male specific material properties for cervical ligaments in finite element Human Body Models and its validation in functional spine units, Proceedings of the IRCOBI conference, 2016, Malaga, Spain.

[27] Clemente CD., Anatomy: a regional atlas of the human anatomy, 6th Edition, Lippincott Williams & Wilkins, Baltimore, 2011.

[28] Delbono O (2000). Regulation of excitation contraction coupling by insulin-like growth factor-1 in aging skeletal muscle. J Nutr Health Aging 4, 162–164.

[29] Erskine, R. M., Tomlinson, D. J., Morse, C. I., Winwood, K., Hampson, P., Lord, J. M., & Onambélé, G. L. (2017). The individual and combined effects of obesity-and ageing-induced systemic inflammation on human skeletal muscle properties. International journal of obesity, 41(1), 102-111.

[30] Ghaffari, G., Brolin, K., Bråse, D., Pipkorn, B., Svanberg, B., Jakobsson, L., & Davidsson, J. (2018, September). Passenger kinematics in Lane change and Lane change with Braking

Manoeuvres using two belt configurations: standard and reversible pre-pretensioner. In Proceedings of the 2018 IRCOBI Conference, Athens, Greece (pp. 12-14).

[31] Janssen I, Heymsfield SB, Wang ZM, and Ross R. (2000) Skeletal muscle mass and distribution in 468 men and women aged 18–88 yr. J Appl Physiol 89: 81–88.

[32] Klein, C. S., Rice, C. L., & Marsh, G. D. (2001). Normalized force, activation, and coactivation in the arm muscles of young and old men. Journal of Applied Physiology, 91(3), 1341-1349.

[33] Larsson, E., Iraeus, J., Fice, J., Pipkorn, B., Jakobsson, L., Brynskog, E., ... & Davidsson, J. (2019). Active Human Body Model Predictions Compared to Volunteer Response in Experiments With Braking, Lane Change, and Combined Manoeuvres. International Research Council on Biomechanics of Injury (IROCBI 2019), Florence, Italy, Sept, 11-13.

[34] Thom, J. M., Morse, C. I., Birch, K. M., & Narici, M. V. (2007). Influence of muscle architecture on the torque and power–velocity characteristics of young and elderly men. European journal of applied physiology, 100(5), 613-619.

[35] Macaluso A, Nimmo MA, Foster JE, Cockburn M, McMillan NC, De Vito G. (2002) Contractile muscle volume and agonist-antagonist coactivation account for differences in torque between young and older women. Muscle Nerve; 25:858-63.

[36] Morse CI, Thom JM, Davis MG, Fox KR, Birch KM, Narici MV. (2004) Reduced plantar-flexor specific torque in the elderly is associated with a lower activation capacity. Eur J Appl Physiol; 92:219-26.

[37] Morse, C. I., Thom, J. M., Reeves, N. D., Birch, K. M., & Narici, M. V. (2005a). In vivo physiological cross-sectional area and specific force are reduced in the gastrocnemius of elderly men. Journal of applied physiology, 99(3), 1050-1055.

[38] Morse, C. I., Thom, J. M., Birch, K. M., & Narici, M. V. (2005b). Changes in triceps surae muscle architecture with sarcopenia. Acta Physiologica Scandinavica, 183(3), 291-298.

[39] Yue, G. H., Ranganathan, V. K., Siemionow, V., Liu, J. Z., & Sahgal, V. (1999). Older adults exhibit a reduced ability to fully activate their biceps brachii muscle. Journals of Gerontology Series A: Biomedical Sciences and Medical Sciences, 54(5), M249-M253.

[40] Günther, M., Schmitt S. and Wank V. "High-frequency oscillations as a consequence of neglected serial damping in Hill-type muscle models," Biological cybernetics, 2007.

[41] Haeufle, D. F. B., Günther, M., Bayer, A. and Schmitt, S. "Hill-type muscle model with serial damping and eccentric force-velocity relation," Journal of biomechanics, 2014.

[42] Wochner, I., Endler, C. A., Schmitt, S. and Martynenko, O. V. "Comparison of Controller Strategies for Active Human Body Models with Different Muscle Materials," in *Proceedings of the IRCOBI Conference*, Athens, Greece, 2019.

[43] Kleinbach, C. G. "Simulation of occupant kinematics using active human body models," Shaker Verlag, Düren, 2019.

[44] Feller, L., Kleinbach, C., Fehr, J. and Schmitt S. "Incorporating Muscle Activation Dynamics into the Global Human Body Model", in *2016 IRCOBI Conference Proceedings - International Research Council on the Biomechanics of Injury*, Malaga, 2016.

[45] Martynenko, O., Kempter, F., Kleinbach, C., Schmitt, S. and Fehr, J. "Integrated Physiologically Motivated Controller for the Open-Source Extended Hil-type Muscle Model in LS-DYNA," in *Proceedings of the International IRCOBI Conference*, Athens, 2018.

[46] Hatze, H. "A myocybernetic control model of skeletal muscle," *Biological Cybernetics,* vol. 25, p. 103–119, 1977.

[47] Iwamoto M. and Nakahira Y. "Development and Validation of the Total HUman Model for Safety (THUMS) Version 5 Containing Multiple 1D Muscles for Estimating Occupant Motions with Muscle Activation During Side Impacts," *SAE Technical Paper Series 2015,* 2015.

[48] Salthouse, T. A. "The speed factor in cognitive aging," Theory of cognitive aging, p. 249–294, 1985.

[49] Stelmach G. E. and Goggin N. L. "Psychomotor decline with age," in Human Kinetics Books, 1989.

[50] Black, O. "The aging vestibular system," in Special senses in aging, 1977.

[51] Smith, B. H. "Aging and the nervous system," Geriatrics, p. 109–115, 1975.

[52] Lewis, R. D. and Brown, J. M. "Influence of muscle activation dynamics on reaction time in the elderly," European journal of applied physiology and occupational physiology, pp. 344-349, 1994.

[53] Bosco, C. and Komi, P. V. "Influence of aging on the mechanical behavior of leg extensor muscles," European journal of applied physiology and occupational physiology, p. 209–219, 1980.

[54] Degens, H. "Human Ageing," in Muscle and exercise physiology, 2019, p. 423–432.

[55] L. S. T. C. LSTC, "LS-DYNA® KEYWORD USER'S MANUAL VOLUME I," 2016.

[56] Iwamoto, M., Nakahira Y. and Kimpara, H. "Development and Validation of the Total HUman Model for Safety (THUMS) Toward Further Understanding of Occupant Injury Mechanisms in Precrash and During Crash," Traffic injury prevention, pp. S36-48, 2015.

[57] Brinkey, L., Savoie, C., Hurvitz, E. A. and Flannagan, C. "Patients' and health care providers' knowledge of wheelchair transportation issues," Assistive Technology, p. 35–46, 2009.

[58] Schneider, L. W., Klinich, K. D., Moore J. L. and MacWilliams, J. B. "Using in-depth investigations to identify transportation safety issues for wheelchair-seated occupants of motor vehicles," Medical engineering & physics, p. 237–247, 2010.

[59] Schneider, L. W., Manary, M. A., Orton, N. R. Hu, J. H., Klinich, K. D., Flannagan C. A. and Moore, J. L. "Wheelchair occupant studies," Final Report (2006-2016), 2016.

[60] Martynenko, O. V., Wochner, I., Nölle, L. V., Alfaro, E. H., Schmitt, S., Mayer, C., Mishra, A., Ghosh, P.., Chitteti, R. K., Weber, J., González-García, M., Beaugonin, M. and Vlachoutsis S. "Comparison of the Head-Neck Kinematics of Different Active Human Body Models with Experimental Data," in Proceedings of the International IRCOBI Conference, online, 2021.

[61] Narici MV, Maganaris CN, Reeves ND, Capodaglio P. Effect of aging on human muscle architecture. J Appl Physiol (1985). 2003 Dec;95(6):2229-34. doi: 10.1152/japplphysiol.00433.2003. Epub 2003 Jul 3. PMID: 12844499.

[62] Banik T, Lennart VN, Schmitt S, Martynenko OV "Representation of the Elderly Population with Active Human Body Models", in Proceedings of the International IRCOBI Conference, online, 2021.

[63] Ghaffari G., Brolin K., Pipkorn B., Jakobsson L. and Davidsson J. (2019) Passenger muscle responses in lane change and lane change with braking maneuvers using two belt configurations: Standard and reversible pre-pretensioner. Traffic Injury Prevention, 20(S1), S43–S51. https://doi.org/10.1080/15389588.2019.1634265.

[64] Ghaffari G. and Davidsson J. (2021) Female kinematics and muscle responses in lane change and lane change with braking maneuvers. Traffic Injury Prevention, 236-241, https://doi.org/10.1080/15389588.2021.1881068.

[65] Östh, J., Ólafsdóttir, J. M., Davidsson, J., and Brolin, K. (2013). Driver kinematic and muscle responses in braking events with standard and reversible pre-tensioned restraints: validation data for human models (No. 2013-22-0001). Stapp - SAE Technical Paper.

[66] Ejima, S., Ito, D., Satou, F., Mikami, K., Ono, K., Kaneoka, K., & Shiina, I. (2012). Effects of pre-impact swerving/steering on physical motion of the volunteer in the low-speed side-impact sled test. In Proceedings of the 2012 International Research Council on Biomechanics Injury Conference (pp. 12-14).

[67] "TUC-Project – THUMS User Community", https://tuc-project.org/. [cited May 2021].

[68] "ESI Group: Empowering Industrial Players to Commit to Outcomes", https://www.esi-group.com. [cited May 2021].

[69] Iwamoto M, Nakahira Y, Tamura A, Kimpara H, Watanabe I, Miki K. (2007) Development of advanced human models in THUMS. Proceedings of the 6th European LS-DYNA Users' Conference, 2007, Gothenburg, Sweden.

[70] Borst, J., Forbes, P. A., Happee, R., Veeger, D. H. E. J. (2011): Muscle parameters for musculoskeletal modelling of the human neck. In Clinical biomechanics (Bristol, Avon) 26 (4), pp. 343–351.

[71] Yigit, E. (2018) Reaktives FE-Menschmodell im Insassenschutz. AutoUni-Schriftenreihe 114, Springer Fachmedien Wiesbaden GmbH, Wiesbaden, Germany. DOI: https://doi.org/10.1007/978-3-658-21226_1-1.

[72] Sugiyama, T, Weber, J, Sandoz, B, Bensler, H. P. (2018) Validation of a Reactive Finite Element Human Body Model under Moderate Lateral Loading. 7th International Symposium: Human Modeling and Simulation in Automotive Engineering, 2018, Berlin.

[73] González-García, M, Weber, J, Kulavi, P. (2019) VPS-SimulationX Coupling for Active Human Body Modelling. ESI Forum, 2019, Berlin.

[74] van der Horst MJ, Thunnissen J, Happee R, Van Haaster R, Wismans J. The influence of muscle activity on head-neck response during impact. SAE transactions. 1997; p. 4003–4023.

[75] Meijer, R., Elrofai, H., Broos, J., van Hassel, E. (2013) Evaluation of an Active Multi-Body Human Model for Braking and Frontal Crash Events. In International Technical Conference on the Enhanced Safety of Vehicles.

[76] González-García, M, Weber, J, Sugiyama, T, Peldschus, S, Sandoz, B. (2020). Closing the gap between sled and in-vehicle volunteer tests under moderate lateral accelerations. In: Proceedings: IRCOBI Conference, September.

[77] A. Özturk, C. Mayer, H. Kumar, G Pronoy, G. Atul, M. Ravi, K. Chitteti, and D. Fressmann, "A step towards integrated safety simulation through pre-crash to in-crash data transfer", in International Technical Conference on the Enhanced Safety of Vehicles, 2019.

[78] González-García M, Weber J, Peldschus S. (2020). Numerical study to quantify the potential influence of pre-activated muscles during the in-crash phase. Presented at: 8th International Symposium Human Modeling and Simulation in Automotive Engineering; 19th–20th November.

[79] Devane K, Koya B, Gayzik FS. (2020). Active human body models and associated risk of injury for out-of-position occupants in frontal crash. Presented at: 8th International Symposium Human Modeling and Simulation in Automotive Engineering; 19th–20th November.

[80] J. Östh, K. Bohman, and L. Jakobsson, “Evaluation of Kinematics and Restraint Interaction when Repositioning a Driver from a Reclined to an Upright Position Prior to Frontal Impact using Active Human Body Model Simulations”, in IRCOBI Conference, 2020, pp. 358–380.

[81] González-García, M., Weber, J., and Peldschus, S., (2021) “Potential effect of pre-activated muscles under a far-side lateral impact”, Traffic Injury Prevention, pp. 1–4, issn: 1538-9588. doi: 10.1080/15389588.2021.1982597.

[82] Ewing, C. L. and Thomas, D. J., (1972) “Human Head and Neck Response to Impact Acceleration”, NAMRL Monograph 21, Pensacola, Florida, Tech. Rep.

[83] Gunby, P., “John Paul Stapp, MD, PhD”, JAMA, vol. 283, no. 14, p. 1894, 2000, issn: 0098-7484. doi: 10.1001/jama.283.14.1894.

[84] Van Vliet, B, de Vlugt, E, Happee, R. (2014) Nonlinear arm responses to continuous and pulse-shaped force perturbations. Experimental Brain Research vol. 233, no. 1.

[85] Hamacher, M., Becker, J., D’Addetta, G. A., Östling, M., Mayer, C., Compigne, S. (2021) Final virtual design of advanced passenger protection principles. Deliverable report D2.4 of EU-funded project OSCCAR (FUTURE OCCUPANT SAFETY FOR CRASHES IN CARS), Grant Agreement Number 768947.

[86] Jeno, S, Schindler, G; Anatomy, Bony Pelvis and Lower Limb, Thigh Adductor Magnus Muscle, Bookshelf ID: NBK534842, PMID: 30521263.

[87] Tobin D. (2018) Shoulder Model Development in the Active Human Model, Master’s Thesis, Trinity College Dublin.

[88] Siemens Industry Software Netherlands; “Simcenter Madymo Quality Report Release Update: Active Human Model, version 3.2 (R2020.1)”, 2019.

[89] Begeman, P. C., King, A. I., Levine, R. S. and Viano, D., C. (1980) Biodynamic Response of the Musculoskeletal System to Impact Acceleration, Stapp Car Crash Conference (24th) Proceedings, pp 477-509, SAE Technical Paper Series, doi: 10.4271/801312.

[90] Meyer, E., Bonnoit, J. (1994) “Le choc lateral sur l’epaule: mise en place d’un protocole experimental en sollicitation dynamique”, *Memoire de DEA,* Laboratoire de biomécanique appliquée, faculté de Marseille.

[91] Siemens Industry Software Netherlands; “Simcenter Madymo Theory Manual (R2020.1)”, 2019.

[92] Holzbaur, K, Murray, W, Delp, S. (2005) “A model of the upper extremity for simulating musculoskeletal surgery and analyzing neuromuscular control”, Annals of Biomedical Engineering.

A. APPENDIX - REVIEW OF DATA FOR THE DEVELOPMENT OF ACTIVE HBMS

Summary

Pre-crash responses due to bracing, steering, braking etc. may alter occupant position relative to safety systems and change injury risk if there is a crash. An important tool to assess these risks is HBMs with some form of muscle control system, but these models need validation and tuning data. The purpose of this document was to review experiments that have measured volunteer kinematic and muscle activity responses to simulated or actual pre-crash events and assess their applicability as validation data for HBMs with muscle control systems.

A total of 25 datasets were identified that involved applying accelerations that mimic pre-crash events to human volunteers. Most of these were from published sources and three additional ones came from unpublished data.

This report provides additional details and is meant to accompany the summary tables provided in the file: “Osccar Review of Pre-impact Volunteer data - Summary 20190508.xlsx”. Save both files to the same folder on your computer for the links between the files to work.

Methods of literature review of volunteers in pre-crash events

The focus of the review was to assess the suitability of the datasets to being used for validation/tuning of HBMs. Mostly datasets that have been published were included in this review, and partner organizations have suggested reports with additional unpublished data. Publications were added to this review if they met two criteria: 1) experiments on human volunteers and 2) the volunteer’s response to pre-crash scenarios was elicited by exposure to appropriate accelerations. In this document pre-crash events include occupant bracing, braking, lane change, cornering or any combination. The articles were found by searching “pre-crash volunteer” and “pre-impact volunteer” in google scholar. In addition, the references of articles found were checked for further articles that should be included.

The datasets found were reviewed for their applicability in validation/tuning of HBMs. The applicability of the datasets as validation/tuning data was evaluated solely from the data that has been made available in the publication. Thus, it is likely that more of these datasets would be more applicable for human body model validation/tuning with access to the underlying data. The loading conditions were considered reproducible if time histories of all the relevant sled or vehicle dynamics are available. Boundary conditions were considered reproducible if enough information about the geometry of the seat, the type of restraints, and occupant initial position etc. where have been made available. Electromyographic (EMG) recordings of muscle activity data that were normalized by maximum voluntary isometric contracts (MVIC) were considered suitable for validation or tuning. This is because in the Hill muscle model activation scales the maximum muscle force, and EMG data normalized by MVIC is interpretable in this context.

Description of each study

Autoliv Germany (1999) In vehicle passengers in emergency braking

References, Institution, Funding

Kümpfbeck, M., Oertel, D., & Pilatus, K. (1999). Occupant kinematics during emergency braking. IRCOBI Sitges, Spain September 19.

Institution

Autoliv GmbH, Dachau, Germany

Funding

Not available.

Summary

Passengers in a vehicle exposed to emergency braking from 80km/h. The effect of steering inputs while braking, belt slack, and occupant head turned posture were investigated.

Experimental Details

Participants

1 male volunteer.

Instrumentation

Two video cameras were used. One mounted outside vehicle looked through the side window and another in the back looking at lateral movements of the passenger. For ‘normal conditions’ 80mm belt slack was used.

Lateral and longitudinal accelerometers were mounted to the test vehicle. Load cell was placed on the shoulder belt.

A pulling string method was used to quantify head and torso displacements.

Load cases

Emergency braking from 80km/h.

Boundary Conditions

Audi A4. Standard seatbelts. Seat position set as per 50th percentile dummy in FMVSS 208.

Data Availability

Peak head excursion as a function of different test environments shown.

Applicability of the Data to Human Body Modelling

Not enough information is provided to model the loading or boundary conditions, so this dataset is currently not suitable as validation data.

U. Munich (2005) Lane change and sinusoidal manoeuvres

References, Institution, Funding

Muggenthaler, H., Adamec, J., Praxl, N., & Schönpflug, M. (2005). The influence of muscle activity on occupant kinematics. In International IRCOBI Conference on the Biomechanics of Impact, Prague (Czech Republic) September.

Institution

Institute for Legal Medicine, University of Munich

Funding

European funded project ROLLOVER (G3RD-CT-2002-00802)

Summary

This study compares the kinematic response of volunteers and the hybrid III ATD when exposed to VDA lane change manoeuvres and sinusoidal motions in a test vehicle. EMG of the volunteer was also collected.

Experimental Details

Participants

No information provided.

Instrumentation

EMG: Bilateral surface recordings of the sternocleidomastoid, trapezius, obliquus externus abdominis, rectus femoris. NORAXON amplifier. 960Hz sampling. Normalization was not performed.

High speed cameras.

Accelerometer on vehicle.

Load cases

Emergency avoidance lane change – uses VDA test track (ISO 3888-2). Also known as the ‘Moose test.’ Speed 60km/h. Volunteer as passenger and driver

Sinusoidal Motions: 60 km/h & 80 km/h. Both speeds with human and ATD as passenger.

Boundary Conditions

Lane changes: Renault Megane Scenic (unknown year), volunteer and ATD in passenger seat.

Sinusoidal: BMW X5 (unknown year), volunteer and ATD in passenger seat.

Data Availability

Exemplar time histories of muscle activity shown with lateral acceleration of vehicle.

Applicability of the Data to Human Body Modeling

The data set is not well suited to validation of HBMs because corridors of volunteer's kinematic or muscle activity are not provided. Further it is unknown how many subjects were tested.

Hongik U. (2005) Bracing volunteers on sled

References, Institution, Funding

Choi, H. Y., Sah, S. J., Lee, B., Cho, H. S., Kang, S. J., Mun, M. S., ... & Lee, J. (2005, June). Experimental and numerical studies of muscular activations of bracing occupant. In 19th ESV Conference, Paper (No. 05-0139).

Institution

Hongik University, Korea Orthopedics and Rehabilitation Engineering Center, IPS International

Funding

Korean ministry of science and technology. Project No.: M10139080002-04L1008-00210

Summary

A dynamometer was used to record the MVIC of volunteer shoulder, elbow, wrist, knee, and ankle joints while recording EMG. Volunteers mimicked a braced posture while sliding down an incline towards a barrier. EMG and reaction forces were measured during these tests. The data was used to optimize muscle activity for human body model.

Experimental Details

Participants

Two stage selection process. Stage 1, 20/128 volunteers were selected based on BMI and body mass targets. Stage 2, 8/20 volunteers were selected based on closest MVIC to mean.

	Age	Height (m)	Weight (kg)	BMI (kg/m²)	RA lean balance* (%)	RL lean balance** (%)
Mean	24	1.75	67	22.1	4.6	13.3
S.D	1.7	0.84	1.6	0.6	0.3	0.6

* Ratio of right arm muscle mass to total body mass (%)

** Ratio of right leg muscle mass to total body mass (%)

Instrumentation

EMG: Surface recordings of the posterior deltoid, anterior deltoid, medial triceps, biceps brachii, extensor carpi radialis, flexor carpi radialis, rectus femoris, biceps femoris, soleus, tibialis anterior. Signals rectified, filtered, and normalized by MVIC.

Uniaxial loadcell on steering wheel and pedals. Pressure pad on seat back

Kinematics were not measured.

Load cases

Sled buck was slid down an incline under the force of gravity. Two drop heights used 0.9 m and 1 m.

Boundary Conditions

Simple sled buck with automotive seat. Geometry of seat, steering wheel and pedals not defined. Detailed information of occupant posture during their trials is provided.

Data Availability

Percentage of MVIC for muscle activity provided for each muscle during bracing. Reaction loads on steering wheel, pedals, and seat back.

Applicability of the Data to Human Body Modelling

In general time histories and response corridors during an event are important data for the purpose of validation. In this case those aren't needed because this dataset is well suited to validating a braced occupant just before impact. For this type of validation, the loading conditions would be the activity of muscles not movement of the sled/vehicle, and those are well defined. It was not feasible to record all of the recruited muscles during bracing, so assumptions would be required assign muscle activity to all of the suitable muscles.

MIRA Ltd. (2005) Volunteer postures in vehicle pre-crash

References, Institution, Funding

Morris, R., Cross, G., & Bingley, L. (2005). Improved understanding of passenger behavior during pre-impact events to aid smart restraint development. In Proceedings of the 19th International Technical Conference on the Enhanced Safety of Vehicles (ESV), Washington DC, USA, June (pp. 6-9).

Institution

MIRA Ltd., United Kingdom

Funding

PRISM is a DG Research project under the 5th Framework, G3RD-CT-2002-00848.

Summary

Volunteers were exposed to a series of pre-crash events in the passenger seat of a vehicle while filmed with on board cameras. The purpose was to see how volunteers would react to pre-crash events while in normal or altered postures or while undertaking various tasks. Hybrid III crash test dummies of different sizes were also exposed to the same pre-crash events.

Experimental Details

Participants

49 volunteers plus four study members who were exposed to the more severe load cases.

Instrumentation

5 on-board cameras.

Longitudinal and lateral accelerometers on vehicle. Brake pedal force transducer.

Load cases

Pre-crash events included: straight line emergency braking, emergency lane change, emergency lane change then braking, rapid direction change with lift-off oversteer with spin or partial spin, rapid direction change as if driving fast on sweeping road.

Postures tested include: Normal (own) posture, FMVSS ATD posture, rear-view mirror, radio adjustment, arm on waist rail, arm on arm rest, holding roof grab handle, arm out of window, holding head restraints (both hands), holding magazine, legs crossed, on phone

Project members were additionally exposed while reaching into footwell, adjusting seatbelt, drinking/eating, sitting on feet, turning to talk to rear seat passengers, unbelted.

Each volunteer exposed to three events.

Boundary Conditions

5-door ford focus. Volunteers in passenger seat.

Data Availability

Exemplar trace of vehicle braking acceleration as a function of time.

Applicability of Data for Human Body Modelling

Kinematics and muscle activity of the volunteers were not measured so the study is not suitable for use as validation/tuning data.

Exponent (2005) Initiation of roll over in vehicle

References, Institution, Funding

Yamaguchi, G. T., Carhart, M. R., Larson, R., Richards, D., Pierce, J., Raasch, C. C., ... & Corrigan, C. F. (2005). Electromyographic activity and posturing of the human neck during rollover tests (No. 2005-01-0302). SAE Technical Paper.

Institution

Exponent Failure Analysis Associates, USA

Funding

Exponent Failure Analysis Associates, USA

Summary

Lateral head motions, torso motions, lateral neck bending angles, and electromyographic (EMG) activity patterns of five human volunteer passengers are compared to lateral motions of a Hybrid III ATD during right-left and left-right fishhook steering manoeuvres leading to vehicular tip-up.

Experimental Details

Participants

5 males.

Subject	Height(m)	Weight (kg)	Age (yrs)
1	1.75	80	33
2	1.78	82	52
3	1.78	79	36
4	1.73	91	35
5	1.80	76	32

Instrumentation

Two-axis optical fifth wheel for speed measurement. Ultrasonic height sensor was used to measure roll angle. Vehicle kinematics were measured with a 6-axis accelerometer / angular rate sensor mounted on the floor between front seats. Video cameras captured front and side views of the passengers. Markers on the head and torso were tracked with software, although precise marker locations were unclear.

Bilateral surface EMG on upper trapezius, sternocleidomastoid, and abdominal oblique muscles. Lateral vasti on left leg for some subjects. EMG was normalized against MVIC, but the details of these procedures was unclear.

In one subject, head accelerometers & gyroscopic rate sensors were strapped to top of head in the sagittal plane aligned with the external auditory meatus.

Load cases

Each subject had two left-right and two right-left manoeuvres resulting in inboard and outboard tip ups. Open-loop controller to modulate steering, driver maintained 35-36mph before manoeuvre.

Boundary Conditions

1992 Isuzu Rodeo. Volunteers in passenger seat.

Data Availability

Response corridors are provided for head and torso excursion, EMG, and vehicle kinematics.

Applicability of the Data for Human Body Modeling

This dataset is generally well suited to validation of occupants in pre-roll over cases. The loading case is very complex, but the linear and angular kinematics of the vehicle have been provided and should be reproducible. Without access to an example of the test vehicle used, it is unlikely that precise boundary conditions could be defined. For example, the geometry of the seat and seat belt retractor properties are unknown which will influence occupant kinematics. Response corridors for the volunteer kinematics and muscle activity were provided. It may be difficult to relate the displacement data measured to model displacements because the exact location of the markers they used is not clearly described.

U. Munich (2005) On sled lateral acceleration & initiation of roll-over

References, Institution, Funding

Adamec, J., Praxl, N., Miehling, T., Muggenthaler, H., & Schonpflug, M. (2005). The occupant kinematics in the first phase of a rollover accident–experiment and simulation. In International IRCOBI Conference on the Biomechanics of Impact, Prague (Czech Republic) September.

Institution

Institute for Legal Medicine, Ludwig-Maximilian University Munich, Germany.

Funding

Unknown

Summary

Comparison of the Hybrid III and EuroSID II ATDs against a MADYMO human body model and volunteers under the early phase of a roll-over crash. Volunteers sat upon a platform that could be tilted to generate roll (i.e. rotation about a forward-facing axis) or the platform could be accelerated on rails to generate lateral acceleration. Volunteer muscle activity and kinematics were measured.

Experimental Details

Participants

2 volunteers. No further information provided.

Instrumentation

Bilateral surface EMG on upper trapezius, sternocleidomastoid, oblique externus, and rectus femoris muscles. Noraxon (Scottsdale, AZ, USA). No normalization attempted.

14 reflective markers: 3 on head, sternum, bilateral on shoulder, elbow, chest, pelvis, and knee. 8 Falcon cameras at 240Hz used to capture motion of markers. Eva Real Time 2.1 motion analysis software (Santa Rosa, CA, USA) was used for analysis.

Load cases

Each volunteer exposed to one slow and one fast translation, in addition to one slow and one fast rotation. Consistency of the applied kinematics was not achieved. These loads were chosen to approximate 30 rollover-cases from accident reconstruction and field tests as part of the ROLLOVER Project (RTD GRD2-2001-50086 “Improvement of Rollover Safety for Passenger Vehicles”) See chart below.

Occupant	y-acceleration peak (g)		roll-rate peak (deg/s)	
	"slow"	"fast”	"slow"	"fast"
Volunteer 1	0,8 (2,0)	0,9 (2,5)	56	62
Volunteer 2	0,7 (2,1)	0,9 (2,8)	36	60
HybridIII	0,6 (1,3)	1,0 (2,6)	44	58
EuroSID	0,9 (1,9)	1,0 (2,5)	55	64

Boundary Conditions

Automotive seat with three-point belt. Hands on lap posture representing passengers. No further information provided.

Data Availability

Exemplar plots of EMG for both subjects in all four load cases. One plot of the motions on the top of the head

Applicability of the Data for Human Body Modelling

The limited number of subjects makes it difficult to know how average these responses are in a larger population, which limits the applicability for validation / tuning. Further, not enough data was provided to recreate the loading conditions (i.e., traces of movement as a function of time, the rotational centre of the rotational perturbations) or boundary conditions (i.e. seat used, posture of volunteers).

Delphi (2006) Lateral acceleration on sled.

References, Institution, Funding

Parenteau, C. (2006). A comparison of volunteers and dummy upper torso kinematics with and without shoulder belt slack in a low speed side/pre-roll environment. Traffic injury prevention, 7(2), 155-163.

Institution

Delphi Corp., Troy, MI, USA.

Funding

Delphi Corp., Troy, MI, USA.

Summary

A buck of a small European car was mounted on a side impact sled. The parameters evaluated were pulses, sitting location, and belt slack. A total of 24 tests were carried out. Three 50th-percentile male volunteers and one Hybrid III 50th-percentile male were tested. The pulses consisted of Pulse 1:+/− 0.7 g's pulse and Pulse 2: a −0.9 g pulse to simulate low-speed pre-roll/side events. Both pulses had a duration of 500 msec.

Experimental Details

Participants

3 male volunteers. Aged 21, 21, and 24 years; height of 175, 172, and 183; weight of 80, 80, 90kg; sitting height of 88, 91, 92cm.

Instrumentation

Two seatbelt load cells were place on the lap and shoulder belts.

Three highspeed camera record maker displacement at 1000f/s. Markers were place on the forehead (2), chin, L & R acromion, just below sternal notch. Note torso markers stuck directly to clothing.

Load cases

The pulses consisted of Pulse 1:+/− 0.7 g's pulse and Pulse 2: a −0.9 g pulse to simulate low-speed pre-roll/side events. Both pulses had a duration of 500 msec.

Boundary Conditions

Automotive seat with three-point belt. No further information provided.

Pulses are repeated with no belt slack and 100mm slack. Volunteers repeated the test in near side and far side seat (there was no steering wheel, and hands were in their lap for both cases). Each condition is repeated three times.

Data Availability

Head and torso excursion for both pulse types, in both seating positions, for both belt slacks are provided for each volunteer. Exemplar acceleration traces are shown for both pulse types.

Applicability of the Data for Human Body Modelling

The limited number of subjects makes it difficult to know how average these responses are in a larger population. There is enough data to produce the loading conditions, but not the boundary conditions and muscle activity were not measured.

JARI (2007) Pre-crash braking on sled.

References, Institution, Funding

Ejima, S., Ono, K., Holcombe, S., Kaneoka, K., & Fukushima, M. (2007). A study on occupant kinematics behaviour and muscle activities during pre-impact braking based on volunteer tests. In Proceedings of ircobi (international research council on the biomechanics of injury) conference 2007, held maastricht, the netherlands, september 2007.

Institution

Japan Automobile Research Institute (JARI); Department of Orthopedic Surgery, University of Tsukuba; Tsukuba Medical Center Hospital.

Funding

Toyota Motor Company

Summary

The objective was to understand postural responses of vehicle passengers to pre-crash braking. Volunteers sat on a sled that was accelerated at ~1g to mimic braking events, while EMG and kinematics were measured.

Experimental Details

Participants

3 males and 2 females that were all 23 years old participated. The height and weight of each volunteers was provided along with estimated locations of the head CG, occiput, head mass, and inertia.

Volunteer	Height (cm)	Weight (kg)	Tragion to vertex height (mm)	Location of acceleration (mm)		Location of Occipital		Head mass (kg)	Head inertia moment(kg-cm^2)		
				X	Z	X	Z		X	Y	Z
YSM	177.7	68	133	130.2	55.4	-8.3	41.6	4.0	194.8	171.9	119.8
AOM	173	63	146.8	121.9	66.5	-19.4	38.8	4.3	220.5	196.5	131.6
SWM	176	67	138.8	128.5	66.8	-15.4	37.3	4.2	208.6	185.0	126.2
TIF	172	62	146.5	138.8	57.8	-15.4	38.8	4.0	200.6	177.3	120.8
AMF	159	53	126.4	119.5	58	-18.6	40.6	3.3	140.0	121.3	90.3

Instrumentation

8 markers were attached to the head (parietal, tragion), shoulder (Acromion), chest (12^{th} rib, sternum), back (T4, T10), lumbar (Iliac crest), arm (elbow), hand (back of wrist), leg (knee). Two cameras (Eagle Digital camera), 1280 x 1024 pixels, and marker location was automatically calculated using Calcium software (NAC Inc.).

Triaxial accelerometers affixed to the Sled, head via a mouthpiece, first thoracic vertebra, the acromion, sternum, iliac crest.

Bilateral surface EMG on sternocleidomastoid, paravertebral, latissimus dorsi, rectus abdominis, obliquus externus abdomens, biceps femoris, rectus femoris, tibialis anterior. EMG normalized by the largest activity experienced across trials for each subject.

Load cases

Sled slid down ramp with 10deg slant with speed limited by a cable attached to an electric motor. At the end of the ramp the sled collided into a damper that controlled the deceleration (0.2-1g with duration of ~200ms).

Each volunteer was exposed to accelerations of 0.2, 0.6, and 1g repeated for a relaxed and a tensed state. In the tensed stated subjects were instructed to co-contract their muscles without altering initial posture. Startle response likely diminished by three practice trials of each condition before data collection.

Boundary Conditions

Rigid seat without seat back or head restraint. Lap belt without pre-tension. Upper and lower legs strapped to sled. The volunteers rested their arms downwards on their sides.

Data Availability

Plots of body segments at beginning and peak motions for each subject at the 1g load level. Exemplar time histories of acceleration and EMG are provided.

Applicability of the Data for Human Body Modeling

The time history of sled velocity and acceleration were only provided for the 1g impact case, so the loading conditions may not be reproducible for other load conditions. The boundary conditions are simple and would likely be easily reproduced. Only trajectories for the five subjects in the 1g case are complete enough to be used for validation or tuning. Accelerations and EMG are only presented as exemplars from one subject and so may not be sufficient. Further, the short duration of 200ms of deceleration may not be relevant to a typical pre-braking event.

JARI (2008) Pre-crash braking on sled

References, Institution, Funding

Ejima, S., Zama, Y., Satou, F., Holcombe, S., Ono, K., Kaneoka, K., & Shiina, I. (2008). Prediction of the physical motion of the human body based on muscle activity during pre-impact braking. In Proceedings of the IRCOBI Conference (pp. 163-175).

Ejima, S., Zama, Y., Ono, K., Kaneoka, K., Shiina, I., & Asada, H. (2009). Prediction of pre-impact occupant kinematic behavior based on the muscle activity during frontal collision. In 21st ESV Conference (No. 09-0913).

Institution

Japan Automobile Research Institute; Department of Orthopedic Surgery, University of Tsukuba; Waseda University, Faculty of Sports Sciences.

Funding

Japan Automobile Manufacturing Association

Summary

Objective was to understand postural responses of vehicle drivers to pre- crash braking. Volunteers sat on a sled that was accelerated to mimic braking events, while EMG and kinematics were measured while their arms were on the steering wheel. Both relaxed and tensed states of muscle activation were investigated.

Experimental Details

Participants

Five males and 2 females aged 22-26 years old participated.

Volunteer	Age (years)	Sex	Height (cm)	Weight (kg)	Sitting height (cm)
I	26	M	174	76	92
II	25	M	168	62	89
III	25	M	172	64	89
IV	23	M	173	70	85
V	25	M	178	65	91
VI	23	F	160	42	86
VII	22	F	157	53	80

Instrumentation

8 markers attached to head (parietal, auditory meatus), shoulder (Acromion), chest (sternum), back (T1, T11), lumbar (L3), arm (elbow), hand (wrist, back), leg (knee). Multiple cameras (Eagle Digital camera), 1280 x 1024 pixels, and marker location was automatically calculated using EVaRT software (NAC Inc.).

Triaxial accelerometers & angular rate sensors were affixed to the Sled, head via a mouthpiece, first thoracic vertebra, twelve thoracic vertebrae, and lumbar vertebrae (L3). Triaxial accelerometers were also affixed to the acromion, and sternum.

Single axis loads cells were placed on the pedals, steering wheel, and shoulder belt.

Bilateral surface EMG recorded from the sternocleidomastoid, paravertebral, latissimus dorsi, erector spinae, rectus abdominis, obliquus externus abdomens, biceps femoris, rectus femoris, gastrocnemius, biceps brachii, triceps brachii, deltoideus muscles. EMG was normalized by the largest activity experience across trials for each subject.

Load cases

A motor was used to accelerate a sled along rails. Each volunteer was exposed to accelerations of 0.8g for ~600ms repeated for a relaxed and a tensed state. In the tensed state, subjects were instructed to co-contract their muscles without altering initial posture.

Boundary Conditions

Rigid seat without head restraint. Three-point belt without pre-tension.

Data Availability

Initial posture variation between subjects is well defined. Only exemplar time histories of loads, body segments, acceleration, and EMG are provided. No time history of sled acceleration.

Applicability of the Data for Human Body Modelling

The number of subjects is likely sufficient to generate response corridors, but uncertainty will remain if this average response really represents a true population average. The initial posture of the

subjects was well defined. The boundary conditions were simple and would likely be easily reproduced. The loading conditions are not possible to reproduce because a time history of sled kinematics was not given. Little volunteer responses are provided, so the utility of the data for validation and tuning would be limited. This could be a useful dataset if more time histories were made available, but the lack of EMG normalized by MVIC would remain problematic.

UMRT24 (2010) Driver simulator and in vehicle pre-crash braking

References, Institution, Funding

Behr, M., Poumarat, G., Serre, T., Arnoux, P. J., Thollon, L., & Brunet, C. (2010). Posture and muscular behaviour in emergency braking: An experimental approach. Accident Analysis & Prevention, 42(3), 797-801.

Institution

Laboratoire de Biomécanique Appliquée, UMRT24 INRETS/University of Mediterranée; Laboratoire d'Anatomie, ERIM EA3295, Université Blaise.

Funding

Not specified.

Summary

This study aims to quantify drivers' behaviour in terms of posture and muscular activity just before a frontal impact. Experiments on volunteers were performed in order to define these conditions, both on a driving simulator and on a real moving car. Brake pedal loads, lower limbs kinematics and muscle activation were recorded

Experimental Details

Participants

Driving simulator: 34 volunteers (24 men, 10 women). Age 36 (SD 16) years, weight 75 (7) kg, and height 174 (7) cm.

Rear car tests: 13 volunteers (11 men, 2 women) aged 30(8) years, weight of 71 (7) kg, and height of 174 (7) cm.

Instrumentation

Driving Simulator:

Retroreflective markers were affixed to the skin at 5 different anatomical points: distal foot (distal end of big toe), tibial malleola (ankle), lateral femoral condyle (knee), greater trochanter (hip), and acromion (shoulder). Six cameras captured the markers at 50Hz.

Load cell on the brake pedal. Contact sensor on accelerometer pedal.

Real car tests:

Vehicle tri-axial accelerometer, load cells on both pedals, car speed transducer.

Surface EMG on the right rectus femoris, vastus lateralis, biceps femoris, tibilais anterior, and gastrocnemius medialis. The RMS EMG was calculated and normalized against MVIC performed by

instructing subjects to “forcibly contract each considered muscle one after the other. For each measurement, the contraction would last for 3–5 s.”

Load cases

Driving Simulator: Brake lights shown to subject ~3m ahead of simulator which signalled to the drive to emergency brake. Five repetitions.

Real car tests: While the participant was driving at 70km/hr, aball was rolled in front of the vehicle and the drivers braked in a straight line with full effort to avoid it. The participants drove past the braking area four times, and the ball was thrown three times per volunteer.

Boundary Conditions

Driving Simulator: Occupant cabin extracted from Renault 19. Actual brakes retained for realistic feel.

Real car test: Peugeot 307.

Data Availability

From the simulator tests, mean and range of joints angles before and during braking were provided. In the real car tests, peak normalized muscle activity during braking were provided. No time histories of measurements were provided.

Applicability of the Data for Human Body Modelling

The joint angles and pedal loads from the static driver simulator could be used to tune or validate a model of a braking occupant. The data from the real car tests would be difficult to use for validation or tuning because the loading conditions cannot be reproduced because the time history of the vehicle kinematics were not provided.

Autoliv. Sweden (2013) Children in vehicle braking and cornering

References, Institution, Funding

Bohman, K., Stockman, I., Jakobsson, L., Osvalder, A. L., Bostrom, O., & Arbogast, K. B. (2011). Kinematics and shoulder belt position of child rear seat passengers during vehicle maneuvers. In Annals of Advances in Automotive Medicine/Annual Scientific Conference (Vol. 55, p. 15). Association for the Advancement of Automotive Medicine.

Stockman, I., Bohman, K., Jakobsson, L., & Brolin, K. (2013). Kinematics of child volunteers and child anthropomorphic test devices during emergency braking events in real car environment. Traffic injury prevention, 14(1), 92-102.

Institutions

Autoliv Research, Vårgårda, Sweden; Karolinska Institutet, Stockholm, Sweden; Chalmers University of Technology, Göteborg, Sweden; Center for Injury Research and Prevention, The Children’s Hospital of Philadelphia, Philadelphia, USA.

Funding

In part by FFI (Fordonsstrategisk Forsknings och Innovation), Vinnova, Sweden.

Summary

The aim of this study was to quantify kinematics of child occupants during swerving manoeuvres (at 50km/h) and emergency braking from 70km/h. 16 children aged 4-12 were filmed during the manoeuvres with four cameras filmed and vehicle kinematics were measured.

Experimental Details

Participants

12 boys, 4 girls aged 4-12 years. Subjects were split into a tall group and short group. The tall subjects were on average 9, 144 cm tall, and had a sitting height of 75cm. Members of the short group were on average 5 years old, 117cm tall, and had a seated height of 59cm.

Instrumentation

Four cameras facing the subject. Markers were placed on shoulder, femur, knee, head gear, and shoulder belts.

Load cell on upper portion of three-point belt.

Vehicle velocity and longitudinal acceleration were measured from the CAN-bus. An additional accelerometer was placed to measure vehicle lateral acceleration.

Load cases

14m radius turn taken at 50km/h. Professional driver produced consistent kinematics.

Emergency braking from 70km/h.

Boundary Conditions

Test vehicle was a 2010 Volvo XC70 with leather upholstery.

Data Availability

Corridors are provided for the lateral acceleration of the vehicle during the turn and longitudinal acceleration during braking.

Applicability of the Data for Human Body Modelling

This data set was designed to investigate the likelihood of the seatbelt slipping off children and it was not designed as validation of HBMs. The lateral acceleration could be easily applied to a simulation, but the full vehicle kinematics cannot be reproduced because the data wasn't provided. Time history traces of the volunteer kinematics weren't presented, and muscle activity was not measured, so validation or tuning may not be possible with this dataset. Further, different subjects used different styles of booster seats or child seats and thus not enough information is provided to simulate the boundary conditions.

Chalmers (2011) On road manual and autonomous braking

References, Institution, Funding

Carlsson, S., & Davidsson, J. (2011). Volunteer occupant kinematics during driver initiated and autonomous braking when driving in real traffic environments. In Proceedings of the International Conference on Biomechanics of Impact IRCOBI, Krakow-Poland.

Institutions

Chalmers University of Technology, Göteborg, Sweden; Volvo Car Corporation, Göteborg, Sweden.

Funding

ASIS project (Algorithm and Software for Improved Safety) which was sponsored partly by The Swedish Governmental Agency for Innovative Systems (VINNOVA) under the Intelligent Vehicle Safety Systems (IVSS) programme.

Summary

The aim of this paper was to quantify the driver and passenger kinematics during medium harsh braking while driving in real traffic. 17 volunteers (8 females, 9 males) were fitted with markers that were tracked with cameras.

Experimental Details

Participants

Participants were split according to sitting height.

Group A: 5th percentile female; 4 females; height 155 (SD 0.8); weight 54.3 (4.9); sitting height 81.8 (0.7) cm; age 43.8 (8.3).

Group B: 50th percentile female; 4 females; height 168 (SD 4.1); weight 68 (5.4); sitting height 88 (0.05) cm; age 42.8 (2.4).

Group C: 50th percentile male; 6 males; height 174.8 (SD 6.8); weight 77.8 (10.5); sitting height 81.8 (0.7) cm; age 43.8 (8.3).

Group D: 95th percentile male; 3 males; height 177 (SD 1.7); weight 72.0 (8.2); sitting height 93.7 (2.4) cm; age 29.7 (3.5).

Instrumentation

Marker targets were placed close to the ear, side of the forehead, the cheek, and a T-shaped holder with a film target on the upper part of the sternum. Further markers were placed on the inside of the vehicle. The positions of these markers were recorded using two cameras mounted inside the vehicle.

Vehicle speed, lateral acceleration, yaw rate, steering wheel angle, brake pedal status, and brake pressure were recorded from the CAN-bus.

Load cases

Both manual and autonomous braking events were recorded. The test drives took place on public roads with speeds between 30-90km/h. Autonomous braking were designed to maintain braking of -3, -4, or -5 m/s^2 for 1.4s. The minimum values of the resulting longitudinal acceleration of the vehicle were: -4.68 ± 0.34 m/s2 for a level of -3 m/s2, -5.69 ± 0.33 m/s2 for -4 m/s2 and -6.73 ± 0.40 m/s2 for -5 m/s2. A subset of the driver braking matching the 5 m/s^2 were also examined.

Boundary Conditions

Volunteers spent an equal amount of time as the driver and as the passenger. The test vehicle was a Volvo XC60. Standard three-point seat belts were used that locked at a vehicle deceleration of 0.5g.

Data Availability

Traces of the vehicle longitudinal acceleration were provided. Time history traces of individual subjects are provided for head angle and displacement.

Applicability of the Data for Human Body Modelling

The data is not presented as corridors, so without access to the underlying data comparisons to HBMs may be difficult. The loading case is straight forward to simulate, but there is a lot of variability in the vehicle accelerations and average accelerations were not provided in the paper. The boundary conditions were complex and would be difficult to simulate.

Graz U. (2011) On sled lateral and braking acceleration

References, Institution, Funding

Kirschbichler, S., Sinz, W., Pruggler, A., Huber, P., & Steiner, K. (2011). Detailed analysis of 3D occupant kinematics and muscle activity during the pre-crash phase as basis for human modeling based on sled tests. In Proceedings of the 22nd International Technical Conference on the Enhanced Safety of the Vehicles (pp. 13-16).

Institutions

Graz University of Technology, Austria; Virtual Vehicle Research and Test Center, Austria.

Funding

COMET K2 – Competence Centres for Excellent Technologies Programme. OM4IS 1 project.

Summary

Sled tests to mimic braking (peak 0.8g, 500ms duration) and lateral acceleration (peak 0.5g, 500ms duration) of volunteers. Volunteer kinematics measured with infrared tracking system and cameras. Muscle activity in upper body measured.

Experimental Details

Participants

11 males with average height of 179 (SD 5) and weight of 74 (4).

Instrumentation

Tests were repeated for the infrared measurement system and high-speed camera system.

For infrared system subjects work a tight-fitting suit wore retro-reflective makers attached to it.

For High-speed camera tests. Subject had markers affixed to head (3), shoulder, elbow, wrist joint, hip, knees, and torso.

Bilateral surface EMG measured from the sternocleidomastoid, rectus abdominis, obliquus externus abdominis, cervical paraspinals, trapezius descending, latissimus dorsi, and erector spinae muscles. No normalization was performed.

Load cases

Frontal acceleration to mimic braking (peak 0.8g, 500ms duration).

Lateral acceleration to mimic steering (peak 0.5g, 500ms duration).

Boundary Conditions

Production automotive seat. Seat pan removed, and a wooden board covered in leather is used. Volunteers are shown in figures holding a piece of Styrofoam in the tests, and it is unclear if they are trying to mimic a driver or passenger posture during the trials.

Data Availability

Exemplar traces of sled acceleration are provided. X vs. Z exemplar head displacement plots are provided.

Applicability of the Data for Human Body Modelling

The loading conditions of this experiment would be simple to simulate, although only exemplar traces of acceleration are provided, and variability is unknown. The boundary conditions should be simple to replicate, but the seat back geometry is unknown and may influence the lateral acceleration tests. There were no response corridors provided, so without some access to the underlying data, validation with this dataset is not possible.

JARI (2012) Lateral accelerations on sled

References, Institution, Funding

Ejima, S., Ito, D., Satou, F., Mikami, K., Ono, K., Kaneoka, K., & Shiina, I. (2012). Effects of pre-impact swerving/steering on physical motion of the volunteer in the low-speed side-impact sled test. In Proceedings of the 2012 International Research Council on Biomechanics Injury Conference (pp. 12-14).

Institutions

Japan Automobile Research Institute; Faculty of sports science, Waseda University; Mito Kyodo General Hospital, Japan.

Funding

Japan Automobile Manufacturing Association.

Summary

In order to simulate the actual pre-crash condition of a car that occurs when the drivers avoid an accident in an emergency situation, low-speed lateral sled tests on human volunteers were conducted using a sled-mounted rigid seat. Muscle activity, kinematics, and reaction loads were measured during these volunteer tests.

Experimental Details

Participants

Three males.

Volunteer	Age (years)	Sex	Height (cm)	Weight (kg)	Sitting height (cm)
I	26	M	176	69	94
II	25	M	166	58	86
III	28	M	178	67	92

Instrumentation

Markers were attached to head (parietal, auditory meatus), shoulder (Acromion), chest (sternum), back (T1, T11), lumbar (L3), arm (elbow), hand (wrist, back), leg (knee). Multiple cameras (Eagle Digital camera), 1280 x 1024 pixels, and marker location was automatically calculated using EVaRT software (NAC Inc.).

Triaxial accelerometers & angular rate sensors were affixed to the sled, head via a mouthpiece, first thoracic vertebra, twelve thoracic vertebrae, and lumbar vertebrae (L3). Triaxial accelerometers were also affixed to the acromion, and sternum.

Single axis loads cells were placed on the pedals, steering wheel, and shoulder belt.

Bilateral surface EMG on sternocleidomastoid, paravertebral, latissimus dorsi, erector spinae, rectus abdominis, obliquus externus abdomens, biceps femoris, rectus femoris, gastrocnemius muscles. EMG was normalized by the largest activity experience across trials for each subject.

Load cases

0.4 & 0.6g lateral accelerations with a duration of 600ms. Each volunteer underwent one exposure to each acceleration with either relaxed or tensed neck muscles.

Boundary Conditions

Rigid seat with seat back. Lap belt. Hands were held at the side of the subject's legs to mimic a passenger.

Data Availability

Exemplar time histories of kinematics, load, and muscle activities for both load levels. Mean and standard deviation of muscle activity for peak activity in different phases of the impact.

Applicability of the Data for Human Body Modelling

With only three subjects, it is not possible to know if the responses recorded are representative of the wider population, so care should be taken when using this data set for tuning or validation. The instrumentation is extensive, but only exemplar traces are provided limiting the utility of the data. Further, the time history of the sled acceleration was not provided, so reproducing the loading conditions is not possible. Finally, the boundary conditions are relatively simple, so they could likely be approximated without difficulty.

VIF, Graz. (2013) In vehicle lane change manoeuvres

References, Institution, Funding

Huber, P., Christova, M., D'Addetta, G. A., Gallasch, E., Kirschbichler, S., Mayer, C., ... & Wallner, D. (2013). Muscle activation onset latencies and amplitudes during lane change in a full vehicle test. In Proceedings of the IRCOBI Conference.

Institutions

Virtual Vehicle Research Center, Graz, Austria; Institute of Physiology, Medical University of Graz, Austria; Robert Bosch GmbH, Schwieberdingen, Germany; Vehicle Safety Institute at Graz University of Technology, Austria; Daimler AG, Sindelfingen, Germany; Sport Science Laboratory, FH Joanneum, University of Applied Sciences, Austria.

Funding

COMET K2 – Competence Centers for Excellent Technologies Programme. OM4IS 1.

Summary

Passengers in a car were subjected to a series of lane change manoeuvres with peak accelerations of around 1 g in the lateral direction. Three awareness conditions were tested: an unaware, an anticipated and an informed condition. Subject kinematics were recorded with an infrared tracking system and muscle activity of three neck muscle and four truck muscles were recorded.

A further series of unpublished results had subjects with a three-point belt in six tests. Part of the OM4IS 1 test series.

Experimental Details

Participants

21 healthy male volunteers (co-driver, age: 33.4 ± 8.8 y, mass: 78.5 ± 6.3 kg, height: 179.2 ± 4.6 cm, sitting height: 91.0 ± 2.0 cm). Attempted to recruit males close to 50th percentile males.

Instrumentation

The vehicle's velocity (sample rate: 10 Hz), acceleration in frontal and lateral directions (50 Hz), steering wheel angel and associated angular velocity (100 Hz), yaw rate and brake pedal activation state (50 Hz) were recorded from the CAN Bus.

Subject wore a tight-fitting suit with a hood that was covered in retro reflective markers. Eight Vicon M2 cameras recorded occupant kinematics, which required the vehicles windscreen and front windows removed with other modifications to the doors.

Bilateral surface EMG on sternocleidomastoideus, trapezius cervicalis and descendants, rectus abdominis, obliquus externus abdominis, latissimus dorsi, erector spinae muscles. No EMG normalization was performed.

Load cases

Lane change manoeuvre: The driver travelling at 50 km/h initiated the manoeuvre by turning the steering wheel by approximately 200° within typically 0.5 s followed by a counter steering action of

around 360° within 0.7 s and a return movement to the neutral position. Lane change performed to the left and right. The first part is meant to closely mimic the VDA lane change manoeuvre.

Manoeuvre was repeated for three conditions of the passenger: unaware (no info given to subject), anticipated (contextual clues make it apparent the manoeuvre was coming), and informed (a countdown was provided)

Boundary Conditions

A Mercedes-Benz S-500 (type: W221, left-hand drive) was used as the test vehicle.

The driver seat was simplified to make it easier to model the boundary conditions. The seat pan and seat back were replaced with wooden boards covered by 40mm of foam, and lateral support structures were added. Seat back angle of 104°, the lateral supports were 314mm apart at 120° angle. The whole seat was wrapped in artificial leather and infrared absorbing material.

The three-point belt was replaced with a lap belt without retractor.

A further series of unpublished tests had a three-point belt.

Data Availability

Visualization of peak trunk displacements are shown. Onset latencies as a function of awareness conditions were provided. Averaged muscle activity between subjects over several time sequences were provided, but unfortunately this data is not valid because the EMG was not normalized and thus you cannot take between subject averages.

Applicability of the Data for Human Body Modelling

This experiment was designed to answer questions about muscle activity during lane changes. It is not suitable to be used for validation or tuning of HBMs because the kinematics were not presented, and EMG was not normalized so applying the data to a model may be difficult.

TNO (2013) On sled lateral and lateral/yaw accelerations

References, Institution, Funding

Van Rooij, L., Elrofai, H., Philippens, M. M. G. M., & Daanen, H. A. M. (2013). Volunteer kinematics and reaction in lateral emergency maneuver tests. Stapp car crash journal, 57, 313.

Institutions

TNO, The Netherlands.

Funding

TASS International.

Summary

The objective of this study was to quantify kinematic behaviour and muscle activation in simulated steering tests in several realistic conditions. Volunteers sat in a custom designed remote-controlled test sled/vehicle and underwent purely lateral manoeuvres at 5 m/s^2 deceleration or simulated lane change manoeuvres at 5 m/s^2 peak acceleration and peak yaw velocity of 25 °/s. Subjects were instrumented with photo markers that were tracked with 3D high-speed stereo cameras and with electromyography (EMG) electrodes on 8 muscles.

Experimental Details

Participants

Ten males participated with average (SD) height of 1.77 (0.04) m, weight of 73.3 (4.5) kg, and age of 41 (9) years.

Instrumentation

Stereo cameras recorded markers that featured high contract speckle pattern on tape that were affixed to the left gleno-humeral joint, the left elbow joint, the left and right wrist joint and the left knee joint. A marker bracket was directly attached to the skin overlaying the spinous process of vertebra T1 and a head cap was developed that contained an array of markers. The markers position in space were tracked with automatic digital image correlation.

Bilateral surface EMG recorded activity of the sternocleidomastoid and longus capitis muscles for all subjects. Other muscle measured on some subjects included bilateral longissimus, obliquus externus abdominis, biceps femoris, and triceps brachii muscles. EMG was normalized based on the largest activity recorded across trials for each muscle and subject.

Load cases

A pure lateral acceleration with a constant acceleration of 5 m/s^2 and an initial jerk of 130 m/s^3. Tests were performed with this motion in both left and right direction.

A lane change manoeuvre in which the occupant experienced a sinusoidal lateral acceleration with approximately 5 m/s^2 peak in combination with a yaw motion with approximately 25 °/s peak. The vehicle was moving with 5 km/h in lateral direction prior to initiation of the lane change manoeuvre. The simulated event was derived from the measured response of a small family car in a Euro NCAP Electronic Stability Control (ESC) test [Euro NCAP, 2011].

Different subjects did different combinations of these two load cases to the left or right while holding the steering wheel or not and relaxed or braced. Table 2 in the paper gives a summary of the conditions and the number of subjects that performed each combination of factors. A total of 108 test were conducted with 10 subjects.

Boundary Conditions

A non-functional steering wheel was mounted inside the vehicle, as well as a footplate. A rigid seat was used (RCI Poly Highback Seat 8000S). This seat is typically used in rally sport, made of polypropylene with an ergonomic shape, lateral support in the hip area and an integrated headrest. A four-point harness (Securon 700) with inertial reel on the shoulder straps was mounted as well. Investigators pre-tensioned the lap belt to approximately 50N.

Data Availability

Extensive volunteer corridors of the kinematics were provided. Exemplar EMG traces were provided along with mean SD of peak muscle activity for the different conditions.

Applicability of the Data for Human Body Modelling

The extensive time histories provided make the kinematics of this data set well suited to being used in tuning or validation as the loading conditions should be easily replicated and kinematic responses easily compared to their corridors. The boundary conditions are relatively simple and well described so with some effort would likely be reproducible in a model. The EMG activity of the longissimus and longus capitis cannot be isolated with surface electrodes and therefore the author's recordings

cannot be attributed solely to the activity of these muscles. Further, the normalization of the EMG was not done against MVIC values, and thus is challenging to interpret for the Hill muscle model.

Chalmers (2012) In vehicle autonomous braking with pre-tensioned belts

References, Institution, Funding

Östh, J., Ólafsdóttir, J. M., Davidsson, J., & Brolin, K. (2013). Driver kinematic and muscle responses in braking events with standard and reversible pre-tensioned restraints: validation data for human models (No. 2013-22-0001). Stapp - SAE Technical Paper.

Ólafsdóttir, J. M., Östh, J., Davidsson, J., & Brolin, K. (2013). Passenger kinematics and muscle responses in autonomous braking events with standard and reversible pre-tensioned restraints. In Ircobi conference 2013 (No. IRC-13-70, pp. 602-617).

Institutions

Chalmers University, Umeå University.

Funding

Autoliv Research AB, Volvo Group, and Volvo Car Corporation.

Summary

Volunteers either as a driver or a passenger in an actual vehicle were exposed to autonomous emergency braking (peak 1.1g) with and without reversible pre-tensioned restraints, and they also performed voluntary emergency braking for a total of five conditions. Kinematics were measured by tracking markers with video cameras and muscle activity was measured in 8 muscles throughout the body.

Experimental Details

Participants

20 volunteers in total. 11 males with average age of 32.7 (SD 12.5), height of 178.2 (5.2) cm, weight 77.5 (5.6) kg, and seated height 946.5 (26.2) mm. 9 females with average age of 28.8 (5.9), height of 166.6 (5.0), weight 59.4 (5.2) kg, and seated height of 893.9 (33.2) mm.

Instrumentation

Film markers were placed on the head (3 markers aligned with Frankfurt plane), sternum, middle deltoid, lateral epicondyles of the humerus, between the styloid processes of the radius and ulna.

Bilateral surface EMG on sternocleidomastoid, cervical paravertebral muscles, rectus abdominis, lumbar paravertebral muscles, biceps brachii, tri triceps brachii, anterior deltoid, and the posterior deltoid. EMG was normalized based on the MVIC measured in a lab before the in-car tests.

Load cells on lap and shoulder belt. Brake pedal and foot well load cells. Accelerometer mounted to front left mount of passenger chair.

Load cases

Five load cases: Passenger autonomous braking with standard belt; Passenger autonomous braking with reversible pre-tension belt; Driver autonomous braking with standard belt; Driver autonomous braking with reversible pre-tension belt; Driver manual braking.

All load cases involved maximum emergency braking from a speed of 70km/h with a speed change of 50km/h which resulted in a peak acceleration of 1.1g.

Autonomous braking events were triggered by researchers at times unknown to the occupant to trigger the vehicle's built-in systems.

Boundary Conditions

Volunteers were driven in or drove a 2012 Volvo V60 T4 with leather upholstery. Volunteers adjusted the car seat for a comfortable fit (fore-aft, seat back angle, steering wheel position and angle). The seat base was at its lowest angle and adjustments of height and angle were not permitted.

The vehicle's three-point seat belt retractor was replaced with an Autoliv supplied Active seatbelt. In reversible pre-tension trials, 170 N was applied to the belt 200 ms before autonomous braking. In standard seat belt trials, no pretension was applied, and the retractor locked at 0.45 g vehicle acceleration, or 1.5 g belt pull-out acceleration.

Data Availability

Extensive corridors of the kinematics of the vehicle and passenger along with muscle activity were provided. Detailed description of the vehicle seat and model characterization of the seat were provided.

Applicability of the Data for Human Body Modelling

This data set is well suited to being used as tuning or validation data and the extensive corridors provided make it a potentially rich dataset. The EMG is normalized by MVIC, so the results are easy to interpret in the Hill muscle model. The loading conditions are well documented and should be easily replicated. Although due to the on-road testing environment, there is variability in the loading conditions and therefore understanding model response for the mean and mean +/- standard deviation of vehicle acceleration may be important. The boundary conditions are complex including interactions with the seat, steering wheel, foot well, and the reversible pretensioned three-point belt. Although, the group responsible for this experiment have mechanically characterized the physical seat used and developed an LS-Dyna model of the vehicle environment. If this model is available, the boundary conditions would be simple to simulate. Without this model the authors have attempted to provide detailed information of the boundary conditions, which may make it possible to approximately model the boundary conditions. One potential downside to this dataset for validation is that volunteer kinematics were not captured with accelerometers or angular rate sensors, and differentiation of displacement is a problematic method to calculate these measures.

JARI (2013) On sled braking acceleration with belt pre-tensioner

References, Institution, Funding

Ito, D., Ejima, S., Kitajima, S., Katoh, R., Ito, H., Sakane, M., ... & Kimura, T. (2013, September). Occupant kinematic behavior and effects of a motorized seatbelt on occupant restraint of human volunteers during low speed frontal impact: mini-sled tests with mass production car seat. In Proceedings of the IRCOBI Conference.

Institutions

JARI; University of Tsukuba, Japan; Takata Corporation.

Funding

n/a.

Summary

The objective was to evaluate the change of posture of volunteers during pre-impact braking. Three volunteers were exposed to 0.82 g with a duration of approximately 1s on a sled. Volunteers were restrained with a standard three-point belt or motorized seatbelt and they were instructed to be relaxed or tensed before the trials. Kinematics were measured with a 3D video capture system and EMG was measured in several body regions.

Experimental Details

Participants

Three males with mean (SD) height of 170.3 (2.5) cm and weight of 68.6 (5.9) kg.

Instrumentation

Three-dimensional motion capturing system was used to track the motion of the markers on the head, T1, T12, L3 and left and right shoulder.

Load cells measured the foot-plate reaction force and shoulder belt force.

EMG was measured in the sternocleidomastoideus, paravertebralis, latissimus dorsi, erector spinae, rectus abdominis, obliquus externus abdominis, biceps femoris, rectus femoris, gastrocnemius. EMG was normalized by maximum voluntary contraction performed before the sled trials, although the details of these procedures were not included in the paper.

Load cases

Acceleration of 0.82 g with a duration of approximately 1 s in a direction mimicking braking. The time history of acceleration was parabolic in shape.

Four exposures were given to each volunteer with one exposure with the standard or motorized seatbelt in a relaxed or tensed state.

Boundary Conditions

Volunteer mimicked the posture of a passenger with their hands in their lap.

An automotive seat (brand and year not provided) and foot plate are use. The headrest was removed from the seat.

Standard three-point belt was utilized for half of the trials, with no further details provided. A motorized three-point belt was used in the other half of trials. This belt takes 120 ms to produce 120 N of pretension force. No details are provided for the timing of the pre-tension relative to the acceleration pulse.

Data Availability

Time history of the applied acceleration were provided. Corridors of the shoulder belt forces, pedal forces, head and T1 fore-aft displacement, and muscle activity were provided for each experimental condition.

Applicability of the Data for Human Body Modelling

This dataset is potentially well suited to validation of HBMs for the type of acceleration applied in this study. With three volunteers it is unknown if the responses measured represent the wider population. The loading conditions are easily replicated with the provided time histories. Although, the researchers did not attempt to produce an acceleration profile representative of pre-impact braking, rather they applied a parabolic acceleration profile. The dataset would still be useful to validate a model's biofidelity under these conditions. The boundary conditions are simple and thus may be roughly approximated. Important information about the type of seat and seatbelt geometry are not provided and the timing of the pre-tensioner is unclear, so modellers will be faced with some uncertainty in trying to reproduce this dataset. Muscle activity was normalized by MVIC, so is well suited to for validating muscle controller output in a model.

VIF, Graz (2014) Braking, lane change, and combined manoeuvres in vehicle

References, Institution, Funding

Huber, P., Kirschbichler, S., Prüggler, A., & Steidl, T. (2015). Passenger kinematics in braking, lane change and oblique driving maneuvers. In Proc. of IRCOBI.

Huber, P., Kirschbichler, S., Prüggler, A., & Steidl, T. (2014). Three-dimensional occupant kinematics during frontal, lateral and combined emergency maneuvers. In International IRCOBI Conference on the Biomechanics of Impact, Berlin, Germany.

Kirschbichler, S., Huber, P., Prüggler, A., Steidl, T., Sinz, W., Mayer, C., & DAddetta, G. A. (2014, September). Factors influencing occupant kinematics during braking and lane change maneuvers in a passenger vehicle. In International IRCOBI Conference on the Biomechanics of Impact, Berlin, Germany.

Institutions

Virtual Vehicle Research Center, Graz, Austria; Vehicle Safety Institute at Graz University of Technology, Austria.

Funding

COMET – Competence Centers for Excellent Technologies – programme. OM4IS 2.

Summary

A series of vehicle-based driving manoeuvres were performed, where occupants in the passenger position were subjected to emergency braking manoeuvres at 12 km/h and 50 km/h, lane change manoeuvres to the left and the right and combined manoeuvres, where a combination of lateral and frontal accelerations occurred.

A further series of tests that are unpublished measured occupants' response in driving around a circle with braking, Slalom, and a vehicle handing course. Part of the OM4IS 2 test series.

Experimental Details

Participants

6 female (mass: 63.0 ± 10.4 kg, height: 169.0 ± 4.1 cm, age: 31.5 ± 9.3 y) and 19 male (mass: 77.8 ± 8.4 kg, height: 178.2 ± 5.0 cm, age: 28.2 ± 3.8 y) subjects.

A further 8 males are unpublished. Approximately 50th percentile.

Instrumentation

The vehicle's velocity (sample rate: 10 Hz), acceleration in frontal and lateral directions (50 Hz), steering wheel angel and associated angular velocity (100 Hz), yaw rate and brake pedal activation state (50 Hz) were recorded from the CAN Bus.

Subject wore a tight-fitting suit with a hood that was covered in retro reflective markers. Eight Vicon M2 cameras recorded occupant kinematics, which required the vehicles windscreen and front windows removed with other modifications to the doors.

Load cases

Manual emergency braking from 12 km/h and 50 km/h.

Lane change manoeuvre: The driver travelling at 50 km/h initiated the manoeuvre by turning the steering wheel by approximately 200° within typically 0.5 s followed by a counter steering action of around 360° within 0.7 s and a return movement to the neutral position. Lane change performed to the left and right.

In the combined manoeuvre the driver again was traveling at 50 km/h and turned the steering wheel by approximately 220° within 0.6 s while simultaneously pressing the brake pedal at sufficient effort to activate the brake assistant system.

Boundary Conditions

A Mercedes-Benz S-500 (type: W221, left-hand drive) was used as the test vehicle.

The driver seat was simplified to make it easier to model the boundary conditions. The seat pan and seat back were replaced with wooden boards covered by 40mm of foam, and lateral support structures were added. Seat back angle of 104°, the lateral supports were 314mm apart at 120° angle. The whole seat was wrapped in artificial leather and infrared absorbing material.

The standard pre-tensioner was disabled on the three-point seat belt.

Data Availability

Extensive corridors of the kinematics of the vehicle and passenger were provided. Detailed description of the vehicle seat and model characterization of the seat were provided.

Applicability of the Data for Human Body Modelling

Extensive response corridors of volunteer kinematics make this data potentially useful for kinematic validation of HBMs, but the lack of muscle activity recorded potentially limits the utility of the dataset. Further, the linear and angular displacements of the head and torso measured in this study may be difficult to relate to a human body model because the authors calculated these as the centroid of several markers and this centroid does not correspond with an anatomically significant or readily identifiable location. The paper mentions their kinematic locations lie at the "ear and T5 level for the head and torso." Loading conditions are well presented in corridors and should therefore be

reproducible. Although, CAN bus data for vehicle kinematics may not be the most accurate source of data. The geometry of the seat they used is generally well defined which will aid in modelling the boundary conditions, but in vehicle tests always have a lot of detail which can be difficult to model.

Chalmers (2016) On sled multidirectional horizontal plane accelerations.

References, Institution, Funding

Ólafsdóttir, J. M., Fice, J. B., Mang, D. W., Brolin, K., Davidsson, J., Blouin, J.-S., & Siegmund, G. P. (2018). Trunk muscle recruitment patterns in simulated precrash events. *Traffic injury prevention*, *19*(sup1), S186-S188.

Ólafsdóttir, J. M., Fice, J. B., Mang, D. W., Brolin, K., Davidsson, J., Blouin, J.-S., & Siegmund, G. P. (2016). Neck muscle activation patterns in dynamic conditions. *Traffic injury prevention,* Vol. 17, pp. 219-221.

Institutions

Chalmers University, University of British Columbia.

Funding

FFI (Strategic Vehicle Research and Innovation) by VINNOVA, the Swedish Transport Administration, the Swedish Energy Agency, and the industrial partners, Autoliv Research AB and Volvo Car Corporation, and partly by Mitacs Inc., AUTO21 and CIHR.

Summary

Volunteers were exposed to accelerations on a sled in eight directions in the horizontal plane. Muscle activity was recorded with indwelling electrodes in the neck and torso.

Experimental Details

Participants

3M and 1F subjects aged 23-56 years old participated in the study.

Instrumentation

Indwelling electrodes were inserted under ultrasound guidance in the neck and torso. In the torso electrodes were place in the left rectus abdominis, internal oblique, iliocostalis, and multifidus (MU) muscles at the L2–L3 level. In the neck electrodes were place in the left sternohyoid, sternocleidomastoid, trapezius, levator scapulae, splenius capitis, semispinalis capitis, semispinalis cervicis, and multifidus muscles at the C4-C5 level. Muscle activity was normalized to MVIC.

Load cases

The sled acceleration for was accelerated at 0.55g for 0.76s with a speed change of 4m/s. This pulse was applied in 8 directions (0°, ±45°, ±90°, ±135°, 180°). The acceleration was meant to mimic the levels of accelerations seen in pre-crash braking or steering.

Boundary Conditions

Subject sat in a 2005 Volvo S40 seat with the head restraint removed and only a lap belt was used. Subjects sat with their hands in their lap looking straight ahead and relaxed before each acceleration.

The seatback angle was 22° and the feet were supported by footplates angled 55° from horizontal and longitudinally adjusted to forma 115° knee angle.

Data Availability

The spatial tuning curves averaged between subjects for each muscle were presented. These spatial tuning curves plot muscle activation level as a function of acceleration direction. Exemplar sled acceleration traces were also provided.

Applicability of the Data for Human Body Modelling

The data provided in these experiments has proved valuable for the development of omni-directional controllers in active HBMs at Chalmers University. The data can inform a muscle controller which muscles need to activate to resist relative motions of the neck or truck as a function of the direction of motion. It is possible for other groups to use the data in the same manor, but this dataset is not typical validation data as only four subjects are included, and time histories of subject kinematics have not been made available.

IfF (2017) Different automation levels in pre-crash braking.

References, Institution, Funding

Florian Krauns, Kajetan Kietlinski, Roman Henze, Martin Tijssens, Ferit Küçükay

171127_VDIFzgsicherheit_Krauns.pdf

Internal Report.

Institutions

Institut für Fahrzeugtechnik (IfF), TASS International Wiesbaden, TASS International Niederlande

Funding

Not available.

Summary

Seven male volunteers in pre-crash braking with manual and autonomous braking in vehicle. For manual braking, relaxed and tensed volunteers were examined. In autonomous braking, a belt reversible pre-tensioner was used and cases with the subject’s hands on the wheel or in their lap were investigated.

Experimental Details

Participants

Seven males near 50th percentile.

179, 181,181,178,178,179cm in height and 71.1,65.2,83.5,82.7,74.1,78.4kg weight.

Instrumentation

2 3D cameras (Sensor GOM Aramis) tracked 6DOF marker plates affixed to the vehicle, chest, shoulders, mounted to glasses, forehead, and upper legs.

Vehicle status was collected from the CAN bus.

An IMU measured vehicle kinematics.

Load cases

Four load cases were considered. All braking from 50km/h.

Manual braking at 4 m/s^2 without reversible pretensioner while related or tensed.

Autonomous braking at 10 m/s^2 with reversible pretensioner while relaxed and holding the wheel or not.

Boundary Conditions

Volunteers were drivers in a Volkswagen Golf (model year unknown).

The reversible pre-tensioner produced a max belt force of 200 N and it began 0.5 s before braking and ended 0.5s after the vehicle stopped.

Data Availability

The internal report shows exemplar displacement and angular measurements of the head and torso.

Applicability of the Data for Human Body Modeling

More information is required for this assessment.

Chalmers (2018) Autonomous lane change manoeuvres in vehicle

References, Institution, Funding

Ghaffari, G., Brolin, K., Bråse, D., Pipkorn, B., Svanberg, B., Jakobsson, L., & Davidsson, J. (2018). Passenger kinematics in Lane change and Lane change with Braking Manoeuvres using two belt configurations: standard and reversible pre-pretensioner. In Ircobi conference 2018 (No. IRC-18-80, pp. 493-511).

Further publications are under preparation.

Institutions

SAFER vehicle and traffic safety centre at Chalmers University, Gothenburg, Sweden

Funding

FFI-Strategic Vehicle Research and Innovation.

Summary

Twenty-five volunteers (13 males, 12 females) were exposed to autonomous lane changes with or without braking and with or without reversible pre-tension belt. Lane change manoeuvres were performed at an initial vehicle speed of 73 km/h and produced maximum lateral acceleration of 6.1 m/s^2 while a lane change with braking manoeuvre produced a maximum lateral acceleration of 5.4 m/s^2 and a longitudinal acceleration of 5.6 m/s^2. Kinematics were measured by tracking markers with a camera and EMG was recorded from 19 bilateral muscles that spanned the neck, torso, and limbs.

Experimental Details

Participants

Thirteen males with an average age of 37.9 (SD 17.3) years, height of 181.3 (5.7) cm, weight of 73.8 (8.3) kg, and sitting height of 949.2 (27.8) mm.

Twelve females with an average age of 37.3 (13.1) years, height of 168.1 (5.8) cm, weight of 66.8 (15) kg, and sitting height of 888.8 (27.1) mm.

Instrumentation

Film markers (white foam spheres 25mm in diameter) were placed on the head (5 markers), sternum, T1 spinal process, left and right acromion, lateral epicondyles of the humerus. These markers were captured with three colour cameras recording at 50 f/s at 1280 x 1080 resolution.

Bilateral surface EMG on sternocleidomastoid, scalene, cervical paravertebral muscles, upper trapezius, posterior and anterior deltoid, lower trapezius, latissimus dorsi, erector spinae, biceps brachii, triceps brachii, external oblique, rectus abdominis, serratus anterior, pectoralis major, gluteus maximus, semitendinosus, rectus femoris, vastus medialis. EMG was normalized based on the MVIC measured in a lab before the in-car tests.

A six axis loadcell was mounted between the steering wheel and steering column. Single axis load cells were also located on the lap and shoulder belt, and foot well. Further a pressure mat between the seat pan and subject measured the pressure distribution during the load cases.

Vehicle status including steering wheel angle, throttle position, and brake pedal position were collect from the CA-bus at 100 Hz. Vehicle kinematics were measured with a roof mounted inertial measurement unit which recorded at 100 Hz.

Load cases

Autonomous lane changes with or without braking and with or without reversible pre-tension belt were performed with volunteers in the passenger or driver seat. Three repetitions were performed for each manoeuvre. The lane changes were performed at an initial vehicle speed of 73km/h and produced maximum lateral acceleration of 6.1 m/s^2 while a lane change with braking manoeuvre produced a maximum lateral acceleration of 5.4 m/s^2 and a longitudinal acceleration of 5.6 m/s^2.

Autonomous events were triggered by researchers at times unknown to the occupant to trigger the vehicle's built in braking system and/or a custom steering robot developed by Autoliv Research.

Boundary Conditions

Volunteers were passengers or drivers in a 2016 Volvo V60 with leather upholstery. Volunteers adjusted the car seat for a comfortable fit (fore-aft, seat back angle, steering wheel position and angle). The seat base was at its lowest angle and adjustments of height and angle were not permitted.

The vehicle's three-point seat belt retractor was replaced with an Autoliv supplied Active seatbelt. In reversible pre-tension trials, 170 N was applied to the belt 200 ms before autonomous braking. In standard seat belt trials, no pretension was applied, and the retractor locked at 0.45 g vehicle acceleration, or 1.5 g belt pull-out acceleration.

Data Availability

At this time kinematic corridors of vehicle and volunteers in the passenger seat have been published. In time extensive corridors of most of the data streams, including muscle activity, will be published.

Applicability of the Data for Human Body Modeling

This dataset will be well suited to being used as tuning or validation data once the likely extensive corridors have been published. This is ongoing work. The EMG is normalized by MVIC, so the results are easy to interpret in the Hill muscle model. The loading conditions are well documented and should be easily replicated. The boundary conditions are complex including interactions with the seat, steering wheel, foot well, and the reversible pretensioned three-point belt. These complexities are amplified due to the lateral acceleration applied in these load cases which may lead to interactions with the inner door and side window or centre console of the vehicle. Although, the group responsible for this experiment have developed an LS-Dyna model of the vehicle environment. If this model is available, the boundary conditions would be simple to simulate. Without this model the authors have attempted to provide detailed information of the boundary conditions, which may make it possible to approximately model the boundary conditions. Potential downside to this dataset for validation is that volunteer pelvis kinematics are not made available and kinematics were not captured with accelerometers or angular rate sensors, and differentiation of displacement is a problematic method to calculate these measures.

UMTRI (2018) Age and BMI influence, in vehicle braking, lane change, and cornering

References, Institution, Funding

Reed, M., Ebert, S.M., Park, B.-K.D., Jones, M.L.H. (2018). Passenger kinematics during crash avoidance maneuvers. Ann Arbor: University of Michigan Transportation Research Institute (UMTRI-2018-5).

Institutions

University of Michigan Transportation Research Institute, Ann Arbor, MI, USA.

Funding

Toyota Collaborative Safety Research Center.

Summary

Several lane change and maximal braking events. Detailed anthropometric data were obtained from each participant, including 3D body scans. Vehicle motions were recorded with an inertial measurement unit and passenger head motions were tracked using a novel system based on a Microsoft Kinect sensor.

Experimental Details

Participants

Eighty-seven adults (44 women and 43 men) participated in the study.

Participants	BMI<30 (kg/m²)	BMI >= 30 (kg/m²)	Age < 55 (years)	Age >= 55 (years)	Total
Female	27	17	23	21	44

Mean (SD)	24.5 (3.1)	39.4 (8.6)	30.7 (10.3)	62.1 (3.4)	
Male	27	16	27	16	43
Mean (SD)	24.6 (3.1)	35.4 (5.2)	32.5 (11.3)	62.1 (4.9)	
Total	53	34	50	37	87

Instrumentation

MicroStrain 3DM-GX5-10 inertial measurement unit (IMU) was installed near the mass centre of the vehicle to quantify the acceleration and rotation rates of the vehicle.

Webcam was installed on the headliner to monitor foot position.

Kinect camera placed near the centre of the dashboard facing the passenger was used to track head kinematics using a 3D facial recognition approach. Further targets were placed on the seat belt webbing where it crossed the sternum, clavicle, and midline of the pelvis. Other targets were placed along the lap and shoulder belt at locations that were visible to the Kinect camera.

Load cases

Braking abruptly while traveling straight; 1g longitudinal acceleration with 2s duration.

Turning sharply on a skid pad followed by abrupt braking; 0.7g lateral and 1g longitudinal with a duration of 3s.

Quick lane-change to the right; 0.7g lateral acceleration with 1.2s duration

Boundary Conditions

Subjects were a passenger (right hand side) in a 2016 Toyota Avalon sedan with leather seats. The standard three-point belts with retractors were utilized. Seat was set to the lowest position, flattest cushion angle, and a back angle of 23 degrees (SAE J826) and moved fully rearward on seat track

Data Availability

Corridors of vehicle acceleration in longitudinal and/or lateral directions when appropriate for each loading condition were provided. Also provided were regression fits for head excursion as a function of age, BMI, and stature. Finally, corridors of head kinematics were presented as a function of age, bmi, and stature.

Applicability of the Data for Human Body Modeling

The kinematics of the volunteers recorded from this study are well suited for human body modeling. The corridors of the vehicle kinematics should make the loading conditions easy to model and the corridors of head displacements are well presented. This data is especially well suited to HBMs of different sizes because the response corridors of head excursion are presented for different ages, statures, and BMI. A deficit of using this data is that torso kinematics are not reported, and muscle activation was not measured. Further, the boundary conditions would be very difficult to model without access to the vehicle used or a similar model to take measurements of the passenger area.

VIF (2018) PRECOONI Sled Tests

References, Institution, Funding

Presented at Human Modelling and Simulation Symposium 2018. Reference needed.

Institutions

VIF, Graz.

Funding

Part of the PRECOONI series of tests. Funded by COMET K2.

Summary

Information needed. Six subjects on a sled. 2D Laser used to carefully characterize initial subject position.

Experimental Details

Participants

Six subjects participated in the study. Detailed seated anthropometrics measured, but not available to include in this report.

Instrumentation

3 Highspeed camera used to track occupant kinematics. Specific body regions tracked unknown.

Muscle activity recorded, but which muscles is unknown.

3D Forces between footrest and sled.

6D Forces & Moments between sled and seat base.

X3 Pro seat mat between subject and seat back.

1d sled accelerometer.

2 belt force transducers.

Load cases

Unknown.

Boundary Conditions

Simplified seat geometry with some details shared.

Data Availability

Unknown.

Applicability of the Data for Human Body Modeling

More information is required to make this assessment.

VIF (2018) Daimler Steering Tests

References, Institution, Funding

Not published.

Institutions

VIF, Graz. Daimler

Funding

Daimler.

Summary

Drivers performed 11 manoeuvres manually on a closed test track. Vehicle tests using what appears to be the same vehicle from OM4IS 2 (0).

Experimental Details

Participants

14 males.

Instrumentation

Vehicle Kinematics with CAN-bus data.

Driver EMG.

Subject Kinematics with adapted Vicon System.

Go Pro videos (top, front, side).

Load cases

Driving straight ahead, Lane change left, Lane change right, Extreme lane change left (max. g), Extreme lane change right (max. g), Slalom course, Turning manoeuvre to the left, Turning manoeuvre to the right, Full braking straight on, Combined: Full braking & turn to the left, Combined: Full braking & turn to the right.

Boundary Conditions

Mercedes S-class (W221) test vehicle. Driver position. Three-point belt. Closed test track.

Data Availability

Unknown.

Applicability of the Data for Human Body Modelling

More information is required to make this assessment.

B. APPENDIX – DATA FOR THE DEVELOPMENT OF ACTIVE HBMS

OM4IS2 data

Emergency braking manoeuvres at **12 km/h and 50 km/h**, single lane change manoeuvres to the left and right side at 50 km/h and combined braking and steering manoeuvres also at 50 km/h were performed. For the braking as well as the combined manoeuvres acceleration level was set to the peak value which could be reached with a **series production car** (~ 1g). The focus of the movement studies was on the kinematics of 50th percentile subjects. 27 male and 6 female subjects were measured.

Three awareness states were investigated. For the determination of the occupant kinematics a Vicon V612 motion-capturing system with eight near infra-red cameras and a sample frequency of 100 Hz was used. The vehicle states (Vehicle accelerations, steering wheel angle, angular velocity and brake status) were determined using Dewetron Dewe5000. For a small subset of 5 volunteers muscle activity was measured bilaterally using surface EMG.

Publications were done in Huber et al. 2013, Huber et al. 2014, Huber et al. 2015 and Kirschbichler et al. 2014.

Ethics

The Ethics Commission of Medical University of Graz approved the volunteer tests from an ethics point of view.

Disclaimer

Volunteer test data – principles of use (derived from CA)

- For the volunteer test data made available by the OSSCAR partners on OSCCAR projectplace/ sharepoint the following shall apply:
- The test data provided by a partner may be used by another OSSCAR partner to validate, improve and extend occupant models.
- In particular a partner using the data is not allowed to disclose the data to any third party.
- For any use of these data after the OSSCAR project Art 11.3.2. and Art 11.3.5 of the OSSCAR Consortium Agreement shall apply meaning that the partner shall make a written request for any access rights to the owner of the data and a written agreement has to be concluded in order to agree on the conditions of granting access rights to these data.
- For the sake of clarification, it is stated that the evaluated and improved models are not subject to any CA related restrictions.

Furthermore, OSCCAR plans to publish a set of data incl. boundary conditions in order to have an OSCCAR harmonized set of data to validate active model behaviour. The detail on that is still subject of future work here and requires prior partner agreement!

Methods

Volunteer description

In total 33 subjects - six female (mass: 63.0 ± 10.4 kg, height: 169.0 ± 4.1 cm, age: 31.5 ± 9.3 y) and twenty-seven male (mass: 77.8 ± 8.4 kg, height: 179.1 ± 4.7 cm, age: 25.4 ± 9.6 y) subjects were tested in this series in various tests[1]. Following tables, Table A - 1, Table A - 2 and Table A - 3, show manoeuvres of the full data pool of trials that were usable.

Some of the volunteers did not arrive for testing or some datasets were corrupt, therefore data from 33 subjects only could be postprocessed (out of a full set of 39). Female IDs: 5, 10, 16, 19, 20, 26 (out of the IDs 1 - 39).

PARAMETERS OF THE MANOEUVRE AND SUBJECT PROPERTIES							
Manoeuvre	velocity [km/h]	#subjects	#male	#female	height [cm] mean ± std.dev.	weight [kg] mean ± std.dev.	Age (years) mean ± std.dev.
Brake12_01	12	26	20	6	176.0 ± 6.1	74.5 ± 10.7	29.0 ± 9.5
Brake12_02	12	25	19	6	176.0 ± 6.1	74.7 ± 10.8	29.0 ± 9.7
Brake50_01	50	23	17	6	175.7 ± 6.4	73.9 ± 10.4	29.0 ± 10.1
LaneLeft50	50	25	20	5	177.1 ± 6.6	75.1 ± 11.4	28.7 ± 8.9
LaneRight50	50	24	19	5	176.8 ± 6.5	74.7 ± 11.4	28.9 ± 9.1
CombinedLeft50	50	30	25	5	177.6 ± 6.1	75.0 ± 10.8	28.5 ± 8.1
CombinedRight50	50	30	26	4	178.0 ± 5.8	77.0 ± 9.0	28.7 ± 10.2

Table A - 1:

[1] Additionally combined braking and swerving manoeuvres, braking during a stationary circle and manoeuvres in a handling and slalom parcours were recorded, but not included in this report. For selected subjects additional electromyography recordings of eight bilateral muscles were performed, which are also not included here. Only selected subjects of test series B are included in this report.

PARAMETERS OF THE MANOEUVRE AND SUBJECT PROPERTIES (**MEN**)					
manoeuvre	velocity [km/h]	#subjects	height [cm] mean ± std.dev.	weight [kg] mean ± std.dev.	Age (years) mean ± std.dev.
Brake12_01	12	20	178.2 ± 4.9	78.0 ± 8.1	28.2 ± 9.4
Brake12_02	12	19	178.2 ± 5	78.4 ± 8.1	28.2 ± 9.6
Brake50_01	50	17	178.0 ± 5.3	77.7 ± 7.4	28.1 ± 10.0
LaneLeft50	50	20	179.1 ± 5.4	78.9 ± 8.6	28.9 ± 9.7
LaneRight50	50	19	178.8 ± 5.4	78.6 ± 8.7	29.0 ± 10.0
CombinedLeft50	50	25	179.2 ± 4.9	78.1 ± 8.5	28.6 ± 8.7
CombinedRight50	50	26	179.2 ± 4.9	78.5 ± 8.3	28.3 ± 9.9

Table A - 2:

PARAMETERS OF THE MANOEUVRE AND SUBJECT PROPERTIES (**WOMEN**)					
manoeuvre	velocity [km/h]	#subjects	height [cm] mean ± std.dev.	weight [kg] mean ± std.dev.	Age (years) mean ± std.dev.
Brake12_01	12	6	169.0 ± 4.2	63.0 ± 10.4	31.5 ± 9.3
Brake12_02	12	6	169.0 ± 4.1	63.0 ± 10.4	31.5 ± 9.3
Brake50_01	50	6	169.0 ± 4.1	63.0 ± 10.4	31.5 ± 9.3
LaneLeft50	50	5	169.2 ± 4.6	59.8 ± 7.7	28.2 ± 5.1
LaneRight50	50	5	169.2 ± 4.6	59.8 ± 7.7	28.2 ± 5.1
CombinedLeft50	50	5	169.2 ± 4.6	59.8 ± 7.7	28.2 ± 5.1
CombinedRight50	50	4	170.7 ± 4.3	67.8 ± 9.5	31.3 ± 11.7

Table A - 3:

For the presented test series, a modified standard seat was used.

Boundary Conditions

Manoeuvres were performed on a closed test track in a Mercedes-Benz S-500 (type W221; width: 1.78 m, length: 5.23 m, wheelbase: 3.17 m, see Figure A - 1a) that used a modified co-driver standard seat that is described in [1].

For the series the standard seat was replaced with a modified seat (see Figure A - 1b) where the original seat frame was used but the cushions were replaced by wooden plates, covered in artificial leather.

(a) (b)

Figure A - 1: Left (a): The vehicle was equipped with eight Vicon infrared motion capturing cameras. Note that the windshield and the passenger window are removed; Right (b): Reference seat having lateral support structures

For the seat in Figure A - 1 b lateral support structures were added, where the geometry was close to the geometry of the original seat (Angle lateral support: 120°, distance between left and right piece: 314 mm). A layer of foam (thickness: 40 mm) was applied to the wooden plates at the seat surface and back rest as well as on the lateral support structures. These were covered in artificial leather and a layer of light absorbing material to reduce reflections in the infrared spectrum. Afterwards the seat was then scanned, and 3D cloud data was generated. The standard three-point belt was used with the pre-tensioner disabled. The seat model was updated in the project PRECOONI; additional information on how to access the model please see Appendix 0.

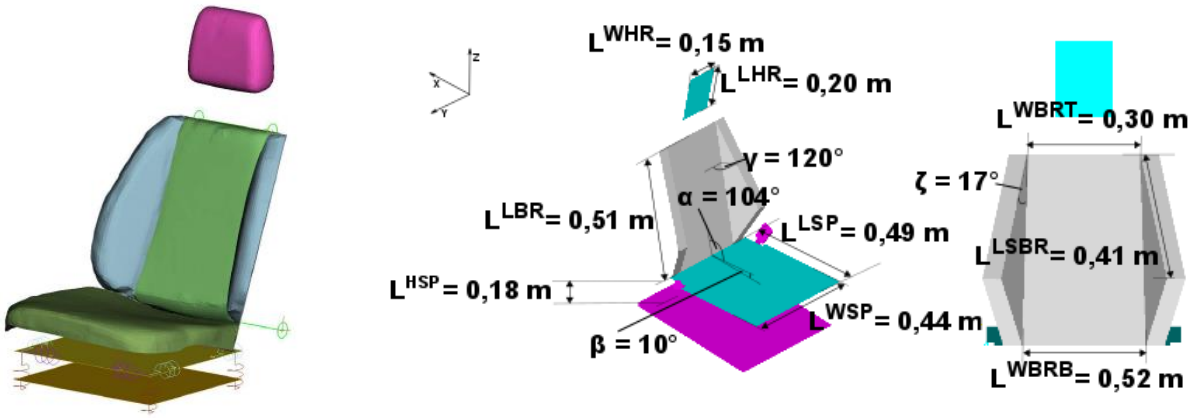

(a) (b)

Figure A - 2: Left (a): Scanned and built-up FE model of seat; Right (b): Main dimensions of seat

The seat foam was represented with *MAT_LOW_DENSITY_FOAM in LS-Dyna with the compression characteristics for the foam derived from foam block tests done at TU Graz as a part of PRECOONI project as illustrated in Figure A - 2.

To evaluate the lateral stiffness of the seat and modify it, impactor tests were done on the FE seat model in a simulation environment (see Figure A - 3:, Figure A - 4:, Figure A - 5:). The substructure was modified with the observations made from the tests and the support for side bolsters was assigned 100GPa elastic material allowing for sideways movement.

Currently further tests are running concerning the seat stiffness (PRECOONI, APROVE). The latest information can be accessed in the OSCCAR deliverables at OSCCAR homepage[2].

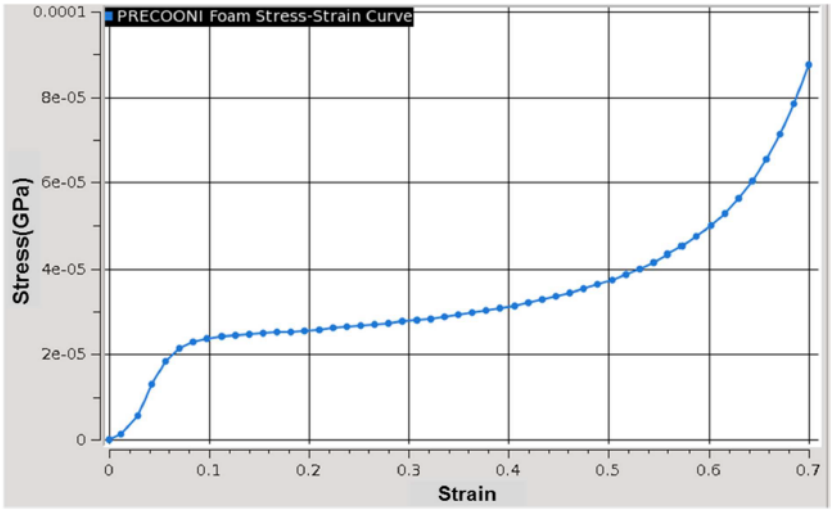

Figure A - 3:– Nominal Stress-Strain Curve for Seat Foam

[2] https://osccarproject.eu

(a) Impactor test conducted on side bolster (b) Coordinate system used in tests

Figure A - 4: Impactor test configuration (Source: TU Graz, Internal Report)

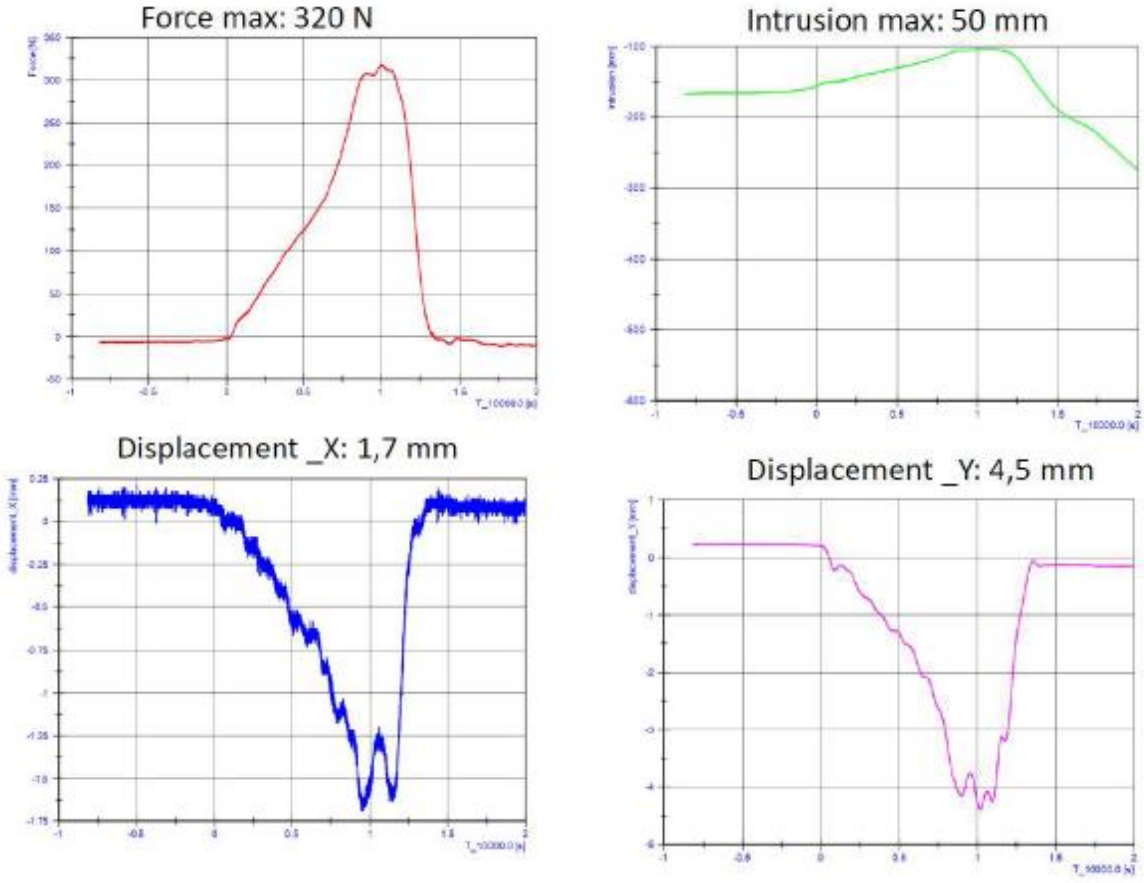

(a) (b)

Figure A - 5: Results Recorded in Impactor Test on Side Bolster

Volunteer posture measurements

For every volunteer a static trial was recorded that was used to calculate geometric centre points. The H-Point was taken from FE Model and was used as centre of coordinate system given in Figure A - 2.

Loading Conditions

Three types of manoeuvres with an initial velocity of 50 km/h are analysed in this study: (I) an emergency braking, induced by the driver with maximum effort, such that the brake-assist was enabled; (II) single lane change, performed to the left and right and at maximum effort; and (III) a combined manoeuvre, where the driver turned the steering wheel at maximum effort (left or right) combined with an emergency braking. The test sequence for each subject started with a braking manoeuvre at 12 km/h, but then the manoeuvres were performed in random order.

In the braking manoeuvre the driver pressed the brake pedal at maximum effort, such that the brake assist system was activated. In the lane change manoeuvre to the right, which was performed to closely resemble the first part of the VDA lane change [Öst et al. 2013], the driver turned the steering wheel to the right around 200°, followed by a countermovement to the left approximately 360° and a rotation to the right to reach the neutral position, again at maximum effort. In the lane change manoeuvre to the left similar levels of acceleration and steering wheel angles were reached, but in opposite directions.

Measured pre manoeuvre speed with variability, peak acceleration with variability.

Instrumentation

In order to identify the vehicle driving state velocity, vehicle speed, acceleration in lateral and frontal direction, steering wheel angle and angular velocity as well as the yaw rate were recorded from the CAN-Bus using a Dewetron Dewe5000. The steering wheel angle and angular velocity were sampled at 100 Hz, the velocity at 10 Hz, while the remaining channels were sampled at 50 Hz. **Summarized: Vehicle kinematic data is available for translational x and y direction and the rotational information for the z-direction.**

There were no measurements taken concerning the interior of the vehicle.

Occupant's kinematic data were captured using a Vicon V612 motion capturing system featuring eight near-infrared cameras (see Fig. 2). Positions of retro-reflective markers on specific locations on the occupant's body were recorded at a sample frequency of 100 Hz and reconstructed to give their 3D positions. To ensure proper operation of the system the windshield and passenger side window and some material from the passenger side door were removed.

Description of time zero

All data sets were synchronized with vehicle kinematics and time-shifted such that t=0 corresponds to the onset of the manoeuvre in consideration.

For the Brake manoeuvre the state of the brake pedal was used to define the starting of the manoeuvre, i.e., t=0. For the lane change manoeuvre, the first-time instance where the steering wheel angle exceeds 20° was identified. The steering wheel angular velocity at this point was then used to extrapolate to steering wheel angle 0° and the corresponding time instance was defined as t=0 (see also Huber et al. 2013).

Kinematics

The occupant's upper part of the torso and head were considered as rigid and selected markers were assigned to those body segments. A purpose-built gap-filling algorithm was applied, that allowed reconstruction of missing marker trajectory, if at least three markers on the subject were visible. Using rigid body constraints displacements of these body segments were determined. A reference posture of the occupant was defined as the posture that occurred at t=0. For further analysis displacements with respect to this reference position were used Kirschbichler et al. 2014.

(a) (b)

Figure A - 6:

Before 3D reconstruction of marker trajectories, a customized algorithm to account for camera motion [Kirschbichler et al. 2014] was applied. No smoothing procedure was performed except for the implicit low-pass filtering that is inherent to the orientation estimation procedure.

After this marker recovery procedure trajectories of each trial were transformed to the H-Point. Center-points from head and torso were calculated and from which angles were measured (Figure A - 7).

From trajectories and angles corridors were derived. In each recorded time instance, the median, 0.16th and 0.84th quantile of the kinematic quantity in consideration was computed and displayed against time.

Angles from hip and neck rotation were taken as reference for the simulation model that acted like a two-segment inverse pendulum (see Figure A - 7. Maximum excursion of torso and head in lateral direction during various lane change manoeuvres can be seen in [Kirschbichler et al. 2014].

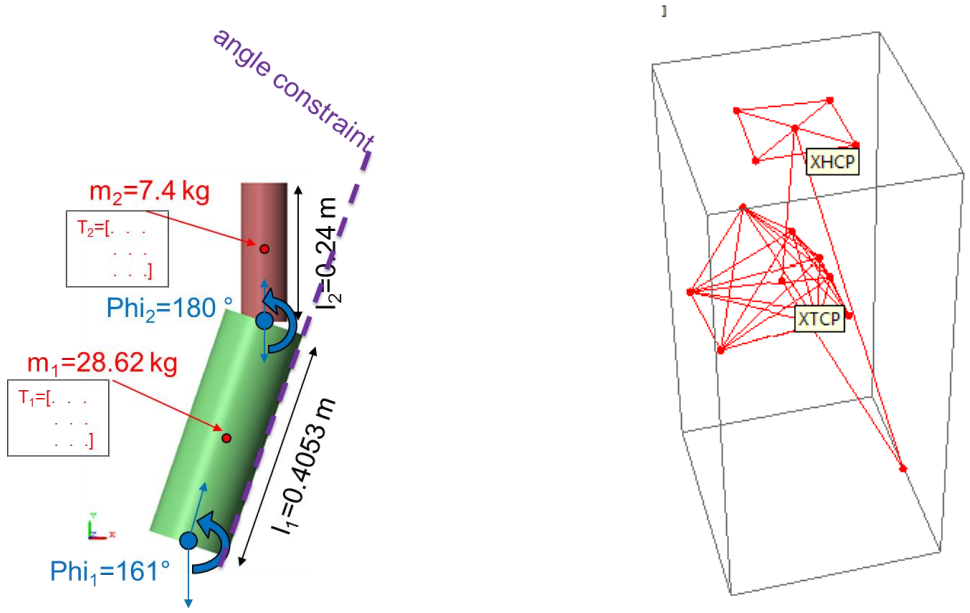

(a) (b)

Figure A - 7: Left (a): Simulation model used in Matlab Simulink;
Right (b): Geometric centre point of head (XHCP) and torso markers (XTCP)

For the calculation of the centre points (Figure A - 7b) the following markers were taken

- LabelsHeadCenterPoint = “LBHD","RBHD","LFHD","RFHD"
- LabelsTorsoCenterPoint ="LBAK","LCLA","LPEC","LSHO","RBAK","RCLA","RPEC","RSHO"

Please check the file “OM4IS2_reconstr.mkr” for the meaning of the labels.

First a single prototype was generated based on all valid trials of a special manoeuvre (e.g. Brake 12 km/h). Afterwards this prototype was used to transform the centre point to each trial. By using this method center points could also be put to trials that lacked a full set of markers (e.g. only 3 head markers).

Trajectories of the markers placed on the subjects were also stored to files.

Coordinate system - In order to derive characteristic kinematic quantities for head and torso 11 markers on the head were used to compute centroid trajectories. The coordinates of these centroids were denoted $r^{Head|Torso}_{x|y|z}$ and given in a Cartesian coordinate system, where the origin was located at the seat’s H-point (Figure A - 9). The x-axis was oriented to the back of the vehicle and the y-axis points to the right of the vehicle (Figure A - 8 a). The relative displacement of the centroid of head and torso markers with respect to the location at t=0 were denoted $\Delta r^{Head|Torso}_{x|y|z}$ (Figure A - 8 b).

From the head and torso segment markers also an orientation relative to the configuration at t=0 was computed. The corresponding rotation angles around the x-, y- and z-axes were denoted $\phi^{Head|Torso}_{x|y|z}$ and referred to as segment orientations (Figure A - 8 c).

The whole torso was assumed to behave like a rigid body. Therefore, an orientation matrix between the vector from the H-point to r^{Torso} and the corresponding vector in the initial position t=0 was computed and the rotation angle around x-, y- and z-axes were then denoted as $\Phi^{Torso}_{x|y|z}$ (Figure A - 8 d). The analogous procedure using the vector r^{Head}-r^{Torso} was performed to obtain $\Phi^{Head}_{x|y|z}$. Note

that due to the definition positive values of Φ relate to negative values in ϕ and vice versa. No distinct smoothing procedure was employed, except for the inherent low-pass filter properties associated with position and orientation estimation described above.

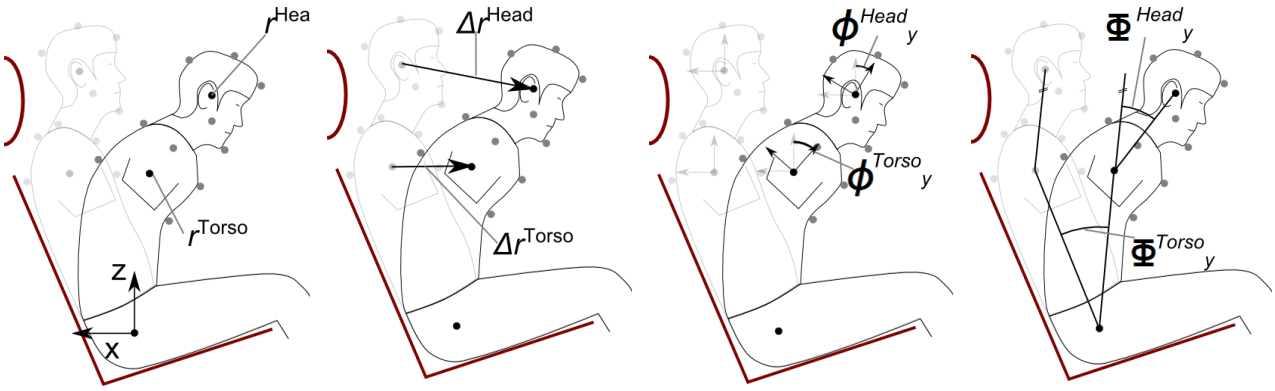

(a) (b) (c) (d)

Figure A - 8: Manoeuvre combined-left Characteristic kinematic quantities for head and torso motion. The light grey pose refers to the initial pose of the, while the dark pose depicts the situation during the manoeuvre.

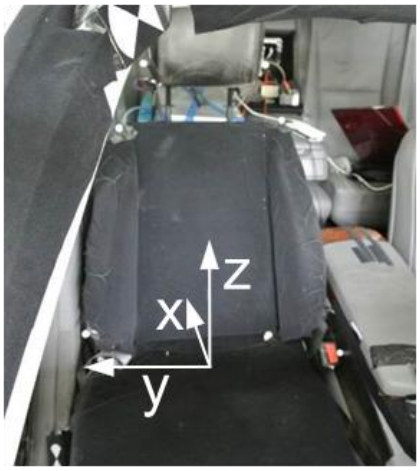

Figure A - 9: Coordinate system of the occupant kinematics

The axis of the measured longitudinal acceleration pointed to the driving direction, lateral acceleration to the left.

Kinetics

Next to vehicle states also the belt forces were measured. The used belt was a 3-point belt (ZF standard series belt).

- Pretensioner was off.
- Validation (component tests,…) were not done
- No belt pay out was measured
- No particular action was taken prior to the test to determine or adjust the belt characteristics (no 100% pullout, no check for the film spool effect,…)

Figure A - 10: shows the roughly location of the belt force sensors.

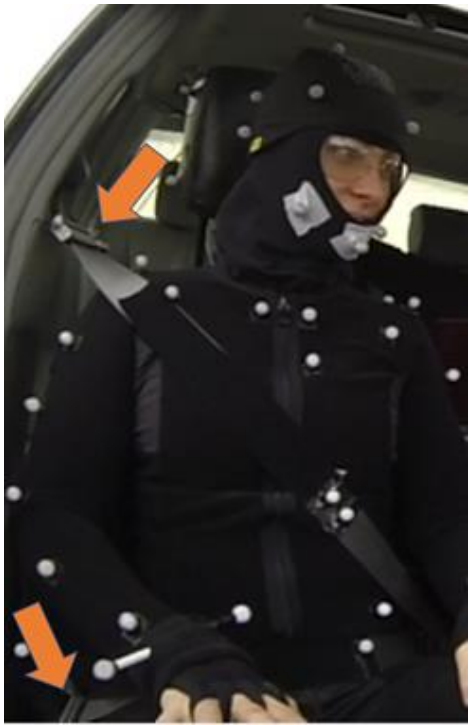

Figure A - 10: Belt force sensor

Muscle Activity

Muscle measurements were done using the surface electromyography (SEMG) that allowed to gain the dimension of the muscle activity and time of activation (onset).

On both sides 2 Ag / AgCI electrodes (Ambu R Blue Sensor N) were put on the prepared skin. Data was captured by the MG-system myon from the company prophysics. Wireless transmitters sent the signals to a receiving station which directed them through a A/D converter. Via software proEMG data was stored to a Dewetron DAQ-BOX at a sampling rate of 1 kHz.

Overall 16 muscles were measured (8 per body side).

- M. vastus medialis (Vast. Med.)
- M. obliqus externus abdominis (Ext. Obliq.)
- M. rectus abdominis (Rect. Abd.)
- M. latissimus dorsi (Lat. Dorsi)
- M. sternocleidomastoideus (SCM)
- Midcervical (C-4) paraspinal placement (Neck ext. C4)

- M. erector spinae, lumbar (ES lumbar)

For all of the trials in the following table muscle mesaurements were done. Co-drivers were *unaware* at the first maneuvre and *anticipated* at the following ones. The time window for measured data relative to the trial start was -1 to 1 second (T_{-10} – T_{10}).

Trial	#01 (unaware)	#02 (anticipated)
Brake 12 kmh	x	x
Brake 50 kmh	x	x
Circle 40 kmh (left / right)	x/x	x/-
Lane 50 kmh (left / right)	x/x	
Combined 50 kmh (left / right)	x/x	

Table A - 4

The physiological frequency range of SEMG signals operate between 10 Hz and 500Hz thererfore a sampling rate of 1 kHz was acceptable.

For gaining amplitude parameters every dataset was processed by a notch-filter (2. order, 200Hz, slope: 150), a Butterworth bandpass filter (6. order, 20-300 Hz) and a rectifier. For the onset detection additionally a teager-kaiser-energy-operator (TKEO) and a Butterworth lowpass filter (2. order, 50 Hz) was used afterwards.

No maximum voluntary isometric contractions (MVIC) measurements were done.

Datasets were successfully checked for normal distribution using the Kolmogorov-Smirnov test.

For co-drivers' average amplitudes were calculated using a time window of 0 to 1s sampled by 100 ms. For drivers a time window of -1 to 1s was used. Electrically low values were taken as reference. For co drivers a time window of -100 to 0 ms was assumed.

For onset detection first a signal between -200 and 0 ms was taken as noise reference. Out of this piece of data mean values such as standard deviation was taken defining a critical threshold of k_{crit} = mean + 5 * standard deviation. A value has to be 12 ms (12 data points) above this level to be taken as onset. Every onset detection was optically reviewed and if necessary, shifted manually to the next muscle activity.

Description of rejected data

Within groups of unaware and aware co-driver datasets those sets were removed that showed a threshold $k_{removed}$ = mean + 2.5 * standard deviation.

Data Description

Available data

ISO MME data is available for all tests and is split into folders named according to the load case ID (e.g., PR01T01). Table A - 9 lists the ISO MME codes of the kinematic data, in particular the sled

acceleration and the trajectories. Table A - 10 lists the ISO MME codes of the kinematic data, in particular the force measurements. Table A - 11 lists the ISO MME codes of the EMG data.

Selected data has been digitized and made available in an open access repository: https://doi.org/10.5281/zenodo.

Data format

Details about data format, used quantities and locations within the provided package can be found in the text below.

Data Format:

- Occupant marker trajectories (extracted from Vicon c3d files) (dat; tab separated)
  - ..\OccupantKinematics\Vicon_ascii_only
- Occupant angle and centerpoint trajectories (dat; tab separated)
  - ..\OccupantKinematics\KinematicsForSimulation\
- Occupant initial position
  - Needs to be extracted from dynamical vicon data
- EMG data (dat; tab separated)
  - ..\EMG\EMG_clean
- Vehicle states (dat; tab separated)
  - ..\Dewetron\
  - ..\OccupantKinematics\KinematicsForSimulation\

For some of the data described, corridors were created using the median, 0.16th and 0.84th quantile of the data. The plots and ascii data can be found in subfolders

- ..\Corrodors\{*Maneuver*}_plots
- ..\Corrodors\{*Maneuver*}_plots

Manoeuvre names {*Maneuver*} are shortened using B12 for Brake12, B50 for Brake50, CL50/CR50 for Combined Left/Right and LL50/LR50 for LaneLeft50/LaneRight50.

Channel names used for kinematic:

All the *.dat files described below include a header (commented by '#') that describes the data and then tab separated columns are appended.

Occupant marker trajectory files include time (100 Hz steps) and positions [mm] in all directions of all available markers in the c3d files. Marker label names can be found in "OM4IS2_reconstr.mkr". The folder structure is

- ..\ OccupantKinematics \Vicon_ascii_only\PreCrashCar2\{*Subject*}\reconstructed\{*Maneuver*}.dat

The *.dat files described below include a header (commented by '#') that describes the data and then tab separated columns are appended. For definitions of the data below please see 0.

Additional data was calculated based on marker data

- Angles.dat

- Holds orientation angles $\phi^{Head|Torso}_{x|y|z}$ [°] of head and torso in all directions (x, y, z) in respect to the location at t=0. The x axis is pointing to the back of the vehicle and y is pointing to the right. Data available for each volunteer.

- AngleCenterPoint.dat
  - Holds angles $\Phi^{Head|Torso}_{x|y|z}$ [°] of head and torso in all directions (x, y, z) in respect to the location at t=0. The x axis is pointing to the back of the vehicle and y is pointing to the right. Data is available for each volunteer + median (q50) with corridors (q16, q84) for every manoeuvre
- CenterPoint.dat
  - Holds positions $r^{Head|Torso}_{x|y|z}$ [mm] of artificial centerpoints of head and torso in all directions (x, y, z) where the x axis is pointing to the back of the vehicle and y is pointing to the right. Data available for each volunteer.
- CenterPointDifferences.dat
  - Holds positions $\Delta r^{Head|Torso}_{x|y|z}$ [mm] of artificial centerpoints of head and torso in all directions (x, y, z) in respect to the location at t=0. Data available for each volunteer.
- AllData.dat
  - Holds all data described above. Data available for each volunteer.

Folder structure is

- ..\OccupantKinematics\KinematicsForSimulation\{*Subject*}\{*Maneuver*}\{*Subject*}_{*Maneuver*}.Angles.dat
- ..\OccupantKinematics\KinematicsForSimulation\{*Subject*}\{*Maneuver*}\{*Subject*}_{*Maneuver*}.AnglesCenterPoint.dat
- ..\OccupantKinematics\KinematicsForSimulation\{*Subject*}\{*Maneuver*}\{*Subject*}_{*Maneuver*}.CenterPoint.dat
- ..\OccupantKinematics\KinematicsForSimulation\{*Subject*}\{*Maneuver*}\{*Subject*}_{*Maneuver*}.CenterPointDifferences.dat
- ..\OccupantKinematics\KinematicsForSimulation\{*Subject*}\{*Maneuver*}\{*Subject*}_{*Maneuver*}.AllData.dat

Channel names used for kinetics:

All the *.dat files described below include a header (commented by '#') that describes the data and then tab separated columns are appended.

Recorded vehicle data can be found at

- Acceleration.dat
  - Acceleration [m/s^2] of the vehicle measured in x and y direction where the x axis is pointing to the back of the vehicle and y is pointing to the right. **As mentioned above data is only available for x- and y translational acceleration and for z-axis rotational acceleration.**
- BeltForce.dat
  - Measured beltforces [kN]. See Figure A - 10:

Folder structure is

- ..\OccupantKinematics\KinematicsForSimulation\{*Subject*}\{*Maneuver*}\{*Subject*}_{*Maneuver*}.Acceleration.dat
- ..\OccupantKinematics\KinematicsForSimulation\{*Subject*}\{*Maneuver*}\{*Subject*}_{*Maneuver*}.BeltForce.dat

Channel names used for muscle activity:

EMG data can be found at

- {Maneuver}.csv
    - Frequency, time and muscle labels are described in the file-header, data is placed afterwards, comma separated.

Folder structure is

- ..\EMG\EMG_clean\{*Subject*}\{*Maneuver*}.csv

Please see [Penasso and Bericht 2013] for more information.

Exemplar plots of the data

In this section plots of some key exemplars should be provided along with detailed and clear description of where in the shared data these exemplars reside.

Occupant kinematic and vehicle acceleration:

Some plots are shown from the dataset of volunteer 5 of trial 1 having the manoeuvre combined-left. Figure A - 11 shows the angles of torso and head calculated from centralised torso and head points of the volunteer. Figure A - 12: shows the vehicle acceleration of x (x axis pointing in driving direction) and y direction. The measured beld force can be seen in Figure A - 13: .

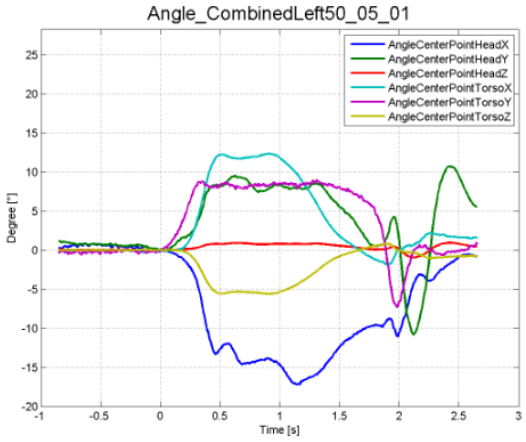


```
# Date created: Wed 15 Jan 2020 19:57:21
# Program name: T:\SIMULATION\Z620\D1T3_MATHEMATICA\biomech\analysis\PreCr
# Original file: T:\SIMULATION\Z620\D1T3_tempdata\Vicon\PreCrashCar2\Subje
# Machine name: insc01340
# OS: Windows
# t AngleCenterPointHeadX   AngleCenterPointHeadY   AngleCenterPointHeadZ
# s °   °   °   °   °   °
-0.85   0.34511583793951417 1.1842326935818073  0.10143740848509333 -0.038
-0.84   0.28465038592769476 1.1274279988028677  0.09686684961996422 -0.017
-0.8300000000000001 0.23089984196355906 1.032157983439788   0.088881002338
-0.8200000000000001 0.2131820214196838  1.0171456430604928  0.087684777172
-0.81   0.43330129230418385 1.1215516889756494  0.09535286204728914 -0.077
-0.8    0.5759318852898192  1.0665998461726254  0.08957956548589642 -0.162
-0.79   0.5476990966487476  1.0536731673611675  0.08863675103782 83  -0.172
-0.78   0.38254385824500564 0.9762235826113361  0.0829610363236741  0.0199
-0.77   0.5152040634711996  1.0118269391765127  0.085188786039013   -0.050
```

Figure A - 11: Manoeuvre combined-left for volunteer 5: Angles of torso and head (..\OccupantKinematics\KinematicsForSimulation\Subject_05\CombinedLeft50_01\Subject_05_CombinedLeft50_01.AnglesCenterPoint_vs_t.dat)

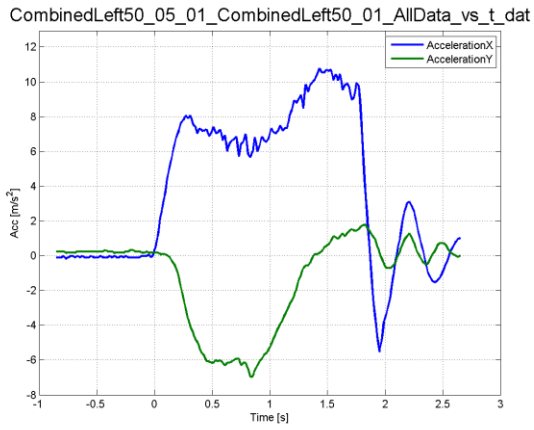


```
# t AccelerationX   AccelerationY
# s m s^-2  m s^-2
-0.8499999999999996 -0.09999996999999994    0.239999998
-0.8399999999999999 -0.09999996999999994    0.239999998
-0.8300000000000001 -0.09999996999999994    0.239999998
-0.8199999999999994 -0.09999996999999994    0.239999998
-0.8099999999999996 -0.09999996999999994    0.239999998
-0.7999999999999998 -0.06274532999999993    0.239999998
-0.79   -0.02352904999999994    0.239999998
```

Figure A - 12: Manoeuvre combined-left for volunteer 5: Acceleration of vehicle (..\OccupantKinematics\KinematicsForSimulation\Subject_05\CombinedLeft50_01\Subject_05_CombinedLeft50_01.Acceleration_vs_t.dat)

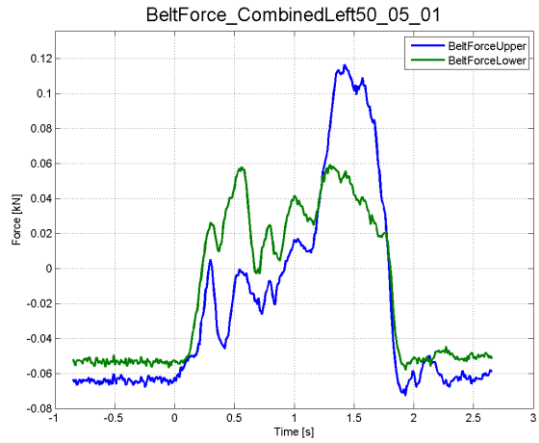


```
# t BeltForceUpper  BeltForceLower
# s kN  kN
-0.8499999999999996 -0.063409925    -0.052013047
-0.8399999999999999 -0.065055192    -0.053746816
-0.8300000000000001 -0.063409925    -0.055480585
-0.8199999999999994 -0.066700451    -0.052446488
-0.8099999999999996 -0.066152029    -0.05287993
-0.7999999999999998 -0.063409925    -0.052446488
```

Figure A - 13: Manoeuvre combined-left for volunteer 5: Measured belt force (..\OccupantKinematics\KinematicsForSimulation\Subject_05\CombinedLeft50_01\Subject_05_CombinedLeft50_01.BeltForce_vs_t.dat)

An example of an occupant marker trajectory is shown in Figure A - 14: .

```
# t    FRO1_x FRO1_y FRO1_z    RCLA_x RCLA_y RCLA_z    CHIN_x CHIN_y CHIN_z    LPEC_
1    53.7728 -19.0002 374.897    98.0615 38.1941 420.872    46.8307 13.2828 500.101
2    53.7122 -19.0704 374.842    96.6764 38.1879 420.651    47.0011 13.2449 500.07
3    53.7141 -19.1209 374.759    93.9166 38.196 420.624    47.0443 13.1994 499.932
4    53.7924 -19.2323 374.66    93.9692 38.0943 420.682    47.1418 13.1293 499.886
5    53.8547 -19.3235 374.657    97.9431 37.8749 420.917    47.265 13.1426 500.003
6    53.905 -19.3173 374.786    94.5584 37.9362 420.695    47.2708 13.0818 500.111
```

Figure A - 14: Manoeuvre combined-left for volunteer 5: Measured marker positions (..\OccupantKinematics\KinematicsForSimulation\Vicon_ascii_only\Subject_05\reconstructed\CombinedLeft50_01.dat)

Corridors were generated from angles $\phi^{Head|Torso}_{x|y|z}$ [°] of head and torso in all directions (x, y, z) for all manoeuvres. An example of Combined 50km/h is shown in Figure A - 15.

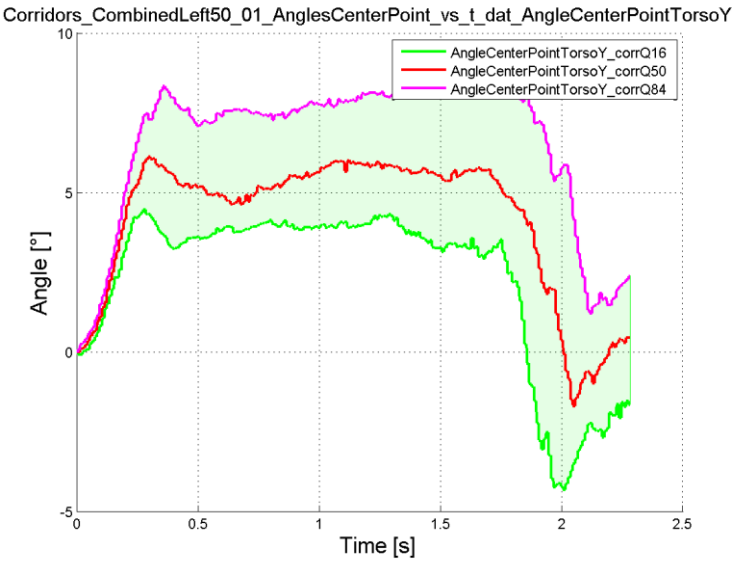

Figure A - 15: Manoeuvre combined-left 50 km/h for all volunteers: Corridor in Y direction for head (..\OccupantKinematics\Corridors\CL50Corr_plots\Corridors_CombinedLeft50_01_AnglesCenterPoint_vs_t_dat_AngleCenterPointTorsoY.txt)

EMG data:

Having the manoeuvre “combined-left” of volunteer 31 all 16 muscles (8 per body side) are plotted in Figure A - 16: . The time 0 is triggered using the brake pedal and steering wheel onset.

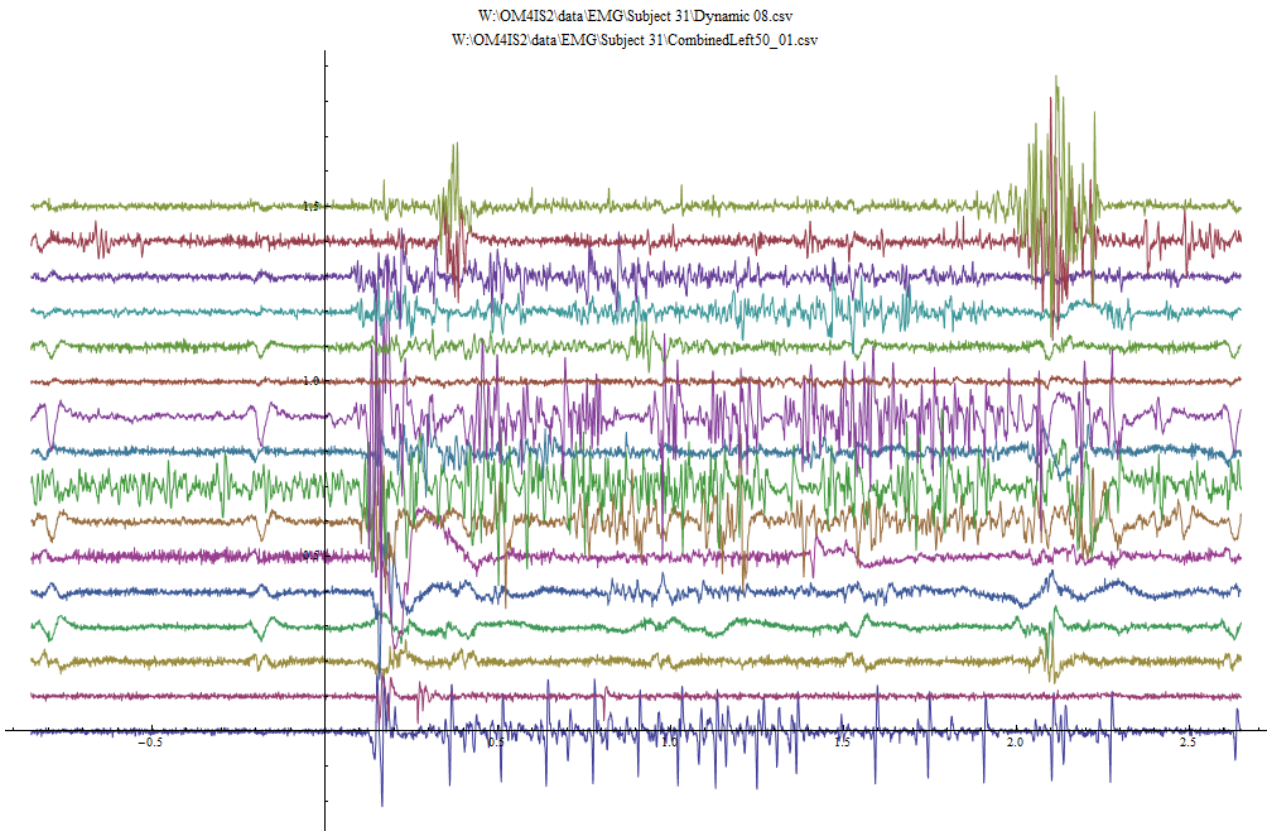

Figure A - 16: Manoeuvre combined-left for volunteer 31: Muscle data
Muscles:
01_r_vast_med,02_l_vast_med,03_r_rect_abd,04_l_rect_abd,05_r_obl_ext_abd,06_l_obl_ext_abd,07_r_erect_spin_lumb,08_l_erect_spin_lumb,
09_r_lat_dorsi,10_l_lat_dorsi,11_r_trap_desc,12_l_trap_desc,13_r_mid_cervi_c4,14_l_mid_cervi_c4,15_r_scm,16_l_scm
(..\EMG\EMG_clean\Subject 31\CombinedLeft50_01.csv)

Example of a trigger execution having a combined left manoeuvre checking Brake and steering wheel angle are shown in Figure A - 17.

Vehicle States:

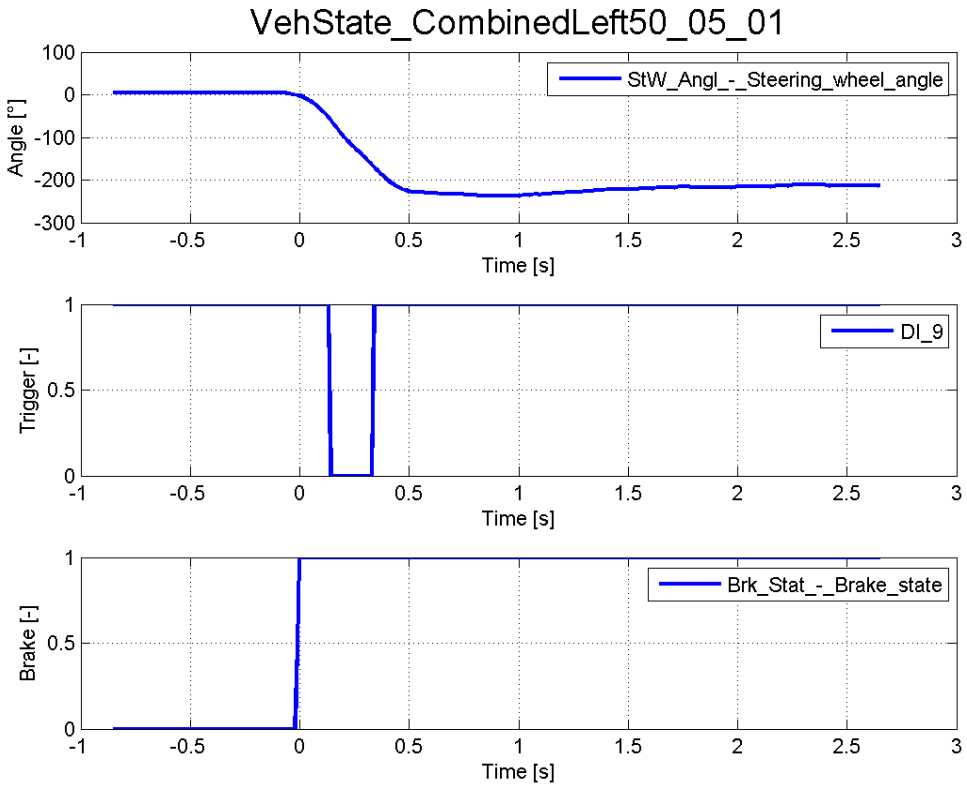

Figure A - 17: Manoeuvre combined-left for volunteer 5: Measured vehicle states (..\Dewetron\ Subject_05_CombinedLeft50_01.dat)

Vehicle kinematics

For further interpretation of the following diagrams see [Huber et al. 2014].

Brake12

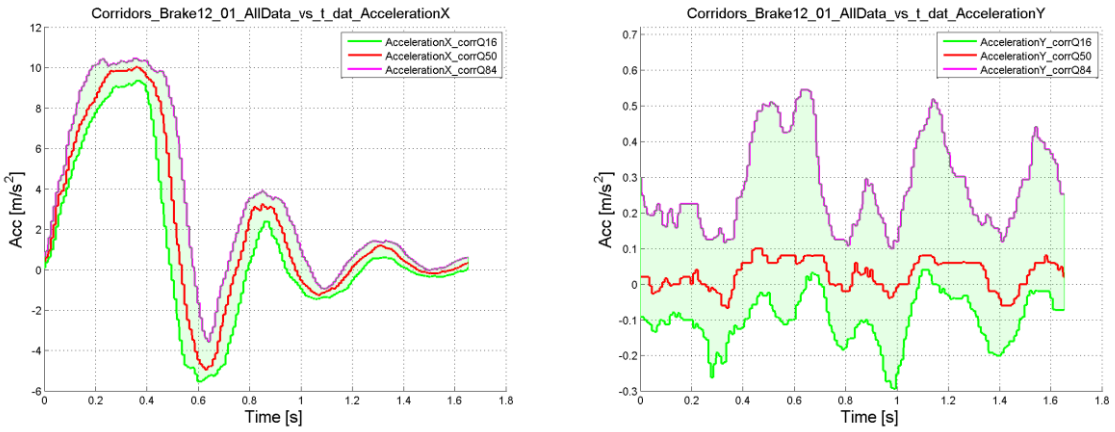

Brake50

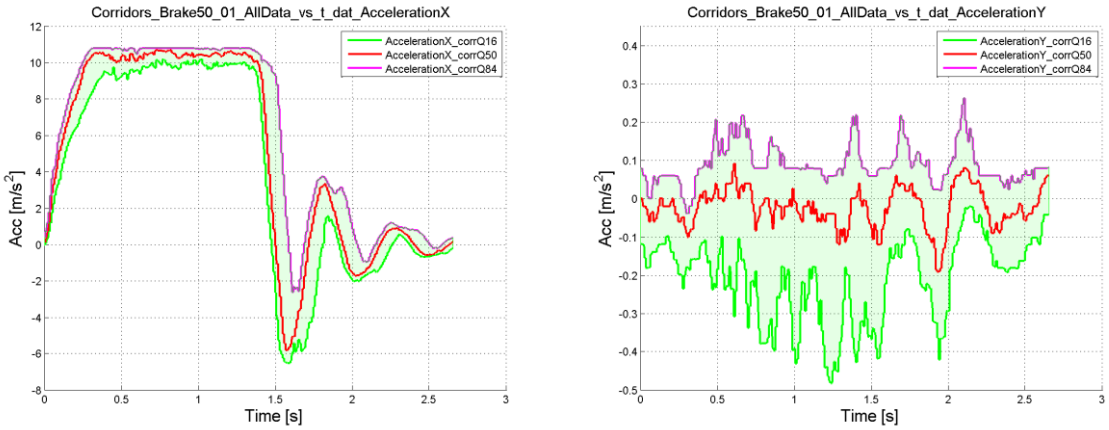

Figure A - 18:

LaneLeft50

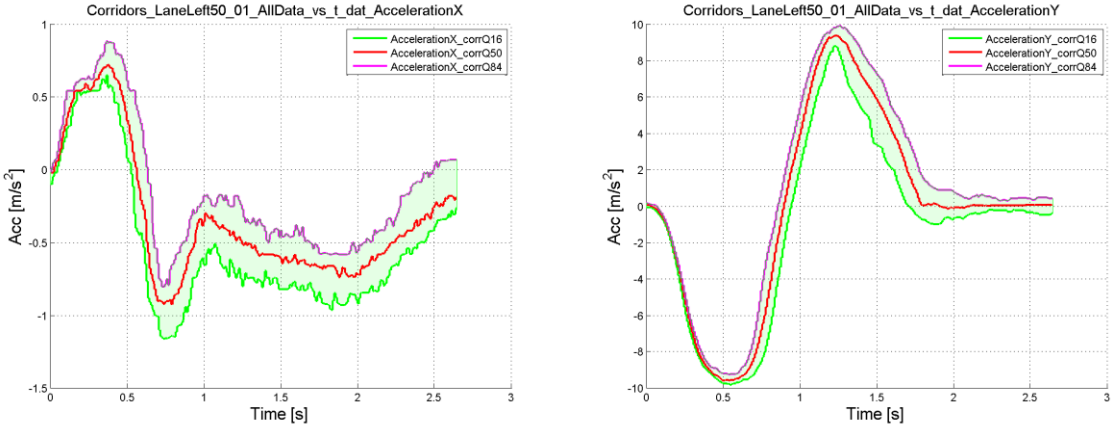

Figure A - 19:

LaneRight50

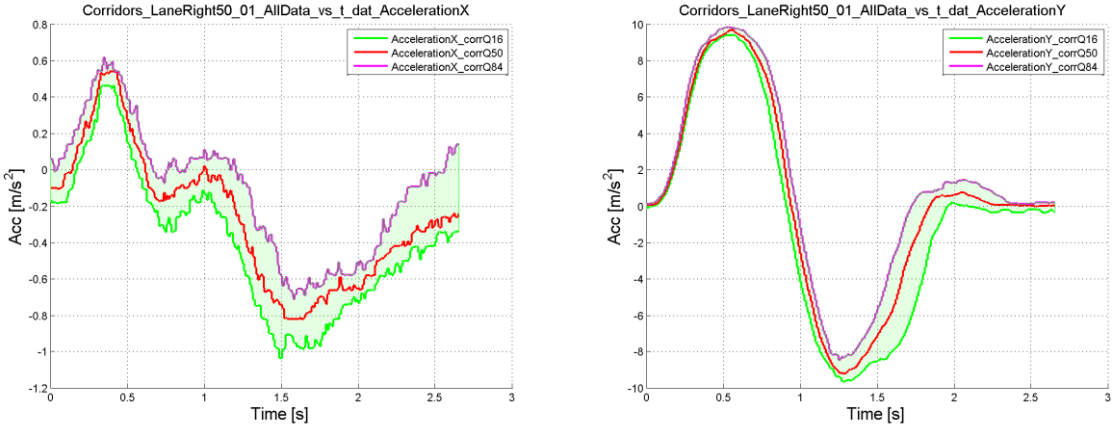

Figure A - 20:

CombinedLeft50

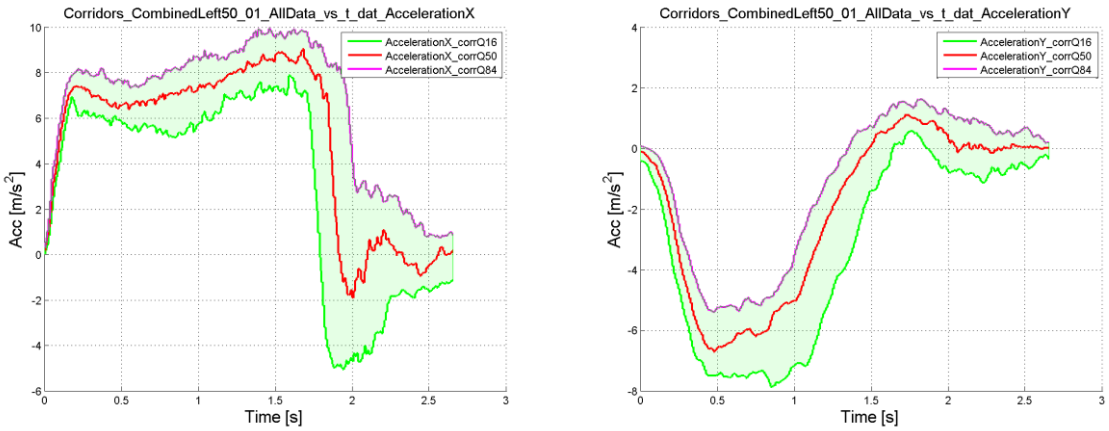

Figure A - 21:

CombinedRight50

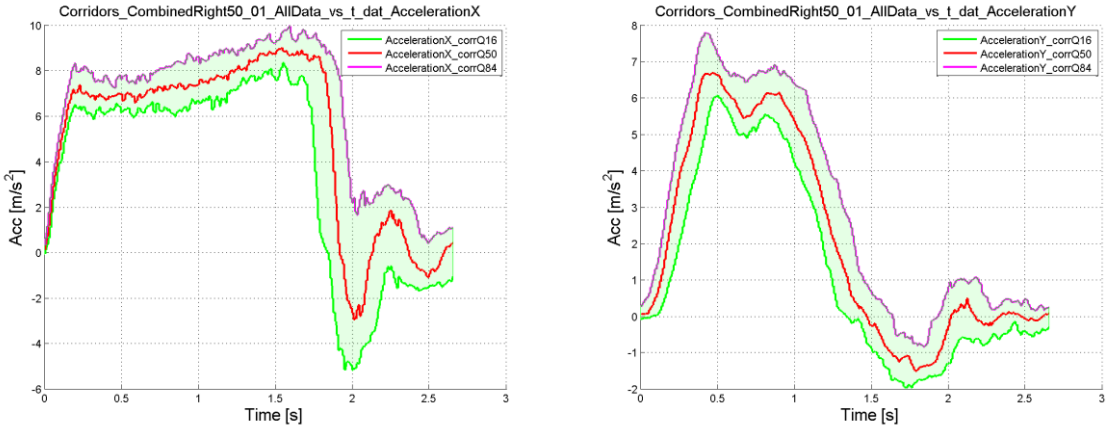

Figure A - 22:

Occupant kinematics

Brake12

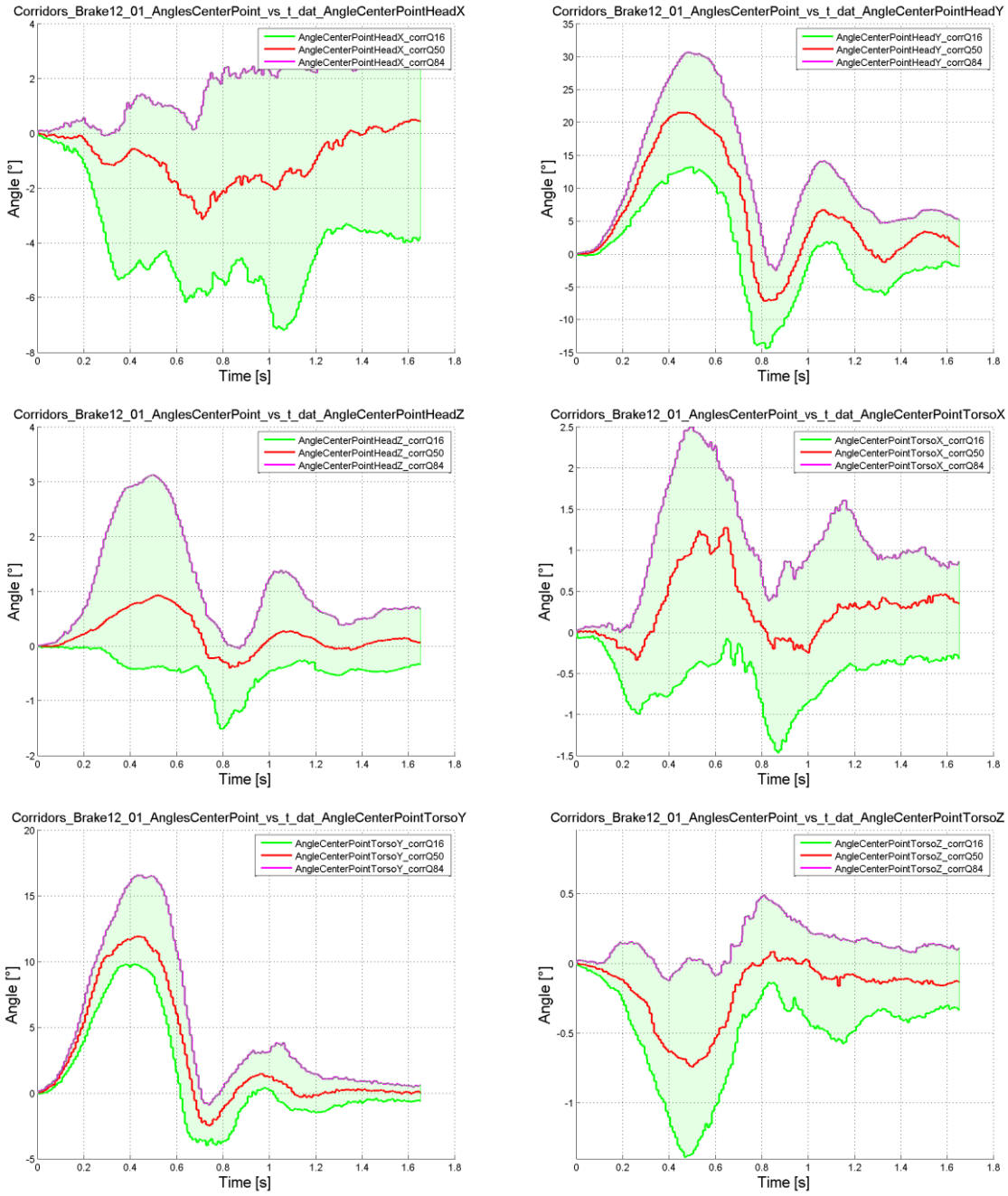
Corridors_Brake12_01_AnglesCenterPoint_vs_t_dat_AngleCenterPointHeadX
AngleCenterPointHeadX_corrQ16
AngleCenterPointHeadX_corrQ50
AngleCenterPointHeadX_corrQ84
Angle [°]
Time [s]
Corridors_Brake12_01_AnglesCenterPoint_vs_t_dat_AngleCenterPointHeadY
AngleCenterPointHeadY_corrQ16
AngleCenterPointHeadY_corrQ50
AngleCenterPointHeadY_corrQ84
Angle [°]
Time [s]
Corridors_Brake12_01_AnglesCenterPoint_vs_t_dat_AngleCenterPointHeadZ
AngleCenterPointHeadZ_corrQ16
AngleCenterPointHeadZ_corrQ50
AngleCenterPointHeadZ_corrQ84
Angle [°]
Time [s]
Corridors_Brake12_01_AnglesCenterPoint_vs_t_dat_AngleCenterPointTorsoX
AngleCenterPointTorsoX_corrQ16
AngleCenterPointTorsoX_corrQ50
AngleCenterPointTorsoX_corrQ84
Angle [°]
Time [s]
Corridors_Brake12_01_AnglesCenterPoint_vs_t_dat_AngleCenterPointTorsoY
AngleCenterPointTorsoY_corrQ16
AngleCenterPointTorsoY_corrQ50
AngleCenterPointTorsoY_corrQ84
Angle [°]
Time [s]
Corridors_Brake12_01_AnglesCenterPoint_vs_t_dat_AngleCenterPointTorsoZ
AngleCenterPointTorsoZ_corrQ16
AngleCenterPointTorsoZ_corrQ50
AngleCenterPointTorsoZ_corrQ84
Angle [°]
Time [s]

Figure A - 23:

Brake50

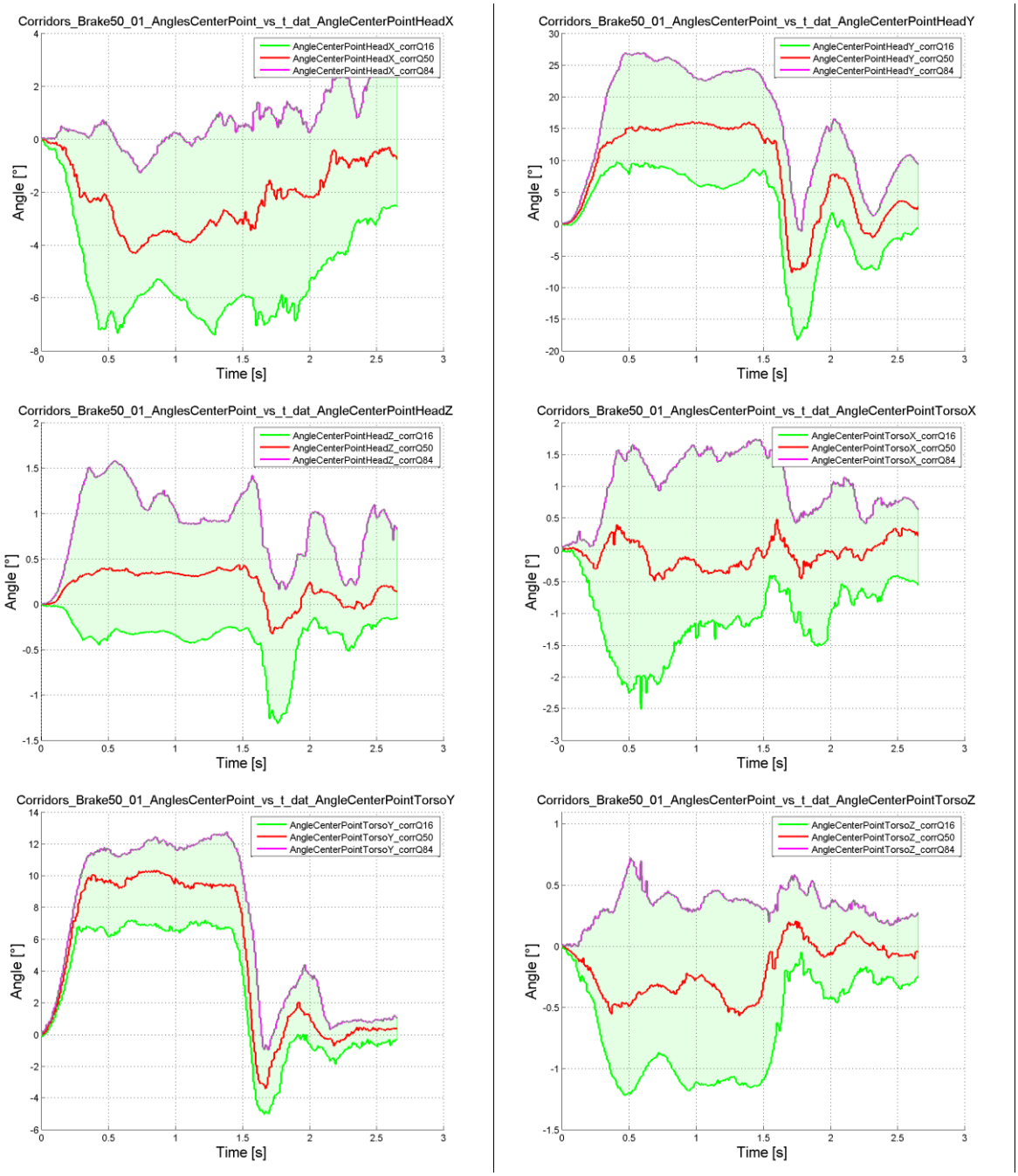

Figure A - 24:

LaneLeft50

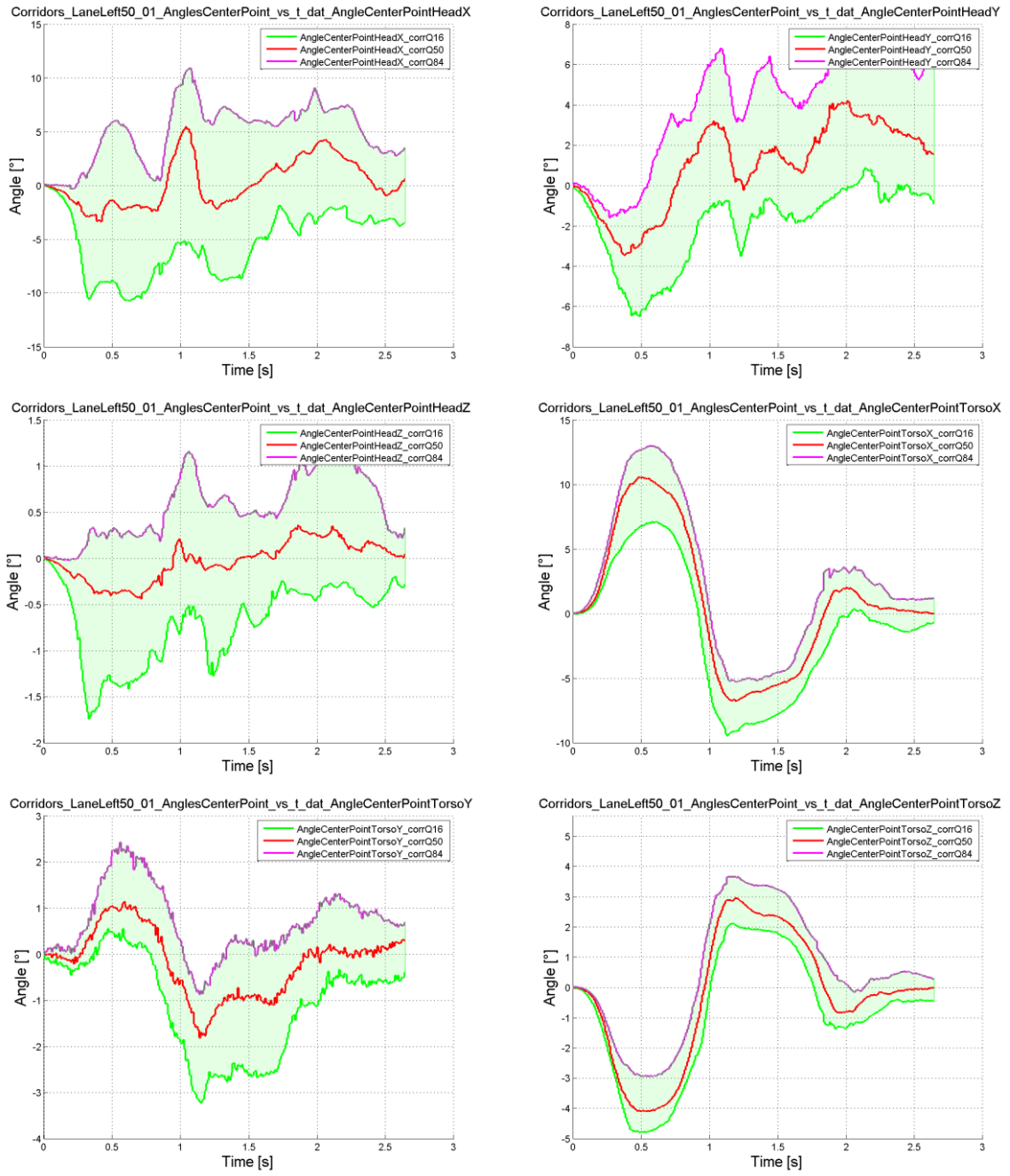

Figure A - 25:

LaneRight50

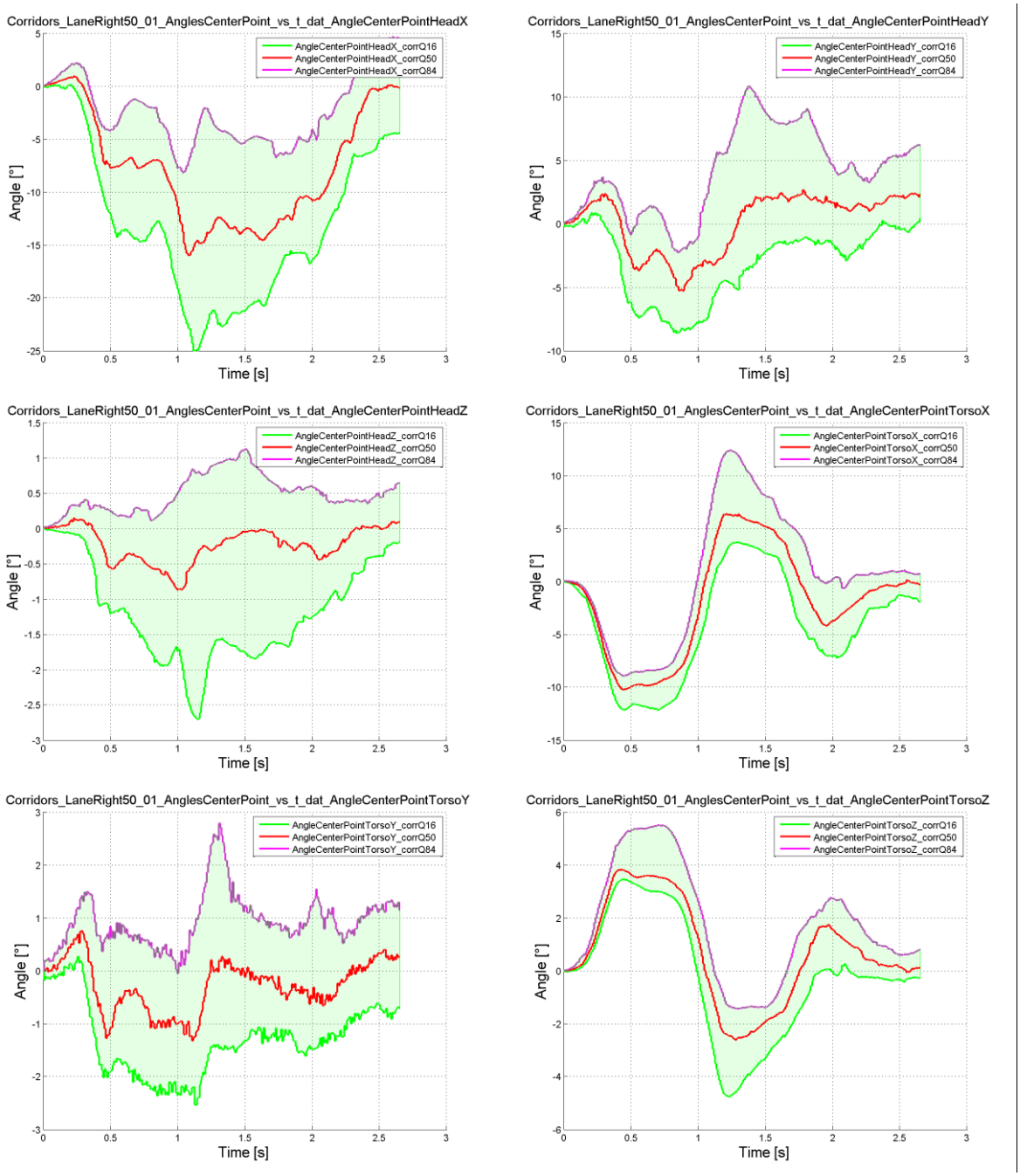

Figure A - 26:

CombinedRight50

Figure A - 27:

CombinedLeft50

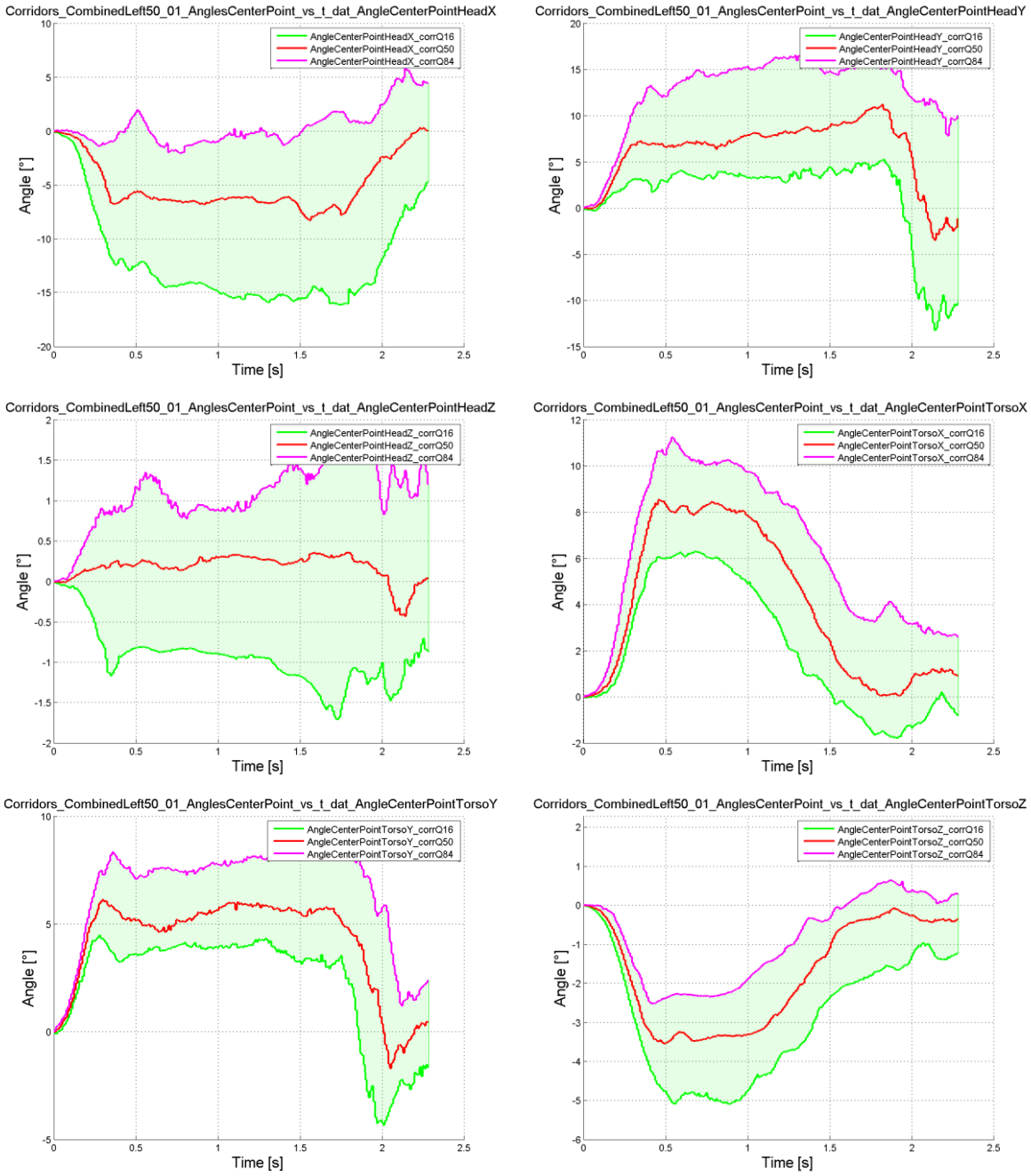

Figure A - 28:

References

Huber P., Christova M., DÀdetta G.A., Gallasch E., Kirschbichler S., Mayer C., Prüggler A., Rieser A., Sinz W., and Wallner D.: Muscle Activation Onset Latencies and Amplitudes during Lane Change in a Full Vehicle Test; Proceedings of IRCOBI; 2013; pp: 628-640.

Huber P., Kirschbichler S., Prüggler A., and Steidl T.: Three Dimensional Occupant Kinematics during Frontal, Lateral and Combined Emergency Maneuvers; Proceedings of IRCOBI (submitted); 12-10-2014.

Huber P., Kirschbichler S., Prüggler A., Steidl T.: Passenger kinematics in braking, lane change and oblique driving maneuvers; In IRC-15-89.; 2015. p. 783-802.

Kirschbichler S., Huber P., Prüggler A., Steidl T., Sinz W., Mayer C. et al.: Factors Influencing Occupant Kinematics during Braking and Lane Change Maneuvers in a Passenger Vehicle; In Proceedings of IRCOBI Conference 2014; IRC-14-70.; 2014; p. 614-625.

Östh J. et al.: Driver Kinematic and Muscle Responses in Braking Events with Standard and Reversible Pre-tensioned Restraints: Validation Data for Human Models; Stapp 2013.

Penasso H.: Bericht zu SEMG-Messungen im Rahmen von Projekt OM4IS 2; Report; 2013.

PRECOONI data

This section describes the execution of volunteer tests in a low-G acceleration setup performed within the PRECOONI project. A modified serial seat is positioned against the driving direction on a sled. The sled is accelerated from static to a certain velocity. The volunteers were belted and exposed to different distractions. A target tracking system and a pressure mat on the seat cushion recorded the movement of the volunteer. Load cells in the seat structure, the footrest and the belt recorded forces and moments. The muscle activity of the volunteer was also recorded with EMG.

A validated finite element model of the seat as well as the measured data in ISO MME format was shared.

Ethics

Tests were performed at Graz University of Technology with approval of the local ethics committee of Medical University of Graz (Reference: EK 30-157 ex 17/18).

Disclaimer

For the volunteer test data made available by the OSSCAR partners on OSCCAR projectplace/ sharepoint the following shall apply:

- The test data provided by a partner may be used by another OSSCAR partner to validate, improve and extend occupant models.
- In particular, a partner using the data is not allowed to disclose the data to any third party.
- For any use of these data after the OSSCAR project Art 11.3.2. and Art 11.3.5 of the OSSCAR Consortium Agreement shall apply meaning that the partner shall make a written request for any access rights to the owner of the data and a written agreement has to be concluded in order to agree on the conditions of granting access rights to these data.
- For the sake of clarification, it is stated that the evaluated and improved models are not subject to any CA related restrictions.

Methods

Volunteer description

The dataset composes of six male volunteers, whose age, height and weight distribution are shown in Table A - 5. Three volunteers that were selected for the OSCCAR dataset are marked with an asterics (*).

Table A - 5: Age, height, weight of the volunteers

VOLUNTEER	AGE	HEIGHT [CM]	BODYWEIGHT[KG]
1*	33	172.1	74.2
2	29	170.7	73.3
3*	30	175.1	73.3
4*	33	177.3	76.8
5	25	178.4	73.4
6	33	173.2	80.1
MEAN	30.5	174.5	75.2
SD ±	3.2	3.0	2.8

Boundary Conditions

The tests were performed on a sled test bench of the Graz University of Technology. The overall setup is shown in Figure A - 29.

Figure A - 29: PRECOONI test setup

A serial seat was modified by replacing the seat cushion and the seat back with a homogenous foam mounted on a wooden plate, as shown in shown in Figure A - 30. The wooden plate was mounted directly to the steel structure of the seat. This modification assured well-defined boundary conditions. The foam was covered with a leather layer. The seat was installed on the sled facing in the opposite driving direction.

The origin of the coordinate system of which the measurements were taken, is located at the upper front edge of the right fixation rail of the seat, see Figure A - 31. The coordinate axes were defined according to SAE standards, with the X-axis facing in driving direction and the Z-axis facing downwards.

Figure A - 30: Set up of the sled tests

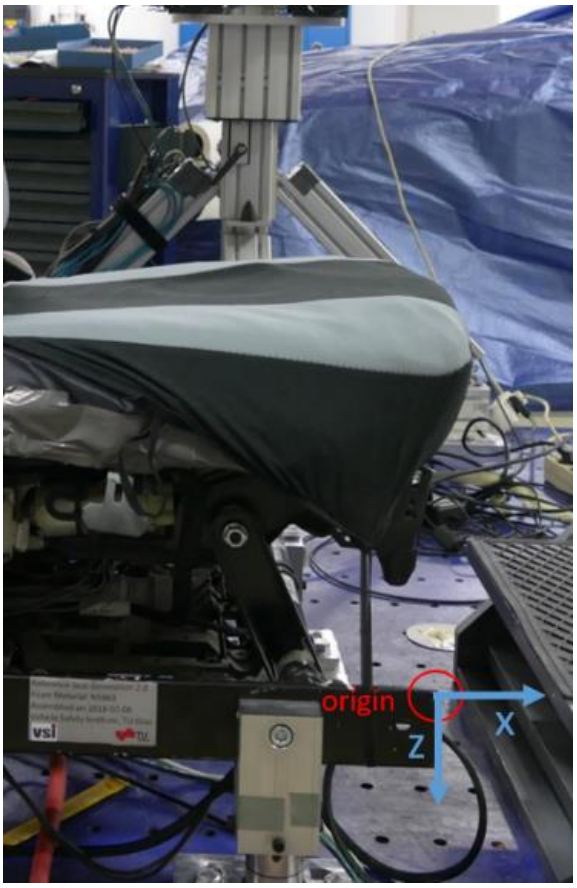

Figure A - 31: Origin of the coordinate system or all measurements and trajectories

The measured geometry of the modified serial seat is illustrated in Figure A - 32.

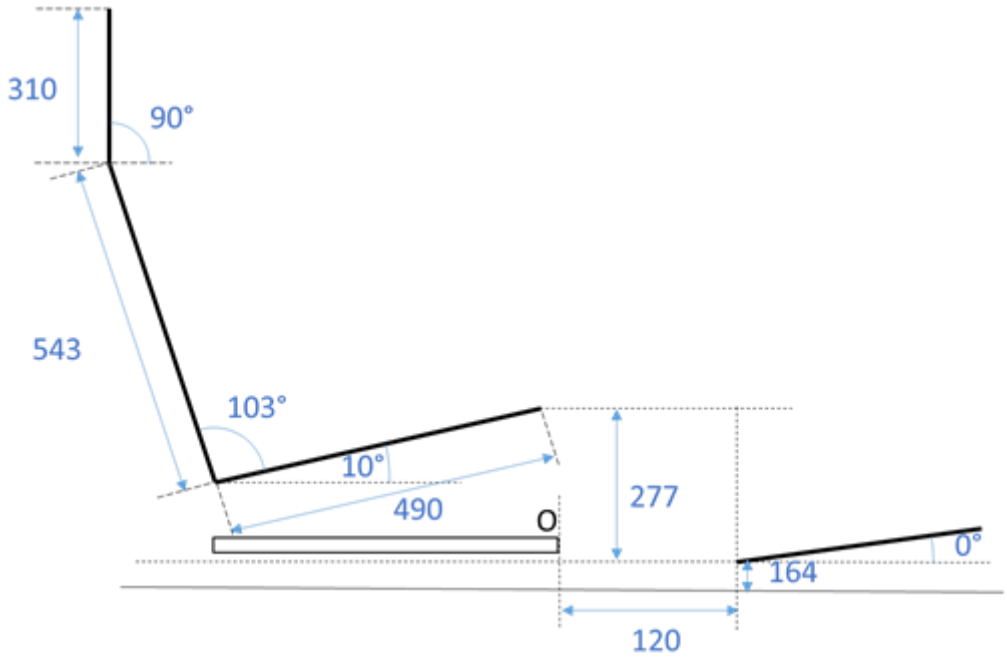

Figure A - 32: Seat Geometry

Volunteer posture measurements

The posture measurements, which were taken, are illustrated in Figure A - 33, including the corresponding naming of the targets.

HA	Head auditory (ear)
HT	Head top
HO	Head orbit (sunglasses)
SHSL	Shoulder side left
ELSL	Elbow side left
WRSL	Wrist side left
CS	Cervical spine
KSL	Knee side left
ASL	Ankle side left
FIX	Fix point on footrest

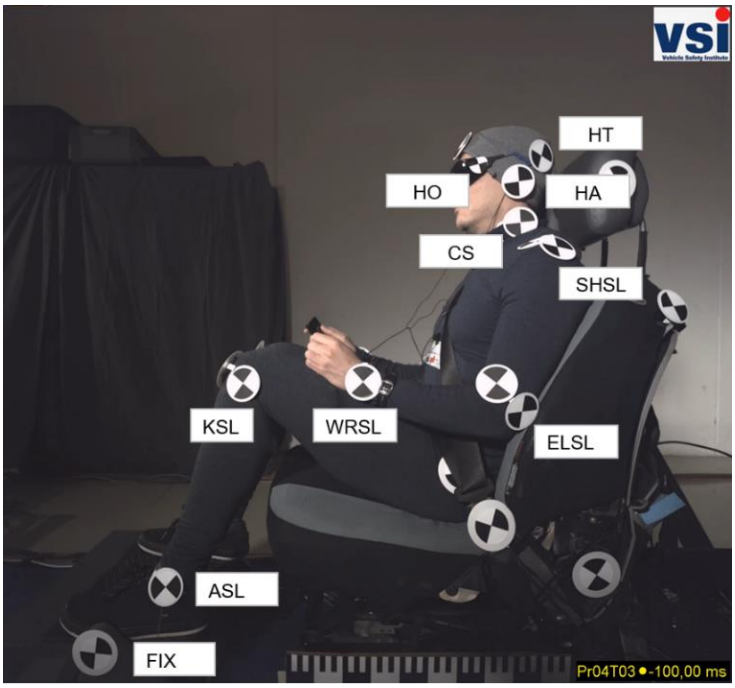

Figure A - 33: Locations of posture measurements

The initial coordinates of the shown posture are listed in Table A - 6 for the volunteers 1, 3 and 4.

TARGET	VOLUNTEER 1		VOLUNTEER 3		VOLUNTEER 4	
	X [mm]	Z [mm]	X [mm]	Z [mm]	X [mm]	Z [mm]
HA - HEAD AUDITORY (EAR)	-550.4	851.8	-550	890.2	-562.5	853.6
HT – HEAD TOP	-	-	-	-	-630.1	908.6
SHLS – SHOULDER LEFT SIDE	-537.4	684	-534.5	708	-558.1	707.4
ELSL – ELBOW SIDE LEFT	-439.5	436.1	-398	430.3	-453	417.9
WRSL – WRIST SIDE LEFT	-239	424.1	-146.9	464.7	-187.8	460.1
CS – CERVICAL SPINE	-537.3	759.1	-557.9	792	-574.3	781
KSL - KNEE SIDE LEFT	44	435.2	11.2	423.9	35.1	437.2
ASL – ANKLE SIDE LEFT	261	24.5	197.2	48.4	181.9	55
FIX – FIX POINT	290.2	33.6	290.2	33.6	290.2	33.6
TM – TROCHANTER MAJOR	-413.1	282.2	-375.5	261.6	-368.0	289.9

Table A - 6: Examples of target coordinates for the targets “Head auditory (ear)” and “Knee side left”

Loading Conditions

Table A - 7 lists the scenarios of each volunteer test chosen for further evaluations. The sled was accelerated within 1.15 s to a speed of 3.55 m/s with up to 0.5 g before the sled decelerated again to come to halt after 50 m. The method of distraction applied on the volunteer was varied.

ID	VOLUNTEER	TEST	DISTRACTION	START POSITON	END POSITION	TARGET VELOCITY
PR01T01	1	1	talking	46 m	40 m	12 km/h
PR03T03	3	3	ipod	46 m	40 m	12 km/h
PR04T03	4	3	ipod	46 m	40 m	12 km/h

Table A - 7: Test matrix

Instrumentation

An accelerometer to record the sled acceleration was mounted on the rigid test sled.

As the sled was accelerated from static, the time zero is defined at the moment when the acceleration is > 0 for the first time.

Response Variables

Figure A - 34 shows a schematic overview of the instrumentation of the test bench. The sled acceleration as well as the reaction forces on the seat structure, seat belt and footrest were measured. A pressure mat with an overlaid textile cover was positioned on the seat cushion to record the pressure distribution of the seated volunteer. Further, the movement of the volunteer as well as the muscle activity was recorded.

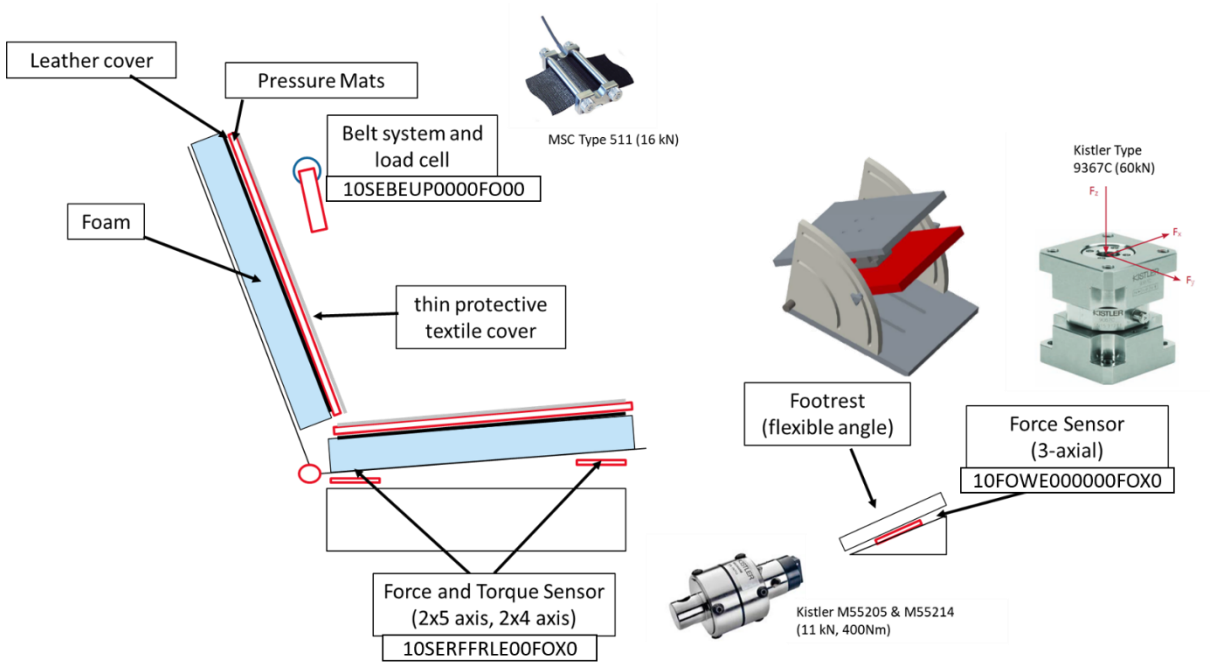

Figure A - 34: Overview of the measurement instrumentation

Three data sets, which represent three different volunteer behaviour, were chosen for further evaluation:

- Volunteer 1 Test 1: braced behaviour (neck muscles activated at t0 and minimum head excursion)
- Volunteer 3 Test 3: reactive behaviour (no muscle activation at t0 and medium head excursion)
- Volunteer 4 Test 3: relaxed behaviour (no muscle activation at t0 and highest head excursion)

Kinematics

The movement of the volunteer was recorded with a stereo camera setup from the side and another camera from the front. Raw data as well as filtered data is provided in the ISO MME files. The measured acceleration signal of the sled was filtered on the one hand with a CFC60 and on the other hand with a CFC 10 filter. To improve the comparability of the tests, the acceleration profiles were normalized on the end of the acceleration phase (when the acceleration became 0 for the first time – between 1.04s and 1.3s).

Distortions in the video data were eliminated by calibration with a chess pattern. The trajectories were calculated by 2D marker tracking, which was performed using the software Blender.

The trajectories were normalized in the same manner as the acceleration data.

The trajectories were calculated in the global coordinates, referred to the coordinate system described in Figure A - 31 .

Kinetics

The seat was mounted on the sled via load cells in each corner. Each load cell recorded the acting forces in X-, Y- and Z-direction as well as moments in X- and Y-direction. The positions of the load cells are listed in Table A - 8. A load cell was installed beneath the footrest and recorded the reaction forces in X-, Y- and Z-direction. A pressure mat placed on the seat cushion measured the change of the pressure distribution in N/cm² of the seated volunteer. Two load cells recorded the forces acting on the seat belt. One load cell was installed on the shoulder belt above the shoulder and the other one measured the forces of the lab belt on the side of the anchor near the pelvis. Figure A - 35 shows the locations of the seat belt load cells.

LOAD CELL	**X** (mm)	**Y** (mm)	**Z** (mm)
Force Transducer Front Right SEFRFRRI	-118	0	131
Force Transducer Rear Right SEFRRERI	-535	0	131
Force Transducer Front Left SEFRFRLE	-115	-540	131
Force Transducer Rear Left SEFRRELE	-526	-540	131

Table A - 8: Locations of the load cells

Figure A - 35: Belt Force measurement

The measured force signals of all load cells were filtered on the one hand with a CFC60 and on the other hand with a CFC 10 filter. Raw data and filtered data are included in the ISO MME files.

The coordinate systems are fixed in each load cell and thereby fixed to the sled. The directions of the axes of the seat and footrest load cells depend on the installation orientation. The belt force was measured in direction of the belt.

Muscle activity

A non-invasive electromyography (EMG) measuring system allowed the recording of the muscle activity. Figure A - 36 shows the evaluated muscles and the locations of the corresponding muscle activity measurements.

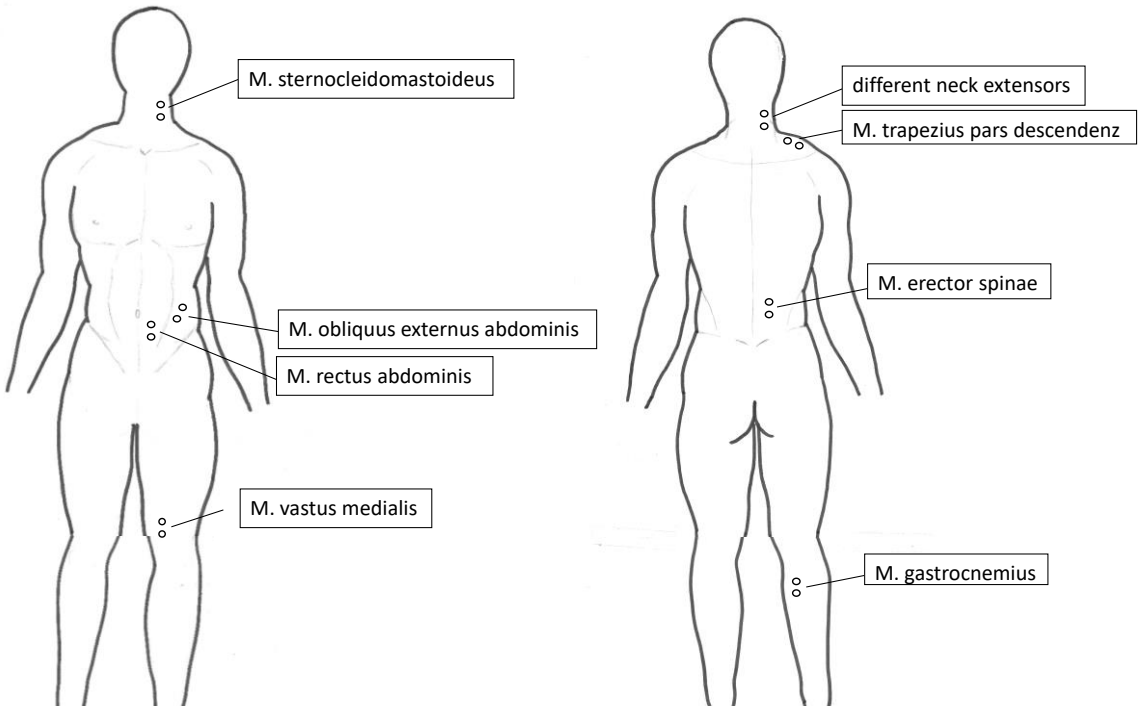

Figure A - 36: Electrode positions from anterior (left) and posterior (right) view.

MVIC measurement

The volunteers were placed in specialized MVIC test positions recommended by the literature (Konrad 2011), which measured maximum activation for each muscle individually. In these positions, the volunteers were asked to apply maximum force for five seconds. This procedure was repeated three times, each time setting the goal to pull or push harder than last time with a 30-60 s break in between.

The digital filtering of the data was carried out using high-pass (10 Hz) and low-pass filters (500 Hz) (Freiwald et al. 2007). As smoothing algorithm, the "Root Mean Square (RMS)" method was applied with a time window of 100 ms (Freiwald et al. 2007).

All Surface Electromyography amplitude values were normalized with the SEMG reference value. The voltage signals [µm] are converted into percent [%] of the maximum possible activation. The largest averaged amplitude value over a time window of 500 ms was used as reference value from the MVC tests.

To assess the activation of the different muscles and the automatic detection of the ECG artefacts, an individual activation threshold was derived for each muscle. The exceeding of this muscle tension threshold which, indicate an ECG-artefact at the resting measurement or an activated muscle activation in the test measurement.

By averaging the signal of the five heartbeats, a mean signal for the heartbeat was derived, for each muscle and for each experiment.

Data below the muscle activation threshold as well as the muscle activation due to the cardiac pulse were neglected.

Data Description

Available data

Test data for the three selected load cases is also made available in an open access repository:

https://doi.org/10.5281/zenodo.5747369

Data format

ISO MME data is available for all tests and is split into folders named according to the load case ID (e.g. PR01T01). Table A - 9 lists the ISO MME codes of the kinematic data, in particular the sled acceleration and the trajectories. Table A - 10 lists the ISO MME codes of the kinematic data, in particular the force measurements. Table A - 11 lists the ISO MME codes of the EMG data.

	MEASUREMENT	SHORTCUT	COMMENT	ISO MME CHANNLE CODE
ACCELERATION	Sled Acceleration	-	CFC 60	00SLED000000ACXD
			CFC 10	00SLED000000ACXS
TRAJECTORIES	Ankle side left	ALS	X Coordinate	D0ANKLLE0000DSXV
			Y Coordinate	D0ANKLLE0000DSYV
			Z Coordinate	D0ANKLLE0000DSZV
	Cervical Spine	CS	X Coordinate	D0CESP000000DSXV
			Y Coordinate	D0CESP000000DSYV
			Z Coordinate	D0CESP000000DSZV
	Elbow side left	ELSL	X Coordinate	D0ELBJLE0000DSXV
			Y Coordinate	D0ELBJLE0000DSYV
			Z Coordinate	D0ELBJLE0000DSZV
	Head Auditory	HA	X Coordinate	D0HEADCG0000DSXV
			Y Coordinate	D0HEADCG0000DSYV
			Z Coordinate	D0HEADCG0000DSZV
	Knee Side Left	KSL	X Coordinate	D0KNEELE0000DSXV
			Y Coordinate	D0KNEELE0000DSYV
			Z Coordinate	D0KNEELE0000DSZV
	Shoulder Left Side	SLS	X Coordinate	D0SHLDLE0000DSXV
			Y Coordinate	D0SHLDLE0000DSYV
			Z Coordinate	D0SHLDLE0000DSZV
	Wrist Left Side	WRLS	X Coordinate	D0WRISLE0000DSXV
			Y Coordinate	D0WRISLE0000DSYV
			Z Coordinate	D0WRISLE0000DSZV
	Fix point on footrest	FIX	X Coordinate	D0FOWE000000DSXV
			Y Coordinate	D0FOWE000000DSYV
			Z Coordinate	D0FOWE000000DSZV
TRAJECTORIES - ERROR	Ankle side left	ALS	X Coordinate	D0ANKLLE0002DSXV
			Y Coordinate	D0ANKLLE0002DSYV
			Z Coordinate	D0ANKLLE0002DSZV
	Cervical Spine	CS	X Coordinate	D0CESP000002DSXV
			Y Coordinate	D0CESP000002DSYV

	MEASUREMENT	SHORTCUT	COMMENT	ISO MME CHANNLE CODE
			Z Coordinate	D0CESP000002DSZV
	Elbow side left	ELSL	X Coordinate	D0ELBJLE0002DSXV
			Y Coordinate	D0ELBJLE0002DSYV
			Z Coordinate	D0ELBJLE0002DSZV
	Head Auditory	HA	X Coordinate	D0HEADCG0002DSXV
			Y Coordinate	D0HEADCG0002DSYV
			Z Coordinate	D0HEADCG0002DSZV
	Knee Side Left	KSL	X Coordinate	D0KNEELE0002DSXV
			Y Coordinate	D0KNEELE0002DSYV
			Z Coordinate	D0KNEELE0002DSZV
	Shoulder Left Side	SLS	X Coordinate	D0SHLDLE0002DSXV
			Y Coordinate	D0SHLDLE0002DSYV
			Z Coordinate	D0SHLDLE0002DSZV
	Wrist Left Side	WRLS	X Coordinate	D0WRISLE0002DSXV
			Y Coordinate	D0WRISLE0002DSYV
			Z Coordinate	D0WRISLE0002DSZV
	Fix point on footrest	FIX	X Coordinate	D0FOWE000002DSXV
			Y Coordinate	D0FOWE000002DSYV
			Z Coordinate	D0FOWE000002DSZV
TRAJECTORIES + ERROR	Ankle side left	ALS	X Coordinate	D0ANKLLE0001DSXV
			Y Coordinate	D0ANKLLE0001DSYV
			Z Coordinate	D0ANKLLE0001DSZV
	Cervical Spine	CS	X Coordinate	D0CESP000001DSXV
			Y Coordinate	D0CESP000001DSYV
			Z Coordinate	D0CESP000001DSZV
	Elbow side left	ELSL	X Coordinate	D0ELBJLE0001DSXV
			Y Coordinate	D0ELBJLE0001DSYV
			Z Coordinate	D0ELBJLE0001DSZV
	Head Auditory	HA	X Coordinate	D0HEADCG0001DSXV
			Y Coordinate	D0HEADCG0001DSYV
			Z Coordinate	D0HEADCG0001DSZV
	Knee Side Left	KSL	X Coordinate	D0KNEELE0001DSXV
			Y Coordinate	D0KNEELE0001DSYV
			Z Coordinate	D0KNEELE0001DSZV
	Shoulder Left Side	SLS	X Coordinate	D0SHLDLE0001DSXV
			Y Coordinate	D0SHLDLE0001DSYV
			Z Coordinate	D0SHLDLE0001DSZV
	Wrist Left Side	WRLS	X Coordinate	D0WRISLE0001DSXV
			Y Coordinate	D0WRISLE0001DSYV
			Z Coordinate	D0WRISLE0001DSZV
	Fix point on footrest	FIX	X Coordinate	D0FOWE000001DSXV
			Y Coordinate	D0FOWE000001DSYV
			Z Coordinate	D0FOWE000001DSZV

Table A - 9: ISO MME coding of the kinematic data

	MEASUREMENT	POSITION	COMMENT	ISO MME CHANNLE CODE
FORCES	Foot Restraint	-	X Force	10FOWE000000FOX0
			Y Force	10FOWE000000FOY0
			Z Force	10FOWE000000FOZ0
	Seatbelt	Upper	X Force	10SEBEUP0000FO00
		Lower	X Force	10SEBELO0000FO00
	Seat	Front Left	X Force	10SERFFRLE00FOX0
			Y Force	10SERFFRLE00FOY0
			Z Force	10SERFFRLE00FOZ0
			X Moment	10SERFFRLE00MOX0
			Y Moment	10SERFFRLE00MOY0
	Seat	Front Right	X Force	10SERFFRRI00FOX0
			Y Force	10SERFFRRI00FOY0
			Z Force	10SERFFRRI00FOZ0
			X Moment	10SERFFRRI00MOX0
			Y Moment	10SERFFRRI00MOY0
	Seat	Rear Left	X Force	10SERFRELE00FOX0
			Y Force	10SERFRELE00FOY0
			Z Force	10SERFRELE00FOZ0
			X Moment	10SERFRELE00MOX0
			Y Moment	10SERFRELE00MOY0
	Seat	Rear Right	X Force	10SERFRERI00FOX0
			Y Force	10SERFRERI00FOY0
			Z Force	10SERFRERI00FOZ0
			X Moment	10SERFRERI00MOX0
			Y Moment	10SERFRERI00MOY0
FORCES CFC 60	Foot Restraint	-	X Force	10FOWE000000FOXD
			Y Force	10FOWE000000FOYD
			Z Force	10FOWE000000FOZD
	Seatbelt	Upper	X Force	10SEBEUP0000FO0D
		Lower	X Force	10SEBELO0000FO0D
	Seat	Front Left	X Force	10SERFFRLE00FOXD
			Y Force	10SERFFRLE00FOYD
			Z Force	10SERFFRLE00FOZD
			X Moment	10SERFFRLE00MOXD
			Y Moment	10SERFFRLE00MOYD
	Seat	Front Right	X Force	10SERFFRRI00FOXD
			Y Force	10SERFFRRI00FOYD
			Z Force	10SERFFRRI00FOZD
			X Moment	10SERFFRRI00MOXD
			Y Moment	10SERFFRRI00MOYD
	Seat	Rear Left	X Force	10SERFRELE00FOXD
			Y Force	10SERFRELE00FOYD
			Z Force	10SERFRELE00FOZD
			X Moment	10SERFRELE00MOXD

			Y Moment	10SERFRELE00MOYD
	Seat	Rear Right	X Force	10SERFRERI00FOXD
			Y Force	10SERFRERI00FOYD
			Z Force	10SERFRERI00FOZD
			X Moment	10SERFRERI00MOXD
			Y Moment	10SERFRERI00MOYD
FORCES CFC 10	Foot Restraint	-	X Force	10FOWE000000FOXS
			Y Force	10FOWE000000FOYS
			Z Force	10FOWE000000FOZS
	Seatbelt	Upper	X Force	10SEBEUP0000FO0S
		Lower	X Force	10SEBELO0000FO0S
	Seat	Front Left	X Force	10SERFFRLE00FOXS
			Y Force	10SERFFRLE00FOYS
			Z Force	10SERFFRLE00FOZS
			X Moment	10SERFFRLE00MOXS
			Y Moment	10SERFFRLE00MOYS
	Seat	Front Right	X Force	10SERFFRRI00FOXS
			Y Force	10SERFFRRI00FOYS
			Z Force	10SERFFRRI00FOZS
			X Moment	10SERFFRRI00MOXS
			Y Moment	10SERFFRRI00MOYS
	Seat	Rear Left	X Force	10SERFRELE00FOXS
			Y Force	10SERFRELE00FOYS
			Z Force	10SERFRELE00FOZS
			X Moment	10SERFRELE00MOXS
			Y Moment	10SERFRELE00MOYS
	Seat	Rear Right	X Force	10SERFRERI00FOXS
			Y Force	10SERFRERI00FOYS
			Z Force	10SERFRERI00FOZS
			X Moment	10SERFRERI00MOXS
			Y Moment	10SERFRERI00MOYS

Table A - 10: ISO MME coding of the kinetic data

	MEASUREMENT	ISO MME CHANNLE CODE
NORMALISED EMG SIGNAL	rectus abdominis left	D0ABDOLAIN00000S
	rectus abdominis right	D0ABDORAIN00000S
	sternocleidomastoideus left	D0NECKLALO00000S
	sternocleidomastoideus right	D0NECKRALO00000S
	neck extensors left	D0NECKLPLO00000S
	neck extensors right	D0NECKRPLO00000S
	trapezius p. descendenz left	D0SHLDLPIN00000S
	trapezius p. descendenz right	D0SHLDRPIN00000S
	obliquus externus abdominis left	D0ABDOLAOU00000S
	obliquus externus abdominis right	D0ABDORAOU00000S
	erector spinae left	D0LUSPLP0000000S
	erector spinae right	D0LUSPRP0000000S
	vastus medialis left	D0ULEGLAIN00000S
	vastus medialis right	D0ULEGRAIN00000S
	gastrocnemius left	D0LLEGLPIN00000S
	gastrocnemius right	D0LLEGRPIN00000S
NORMALISED MEAN CARDIAC PULSE	rectus abdominis left	D0ABDOLAIN02000S
	rectus abdominis right	D0ABDORAIN02000S
	sternocleidomastoideus left	D0NECKLALO02000S
	sternocleidomastoideus right	D0NECKRALO02000S
	neck extensors left	D0NECKLPLO02000S
	neck extensors right	D0NECKRPLO02000S
	trapezius p. descendenz left	D0SHLDLPIN02000S
	trapezius p. descendenz right	D0SHLDRPIN02000S
	obliquus externus abdominis left	D0ABDOLAOU02000S
	obliquus externus abdominis right	D0ABDORAOU02000S
	erector spinae left	D0LUSPLP0002000S
	erector spinae right	D0LUSPRP0002000S
	vastus medialis left	D0ULEGLAIN02000S
	vastus medialis right	D0ULEGRAIN02000S
	gastrocnemius left	D0LLEGLPIN02000S
	gastrocnemius right	D0LLEGRPIN02000S
NORMALISED MEAN CARDIAC PULSE + 1SD	rectus abdominis left	D0ABDOLAIN03000S
	rectus abdominis right	D0ABDORAIN03000S
	sternocleidomastoideus left	D0NECKLALO03000S
	sternocleidomastoideus right	D0NECKRALO03000S
	neck extensors left	D0NECKLPLO03000S
	neck extensors right	D0NECKRPLO03000S
	trapezius p. descendenz left	D0SHLDLPIN03000S
	trapezius p. descendenz right	D0SHLDRPIN03000S
	obliquus externus abdominis left	D0ABDOLAOU03000S
	obliquus externus abdominis right	D0ABDORAOU03000S
	erector spinae left	D0LUSPLP0003000S
	erector spinae right	D0LUSPRP0003000S

	vastus medialis left	D0ULEGLAIN03000S
	vastus medialis right	D0ULEGRAIN03000S
	gastrocnemius left	D0LLEGLPIN03000S
	gastrocnemius right	D0LLEGRPIN03000S
NORMALISED MEAN CARDIAC PULSE - 1SD	rectus abdominis left	D0ABDOLAIN01000S
	rectus abdominis right	D0ABDORAIN01000S
	sternocleidomastoideus left	D0NECKLALO01000S
	sternocleidomastoideus right	D0NECKRALO01000S
	neck extensors left	D0NECKLPLO01000S
	neck extensors right	D0NECKRPLO01000S
	trapezius p. descendenz left	D0SHLDLPIN01000S
	trapezius p. descendenz right	D0SHLDRPIN01000S
	obliquus externus abdominis left	D0ABDOLAOU01000S
	obliquus externus abdominis right	D0ABDORAOU01000S
	erector spinae left	D0LUSPLP0001000S
	erector spinae right	D0LUSPRP0001000S
	vastus medialis left	D0ULEGLAIN01000S
	vastus medialis right	D0ULEGRAIN01000S
	gastrocnemius left	D0LLEGLPIN01000S
	gastrocnemius right	D0LLEGRPIN01000S

Table A - 11: ISO MME coding of the EMG data

Exemplary plots of the data

Figure A - 37 shows exemplarily the response force of the load cells under the seat and Figure A - 38 shows the measured sled acceleration.

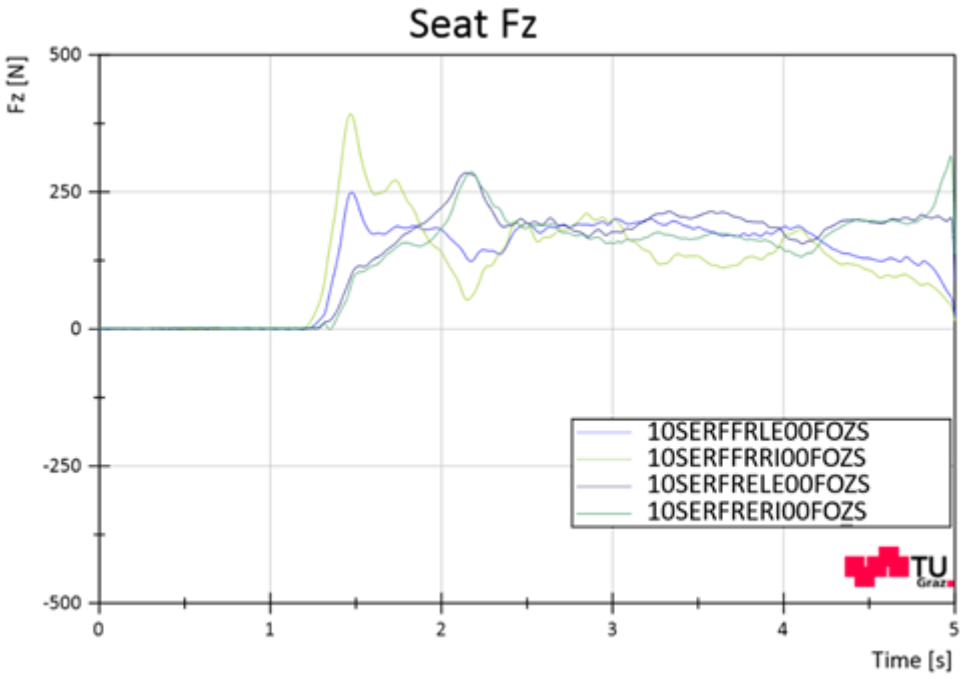

Figure A - 37: Seat Force in Z-axis of volunteer 01

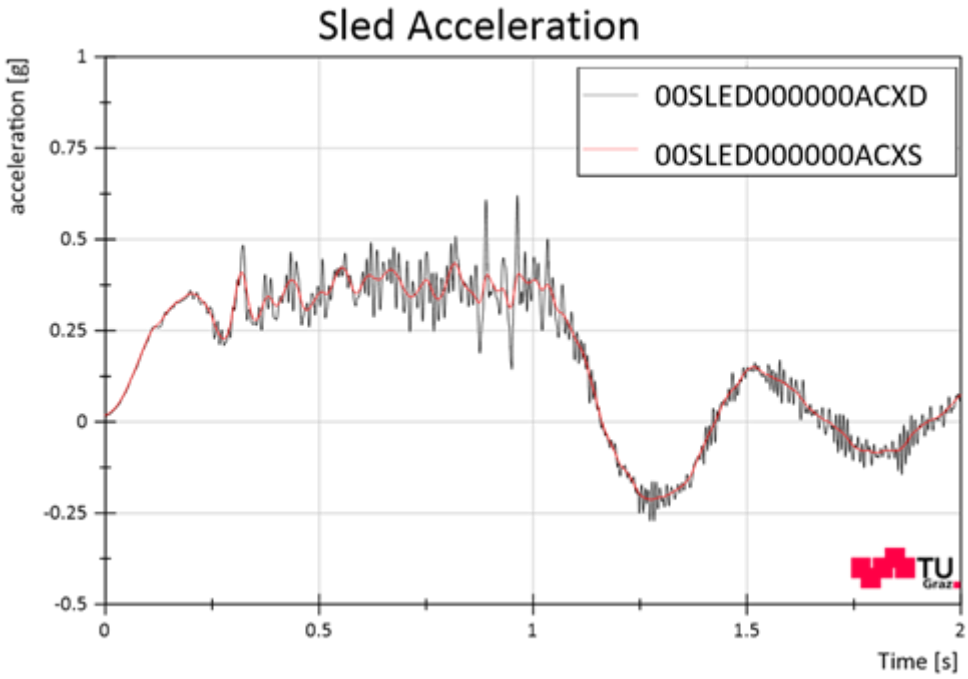

Figure A - 38: Seat Acceleration of volunteer 01

Figure A - 39 shows an exemplar of the EMG data of the sternocleidomastoideus. The measured muscle activity is highlighted in pink. The area below the activation threshold is greyed out, as the data is neglected. The blue lines indicate the time midpoint of the cardiac pulse and the grey lines the averaged pulse beats.

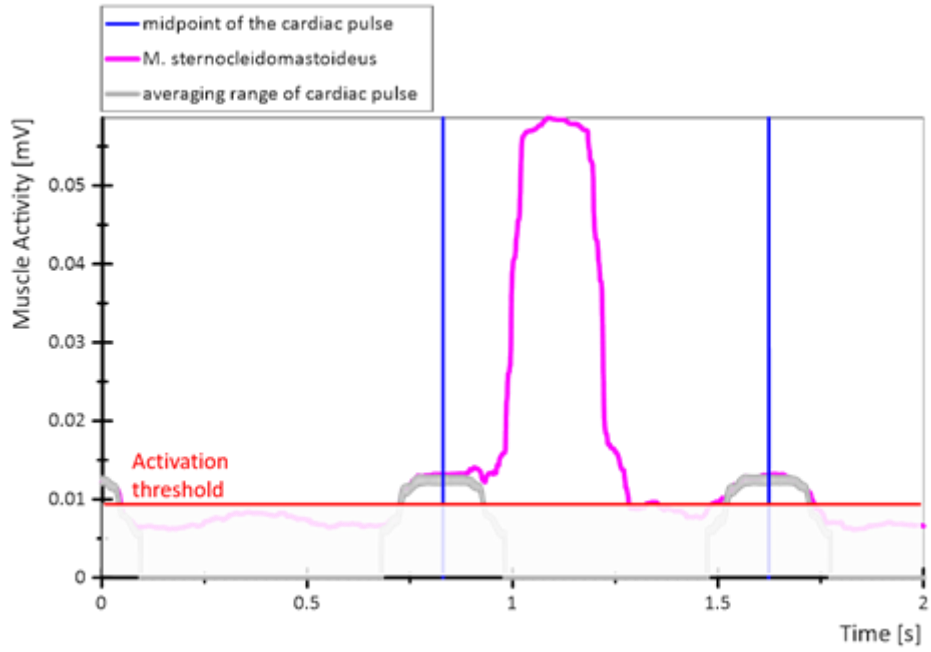

Figure A - 39: EMG measurment of the sternocleidomastoideus and the average cardiac pulse

References

Freiwald, J., Baumgart, C., & Konrad, P. (2007). Einführung in die Elektromyographie. Sport - Prävention - Rehabilitation (Spitta-Fachbuchreihe Medizin). Balingen: Spitta-Verl.

Konrad, P. (2011). EMG-Fibel - Eine praxisorientierte Einführung in die kinesiologische Elektromyographie.

TNO data

Introduction

The test series seated and restrained 10 male volunteers in a multidirectional mobile platform that subjected them to varying loading representing lateral and lane-change manoeuvres of around 5 m/s^2. High-speed camera data tracked the kinematics of their response. This work was carried out and detailed in van Rooij (2013)

Methods

The volunteers were strapped into a rigidly supported monocoque seat with a four-point harness-style seatbelt, inside a rigid cage mounted on a moving base. Inside the cage was also a non-functional steering wheel and a footplate, representing typical support points in a vehicle.

A steering wheel was placed in the test cabin. The wheel was non-functional and locked, preventing rotation. Tests were carried out in which the occupants were asked to hold the steering wheel, representing a driver, and with their hands in their lap, representing a passenger. For the lane change tests, volunteers were asked to either relax, or to brace themselves.

The belt system was anchored at the lap belt end. This portion was pretensioned to 50 N. The shoulder belts were connected to an inertia reel; in none of the tests did the reel lock. The friction of the reel was measured as 10 N. As a result, the restraining effect of the belts was not considered to be significant.

Moving base

The positions of the salient points, given as global co-ordinates relative to the moving base body, are as presented in Table A - 12.

Point	X (mm)	Y (mm)	Z (mm)
Seat: front edge, centreline	-132	-2	622
Seat: top of head restraint, centreline	-752	0	1375
Shoulderbelt seat insertion: right	-710	-40	1146
Shoulderbelt seat insertion: left	-710	40	1146
Lapbelt seat insertion: right	-470	-208	655
Lapbelt seat insertion: left	-470	208	655
Lapbelt anchor: right	-467	-302	500
Lapbelt anchor: left	-467	-292	466
Shoulderbelt joint (point A, fig.1)	-815	498	651

Point	X (mm)	Y (mm)	Z (mm)
Belt end point (point B, fig.1)	-867	850	315
Steering wheel centreline of plane/centre of rotation	48	0	928
Footplate lower centreline	256	0	304

Table A - 12: Model coordinates

The steering wheel has an outer diameter of 350 mm and a rim thickness of 40 mm. It is angled backwards 15 degrees from vertical.

The footplate is 350 mm wide and angled backwards 38 degrees from vertical.

Measurements

The kinematics of the volunteers was measured with a 3D video system tracking markers at 200Hz. Markers were tracked in the following locations: Head c.o.g., T1, left shoulder, elbow and wrist, left knee. Multiple markers were used around the head in order to calculate rotation, and a bracket was used at the T1 in order to extrapolate T1 position.

Multiple volunteer traces were recorded for each load case. These were combined into corridors, given as a mean +/- 1 standard deviation

As the tests were of different lengths, the number of data points varies with time; the longer the measurement continues, the fewer traces remain. This naturally affects the confidence in the standard deviations at later times. To address this, corrected corridors were also calculated; for a given test n our of N total tests, the following equation can be used:

$$s^2 = \sqrt{\frac{N-1}{n-1}} \frac{1}{n-1} \sum_{i=1}^{n} (x_i - \bar{x})^2$$

Load Cases

The moving base was free to move in any direction relative to the occupant. Two different accelerations were prescribed for these tests:

Lateral – a purely lateral acceleration (for the occupant) of 5m/s^2 and an initial jerk of 130 m/s^3. The vehicle had an initial velocity of 25km/h, reducing to 5km/h. Tests were performed separately in both the left and the right directions for the occupant.

Lane Change – the vehicle simulated a lane change manoeuvre derived from a EuroNCAP stability test. The vehicle moved laterally at 5km/h, and an approximately sinusoidal lateral acceleration was applied, peaking at 5 m/s^2 with a yaw of 25 deg/s. Longitudinal acceleration and other rotations were considered negligible and not applied.

The load cases are referred to as

[LaneG/Lateral]_[SW/noSW]_[R/B]_[L/R]

Corresponding to

(lanechange/lateral), (steering wheel/no steering wheel), (relaxed/braced), (left/right)*

*lateral only

Each participant was only tested once per load case. The number of participants varied per configuration (Table A - 13).

Test	Number of participants
Lateral_noSW_R_L	13
Lateral_SW_R_L	9
Lateral_SW_R_R	10
LaneG_noSW_R	21
LaneG_noSW_B	17
LaneG_SW_R	17
LaneG_SW_B	18

Table A - 13:Number of participants tested per load case.

Data Description

Available data

The data was available for OSCCAR partners during the time the project was running. Some of the published data has been digitized and is available:

https://doi.org/10.5281/zenodo.5786677

AHBM 2 data

This report details the experimental setup and available results from a 2012 series of human volunteer tests in which volunteers were exposed to both autonomous and manual braking in a production automobile. The purpose of this report is to detail the study such that its results can be used for evaluations of active HBMs during pre-crash events in the OSCCAR project.

In summary, this series of tests exposed 20 volunteers (11 male 9 female) to braking events from 70 km/h. Occupants in the passenger seat were exposed to autonomous braking with either a pre pre-tensioner or regular seat belt. Occupants in the driver seat were exposed to the same braking events with same seat belt systems but with the additional load case of manual braking with a standard belt. In these experiments a pre pre-tensioner seat belt is one that tensions the seatbelt before an aggressive steering or braking manoeuvre. This is differentiated from a pre-tensioner seat belt that applies tension to the belt during the early phase of a collision. During these experiments the occupant's kinematics were measured with markers tracked with cameras, kinetics were measured with pedal, belt, and steering wheel loadcells, and muscle activity was recorded in 8 bilateral muscles in the neck, torso, and upper extremities. Muscle activity was normalized to maximum voluntary isometric contractions.

Ethics

All volunteers gave their informed consent to participate in this study which was approved by the Ethical Review Board of the University of Göteborg. Volunteer were recruited using advertisements posted at the SAFER offices, emails to recipients at SAFER and Chalmers Applied Mechanics, social media, and personal contacts.

Disclaimer

Volunteer test data – principles of use (derived from CA)

For the volunteer test data made available by the OSSCAR partners on OSCCAR project place/ SharePoint the following shall apply:

- The test data provided by a partner may be used by another OSSCAR partner to validate, improve and extend occupant models.
- In particular, a partner using the data is not allowed to disclose the data to any third party.
- For any use of these data after the OSSCAR project Art 11.3.2. and Art 11.3.5 of the OSSCAR Consortium Agreement shall apply meaning that the partner shall make a written request for any access rights to the owner of the data (Chalmers and their partners) and a written agreement must be concluded to agree on the conditions of granting access rights to these data.
- For the sake of clarification, it is stated that the evaluated and improved models are not subject to any CA related restrictions.

Methods

Volunteer description

A total of 20 volunteers (11 male, 9 female) were tested, with the males being a mean (S.D) of 32.7 (12.5) years old, 178.2 (5.2) cm tall, and 77.5 (5.6) kg in weight (Table A - 14). The females had a mean (S.D.) age of 28.8 (5.9) years old, and were 166.6 (5.0) cm tall, and 59.4 (5.2) kg in weight.

Male volunteer no.	Age (Years)	Stature (cm)	Weight (kg)	Sitting height (mm)	Female volunteer no.	Age (Years)	Height (cm)	Weight (kg)	Sitting height (mm)
1	27	184	78	977	1	28	173	72	940
2	26	173	79	930	2	44	160	60	847
3	26	175	82	967	3	29	168	60	900
4	38	184	85	945	4	27	158.5	56	845
5	68	184	81	965	5	27	163.5	58	877
6	29	169	75	896	6	28	166	60	910
7	28	183	75	962	7	27	168	58	885
8	36	176	85	913	8	24	171	53	917
9	30	180	72	970	9	25	171	58	924
10	23	177	68	929					
11	29	175	72	957					
Mean	32.7	178.2	77.5	946	Mean	28.8	166.6	59.4	894
Std.	12.5	5.2	5.6	26.2	Std.	5.9	5.0	5.2	33.2

Table A - 14: Volunteer anthropometric data. Std. – Standard deviation.

Boundary Conditions

The test vehicle used in these experiments was a Volvo V60 T4 (180 hp turbocharged two-liter petrol engine with automatic gearbox). The car was equipped with new, but worn in, summer tires (Continental Sport Contact 3 235/45/R17 inflated with 2.5 bar). The seats in the vehicle were equipped with leather upholstery.

Autonomous braking was implemented using a PC running Canalyzer v7.6 (Vector GmBH, Stuttgart, Germany). Two VN1640 (Vector GmBH, Stuttgart, Germany) cases were used for communication with the vehicle and triggering of the autonomous braking events (through three separate digital inputs controlled by the experimenter). The autobraking of the vehicle was actuated by the hydraulic pump in the car's brake system.

The driver and passenger seatbelts were replaced with active seatbelts (Autoliv, Stockholm, Sweden), incorporating an electrical motor that allows for reversible pre-tension. The active seatbelts were controlled using the same equipment as the autonomous braking interface. Installation of the seatbelts was performed by a research engineer from Autoliv. The active seatbelts were used both in active and passive mode. In the active mode a nominal tension of 170 N was applied and in the passive mode no tension was applied, and the retractor locked at 0.45 g vehicle deceleration or a belt pay-out acceleration of 1.5 g.

Volunteer posture measurements

Drivers were instructed to always keep their left foot on the foot rest (support surface to the left of the brake pedal), and their hands in a symmetrical position on the steering wheel at positions 3 & 9 or 2 &10. The passengers were instructed to keep both feet on the floor symmetrically around the force transducer (see additional details in [65]).

The volunteers could partially adjust the driver seat and steering wheel to find a comfortable driving position. Allowed adjustments were translation of the seat, change of the inclination angle of the seat back, and the steering wheel position and angle. The seat cushion was in its lowest position and the volunteers were not allowed to change its height or angle. Seat and steering wheel positions chosen by the volunteers are provided in [65]. The initial posture of the volunteers was calculated as their average position just before braking and are presented in Östh et al. [65] in a car fixed reference system. Additional details on driver and passenger initial postures can be found in [65].

Loading conditions

The data from three combinations of vehicle braking and seat belt functions are included in this dataset. This is a subset of the five conditions conducted during the experiments.

A – Autonomous braking (Autobrake) with 170 N electrically driven seat belt pre-tension 200 ms before initiation of braking.

C – Autobrake without electrical seat belt tensioning, i.e., a standard passive seatbelt.

E – Driver Braking: maximum emergency braking initiated by visual stimuli and standard seatbelt.

All tests were from a nominal vehicle speed of 70 km/h, which was the speed limit of the country roads were testing was conducted. The experiment leader checked the traffic situation, using an extra rear-view mirror mounted to the roof in the middle of the passenger compartment, to ensure it was safe to perform the braking events.

Events A & C were initiated by the experiment leader without prior notification to the volunteer. The target deceleration for the autobrake requests was maximum vehicle deceleration over a 2 s period, resulting in a mean vehicle deceleration of approximately 11 m s-2 once fully developed. Wheel lock

and maximum vehicle deceleration was achieved approximately 0.7 s after initiation of the braking. The change of velocity was approximately 50 km/h.

In Event E the volunteer braked in reaction to an array of 10 red Light Emitting Diodes (LEDs), 6 cm long, flashing with 7 Hz for 2 s on the dashboard in front of the driver (Figure A - 41 d). The LED array was triggered by the experiment leader without prior notification to the volunteers.

Testing was divided into two parts, in the first the volunteer was driving the test vehicle, in the second the volunteer was in the passenger seat. In the driver seat, all events A-E were tested four times. In the passenger seat only the Autobrake events, A-C, were tested three times each. The order of the events was randomized for each volunteer except for the first event, which was of type A for all volunteers and on both the driver and passenger side.

Kinematics

Camera system

The kinematics of the volunteers during the braking manoeuvres were measured using motion capture of markers fixed to the skin. Three video cameras (UI-5220CP-C Gigabit Ethernet CMOS colour cameras, IDS GmbH, Obersulm, Germany) with wide angle lenses recorded occupant motions (4.5 mm focal length, LM5NCL, Kowa Co., Tokyo, Japan). The cameras were placed on the on the driver's side roof near the sunscreen for a side view of the passenger (Figure 3c), the passenger side door with a side view of the driver (Figure 3e), and on the dashboard with a front view of the driver (Figure 3c). Note that the front view of the driver was only used to check if the driver was out of position (from mid-plane) before the manoeuvres, and no further analysis was performed on this data.

Data was recorded with custom written LabVIEW code (National Instruments, Austin, Texas). A synchronization pulse was used to sync the other data channels to the camera images, and a timestamp saved with the frames was used to identify missed frames. Images were 768x480 pixels and were saved in uncompressed .png format. Images were recorded at 50Hz.

The tracked film markers consisted of yellow and back stickers that were placed to track head, torso and upper extremity motions (Figure A - 40). Specifically, three markers were placed on each side of the head in a triangular pattern aligned with the Frankfort plane, approximately 20 mm forward of the auditory canal. Further, a marker on a bracket was placed the manubrium via double sided tape a fixed to the skin. The centre of the marker was approximately 25 mm below the sternal notch and 35 mm in front of the chest. The right upper extremity was tracked with three markers: the shoulder on the middle deltoid, the elbow at the lateral epicondyle of the humerus, and the wrist between the styloid processes of radius and ulna on the lateral aspect. Finally, a marker was placed on the left shoulder at the middle deltoid.

Figure A - 40: Film marker placements on the right and left side of the volunteers.

Post-processing

The calculation of marker position was performed using TEMA Automotive (Image Systems, Linköping, Sweden) which adjusts for lens distortion. Lost frames were identified and replaced with a copy of the previous frame using a MATLAB script (MathWorks, Natick, MA, USA).

TEMA Software (option skewed motion plane) was used to correct the tracked marker positions from a coordinate system fixed relative to the camera to one fixed to the vehicle aligned with global vertical and horizontal when the vehicle is static (i.e., Z positive upwards, X positive forward, Y positive left) and confirmed by the use of a pattern on a checkerboard.

The displacements of the head were reported at the center of gravity of the head using rigid body transformation. In this transformation, the marker kinematics in the sagittal plane were transferred to the auditory duct (origin of the Frankfort plane) and then transferred to head center of gravity. The latter was assumed to be located at 8.7 mm in front and 26.8 mm above the auditory duct for males (weighted average of 19 subjects from Beier et al. (1980) and 17 subjects from Walker et al. (1973)) and 0.2 mm in front and 29.1 mm above the auditory duct for females (average of 7 subjects from Yoganandan et al. (2005)) in the local head coordinate system.

Coordinate system and time zero

The coordinate system used is fixed relative to the vehicle and with the vehicle in a static position aligns with world vertical with Z positive upwards, horizontal with X positive forward, and horizontal with Y positive leftwards). The origin of this coordinate system is 792 mm rearward and level with the head of the front right bolt holding the driver's seat.

For the Autobrake load cases, time zero is the time when the trials were started by the trigger. For the Driver Brake load case, time zero is when the driver first contacted the brake pedal.

Description of rejected data

During a single trial, a maximum of ten motion tracking frames were lost due to buffer capacity, but on average two to three frames were lost per trial. These lost frames were replaced with a copy of the previous frame to maintain synchronization with other data channels.

Some of the kinematic data from the film analysis was missing due to insufficient visibility, e.g. the sun was shining directly into the camera or the marker was obscured. Of 44 and 36 possible data sets for each test case, for males and females respectively, the head markers were not tracked in three male driver brake load cases. Moreover, the sternum marker data was missing from one male and nine female Autobrake PT load cases, seven male and eight female Autobrake SB load cases, and twelve male and fifteen female Driver Brake load cases; data from the upper extremity markers was missing from three female Autobrake PT and driver brake load cases, and from two female Autobrake SB load cases.

Kinetics

The interactions of the volunteers with the car interior were measured with a series of sensors (Table A - 15, Figure A - 41). These signals were recorded using an USB-6251 AD-converter (National Instruments, Austin, Texas) running at 2048 Hz. Sensor excitation and pre-amplification were made with multiple DAQ-P Bridge B (Dewetron, Wernau, Germany) bridge amplifiers. For the DAQ-P bridge amplifiers, no anti-aliasing filters were utilized.

Steering column force was measured with a strain gauge glued to the column using a wireless telemetry transmitter (dt1001T-S, Telemetrie Elektronik GmbH, Langenhagen, Germany).

Vehicle accelerometer (10g; EGCS-D1CM-10; Entran, Hampton, Virginia, USA) mounted to the passenger front left seat mount bolt, Figure A - 41.

A: View from driver side showing camera used when recording driver kinematics (see arrow).
B: View of passenger seat environment.
C: View from driver seat showing driver front camera (see arrow) and LED array used as visual trigger for some of the events (left of camera).
D: View from passenger side. Driver front camera visible on top of dashboard (see arrow) and passenger side camera (see arrow) visible above driver sunscreen. In the right lower corner; passenger floor force transducer position.
E: Driver seat indention positions
F: View through rear left door, back of driver seat showing wire potentiometers used for seat compression measurements.
G: Trunk of the car included an AD-converter, a bridge amplifier, a computer), an extra 12V battery and 240V inverter.
H: Brake pedal and driver left foot force transducers.

Figure A - 41: Sensor and equipment placement in the test vehicle.

Signal(s)	No.	Sensor(s)	Model	Manufacturer	Details
Brake pedal force	1	Force transducer	GKR2	Volvo Car Company, Göteborg, Sweden	Mounted on the brake pedal, Figure A - 41b (1).
Footrest force	1	Force transducer	2358FL	Denton ATD Inc. Rochester Hills, Michigan, USA.	Mounted using a steel plate with hinge joint, Figure A - 41b (2).
Passenger footwell force	1	Force transducer	PZ1,0	Load Indicator AB, Göteborg, Sweden	Mounted under passenger floor, Figure A - 41c (4).
Steering wheel force	1	Strain gauge	GTÖJ	Volvo Car Company, Göteborg, Sweden	Glued to the steering column, Figure A - 41e (1). The force from the strain gauge was calibrated in tension.
Lap belt force	1	Belt force transducer	EL20-S458-7B	Altheris bv, Den Haag, Netherlands	Low-range belt force transducer (maximum 6 kN), Figure A - 41a (2).
Shoulder belt force	1	Belt force transducer	DK11-13	Messring GmbH, Krailling, Germany	Low-range belt force transducer (maximum 6 kN), Figure A - 41a (3).
Belt payout	1	Optical belt movement sensor	IES 2098	IES, Braunschweig, Germany	Mounted with double adhesive tape on the inside of B-pillar, between the retractor and D-ring.
Seat indention	6	Wire potentiometer	Series 160	Firstmark Controls, Creedmoor, North Carolina,USA	Mounted through the seat upholstery, Figure A - 41a (1).

Table A - 15: Signals that were recorded and the sensors used in the test vehicle.

Post-processing

All sampled signals were post-processed with a CFC15 low pass filter (J211, SAE 2003).

The inertia sensitivity of the force sensors was assessed by means of six maximum autonomous braking events without any external loads. The steering column force was found to be affected by the 3.3 kg weight of the steering wheel mounted to it. This weight, multiplied with the filtered acceleration signal in each braking event, is subtracted from the steering wheel forces presented in the results. The steering column strain gauge was also found to be sensitive to bending moments; corrections, according to volunteer hand positions from the film data were applied. The other force sensors were found to be affected by less than 2 N, therefore no compensations were made.

Coordinate system

All force measurements are uniaxial and reported with positive values as tension, and negative as compression.

Muscle Activity

Surface electrodes were used to record electromyographic (EMG) signals from 8 bilateral pairs of muscles in the neck, torso, and upper extremities. EMG was recorded with a Grael amplifier (Compumedics, Abbotsford, Australia). For these channels, the input impedance is 24 MΩ, the

Common Mode Rejection Ration above 100 dB, and the input range of +/-300 mV with 24-bit resolution gives a resolution of approximately 0.02 µV (Compumedics 2009).

EMG was recorded with pairs Ag/AgCl electrodes (Blue Sensor N–00–S, Ambu A/S, Ballerup, Denmark) with an interelectrode spacing of 20 mm. A single electrode placed on the iliac crest served as the reference electrode. Before application of the electrodes, the skin was prepared by shaving, abrading with sandpaper (P180) and wiping with 70% ethanol solution. The lead wires were secured using surgical tape at each electrode location and a central strain relief consisting of a Velcro strap fastened around the chest of the volunteer.

Electrodes were placed bilaterally on muscles of the neck, torso, and upper extremities (Figure A - 42). Electrode placement was based on recommendations from SENIAM (SENIAM, 2012); Björn Äng, a physiotherapist and PhD with broad experience from EMG measurement from the Karolinska Institute (Stockholm, Sweden; Äng, 2012); or on other literature sources (Blouin et al. 2003; Cram et al. 1998).

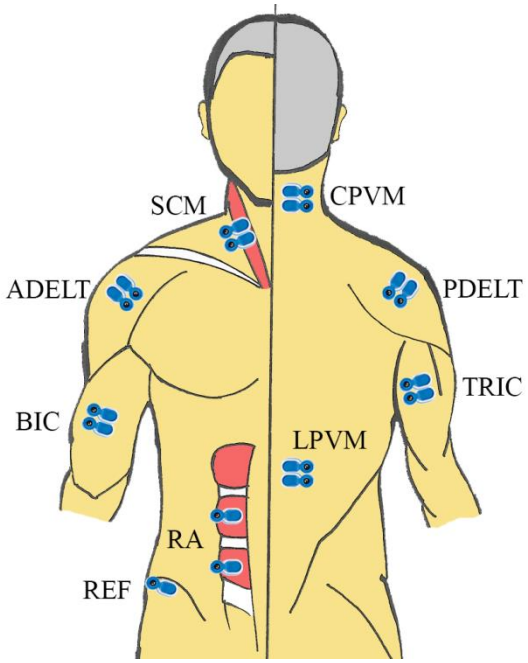

Figure A - 42: Electrode locations on the anterior side of the body shown to the left, on the posterior side to the right. Muscle name acronyms according to Table 2.

Antialiasing filters, amplification, sampling rate

EMG sampling rate was 2048 Hz.

MVIC measurement

Maximum voluntary isometric contractions (MVIC) were conducted for each muscle tested by pulling against a cable with a single axis loadcell in several configurations. MVICs were made in the following order: Cervical flexion – Lumbar flexion; Cervical extension – Lumbar extension; Elbow flexion, right arm – left arm. Elbow extension, right arm – left arm; Shoulder flexion, right arm – left arm; Shoulder extension, left arm – right arm. EMG was recorded during these trials and processed in the same manner as the car manoeuvre trials. A screen in front of the volunteers provided force feedback to motivate maximal effort. MVIC measurements were conducted to normalize the muscle activity measurements from the experimental trials.

Force measurements in the MVIC rig were recorded with an USB-6009 AD-converter (National Instruments, Austin, Texas) at 1000 Hz. Sensor excitation and pre-amplification were made with multiple DAQ-P Bridge B (Dewetron, Wernau, Germany) bridge amplifiers. For the DAQ-P bridge amplifiers, no anti-aliasing filters were utilized.

Post Processing EMG data

EMG was post-processed using MATLAB (The MathWorks Inc., Natick, MA, USA). The raw EMG signals were band-pass filtered (4th order Butterworth, 10-350 Hz), full wave rectified and smoothed with a 40 ms (82 sample) Root Mean Square (RMS) window. For the rectus abdominis and the erector spinae longissimus the low-pass filter limit was increased to 50 Hz to remedy heart rate artifacts. Furthermore, EMG is normalized with the maximum 1 s RMS window found in any of the three MVICs made for each muscle. The corridors were calculated as the mean +/- a standard deviation for each time point.

Data Description

Available data

Selected data has been digitized and made available in an open access repository: https://doi.org/10.5281/zenodo.5774088

Data format

The data was available for OSCCAR partners during the time the project was running. Some of the published data has been digitized and is available:

The data shared were provided either in a MATLAB database by name “Chalmers_Autobrake_2012.mat” or in .csv files.

This MATLAB file was only accessible in the software MATLAB (MathWorks Inc., Natick, MA, USA) later than version 2006a. The database files contains three variables set up as data structures holding the corridors (mean +/- SD) of the muscle activity, boundary conditions, and kinematics.

The data structures for muscle activity, boundary condition, and kinematics are each broken into between four to five levels (Figure A - 43). See acronyms in the following list:

EMG_Corr – Muscle activity corridors

KIN_Corr – Kinematics corridors

BC_Corr – Boundary condition corridors

Driv – Volunteer in the driver position

Pass – Volunteer in passenger position

F – females

M – males

AutoPT_1st – First trial from autobraking with pre pre-tensioner seatbelt

AutoPT – Autobraking with pre pre-tensioner seatbelt (other trials for ‘Driv’ or all trials for ‘Pass’)

AutoSB – Autobraking with standard seatbelt (all trials)

SB – Driver braking with standard seatbelt (all trials)

RA to CPVM – Eight muscles recorded, see section 5.3 for details

HeadCG – Head centre of gravity

Sten – Sternum

Shldr – Shoulder acromion marker

Elbow – Elbow flexion/extension angle

T1 – first thoracic vertebral marker

Acc – Vehicle acceleration

ShBeltF – Shoulder belt force

LapBeltF – Lap belt force

SteerWF – Steering wheel resultant force

BrakePF – Brake pedal force

FootRF – Footrest force

FootWF – Footwell force

L – left

R – right

X – Fore-aft direction

Z – Vertical direction

Rot – rotation in sagittal plane

The first level is for drivers or passengers; followed by the gender of the volunteers; then the four or two load cases for respectively for the drivers and passengers; then response variables, and finally some response variables have directionality or left/right. See the associated figure for more details (Figure A - 43). In the data structures every variable consists of labelled ‘Table’ datatype with the four columns being time, mean response, +1 standard deviation, and minus one standard deviation. The rows correspond to time.

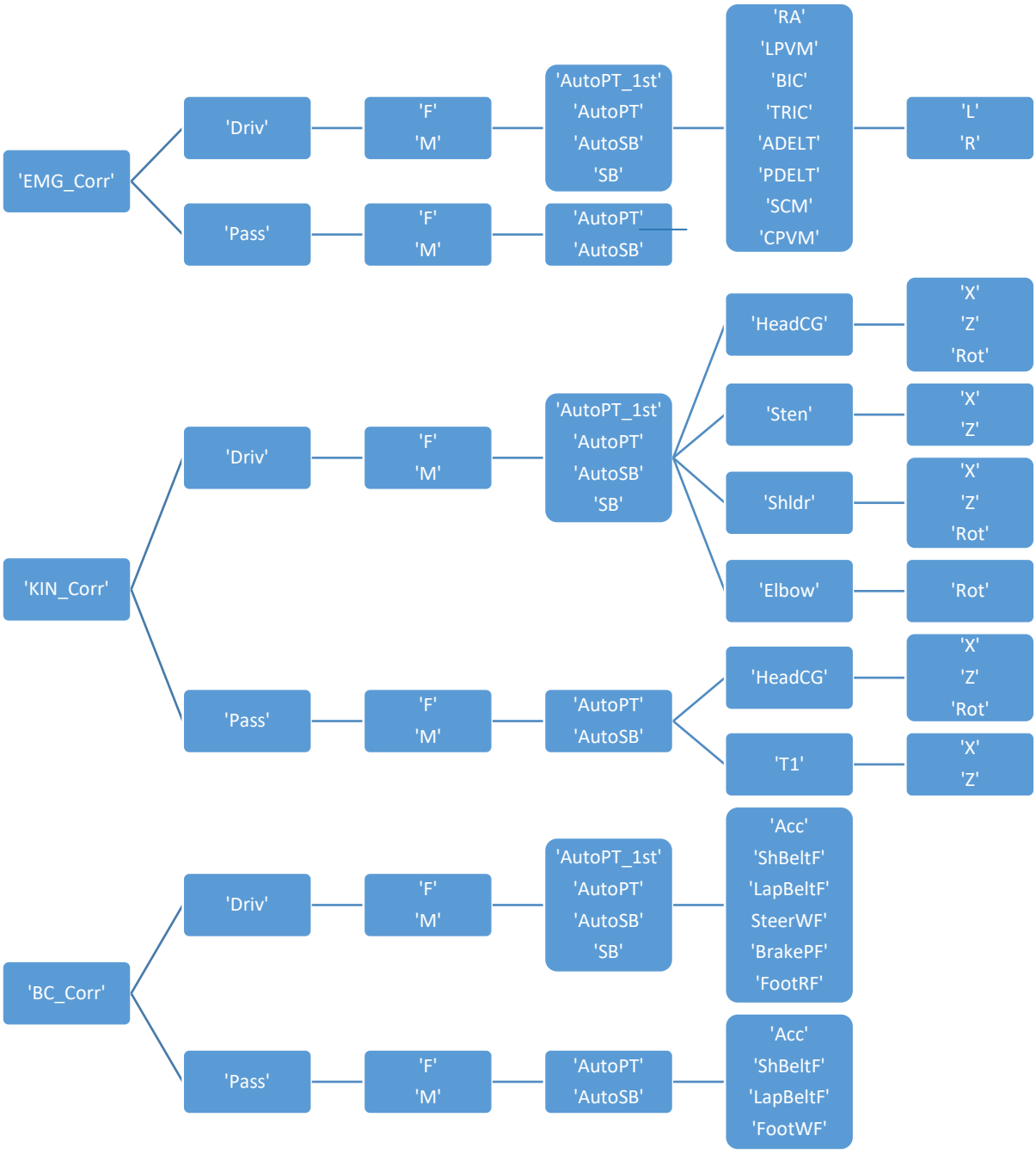

Figure A - 43: The outline of structures containing the validation data for this load case. Data structure names are as follows.

References

Äng, B (2012) Personal communication, 2012-04-17.

Blouin J-S, Descarreaux M, Belanger-Gravel A, Simoneau M, Teasdale N. (2003) Attenuation of human neck muscle activity following repeated imposed trunk-forward linear acceleration. Exp. Brain Res. 150:458–464.

Compumedics (2009) Grael User Guide. Compumedics Limited, Abbotsford, Victoria, Australia.

Cram JR, Kasman GS, Holtz J (1998) Introduction to Surface Electromyography. Aspen Publishers, Inc. Gaithersburg, Maryland.

AHBM 3 data

This report summarizes the experimental setup and some of the results from a 2016 series of human volunteer tests in which volunteers were exposed to autonomous lane change with and without braking in a regular car (Figure A - 44). The purpose of this report is to detail the study such that its results can be used for evaluations of active HBMs during pre-crash events in the OSCCAR project.

This report should be read in parallel with the published articles:

- Ghaffari, G., Brolin, K., Bråse, D., Pipkorn, B., Svanberg, B., Jakobsson, L., & Davidsson, J. (2018). Passenger kinematics in Lane change and Lane change with Braking Manoeuvres using two belt configurations: standard and reversible pre-pretensioner. In *Proceedings of the 2018 International IRCOBI Conference on the Biomechanics of Impact, September 12-14, Athens, Greece*.
- Ghaffari, G., Brolin, K., Pipkorn, B., Jakobsson, L., & Davidsson, J. (2019) Passenger muscle responses in lane change and lane change with braking manoeuvres using two belt configurations: Standard and reversible pre-pretensioner, Traffic Injury Prevention, 20:sup1, S43-S51, DOI: 10.1080/15389588.2019.1634265

Ethics

All volunteers gave their informed consent to participate in this study which was approved by the Ethical Review Board at the University of Göteborg, application 602-15.

Disclaimer

Volunteer test data – principles of use (derived from CA)

For the volunteer test data made available by the OSSCAR partners on OSCCAR projectplace/ SharePoint the following shall apply:

- The test data provided by a partner may be used by another OSSCAR partner to validate, improve and extend occupant models.
- In particular, a partner using the data is not allowed to disclose the data to any third party.
- For any use of these data after the OSSCAR project Art 11.3.2. and Art 11.3.5 of the OSSCAR Consortium Agreement shall apply meaning that the partner shall make a written request for any access rights to the owner of the data (Chalmers and their partners) and a written agreement must be concluded in order to agree on the conditions of granting access rights to these data.
- For the sake of clarification, it is stated that the evaluated and improved models are not subject to any CA related restrictions.

Figure A - 44: Photos of the test vehicle on the test track (airfield) used in the AHBM 3 tests.

Data Description

Available data

Selected data has been digitized and made available in an open access repository:

https://doi.org/10.5281/zenodo.5784240

Data format

The data was available for OSCCAR partners during the time the project was running. Then the data shared were provided either in a MATLAB database by name “Chalmers_LaneChange_2016.mat.” or in .csv files.

This MATLAB file was only accessible in the software MATLAB (MathWorks Inc., Natick, MA, USA) later than version 2006a. The database files contain three variables set up as data structures holding the corridors (mean +/- SD) of the muscle activity, boundary conditions, and kinematics.

The data structures for muscle activity, boundary condition, and kinematics are each broken into between four to five levels (Figure A - 45. The first level only has a passenger entry as the driver data hasn’t been published at this time; followed by the gender of the volunteers; then the four load cases; then response variables, and finally some response variables have directionality or left/right. See the associated figure for more details (Figure A - 45). In the data structures every variable consists of labelled ‘Table’ datatype with the four columns being time, mean minus a standard deviation, mean, mean plus a standard deviation. The rows correspond to time. The exemplar code in section 7 of this document is provided to add clarity to the description of the data structures provided here. See acronyms used in the following table:

EMG_Corr – Muscle activity corridors;

KIN_Corr – Kinematics corridors;

BC_Corr – Boundary condition corridors;

Pass – Volunteer in passenger position;

M – males;

LB_AutoPT – Autonomous lane change with braking, pre-pretensioner seat belt;

LB_AutoSB – Autonomous lane change with braking, standard seat belt;

L_AutoPT – Autonomous lane change without braking, pre-pretensioner seat belt;

L_AutoSB – Autonomous lane change without braking, standard seat belt;

SPVM to RF– Eighteen muscles recorded;

Head – Head;

T1 – First thoracic vertebrae;

UppTorso – Upper Torso;

Acc – Vehicle acceleration;

ShBeltF – Shoulder belt force;

LapBeltF – Lap belt force;

BeltPayout – Belt payout.

L – Left;

R – Right;

X – fore-aft direction in vehicle fixed coordinate system;

Y – lef-right direction in vehicle fixed coordinate system; Z – up-down direction in vehicle fixed coordinate system;

RotX, RotY and RotZ – projection of rotation in the YZ plane, XZ plane and XY plane, respectively;

Roll, Pitch, Yaw – Intrinsic Euler angles with a yaw, pitch, roll decomposition order.

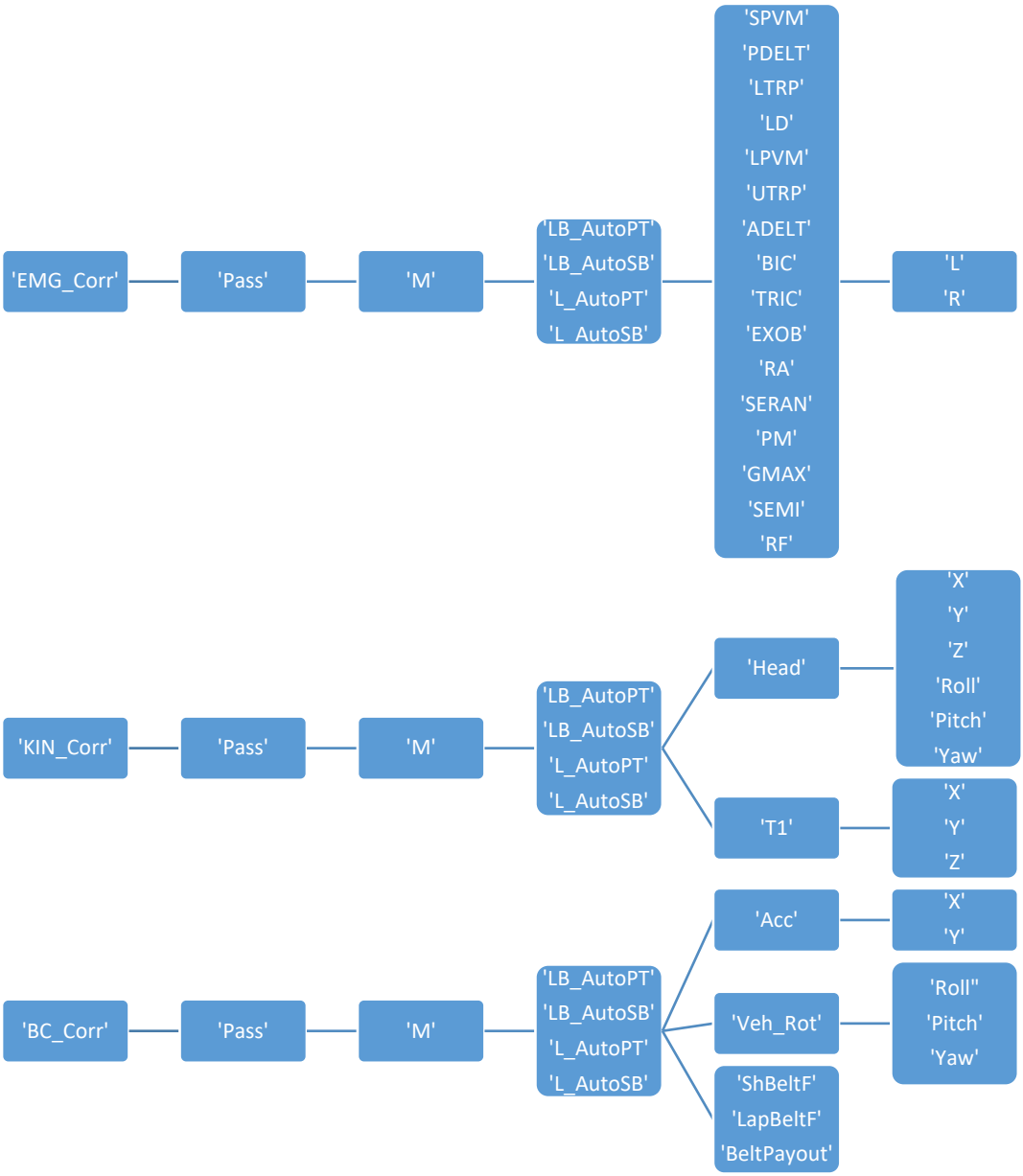

Figure A - 45: The outline of structures containing the validation data for this load case. Data structure names are as follows.

Exemplar plot of the data

Exemplar plots are provided in Figure A - 46 is presented code used to generate it.

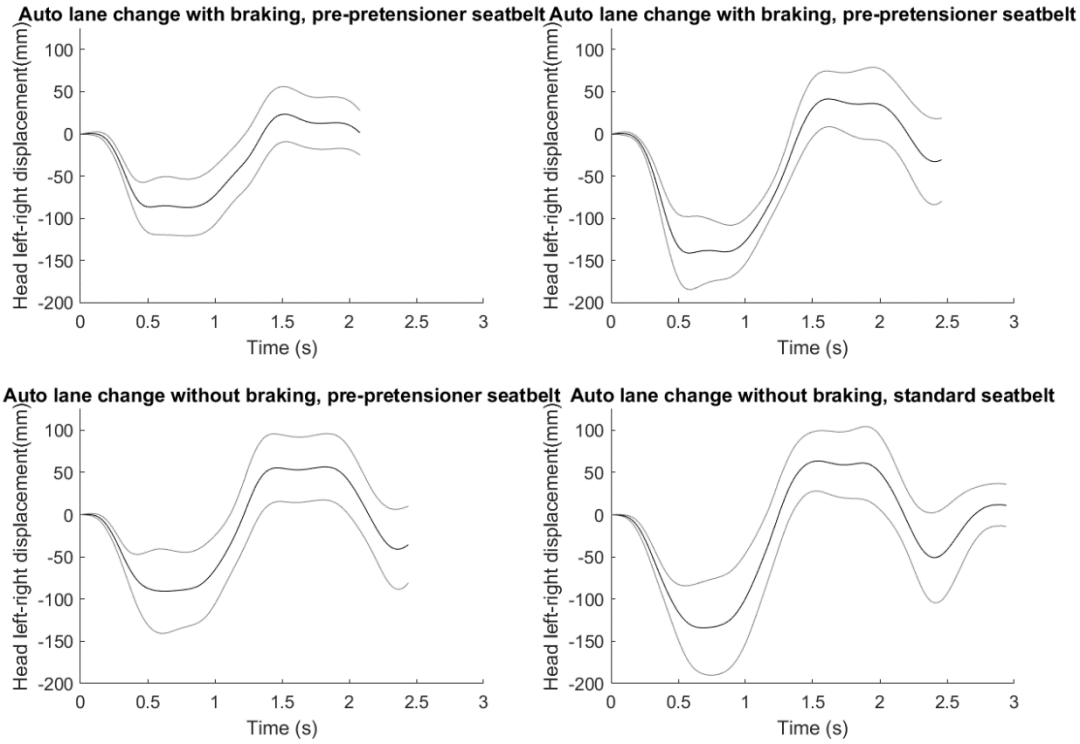

Figure A - 46: Exemplar plot of head response corridors in the left-right direction for male passengers with four load cases considered: 1) Autonomous lane change with braking, pre-pretensioner seat belt; 2) Autonomous lane change with braking, standard seat belt; 3) Autonomous lane change without braking, pre-pretensioner seat belt; 4) Autonomous lane change without braking, standard seat belt.

C. APPENDIX - MODELS OF THE LOADING ENVIRONMENTS USED IN THE VOLUNTEER TESTS

Models for the use of OM4IS2 and PRECOONI data

An FE model of the seat used in the OM4IS2 and PRECOONI tests was developed and validated. The FE model tests was available for OSCCAR partners on their platform. The model is also available for the public on the open VT platform at: https://openvt.eu/osccar/precrash_seat_models/precooni-om4is

Development of the OM4IS2 and PRECOONI seat model

The original seat was scanned with a 3D FARO laser scanner, which output is shown in Figure A - 47 on the left side. Based on the derived geometry, a finite element model was developed by Mercedes, see Figure A - 47 right. The foam was meshed with solid elements and the leather cover with shell elements. The seat structure beneath the seat cushion as well as the seat back is simplified and modelled via beam elements. The behaviour of the seat cushion structure is modelled via beams in x, y and z direction in each corner. A joint defines the connection between the seat cushion and seat back.

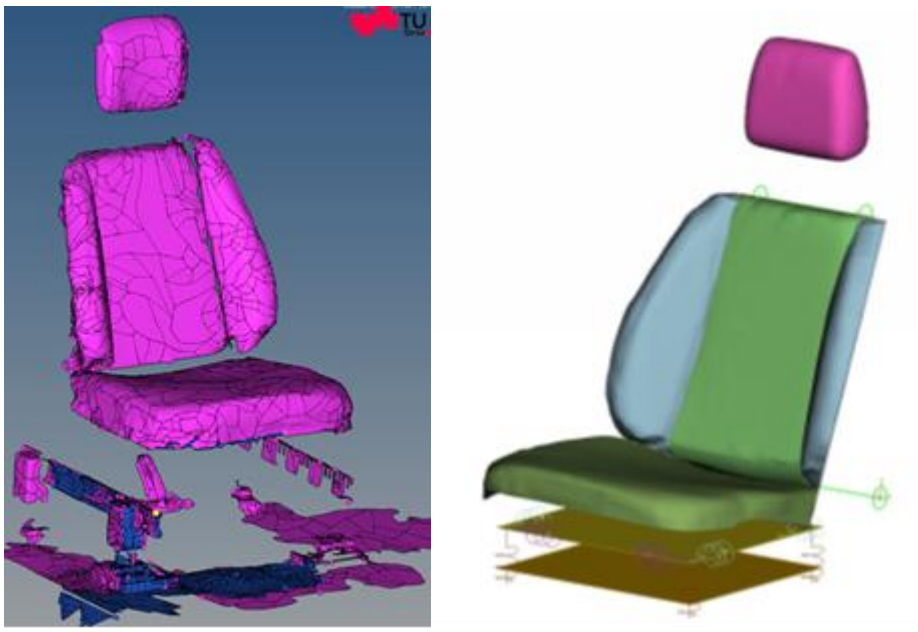

Figure A - 47: Generation of the seat model

For the first generation of the seat (PRECOONI_SEAT_FOAM_HR_v1_14_28022020.key) only compression tests of the foam (according to ISO 3386) were included in the development of the seat model.

For the second generation developed within OSCCAR, additional mechanical tests with the whole seat were considered.

The characteristic of the seat structure was determined by executing several tests, which are shown in Figure A - 48. The test setups in the top row were performed on the bare wooden plate and

additionally with the seat foam mounted on the wooden plate. For each test, the force acting on the impactor and the deflection of the seat were measured.

Seat cushion – global: impactor on the middle on the seat cushion → global seat structure deflection

Seat cushion – local: impactor in each corner of the seat cushion → deflection behaviour to address each z-axis beam of the simulation model separately

Backrest: impactor on the most upper point of the seat back → bending behaviour of the seat back structure

Seat structure – frontal: lateral push on the seat cushion structure → deflection behaviour to address y-axis beams of the simulation model

Seat structure – lateral: frontal push and pull on the seat cushion structure → deflection behaviour to address x-axis beams of the simulation model

Seat cushion – global	Seat cushion – local	Backrest
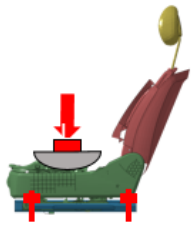	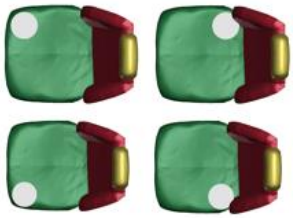	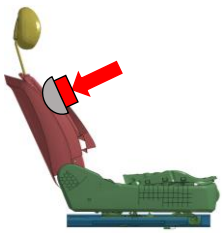
Seat structure – frontal	Seat structur – lateral	Side structure
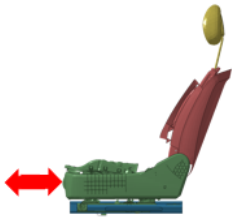		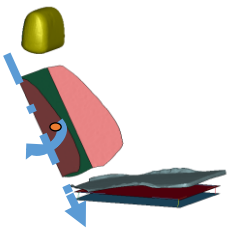

Figure A - 48: Test setups for the seat model validation

Calibration of the OM4IS2 and PRECOONI seat model

The investigations in the previous studies revealed an influence of the seat model setup on the occupant kinematics. To further analyse the influence of potential differences between the seat model and the physical seat, the differences needed to be identified in the first place. To do so, a comparison of the mechanical response of the seat to the response of the seat model in several test setups was targeted.

To further evaluate the influence of the changes in the seat model, which were needed to reproduce the physical test results, simulations with the seated THUMS v4 were performed with the original seat model as well as the enhanced seat model.

Method

Several test setups were defined in order to generate data on the mechanical behaviour of the physical seat. Hemispheric impactors in two sizes were mounted on a hydraulic cylinder and pressed against the seat. A load cell behind the cylinder recorded the applied force. In addition, the deflection of the impactor was measured. In order to determine the characteristic behaviour of the seat due to loadings induced by a seated and moving occupant, press test scenarios were developed as shown in Figure A - 48.

The behaviour of the structure underneath the seat cushion was determined by a global test (“Seat cushion – global”) with a ø250 mm impactor pressing vertically on the seat cushion centre and four local tests (“Seat cushion – local”) with a ø150 mm impactor pressing on each edge of the seat cushion. The behaviour of the backrest joint in combination with the seat structure was tested by pressing the ø150 mm impactor at a 20° angle against the top of the backrest (“Backrest”). All tests were conducted with and without the covering foam layer.

The seat structure was further tested regarding its behaviour due to lateral and frontal loading. For the frontal test setup (“Seat structure – frontal”) a console was manufactured which allowed a pulling and pushing movement of the seat structure. Only a push test was conducted for the lateral test (“Seat structure – lateral”), as the construction of the seat structure did not allow a mounting of a pulling device.

The side wings of the seat (“Side structure”) were not tested physically but via simulation. The two wooden side wings are connected to the backrest via two steel flanges. Performing press tests on those wooden plates did not seem possible without causing damage to the structure. Therefore, the flanges were scanned, meshed for FE-simulation, and allocated with steel material. A rotation about the mounting axis of the wings was simulated and the applied moment was recorded.

For the calibrated of the FE seat model, simulations reproducing the prescribed tests were set up. The seat model was adapted to reproduce the mechanical behaviour of the seat in the physical tests. The correspondence was evaluated by comparing the measured force-deflection curves from the tests with the moment-deflection curve from the simulation.

In a further step, HBM simulations were conducted in order to evaluate the influence of the enhanced seat model in comparison to the original seat. The original simulations were repeated with the new seat model. Subsequently, the trajectories of the HBM were compared to those from simulations with the original seat model. The comparison was made for two HBM postures: the occupant postures the HMB gets delivered in (original posture) and the positioned posture according to volunteer P03T03 (T03s posture).

Results

During the calibration process adaptations of the seat model were made regarding the material properties of the leather skin as well as the spring and damper definitions in the seat structure. Furthermore, the side wings were detached from the backrest and connected via cylindrical joints with defined stiffness parameters. Overall, a comparable behaviour between simulations and tests was observed, which is shown in the figures below.

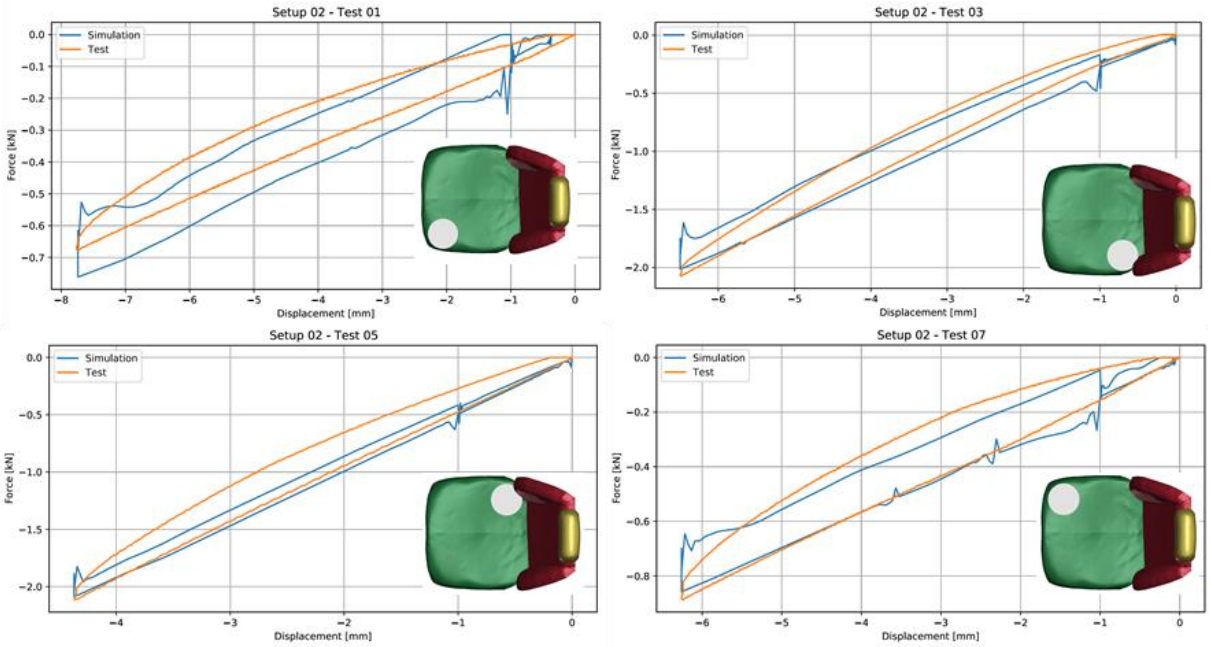

Figure A - 49: Comparison of the OM4IS / PRECOONI seat response from tests and simulations on seat cushion

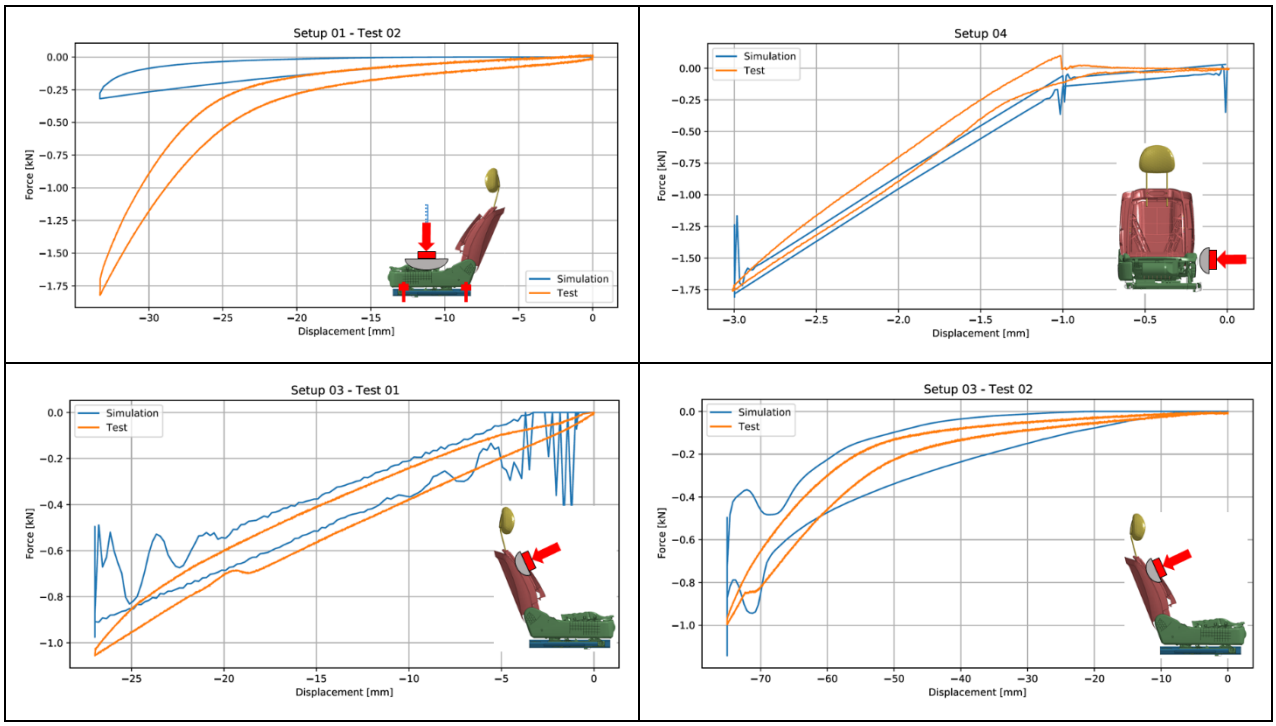

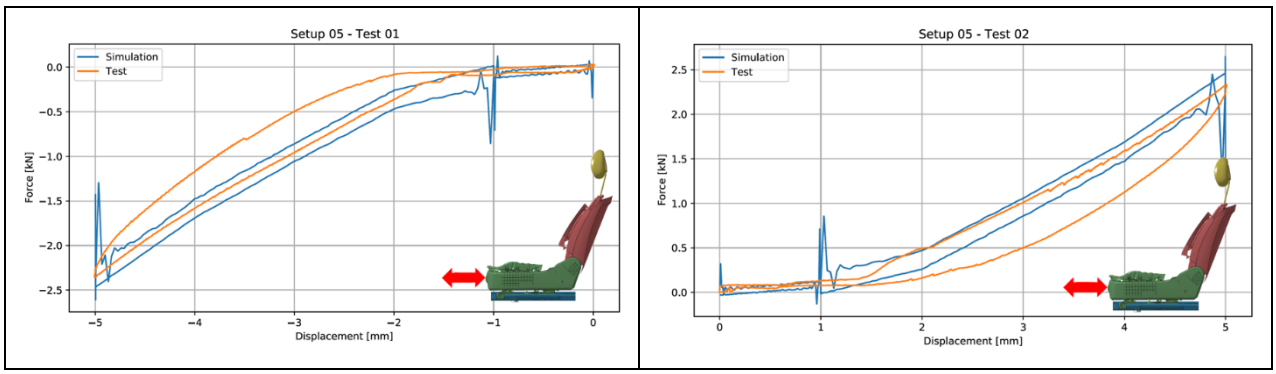

Figure A - 50: Comparison of the OM4IS / PRECOONI seat response from tests and simulations after calibration

Figure A - 51 shows the deviations of the peak forward excursion (left) and the peak downward excursion (right) of the seated HMB between the original and the enhanced seat model with deformable structure. The comparisons were made for the landmarks trochanter major (TM) and head audit (HA). The HBM in the original posture experiences an increased forward and downward excursion of TM (+7% and +40%) but decreased forward and downward excursion of HA (-1% and -6%). The HBM in the T03s posture experiences an increased downward excursion of TM (+81%) and increased downward excursion of HA (+2%) but a decreased forward excursion of HA (-5%).

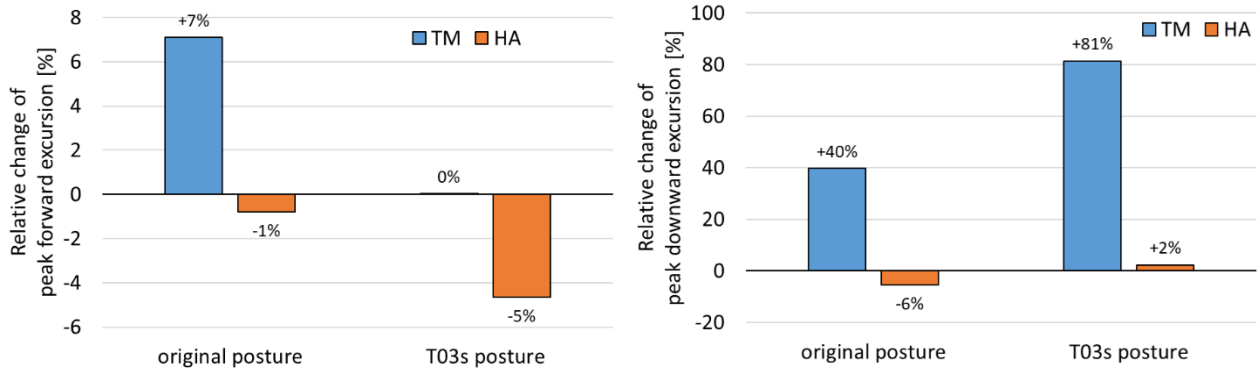

Figure A - 51: Comparison of the peak forward and downward excursion of the seated HBM

The plots of the simulations showed a movement of the upper rigid plate of the seat structure of the validated seat model. The rotational angle of the rigid plate about the y axis peaks up to 0.3 degrees. The original seat model did not show any movement of the rigid seat structure plates.

Conclusion

The original seat model was adapted with regard to the material properties of the leather skin as well as spring and damper definitions to meet the determined force-deflection curves from the tests. As the results match well for the tests without foam layer but showed deviations for the tests with the foam layer, it is assumed, that further testing of the foam itself could further improve the seat model. The fact that the leather canvas was not connected to the seat structure in the tests may also influence the deformation behaviour.

In both HBM postures, an increased forward and downward excursion of the TM was noticed when seated on the validated seat model. The less stiff springs in the seat structure allow a slight movement of the upper rigid plate to which the seat cushion is connected. The resulting rotation of the seat cushion about the y-axis supports the forward movement of the HBM pelvis. Nevertheless,

the differences in the excursions are limited to millimetre range, which means the seat structure stiffness did not have major influence on the occupant's kinematics.

Models for the use of AHBM 2 and AHBM 3 data

The goal of sharing human volunteer test data from the Chalmers 2012 autobrake (AHBM 2) and 2016 lane change test series (AHBM 3) was to provide OSCCAR partners with a common dataset to validate their HBMs. To facilitate this goal, a FE-model for LS Dyna of the set up that was used in these original experiments were developed and made available to OSCCAR partners during the project period and thereafter to the public.

The FE model of the the set up used in AHBM 2 and AHBM 3 volunteer tests is available for OSCCAR partners on the Osccar platform. The same model is also available for the public on the Virtual open VT platform at: https://openvt.eu/osccar/precrash_seat_models/safer-ahbm_2-3

This report outlines the development of this model including a generic model of the seat and restraints used.

Development of the generic AHBM 2 and 3 seat model

The test vehicle used in the 2012 autobrake experiments was a 2012 Volvo V60 T4. In the 2016 lane change experiments, a 2016 Volvo V60 was utilized. Note that the generic seat model is suitable for use with both these experiments. Chalmers internal results have shown that the geometry and mechanical stiffness of these two experimental seats is very similar.

As part of the OSCCAR project, Chalmers has delivered a single generic seat model that represents the experimental seat used in both the lane change and autobrake test series. The geometry for this simplified seat model is derived from an LS-Dyna model of a 2016 Volvo V60 driver's seat provided by Volvo Cars. The Volvo owned seat model is not available to share, so a generic seat model developed by Johan Iraeus (J. Iraeus, PhD Thesis, 2015) was morphed to match the surface geometry of the Volvo seat model (Figure A - 52).

Figure A - 52: Morphed generic seat model (left) shown with the original Volvo supplied seat model (middle) and a superposition of the two models to show similarity (right).

Tuning of the AHBM 2 and 3 seat model

Physical tests from the AHBM 2 project

A series of quasi-static indentation tests on the physical seat used in the 2012 Autobrake experiment were performed to generate data to be used to validate the LS-DYNA seat model. The driver seat was put on plywood stands to orient the top surface of the cushion in the horizontal plane (Figure A - 53). The cushion was loaded in the direction normal to the top surface using an indenter plate measuring 260 × 200 × 13 mm. The indenter plate was mounted with a revolute joint to a square aluminum shaft. The shaft was constrained by 4 ball bearing supports, which only allow vertical translation movement. The indentation depth was measured relative to the position of the unloaded rig (weight 2.25 kg) resting on the cushion using a steel scale and a needle attached to the profile. The load was applied in 5-kg increments to a plate on the top of the profile. Each measurement was made shortly after each load increment. Two positions were tested twice, one rearward and one forward (Figure A - 53). The rearward position was found to be more compliant (Figure A - 54).

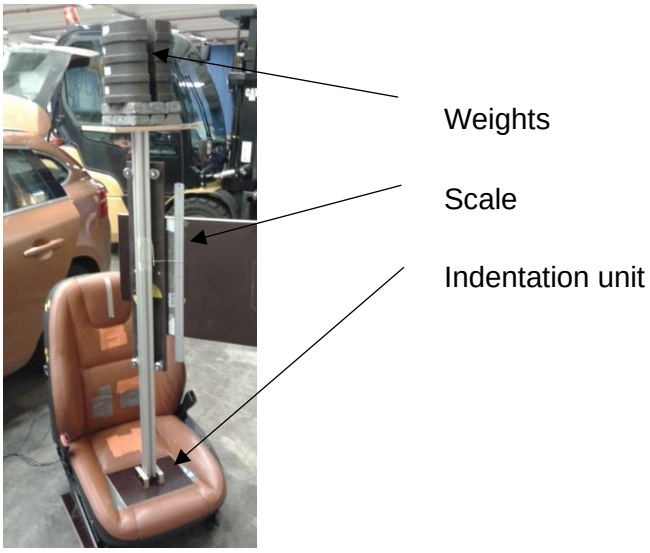

Figure A - 53: Picture of a physical indentation tests performed on the one of the seats used in the AHBM 2 tests.

Tuning of the model to match the physical test results

The physical indentation tests were simulated in LS-Dyna. A rigid plate connected with a revolute joint was loaded with increasing load in increments of 5 kg up to a max of 80 kg. The load was linearly ramped over 50 ms then held for 50 ms until the max load was applied. With additional settling time at the start and end of the simulation, the total simulation time was 1000 ms. The front and back loading positions and angle of applied load (Figure A - 53) were matched to the experiments via pictures and measurements taken. The nodal displacement at the centre of the plate in the direction of applied load vs. the joint reaction force were compared to the load displacement measured in the experiment (Figure A - 54). A scale factor on the stress-strain curve of the seat foam and spring stiffness were manually tuned to match the experimental results without deviating too far from the Volvo supplied seat model. Similar simulations were conducted to match the seatback and side bolsters of the Volvo and generic seat models, but the results are not shown here. To match the side bolster stiffness between the two models, the tension modulus of the seat foam was also tuned.

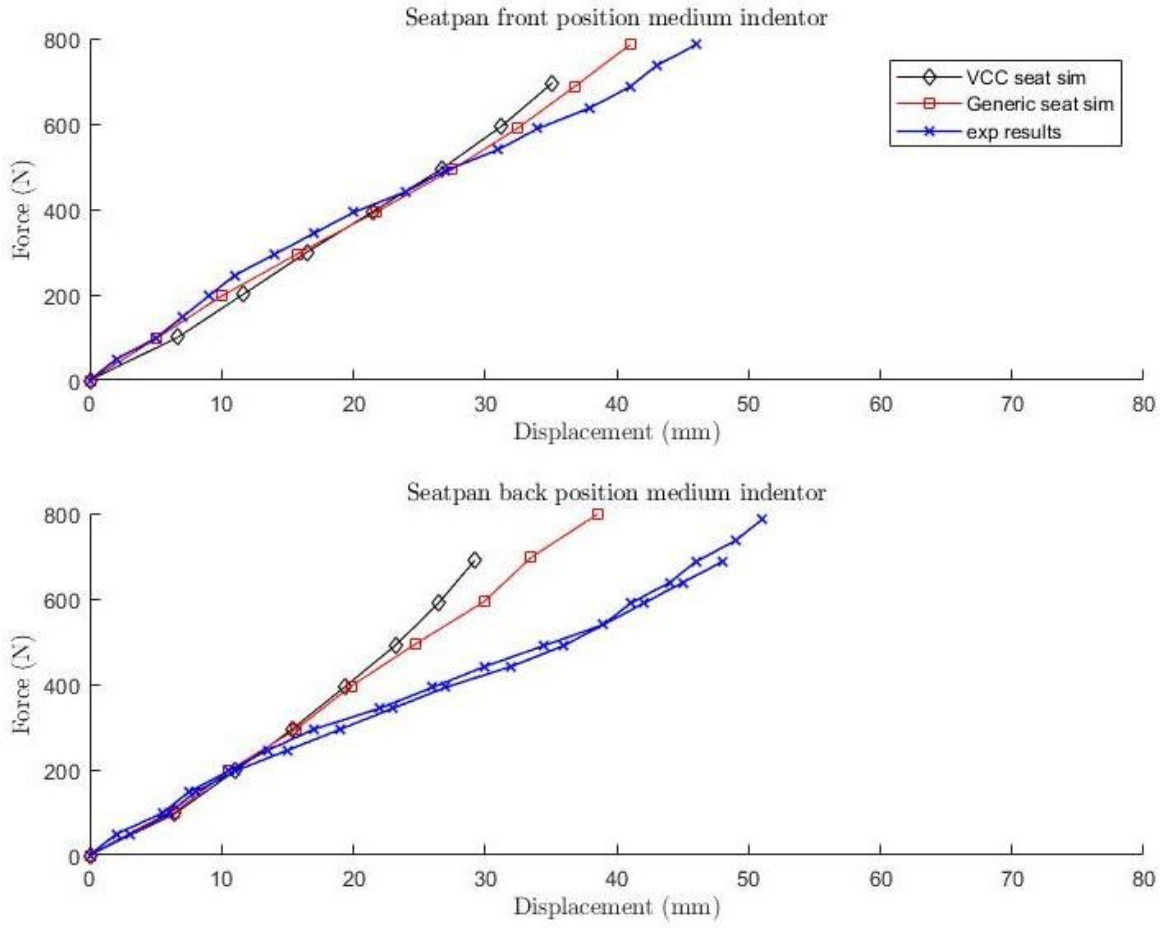

Figure A - 54: Indentation results for the frontward position (top) and rearward (bottom). Physical seat (exp results) vs. LS-DYNA generic seat model vs. Volvo Car Corporation (VCC) provided LS-DYNA model.

Validation of the AHBM 2 and 3 seat model

Once the generic seat model was tuned to match the indentation results of the experimental seat and the Volvo seat model, we wanted to test the response of the generic seat in more complex loading.

Methods

A simulation with the SAFER HBM v9 during a lane change manoeuvre with braking using a standard belt from the Chalmers 2016 lane change test series was chosen. This load case was chosen because interaction with the seat is potentially important during lateral accelerations. For details of the simulation setup and the SAFER HBM v9 whole body HBM, please see Larsson et al., 2019 IRCOBI. Note that in the generic model, the seat belt anchors, and material properties were simplified to remove Volvo intellectual property.

Results

The generic seat simulations produced similar responses in the HBM when compared to the Volvo supplied seat model (Figure A - 55 Figure A - 60).

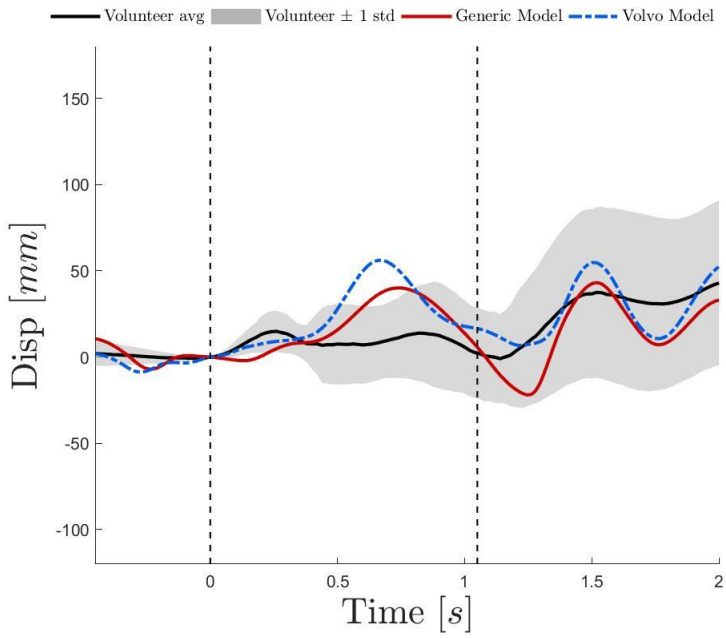

Figure A - 55: Head centre of gravity displacement in the fore-aft direction. Lane change with braking using standard belt - generic seat model and Volvo seat model simulation results compared to volunteers' responses.

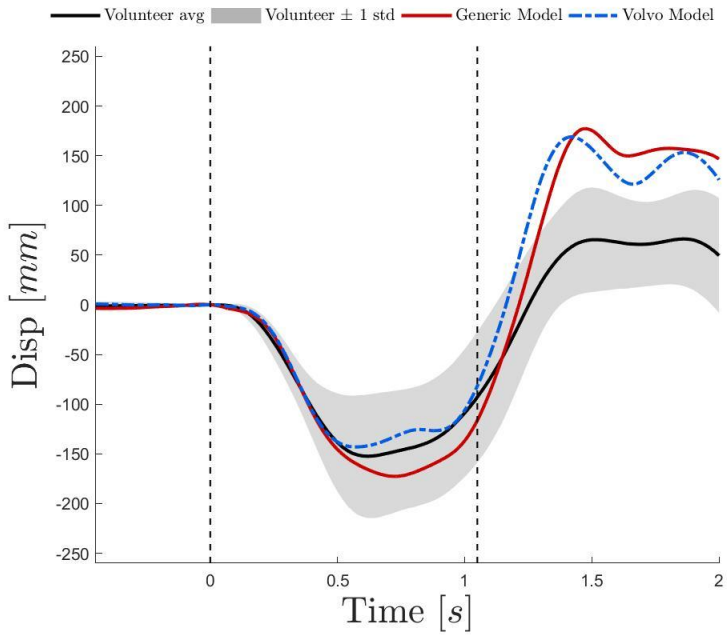

Figure A - 56: Head centre of gravity displacement in the lateral direction. Lane change with braking using standard belt - generic seat model and Volvo seat model simulation results compared to volunteers' responses.

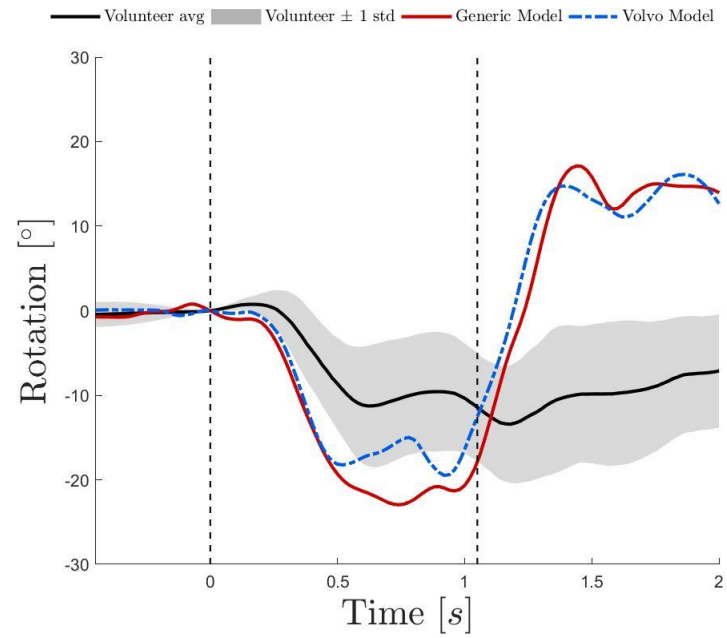

Figure A - 57: Head roll rotation. Lane change with braking using standard belt - generic seat model and Volvo seat model simulation results compared to volunteers' responses.

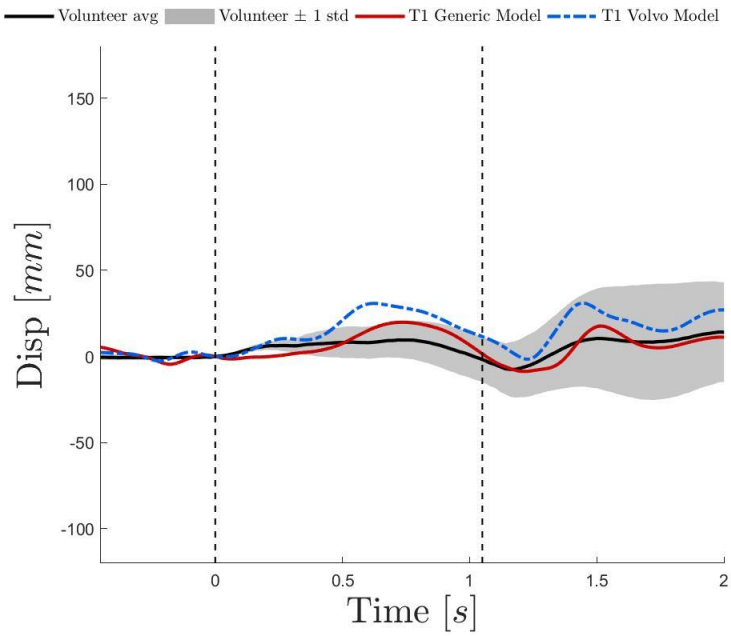

Figure A - 58: Volunteer upper torso fore-aft displacement compared to simulation T1 displacements. Lane change with braking using standard belt - generic seat model and Volvo seat model simulation results compared to volunteers' responses.

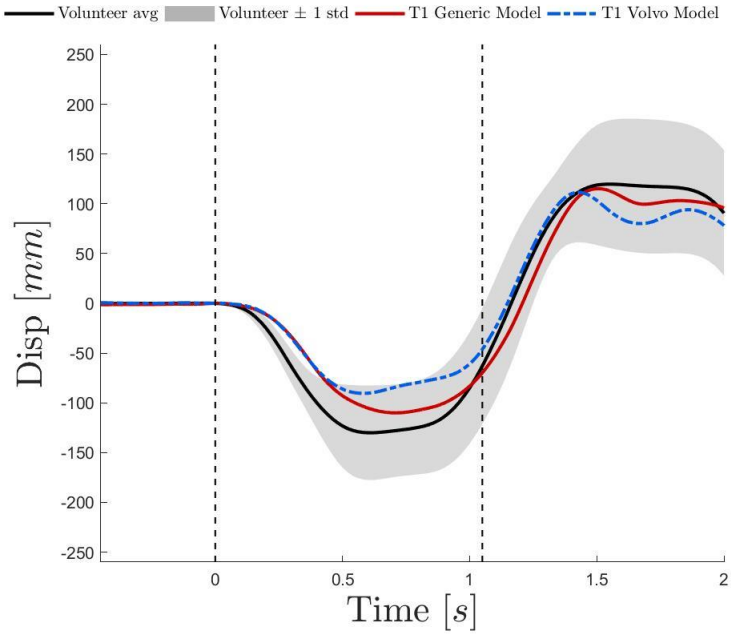

Figure A - 59: Volunteer upper torso lateral displacement compared to simulation T1 displacements. Lane change with braking using standard belt - generic seat model and Volvo seat model simulation results compared to volunteers' responses.

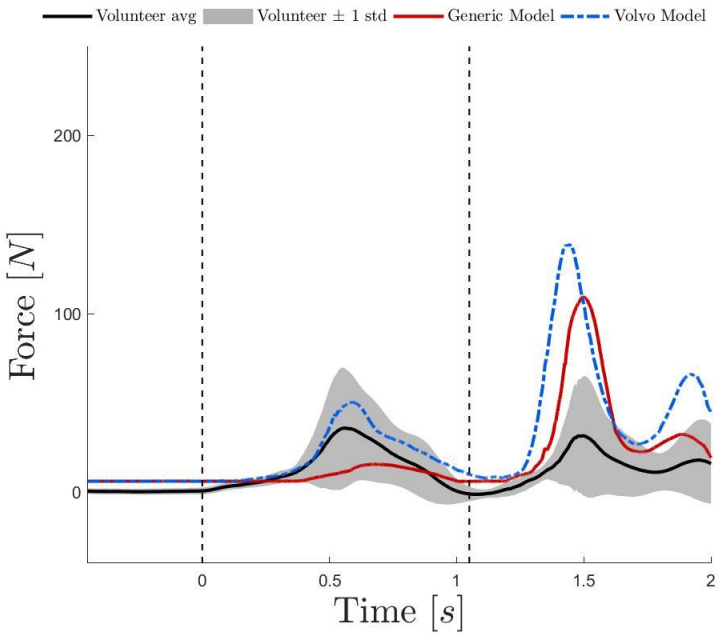

Figure A - 60: Shoulder belt force. Lane change with braking using standard belt - generic seat model and Volvo seat model simulation results compared to volunteers' responses.

D. APPENDIX – IMPLEMENTATION OF EHTM MODEL IN VPS

VPS EHTM model input

VPS ETHM model input follows the architecture already implemented to define an 1D muscle based on previously available standard VPS MATER type 240. It contains three sections: definition of Part of MUSCLE type, EHTM material definition and Fascicle activation definition, as illustrated in Figure A - 61.

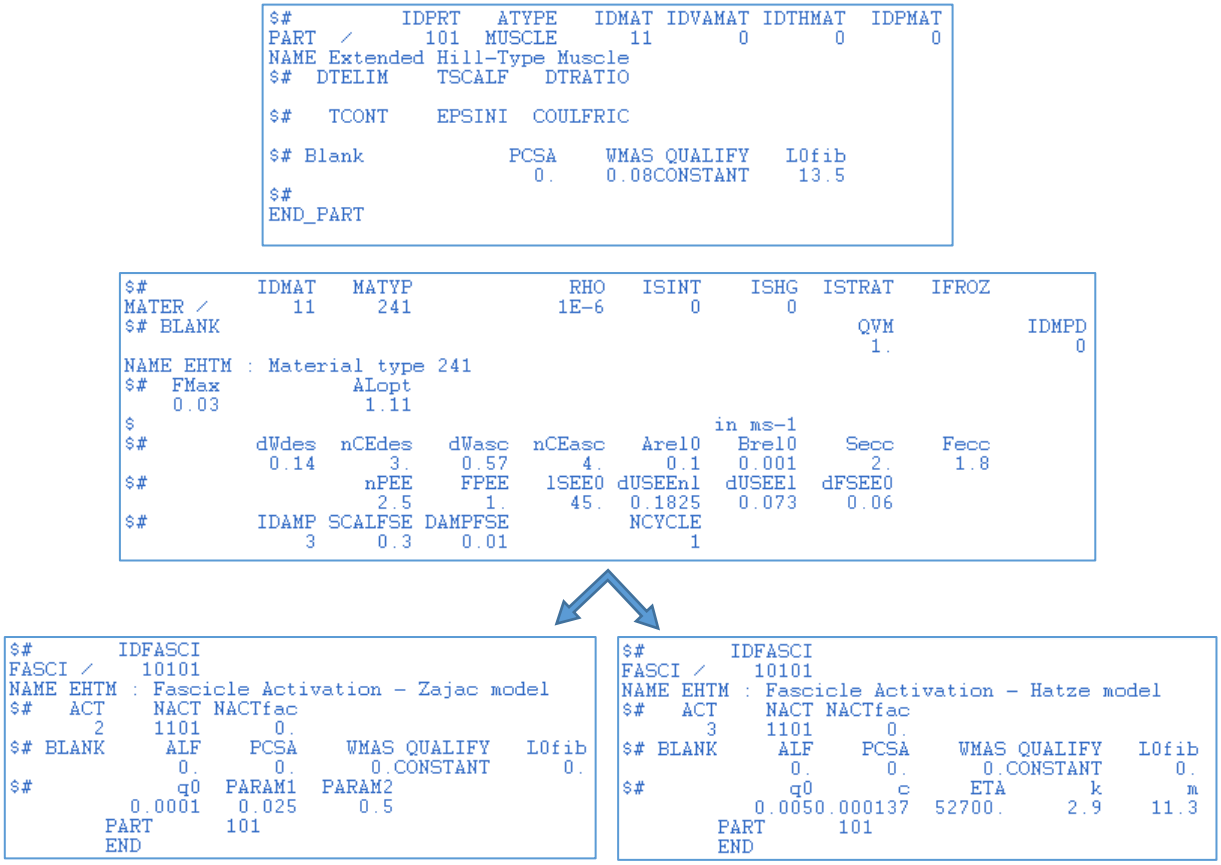

Figure A - 61: VPS EHTM model input – Zajac and Hatze models

Evaluation of the VPS EHTM under isometric concentric load cases

Figure A - 62 and Figure A - 63 present the VPS EHTM model characterisation of Cat and Rat muscles, based on parameters defined in [8] and [9] respectively.

```
$#          IDMAT    MATYP              RHO    ISINT     ISHG  ISTRAT    IFROZ
MATER /        11      241             1E-6        0        0
$# BLANK                                                    QVM             IDMPD
                                                            1.                 0
$      kN
NAME Muscle type 241 - cat soleus muscle (Morl)
$#  FMax            ALopt
0.01                 1.11
$                                                 in ms-1
$#          dWdes   nCEdes    dWasc   nCEasc    Arel0    Brel0     Secc     Fecc
             0.35      1.5     0.35       3.     0.07   0.0002       2.      1.5
$                                          mm                      kN
$#                    nPEE     FPEE    lSEE0 dUSEEnl   dUSEEl  dFSEE0
                       2.5       2.       60.  0.0425    0.017   0.004
$#          IDAMP SCALFSE DAMPFSE             NCYCLE
                3     0.3    0.01                  1
```

```
$#        IDFASCI
FASCI /     10101
NAME Cat Muscle Fascicle - Hatze model
$#    ACT     NACT NACTfac
          3     1101       0.
$# BLANK      ALF     PCSA     WMAS QUALIFY    L0fib
               0.       0.    0.08CONSTANT     47.7
$              0.       0.       0.       0.       0.
$#             q0        c      ETA        k        m
          0.00010.000137  52700.      2.9   22.54
        PART       101
        END
```

Figure A - 62 :Cat VPS EHTM characterization (Units: mm, kg, ms)

```
$#          IDMAT    MATYP              RHO    ISINT     ISHG  ISTRAT    IFROZ
MATER /        11      241             1E-6        0        0
$# BLANK                                                    QVM             IDMPD
                                                            1.                 0
$      kN
NAME Muscle type 241 - rat gastrocnemius medialis (Sierbert)
$#  FMax            ALopt
0.0112               0.32
$                                                 in ms-1
$#          dWdes   nCEdes    dWasc   nCEasc    Arel0    Brel0     Secc     Fecc
             0.35      1.5     0.35       3.     0.06  0.00142     0.99     1.35
$                                          mm                      kN
$#                    nPEE     FPEE    lSEE0 dUSEEnl   dUSEEl  dFSEE0
                       2.5       2.     12.3  0.0425    0.017 0.00448
$#          IDAMP SCALFSE DAMPFSE             NCYCLE
                3     0.3    0.01                  1
```

```
$#        IDFASCI
FASCI /     10101
NAME Rat Muscle Fascicle - Hatze model
$#    ACT     NACT NACTfac
          3     1101       0.
$# BLANK      ALF     PCSA     WMAS QUALIFY    L0fib
               0.       0.    0.08CONSTANT   46.176
$              q0        c      ETA        k        m
          0.0060.000137  52700.      2.9   22.54
        PART       101
        END
```

Figure A - 63: Cat VPS EHTM characterization (Units: mm, kg, ms)

For Cat muscle, the same stimulation curve is used as for the Piglet muscle. Figure A - 64 presents the behaviour simulated by VPS EHTM model defined with Hatze dynamic activation model, which is in agreement with that measured in experiments and also that simulated by LS-DYNA EHTM model.

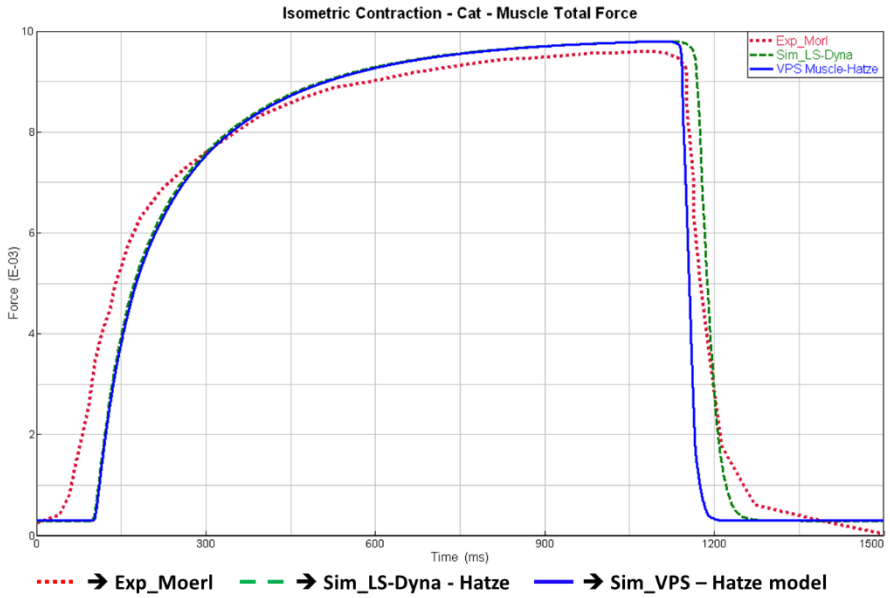

Figure A - 64: Cat – Isometric Contraction – VPS EHTM Hatze: Muscle total force

For Rat muscle, different stimulation curves (see Figure A - 65) have been defined to illustrate its effect on VPS EHTM Hatze model response in terms of total force, shown in Figure A - 66.

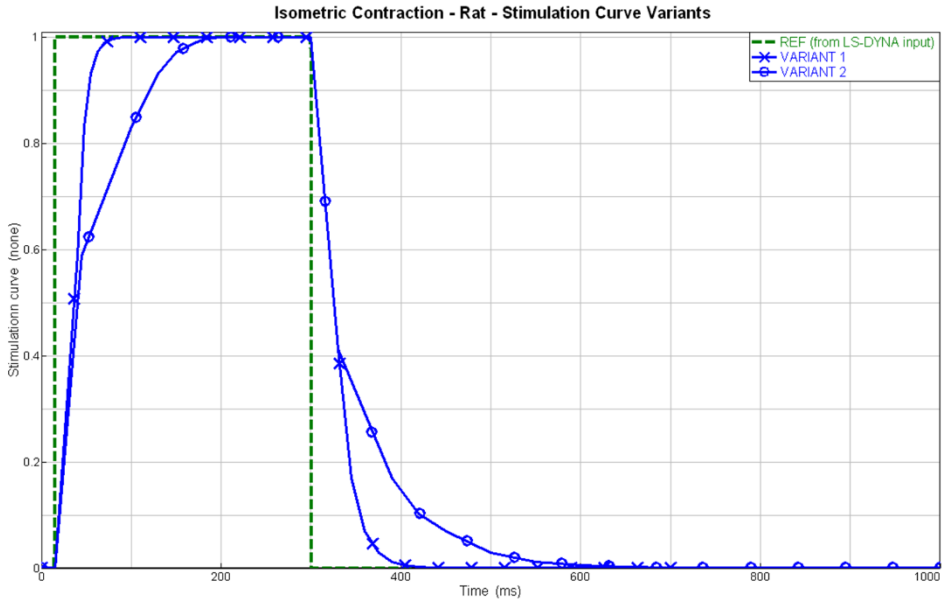

Figure A - 65: Rat – Isometric Contraction - Stimulation curve variants

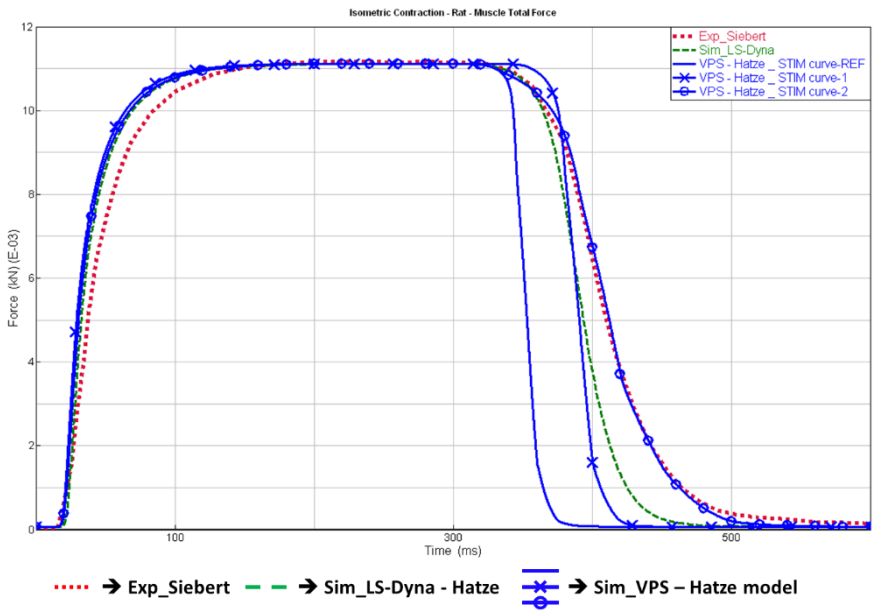

Figure A - 66: Rat – Isometric Contraction – VPS EHTM Hatze: Muscle total force

E. APPENDIX - A SUMMARY OF VALIDATION DATA IN STUDIES OF SHOULDER JOINT STABILITY

Volunteer arm-drop tests were carried out by Tobin [87] to investigate recovery time. The original reference is difficult to obtain, and a summary of the works follows.

In the original experiments, volunteers had their left and right arm extended and supported by cords. The instructions were to remain standing straight and to relax and when the arm fall try to return the arm to its original horizontal position. The cords were released without warning, and the time taken to recover the position was measured (Figure A - 67).

Figure A - 67: Volunteer arm drop test, before (left) and after (right) release

The response time before the arms returned to horizontal averaged 1.22 seconds.

All volunteers overcompensated when recovering their initial arm posture; arms passed the original position (Figure A - 68) before settling back to the original posture.

Figure A - 68: Volunteer arm position at t=0 (left) and t=1.5 (right), showing overcompensation

F. ABBREVIATIONS AND DEFINITIONS

Term	Definition
AHBM	Active Human Body Model
CNIS	China National Institute of Standardization
EHTM	Extended Hill-type Muscle
EMG	Electro Myo Graphy
FE-HBM	Finite Element Human Body Model
HBM	Human Body Model
LS-DYNA	Livermore Software – DYNA; a nonlinear transient dynamic finite element analysis program that uses explicit time integration
MVC	Maximum Voluntary Contraction
OM4IS	Occupant Model for Integrated Safety
PCSA	Physiological Cross-Sectional Area
PID	Proportional–Integral–Derivative (controller)
PRECOONI	COMET K2 funded research project
SAFER	Vehicle Traffic Centre at Chalmers
TNO	Netherlands Organisation for Applied Scientific Research
TUC	Thums User Community
VPS	Virtual Performance Solution
Passive configuration	No muscles are activated in the model
Relaxed configuration	Muscles are activated in the model with low co-contraction
Reactive configuration	Muscles are activated in the model with high co-contraction
Braced configuration	Muscles are activated in the model with high co-contraction

G. DISCLAIMER

The results, opinions and conclusions expressed in this publication are not necessarily those of Volkswagen Aktiengesellschaft.